C55.612/3:973

PENNSYLVANIA STATE UNIVERSITY
MAY 23 1975
DOCUMENTS COLLECTION

ATMOSPHERIC PHYSICS and CHEMISTRY LABORATORY

Collected Reprints 1973

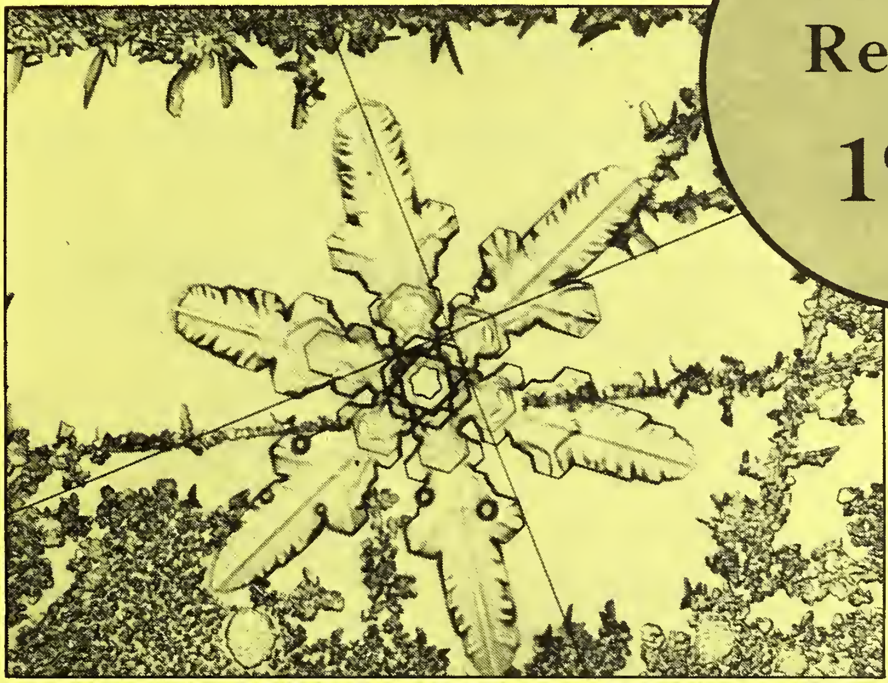

U. S. DEPARTMENT OF COMMERCE
National Oceanic and Atmospheric Administration
Environmental Research Laboratories
Boulder, Colo.

November 1974

Digitized by the Internet Archive
in 2012 with funding from
LYRASIS Members and Sloan Foundation

http://archive.org/details/collectedreprint00atmo

U.S. DEPARTMENT OF COMMERCE
Frederick B. Dent, Secretary

NATIONAL OCEANIC AND ATMOSPHERIC ADMINISTRATION
Robert M. White, Administrator
ENVIRONMENTAL RESEARCH LABORATORIES
Wilmot N. Hess, Director

ATMOSPHERIC PHYSICS AND CHEMISTRY LABORATORY

Collected Reprints 1973

BOULDER, COLO.
November 1974

For sale by the Superintendent of Documents, U. S. Government Printing Office, Washington, D. C. 20402

U. S. Depository Copy

COVER FIGURE

The cover figure is a microscopic view of a snow crystal. It is a reminder of how little we know about it - about its habit, how it grows, how it scavenges aerosol particles and collects droplets from the cloud through which it falls; moreover, we do not know its efficiency in snowing out a cloud. It is a neglected - yet so important - little hydrometeor.

TABLE OF CONTENTS

Page

Allee, P. A.

An Ice Nuclei Concentration Benchmark Network, Proceedings of International Conference on Weather Modification, Tashkent, USSR, October 1-7, 1973. 1

Allee, P. A.

Atmospheric Particulate Concentration Measured During the 1969 BOMEX Experiment, presented at VIII International Conference on Nucleation, Leningrad, USSR, September 23-29, 1973, and at the International Symposium on the Chemistry of Sea/Air Particulate Exchange Processes, Nice, France, October 4-10, 1973. 7

Cobb, W. E.

Atmospheric Electric Program, Antarctic Jounral, *245*, September-October 1973. 14

Cobb, W. E.

Oceanic Aerosol Levels Deduced from the Measurements of the Electrical Conductivity of the Atmosphere, Journal of Atmospheric Sciences, *30*, No. 1, 101-106, January, 1973. 15

Cobb, W. E.

Reply, Journal of the Atmospheric Sciences (Notes and Correspondence) *30*, No. 7, 1460-1462, October 1973. 21

Gille, J. C., and P. M. Kuhn

The International Radiometersonde Intercomparison Programme (1970-1971), Technical Note 128, World Meteorological Organization, WMO-No. 358, 1973. *(Table of contents and preface only)* 24

Grote, H. H.

MINIMAX - A FORTRAN Computer Program to Assemble the Machine Code for the Interdata Model 70 Minicomputer on the Control-Date 3800, NOAA Technical Report ERL 269-APCL 28, 124 pages, April 1973. *(Abstract only)* 28

Jiusto, J. E. and H. K. Weickmann

Types of Snowfall, Bulletin of the American Meteorological Society, *54*, No. 11, 1148-1162, November 1973. 29

Kasemir, H. W.

The Effect of Chaff Seeding on Lightning and Electric Fields of Thunderstorms, Proceedings of the International Conference on Weather Modification, Tashkent, USSR, October 1-7, 1973. 44

Kuhn, P. M. and L. P. Stearns

Long Wave Antarctic Radiation Budget Anomaly, Antarctic Journal, 245-246, September-October 1973. 51

Kuhn, P. M. and L. P. Stearns

Radiometric Observations of Atmospheric Water Vapor Injection by Thunderstorms, Journal of Atmospheric Sciences, *30*, No. 3, 507-509, April 1973. 52

Kuhn, P. M. and L. P. Stearns

Reply: to comments on "Radiosonde Humidity Retrieval by Simultaneous Radiation Measurements" by D. O. Staley and B. M. Herman, Journal of Applied Meteorology, *12*, No. 1, 230-233, February 1973. 55

Kuhn, P. M., W. D. Komhyr, T. B. Harris, P. A. Allee, and W. E. Marlatt

Observations of the Vertical Transport of Water Vapor, Ozone, and Aerosols by Thunderstorms, NOAA Technical Report ERL 253-APCL 25, 57 pages, February 1973. *(Abstract only)* 59

Magaziner, E. L.

A Numerical Model of the Effects of Seedings on the Evolution of a Lake-Effect Storm, Journal of Applied Meteorology, *12*, 948-954, September 1973. 60

Magaziner, E. L. and H. K. Weickmann

The Effect of Hailswath Structure on Hail Suppression Experiments, Journal of Atmospheric Sciences, *30*, No. 2, 334-336, March 1973. 67

Parungo, F. P.

Electron-Microscopic Study of Silver Iodide as Contact or Sublimation Nuclei, Journal of Applied Meteorology, *12*, No. 3, 517-521, April 1973. 70

Parungo, F. P. and R. F. Pueschel

Elemental Identification of Natural and Artifical Ice Nuceli, Proceedings of International Conference on Nucleation, Leningrad, USSR, September 23-29, 1973. 75

Parungo, F. P. and R. F. Pueschel

Ice Nucleation: Elemental Identification of Particles in Snow Crystals, Science, *180*, 1057-1058, June 1973. 80

Parungo, F. P. and H. K. Weickmann

Growth of Ice Crystals from Frozen Cloud Droplets, Beitrage zur Physik der Atmosphare, *46*. Band, 289-304, 1973. 82

Parungo, F. P. and. H. K. Weickmann

Ice Nucleation and Crystal Growth Studied by Electron Microscopy, Proceedings of the VIII International Conference on Nucleation, Leningrad, USSR, September 1973. 98

Phillips, B. B.

Precipitation Characteristics of a Sheared, Moderate Intensity, Supercell-Type Colorado Thunderstorm, Journal of Applied Meteorology, *12*, No. 8, 1354-1363, December, 1973. 102

Pueschel, R. F.

Recent Developments in Chemical Aerosol Analysis, Proceedings of the Workshop on Inadvertent Weather Modification, Utah State University, Logan, Utah, August 13-31, 1973. 112

Pueschel, R. F. and G. Langer

Sugar Cane Fires as a Source of Ice Nuclei in Hawaii, Journal of Applied Meteorology, *12*, No. 3, 549-551, April 1973. 132

Shlanta, A. and P. M. Kuhn

Ozone and Water Vapor Injected into the Stratosphere from Two Isolated Thunderstorms, Journal of Applied Meteorology, *12*, No. 8, 1375-1378, December 1973. 135

Weickmann, H. K.

Welcoming Speech to the Participants, Bulletin of the American Meteorological Society, *54*, No. 2, 100-101, February 1973. 139

Weickmann, H. K.

Closing Remarks by Dr. Weickmann, 26 August, Bulletin of the American Meteorological Society, *54*, No. 2, 103-104, February 1973. 140

Weickmann, H. K., Coordinator

Cloud Physics Program in Support of GATE, NOAA Technical Memorandum ERL APCL-16, 34 pages, December 1973. *(Abstract only)* 141

Weickmann, H. K.

The Modification of Great Lakes Winter Storms, NOAA Technical Report ERL 265-APCL 26, 103 pages, January 1973. *(Abstract only)* 143

Weickmann, H. K.

Snowfall Enhancement, Proceedings of the International Conference on Weather Modification, Tashkent, USSR, October 1-7, 1973. 144

Weickmann, H. K. and R. F. Pueschel

Atmosheric Aerosols: Residence Times, Retainment Factor and Climatic Effects, Beitrage zur Physik der Atmosphare, *46*. Band, 112-118, 1973. 165

Whitaker, S. D.

Computer Simulation of Multi-Aircraft Flights: An Aid to Mission Planning, NOAA Technical Report ERL 281-APCL 29, 27 pages, October 1973. *(Abstract only)* 171

Whiteman, C. D.

Some Climatological Characteristics of Seedable Upslope Cloud Systems in the High Plains, NOAA Technical Report ERL 268-APCL 27, 43 pages, March 1973. *(Abstract only)* 172

Whiteman, C. D.

Variability of High Plains Precipitation, NOAA Technical Report ERL 287-APCL 31, 43 pages, March 1973. *(Abstract and introduction only)* 173

Reprinted with permission of the International Conference on
Weather Modification, Tashkent, USSR, October 1-7, 1973.

An Ice Nuclei Concentration Benchmark Network

Paul A. Allee

Atmospheric Physics and Chemistry Laboratory
National Oceanic and Atmospheric Administration
Boulder, Colorado 80302

Introduction

It is important for the atmospheric scientist to know the concentration of atmospheric ice nuclei and the variation of those concentrations with time. These nuclei are involved in the process of converting supercooled water clouds to ice clouds and any theoretical consideration of weather modification processes must be concerned with their presence in the atmosphere. Measurements to determine the atmospheric concentrations of ice nuclei have been made at many specific locations for varying time periods. However, organized large scale measurements of the atmospheric ice nuclei concentration, coordinating a number of widespread specific sites over a considerable interval of time, have been carried out by only a few projects.

Bowen [1] reported on the results of a one-month examination of the simultaneous concentrations of ice nuclei at eight stations, six Australian, two in the United States. Bigg and Miles [2]carried out a lengthy experiment in which simultaneous measurements of ice nuclei concentrations were made at 24 locations in eastern Australia. Kline [3] reported on extensive measurements derived from a cooperative ice nuclei observational program at 15 locations in the United States during the period from 1959 to 1962. His results give evidence of a geographical difference in ice nuclei concentrations. The most comprehensive survey of the global distribution of ice nuclei concentration was reported by Bigg and Stevenson [4] at 44 locations throughout the world during January, February, and March of 1969. A three station network in the north Pacific Ocean during portions of 1968 and 1969 has detected the advection of enhanced ice nuclei concentrations eastward across the Pacific Ocean (Hobbs, Bluhm and Ohtake [5]).

Discussion

An ice nuclei concentration benchmark network has been established in the western United States by the National Oceanic & Atmospheric Administration. The purpose of the network is to determine the climatological mean and variation for the ice nuclei concentration throughout the seventeen westernmost of the United States and the north Pacific Ocean. The network consists of field monitors located at nineteen National Weather Service locations selected as most likely to be free from anthropogenic sources of ice nuclei. Fig. 1 is a map showing the location of the field monitor sites, identified according to the National Weather Service call letters assigned as location identifiers.

The instrumentation of the network consists of two parts: (1) The equipment for collecting ice nuclei at the field monitoring site. Its major components are a timer, vacuum pump, airflow meter, an elapsed running time meter and an encapsulated membrane filter. (2) An NCAR Ice Nucleus Analyzer for the activation and counting of ice nuclei particles on the membrane filter. This equipment is located in Boulder, Colorado.

The field monitor is designed to filter air through a membrane filter at a known time-rate. The timer is set so that the air is drawn through the membrane filter for a few minutes each hour for each of the twenty-four hours of the day. Thus, the particulate sample obtained on a membrane filter that is changed daily will be representative of the conditions present throughout a twenty-four hour period. The time intervals of pump operation and air flow are coordinated so that about 300 liters of air per day pass through the filter.

The filters are being changed daily at midnight, local time, or as near thereto as possible. The daily atmospheric ice nuclei concentration can then be compared to the daily weather records obtained by the cooperating National Weather Service station for any correlation or anomalies of ice nuclei concentration that are weather dependent. When a number of exposed membrane filter capsules have been collected at the monitor station, they are mailed to the Atmospheric Physics and Chemistry Laboratory at Boulder, Colorado for processing.

The investigation of the ice nuclei concentrations by Hobbs, Bluhm and Ohtake [5] indicates that the time of variation of the climatological ice nuclei concentration is on a greater-than-one-day time scale. Accordingly, the filters from a station are activated at -15°C and -20°C on alternate days. This will give ice nuclei concentration data for two temperatures, yet not interfere seriously with the expected climatological variation time scale. This also reduces the hazards of bookkeeping and contamination due to handling that would result from cutting filters in half for processing at the two temperatures. It is expected that in excess of 7500 filters will be analyzed during the first year of the project. The program will be reviewed at that time to determine the feasibility of operation of the network for a second year.

The daily ice nuclei concentration values are being placed on computer punch cards, along with daily local climatological data obtained by the National Weather Service station where the field monitor is located. The climatological data on the punch cards include:

1. Temperature, maximum
2. Temperature, minimum
3. Temperature, average

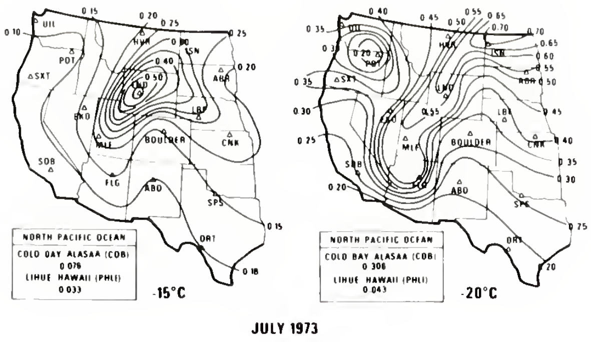

Fig. 1. Location of the benchmark field monitor sites.

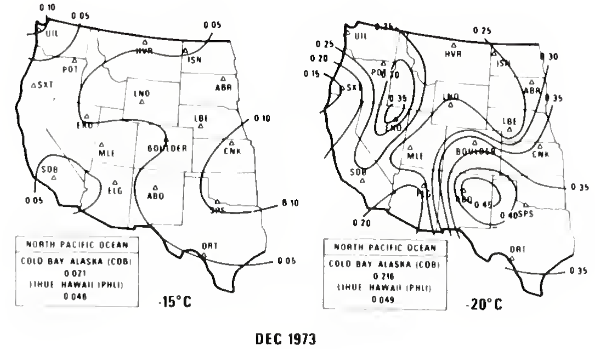

Fig. 3. Isopleths of the average ice concentration over the nuclei benchmark network at -15°C and -20°C for the month of July 1973.

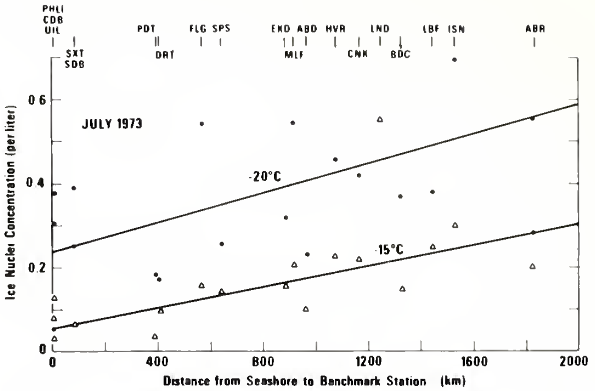

Fig. 2. The daily ice nuclei concentrations at eight of the monitor stations during the month of July 1973.

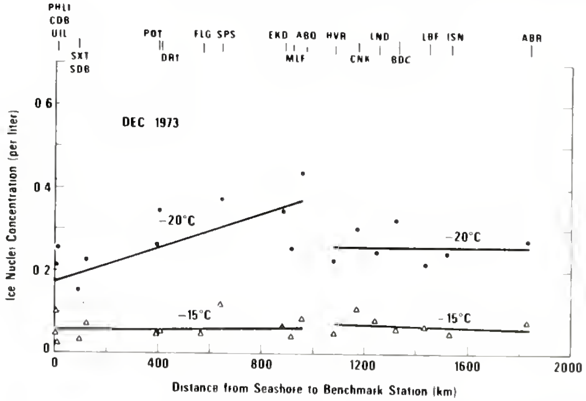

Fig. 4. A plot of the monthly average ice nuclei concentration at a benchmark station for -15°C and -20°C versus its distance from the nearest seashore, either the Pacific Ocean or the Gulf of Mexico.

4. Temperature, dew point, average
5. Weather types on date of occurrence.
6. Snow, ice pellets, or ice on ground.
7. Precipitation, water equivalent.
8. Precipitation, snow, ice pellets.
9. Pressure, average.
10. Wind, resultant direction.
11. Wind, resultant, speed.
12. Wind, average speed.
13. Wind, fastest mile, speed.
14. Wind, fastest mile, direction.
15. Sunshine, percent of possible.
16. Sky cover, tenths, midnight to midnight.

The data from the punch cards are being processed by computer to derive the correlation between the ice nuclei concentration and the climatological weather data on a daily and monthly basis. The computer will also furnish daily and monthly synoptic charts with isopleths of ice nuclei concentration and change charts with isopleths of the increased or decreased ice crystal ice nuclei concentration for the western United States. These charts will be compared to standard meteorological synoptic charts to determine whether any similarity exists between the various types of charts.

Results

The analysis of the data has been made to date on the accumulation of data during May, June, and July, 1973. The ice nuclei concentration has been partially analyzed on both a daily and a monthly summary basis.

Fig. 2 represents the daily ice nuclei concentration at eight of the monitor stations during the month of July, 1973. Because of the volume effect associated with the membrane filter method of counting ice nuclei, the actual ice nuclei concentration on this and the succeeding two figures should be increased by a factor of about 3X (Bigg, Mossop, Meade and Thorndike [6], Gagin and Aroyo [7]. Although plotting the ice nuclei concentration on a logarithmic scale does not emphasize daily variation, there are a few occasions where the daily change of concentration is considerable, such as the July 25-30 increase at FLG (Flagstaff, Arizona). Occasionally the two-day change of concentration increases by more than a factor of 10X, as does the -20°C ice nuclei concentration at SDB (Sandberg, California) on July 29-31. There appears to be no connection between these incidents of increasing ice nuclei concentration since SDB is upwind from FLG by about 500 km.

It is interesting to note that individual stations have a characteristic ratio of ice nuclei concentration at -20°C to that at -15°C. For example, SDB has an average monthly ratio of 3.7 and CNK (Concordia, Kansas) has a ratio of 1.9. SDB is near the Pacific Ocean, CNK is at an inland continental type location. Apparently the ice nuclei at the two locations were of differing chemical composition and/or physical characteristics.

A computer comparison of the daily variation of ice nuclei concentration with the 16 meteorological elements listed in the discussion has not yet detected any strong correlation between the ice nuclei concentration and any of the meteorological elements.

Fig. 3 shows the isopleths of the average ice nuclei concentration over the benchmark network at -15°C and -20°C for the month of July, 1973. It is apparent that the ice nuclei concentrations are less along the coastal areas than they are in the continental interior. The high monthly average of ice nuclei concentration at LND (Lander, Wyoming) could be due to two anthropogenic factors: a rodeo during the first week of July that generated enough dust to occasionally reduce the visibility to two miles, and activities associated with construction of a new airport terminal building.

Fig. 4 is a plot of the monthly average ice nuclei concentration at a benchmark station for -15°C and -20°C versus its distance from the nearest seashore, either the Pacific Ocean or the Gulf of Mexico. Linear regression lines have been calculated for the -15°C and -20°C data and drawn on the graph. Except for LND, the regression line fits the -15°C data points very well. The slope of the line can be interpreted to mean that as the atmosphere crosses the coastline and flows inland, the ice nuclei concentration increases within the atmosphere in direct proportion to the distance from the seashore. If the source of ice nuclei is the surface of the earth and is then convected throughout the troposphere, it can be shown that there are generated at the earth's surface about 2 ice nuclei m^{-2} min^{-2}.

The -20°C regression line does not match the data quite so well, but an interesting stratification of the stations according to geographic location is possible, reflecting the path of motion of the atmosphere across various portions of the western United States.

Comparison of the monthly average values of the ice nuclei concentrations shows that the average concentration has been increasing at all the network stations during the months of May, June and July with the single exception of PHLI (Lihue, Hawaii).

Conclusion

No strong correlations between the daily ice nuclei concentration and local meteorological elements have been found. No evidence of "ice nucleus storms" progressing across the network have been detected to date as previously shown to exist over the North Pacific Ocean by Hobbs, Bluhm and Ohtake [5].

Monthly ice nuclei concentration averages at the network stations show a monotonic increase when related to the distance of the station from the seashore, which can be interpreted that the earth's surface is a source of ice nuclei. Monthly ice nuclei concentration averages at the network stations increased during the months of May, June and July, 1973.

Additional studies need to be carried out in conjunction with the project to determine: (1) Whether an average correction factor for the volume effect can be assigned to the ice nuclei concentration network data on a whole, regional, or seasonal basis. (2) The ice nuclei concentration by aircraft measurements simultaneously with ground measurements to test the extent of the possible stratification of ice nuclei concentration within the atmosphere by such meteorological factors as temperature inversions. (3) The ice nuclei chemical and physical characteristics from various portions of the network.

Bibliography

[1] BOWEN, E.G. (1958). Freezing nucleus measurements in January 1957. Aust. J. Phys., 11, pp. 452-455.

[2] BIGG, E.K., and G.T. MILES. (1968). The results of large-scale measurements of natural ice nuclei. J. Atmos. Sci., 21, pp. 396-403.

[3] KLINE, D.B. (1963). Evidence of geographic differences in ice nuclei concentrations. Mon. Wea. Rev., 91, pp. 681-686.

[4] BIGG, E.K. and C.M. STEVENSON. (1970). Comparison of concentrations of ice nuclei in different parts of the world. J. Rech. Atmos., Vol. IV, 2^{e} annee, no. 2., pp. 41-58.

[5] HOBBS, P.V., G.C. BLUHM, and T. OHTAKE. (1971). Transport of ice nuclei over the north Pacific Ocean. Tellus, XXIII, 1, pp. 28-39.

[6] BIGG, E.K., S.C. MOSSOP, R.T. MEADE and N.S. THORNDIKE. (1963). The measurement of ice nucleus concentrations by means of Millipore filters. J. Appl. Meteor., 2, pp. 266-269.

[7] GAGIN, A., and M. AROYO. (1969). A thermal diffusion chamber for the measurement of ice nuclei concentrations. J. Rech. Atmos., Vol. IV, I^{re} annee, no. 3, pp. 115-122.

Reprinted with permission of the Eighth International Conference
on Nucleation Leningrad, USSR, September 23-29, 1973 and the
International Symposium on the Chemistry of Sea/Air Particulate
Exchange Processes, Nice, France, October 4-10, 1973.

Atmospheric particulate concentration measured during the 1969 BOMEX experiment

by Paul A. Allee

Atmospheric Physics and Chemistry Laboratory
National Oceanic and Atmospheric Administration
Boulder, Colorado 80302

Introduction

During the 1969 BOMEX experiments the Atmospheric Physics and Chemistry Laboratory of NOAA operated atmospheric particulate sampling equipment on a NOAA Research Flight Facility DC-6 aircraft and on the NOAA Ship DISCOVERER. Three types of atmospheric particulate concentrations were measured on most of the DC-6 flights: (1) The Aitken nuclei, the concentration of all particulate material in the atmosphere. (2) The cloud droplet condensation nuclei (CCN), that portion of the Aitken nuclei that are active at low water vapor supersaturation, and around which cloud droplets are formed. (3) The ice nuclei, those Aitken nuclei that are active as freezing nuclei, converting supercooled water droplets to ice crystals. On the NOAA Ship DISCOVERER, only the Aitken nuclei concentration was measured.

Data were obtained on 18 flights, and a portion of one flight was specifically planned to investigate the extent and characterization of the aerosol plume downwind from and generated by Barbados.

Instrumentation

The DC-6 was equipped with an isokinetic sampling intake that brought outside air into the aircraft cabin into a 9.5 mm I.D. Tygon tube, where the air sample was divided between three instruments that measured the concentrations of three types of nuclei. The air intake would not accept air when the cabin was pressurized, so that, except for one event, data at higher than 10,000 feet are not available.

The Aitken nuclei concentrations were measured with a Gardner Small Particle Detector, corrected for altitude according to Auer

(1965). Cloud droplet condensation nuclei concentrations measured with a thermal diffusion chamber, such as discussed by Twomey (1963), at 1 percent water vapor supersaturation. The construction features of the NOAA APCL thermal diffusion chamber have been described by Allee (1971). The ice nuclei concentrations were measured with an NCAR acoustic ice nucleus counter at a temperature of -20°C. For the type of conditions that were encountered during the BOMEX experiments the correction factor would be about 10X, according to Langer (1971).

On the NOAA Ship DISCOVERER, only the Aitken nuclei concentration was measured with a Gardner Small Particle Detector.

None of the instruments used to measure nuclei concentration were capable of measuring the size distribution of the nuclei.

Results

Only a summary of some of the results are presented in this publication . Complete documentation of the individual observations will be found in the future in the BOMEX Permanent Archive of NOAA.

Although the general appearance of the maritime atmosphere was that of considerable haze, visibility sometimes being less than 10 miles, the concentration of Aitken particles was usually less than 400 ml^{-1} at all measurable levels, except in the vicinity of a source of atmospheric pollutants. Visual observation from high flying aircraft indicate that the height of the haze layer was about 12,000 feet.

Figure 1 shows the variation of Aitken nuclei concentration with altitude. The graph has been derived by averaging all of the flight data obtained. The average surface nuclei concentration was derived from data obtained by the NOAA Ship DISCOVERER.

Figure 2 is a comparison of concurrent values of Aitken nuclei and cloud droplet condensation nuclei (CCN) concentrations, and their variation with altitude. It is apparent that there is a strong correlation between the two types of nuclei, except at the 2000 foot level.

Figure 3 is a comparison of concurrent values of Aitken nuclei and ice nuclei concentrations at $-20^{\circ}C$ and their variation with altitude. There is no apparent correlation between the two types of nuclei. For the type of conditions encountered during the BOMEX experiment the correction factor for the ice nuclei concentrations is a multiplication of 10X the ice nuclei concentration shown on Figure 3. The ice nuclei concentration increases with altitude, and is probably associated with the observed increase of the concentration of red dust with increasing altitude. The source of this red dust appears to be the dust storms of the Sahara Desert of Africa.

Conclusion

The atmosphere above BOMEX experiment area of the Atlantic Ocean appears to be an area free of industrial pollution when the atmospheric particulate concentration is considered. It is recommended that areas of the world such as this be monitored at appropriate intervals to measure any increase of the atmospheric particulate concentration at these levels, and to ascertain whether or not the capability of the atmosphere to purge itself of particulate pollutants of industrial origin is being exceeded.

The Atmospheric Physics and Chemistry Laboratory is planning to measure the same particulate concentrations from a DC-6 aircraft during the summer of 1974 GATE experiment. This experiment area is east of the BOMEX experiment area and subsequent comparison of the two sets of data may show how much, if any, the continent of Africa influences the concentration of atmospheric particulates over the GATE experiment area. Membrane filters will also be exposed during the GATE experiment and will be analyzed in the laboratory by a scanning beam electron microscope for particulate size and by an x-ray energy spectrometer for their elemental constituents.

Bibliography

Allee, P.A., 1971: A description of the ESSA-APCL portable thermal diffusion cloud chamber. The Second International Workshop on Condensation and Ice Nuclei, 5-19 August, 1970.

Compiled by L.O. Grant, Dept. of Atmos. Sci., Colorado State University, Ft. Collin , Colorado. Pp. 39-40.

Auer, A., 1965: The vertical distribution of Aitken nuclei in the vicinity of Ft. Collins, Colorado. Tech. Paper No. 68, Dept. of Atmos. Sci., Colorado State University, Ft, Collins, Colorado.

Langer, G., J. Rosinski and C.P. Edwards, 1967: A continuous ice nucleus counter and its application to tracking in the troposphere. J. Appl. Meteor., 6 , pp. 114-125.

Langer, G., 1971: Detailed evaluation of the NCAR ice nucleus counter-- initial report. International Conference on Weather Modification, 6-11 September, 1971, Canberra, Australia.

Twomey, S., 1963: Measurements of natural cloud nuclei. J. Rech. Atmos., I, No. 3, pp. 101-105.

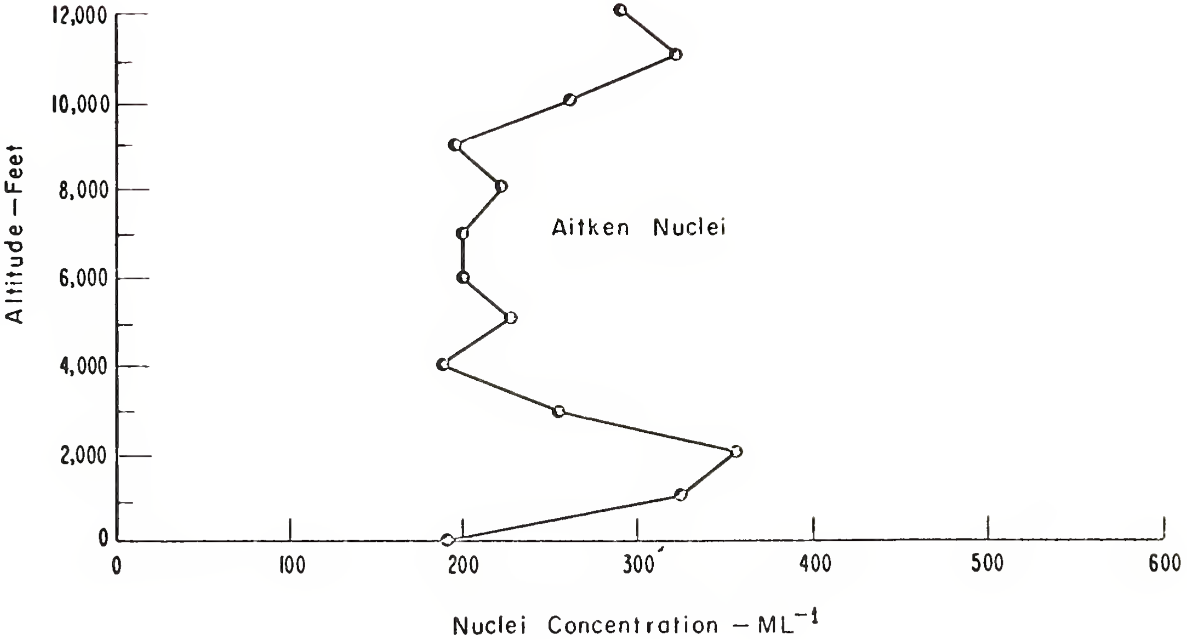

Figure 1. The variation of Aitken nuclei concentration with altitude.

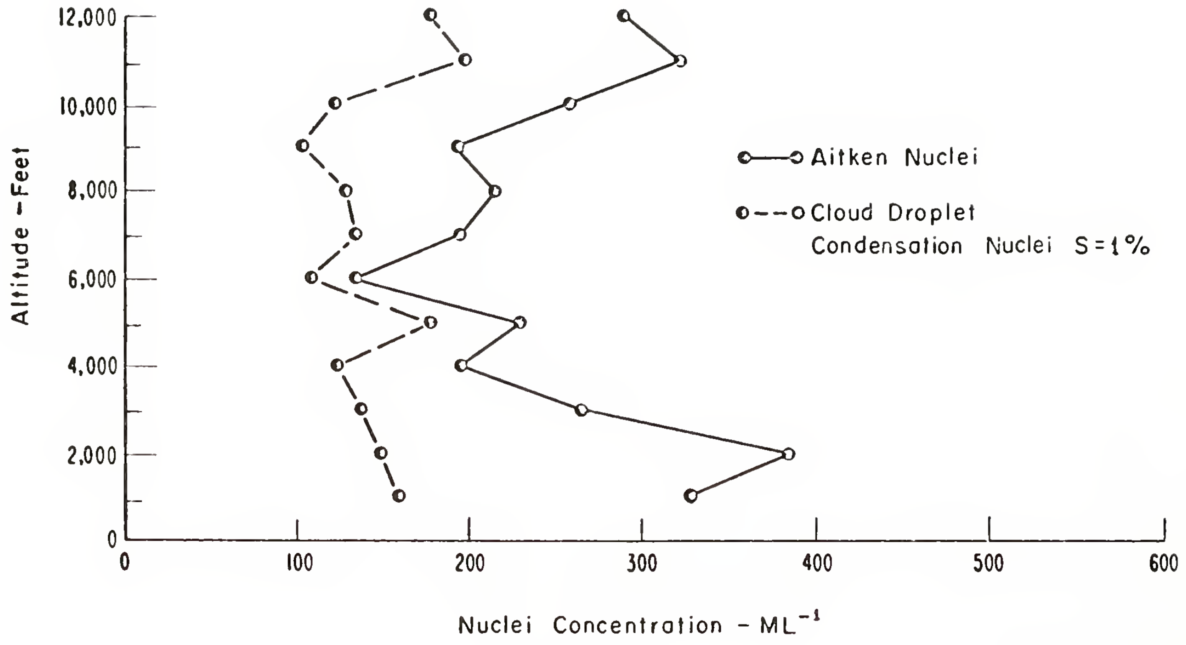

Figure 2. A comparison of concurrent values of the concentration of Aitken nuclei and cloud droplet condensation nuclei with altitude.

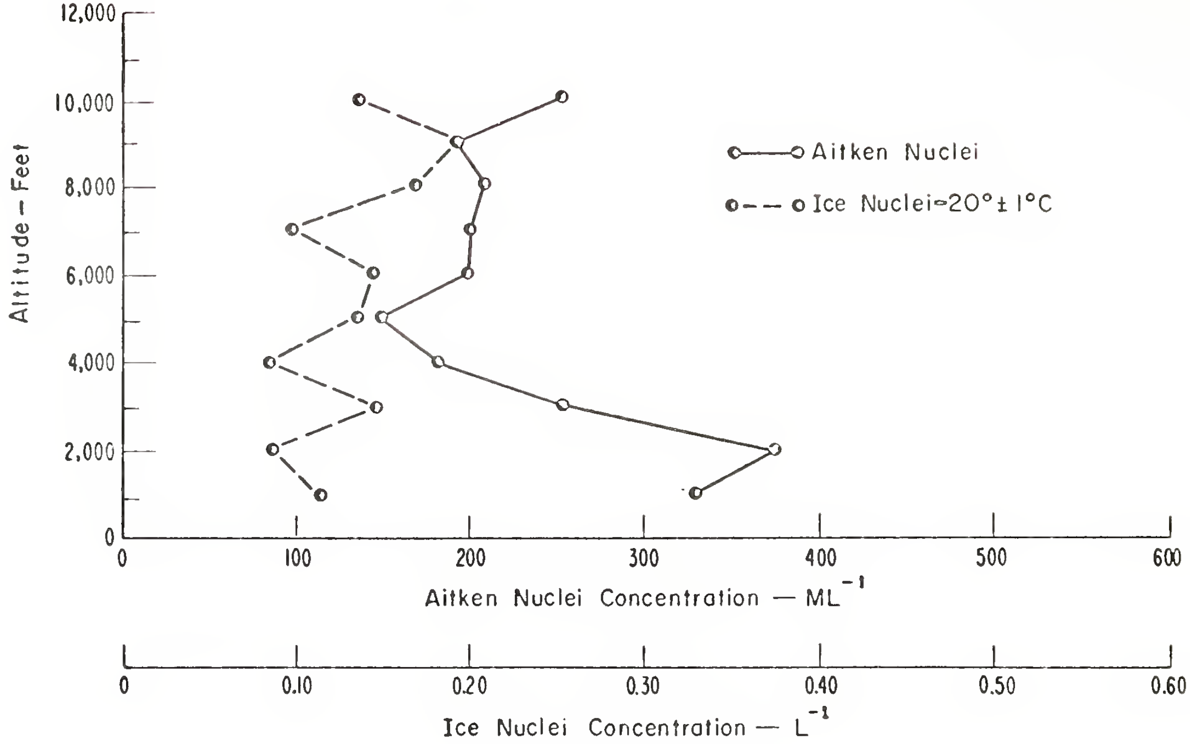

Figure 3. A comparison of concurrent values of the concentration of Aitken nuclei and ice nuclei at -20^{0}C with altitude. The correction factor for the ice nuclei concentration is a multiplication of 10X.

Reprinted with permission of the Antarctic Journal,
September-October 1973.

Atmospheric electric program

WILLIAM E. COBB

National Oceanic and Atmospheric Administration
Atmospheric Physics and Chemistry Laboratory, Boulder

New instruments designed to measure atmospheric electric parameters at South Pole Station were tested during the 1972-1973 austral summer, in preparation for the 5-year measurement program to begin in November 1973. The program's purpose is to establish an "environmental benchmark" of atmospheric electrical parameters sensitive to air pollution levels, and also to investigate the mechanisms that control and maintain the constant flow of electrical current between the earth and the ionosphere.

Ten successful balloon flights were made, using radiosondes modified to measure the ionosphere-earth conduction current. This was the first time such measurements have been made from South Pole Station. Simultaneous balloon measurements were made at several northern hemisphere sites: Boulder, Colorado, White Sands, New Mexico; Duluth, Minnesota; and Thule, Greenland. A cooperative program between the Atmospheric Physics and Chemistry Laboratory, National Oceanic and Atmospheric Administration, Boulder, and the University of Minnesota, Duluth, has been established to coordinate simultaneous balloon flights in both hemispheres.

A widely accepted hypothesis claims that the flow of electrical current from the ionosphere to the earth, in fair-weather regions, is returned to the ionosphere where there are thunderstorms. Balloon measurements of the current flow at different latitudes are expected to help explain this hypothesis as well as extra-terrestrial effects often manifested in polar auroral activity.

Reprinted with permission of the Journal of Atmospheric Sciences
Vol. 30, No. 1, January 1973.

Oceanic Aerosol Levels Deduced from Measurements of the Electrical Conductivity of the Atmosphere

WILLIAM E. COBB
Atmospheric Physics and Chemistry Laboratory, NOAA, Boulder, Colo. 80302

(Manuscript received 8 May 1972, in revised form 6 October 1972)

ABSTRACT

The electrical conductivity of the atmosphere, monitored at sites remote from sources of anthropogenic aerosols, may be used to provide an index of the level of suspended particulates for the area representative of the sampling site. Conductivity measurements taken at Mauna Loa, Hawaii, and from ocean research vessels, indicate that most of the oceanic regions of the world are maintaining a natural aerosol level unchanged by the activities of mankind. Significant exceptions are the paths of aerosol pollution extending eastward from the United States in the North Atlantic, from Japan in the North Pacific, and southward from Asia in the Northern Indian Ocean. These regions are discussed with respect to the lifetime of the suspended particulates and the influence of large-scale atmospheric circulation. Anthropogenic aerosols are largely produced from the burning of fossil fuels such as coal and oil. The present trend is toward control of these particulate emissions and an inevitable switch to other forms of energy production. It is concluded that the anthropogenic aerosols now detectable in some oceanic regions will begin to decline by the end of the century and that any global climatic changes due to the current increase will be insignificant.

1. Introduction

It has become important to the well-being of mankind on this planet to assess the consequences of the particulate material which is produced and injected into the atmosphere through the activities of an expanding human population. The task is to document aerosol levels in the past; to establish environmental benchmarks of the present state of the atmosphere; and to predict, if possible, future trends and effects.

It is well known that the electrical conductivity of the atmosphere, monitored at sites remote from sources of pollution, will yield data interpretable as an index of the amount of particulate matter suspended in the atmosphere. The conductivity is a particularly important parameter because new measurements may be compared to those taken on the scientific cruises of the sailing vessel *Carnegie*.

Wait (1946) was probably the first to attempt on a global scale to correlate aerosol levels with the atmospheric conductivity. He reported an alarming decrease in oceanic conductivity and attributed it to an increase in anthropogenic aerosols. Gunn (1964) found Wait's conclusions to be in error due to an instrumental air-sampling problem which existed during Cruise VII of the *Carnegie*. Gunn, nevertheless, reported a measureable increase in air pollution over the mid-Atlantic between 1928 and 1962. Cobb and Wells (1970) measured the conductivity during the global voyage of the *Oceanographer* in 1967. They reported that the aerosol concentration in the North Atlantic had approximately doubled in the preceding 60 years but found no significant change in the South Pacific.

This report presents new conductivity data from the Mauna Loa high altitude observatory in Hawaii and discusses recent oceanic measurements made in the western North Pacific (Misaki and Takeuti, 1970; Morita, 1971).

2. The electrical conductivity of the atmosphere

The atmosphere is a poor electrical conductor. This fact is easily demonstrated by observing that an electrically charged and highly insulated conductor placed in the atmosphere will systematically lose its charge in the surrounding air. The conductivity is due to the presence of highly mobile ions produced in the atmosphere by cosmic rays and local radioactive sources. Over the oceans, ionizing radiations produce about 2 ion pairs $\mathrm{cm}^{-3}\ \mathrm{sec}^{-1}$ and a resulting small ion density and conductivity, near sea level, of roughly 1000 ions cm^{-3} and $2.5\times10^{-14}\ \Omega^{-1}\ \mathrm{m}^{-1}$, respectively. A balance is maintained since the small ions are being removed from the atmosphere at the same rate that they are being produced. They are removed by recombination with oppositely charged small ions, thus neutralizing the charge, and by attachment to much larger aerosols, both charged and uncharged. These recombination and attachment processes thus determine the lifetimes of small ions in the atmosphere and the existing conductivity and small ion population. Ionic lifetimes near the earth's surface vary from ~20 sec in highly polluted air to ~300 sec in very clean air. The particulates which have appreciable atmospheric suspension times are largely sub-micron sized; however, they are much larger than the molecular sized small ions. Their role is mainly a passive one, that of providing relatively immobile surfaces for the diffusional attachment of small ions thus leading to a subsequent reduction in the electrical conductivity.

3. Aerosols: Natural and anthropogenic

The fine-particle aerosol content of the atmosphere is largely composed of condensation nuclei. While the size distribution of these nuclei is very large, the majority have radii of less than 10^{-5} cm. The relative abundance or scarcity of condensation nuclei can be of great importance to the physics of precipitation since nearly each cloud droplet requires a grain of particulate matter at its birth. Of equal or greater importance is the effect of the total particulate suspension on the global heat balance.

The distribution of particulate matter in the atmosphere results from the dynamic balance of processes which continuously cleanse and replenish the air with nuclei. Sources are both natural and anthropogenic. Nuclei are produced from the oceans and the continents, and from forest fires, volcanoes, dust storms, etc. They are also produced through the activities of mankind, particularly from the burning of fossil fuels. Thus, a continuing flux of material from the earth's surface is borne aloft by the mechanisms of convection, diffusion and large-scale circulation.

Within the troposphere, where most of our global weather occurs, washout by precipitation and other aerosol removal processes tend to reduce the amount of material in suspension. The average atmospheric residence times of these fine-particle aerosols is of the order of days to a few weeks. Aerosols, which in some manner are transported to above the tropopause, may remain suspended for months, even years, drifting with the prevailing winds, until the processes of coagulation and gravitational settling slowly bring the particles down into the region of clouds and storms to become moisture laden and eventually precipitated to earth.

The atmospheric mechanisms of particle injection, transport, and eventual deposition have maintained a balanced aerosol level presumably for centuries, with the exception of periods of up to a few years following great volcanic eruptions. Within this century particulates produced by human activities have become a factor to be considered.

It has been estimated (Squires, 1966; Selezneva, 1966; Hidy and Brock, 1970; Robinson and Robbins, 1970) that the anthropogenic component of the global particulate burden of the atmosphere amounts to 5–12%; not, it would seem a very alarming figure. The ratio of natural to anthropogenic aerosols, however, varies greatly. The author recently measured the Aitken nucleus concentration at the Amundsen-Scott South Pole station and found less than 200 nuclei cm^{-3}, probably all of natural origin. The same instrumentation, in Boulder, Colo., a typical urban non-industrial community, measured from 50,000 to 300,000 nuclei cm^{-3} of which more than 90% were considered to be anthropogenic. Weickmann (1971) has considered, on a global basis, areas of industrialization and population density and concluded that nearly all of the man-made aerosol pollution is produced from only 2.5% of the earth's surface. Particulates injected from this relatively small area, however, may be transported over long distances. Smoke from forest fires in North America, for example, is sometimes observed over Europe. Volcanic ash has been known to circle the globe for several years. Libby and Palmer (1960) have shown that radioactive debris can remain suspended for many months, accumulating at high levels over the poles during the winter season and descending toward mid-latitude troposphere in the following spring. Harmattan dust has been traced across the equatorial Atlantic from North Africa to Barbados (Prospero and Carlson, 1972). Thus, there is no doubt that suspended particulates, whether natural or anthropogenic, may be transported great distances and remain aloft for extended periods.

An unknown fraction of the total particulate suspension of the atmosphere results from the transformation of pollutant gases. Such aerosols may also be natural or anthropogenic, resulting, for example, from gases produced from the biological decay of vegetation; from volcanic gases; or in the case of human activity, from gases produced from the burning of fossil fuels.

4. Atmospheric conductivity measurements at Mauna Loa: Comparison of 1960 and 1968 data

The Gerdian-type conductivity sensors used in 1960 and in 1968 have been previously described (Cobb and Phillips, 1962). An important change was made in the air intake system prior to the 1968 measurements. As suggested by Cobb (1968a), the intake ahead of the Gerdian chamber was reduced to a short length (50 cm) of straight flow pipe. The air transit time from the intake entrance to the Gerdian chamber was thus reduced from 0.5 to 0.1 sec. It was experimentally determined that the earlier intake system used at Mauna Loa resulted in a 3% loss in conductivity and small-ion density from the free-air values, the loss being primarily due to the diffusion of ions to the walls of the intake system. The 1960 data in Fig. 1 have been adjusted accordingly.

The data in Fig. 1 consist of mean hourly values of the electrical conductivity measured in fair weather during the respective 1-year measurement periods. A "fair weather" day, more restrictive than that originally used, is defined as follows: 24 hr of record with no clouds above the Observatory level other than the possible existence of cirrus; no restrictions to visibility such as smoke from brush fires or a local volcanic eruption; and no upslope wind. Fifty-six such fair-weather days occurred during the initial measurement period, 1 September 1960–1 September 1961, and 72 days in the latter period, 1 June 1968–1 June 1969. The fair-weather restrictions were imposed to make the sampled atmosphere representative of as large an area as possible. Cobb (1968b) has described the Observatory environment during downslope wind conditions, as typical of the free atmosphere over the mid-Pacific at 3–5 km.

The only conclusion to be drawn from the data in Fig. 1 is that there is no measurable difference in the electrical conductivity, and thus of the aerosol level, between that found in 1960 and again in 1968. The double oscillation which occurs diurnally, is a persistent feature of the conductivity measurement at Mauna Loa entirely due to the mountain's presence. The mean diurnal variations are small, however, amounting to $\pm 5\%$ from the mean conductivity of $7.23\times10^{-14}\,\Omega^{-1}\,\mathrm{m}^{-1}$ in 1960 and $7.25\times10^{-14}\,\Omega^{-1}\,\mathrm{m}^{-1}$ in 1968. The early morning conductivity minimum is associated with the electrode effect (Cobb, 1968b) which becomes progressively stronger during the night and reduces the negative and total conductivity. The mid-afternoon minimum occurs at the time of greatest heating of the mountain's lava surface and a subsequent increase in particulates raised from the surface by thermal convective processes. It may be deduced, then, that the free-air conductivity at the Observatory's elevation would, in the absence of the mountain effects described above, approach a constant level equivalent to the maximum values shown in Fig. 1.

5. The oceanic distribution of anthropogenic aerosols

Depicted on the world map in Fig. 2 are ocean areas where measurements of the atmospheric electrical conductivity indicate a secular increase in aerosol pollution. Conductivity values are shown which also indicate areas where the natural aerosol level remains unaffected by human activity. The size and intensity of the three regions of aerosol pollution must remain in doubt since oceanic measurements are not frequently made. Nevertheless, there is sufficient evidence to state that the three areas do indeed exist, and that they are extensions of anthropogenic aerosol concentrations produced in populated land areas.

The secular decrease in atmospheric conductivity over the North Atlantic is based on the report of Cobb and Wells (1970). No new data have been reported although some overlooked measurements of Anderson and Trent (1962) made in 1960 agree with the downward trend of atmospheric conductivity in the region.

Recent investigations in the Pacific indicate an aerosol increase east of the Asian continent and the islands of Japan similar to that found in the North Atlantic. Misaki and Takeuti (1970) measured the electrical conductivity around the Japanese Islands on the research vessel *Fuji* and found a mean conductivity of $1.35\times10^{-14}\,\Omega^{-1}\,\mathrm{m}^{-1}$. While the conductivity increased with the distance from land, the vessel was never more than 150 km at sea and the measurements are probably more representative of the land than of the ocean. Morita (1971) made atmospheric electric measurements in the western North Pacific aboard the research vessel *Hakuho-Maru* and reported a mean conductivity, in fair weather and more than 1000 km from shore, of $2.2\times10^{-14}\,\Omega^{-1}\,\mathrm{m}^{-1}$. This is 20–25% less than the conductivity measured by the *Carnegie* on cruises IV and VII in the area from 10–50N and 140–180E in 1915 and 1929 (Ault and Mauchly, 1925; Torreson *et al.*, 1946).

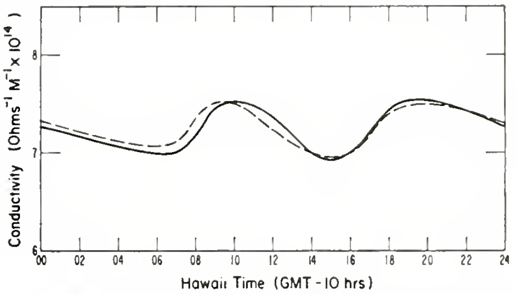

FIG. 1. Mean hourly conductivity at Mauna Loa in fair weather in 1960 (dashed) and 1969 (solid), indicating no change in conductivity and consequently in the aerosol level at the Observatory.

The increased aerosol pollution reported by Cobb and Wells in the northern Indian Ocean is considered to be a special case. Drought conditions over the past decade in India have helped produce large areas of barren soil and dust particles which may be borne aloft and transported by the monsoon circulation. Thus, the aerosol pollution found at sea is probably seasonal and not as extensive as the areas in the North Pacific and North Atlantic.

It should be noted that some regions have always had a relatively high natural aerosol level. The conductivity measured, for example, in the Red Sea in 1911 (Angenheister, 1914), is the same as that found by the *Oceanographer* in 1967. This is an arid region which has always had a high level of haze and dust particles and a lack of rainfall to remove them.

6. Summary and conclusions

Conductivity measurements made at Mauna Loa and from ocean research vessels indicate that most of the global ocean environment, within the planetary boundary layer at least, has maintained a natural aerosol level unchanged by the activities of mankind. Significant exceptions are the paths of aerosol pollution extending eastward from the United States in the North Atlantic, from Asia and Japan in the North Pacific, and southward from Asia in the northern Indian Ocean. These regions comprise less than 10% of the earth's ocean

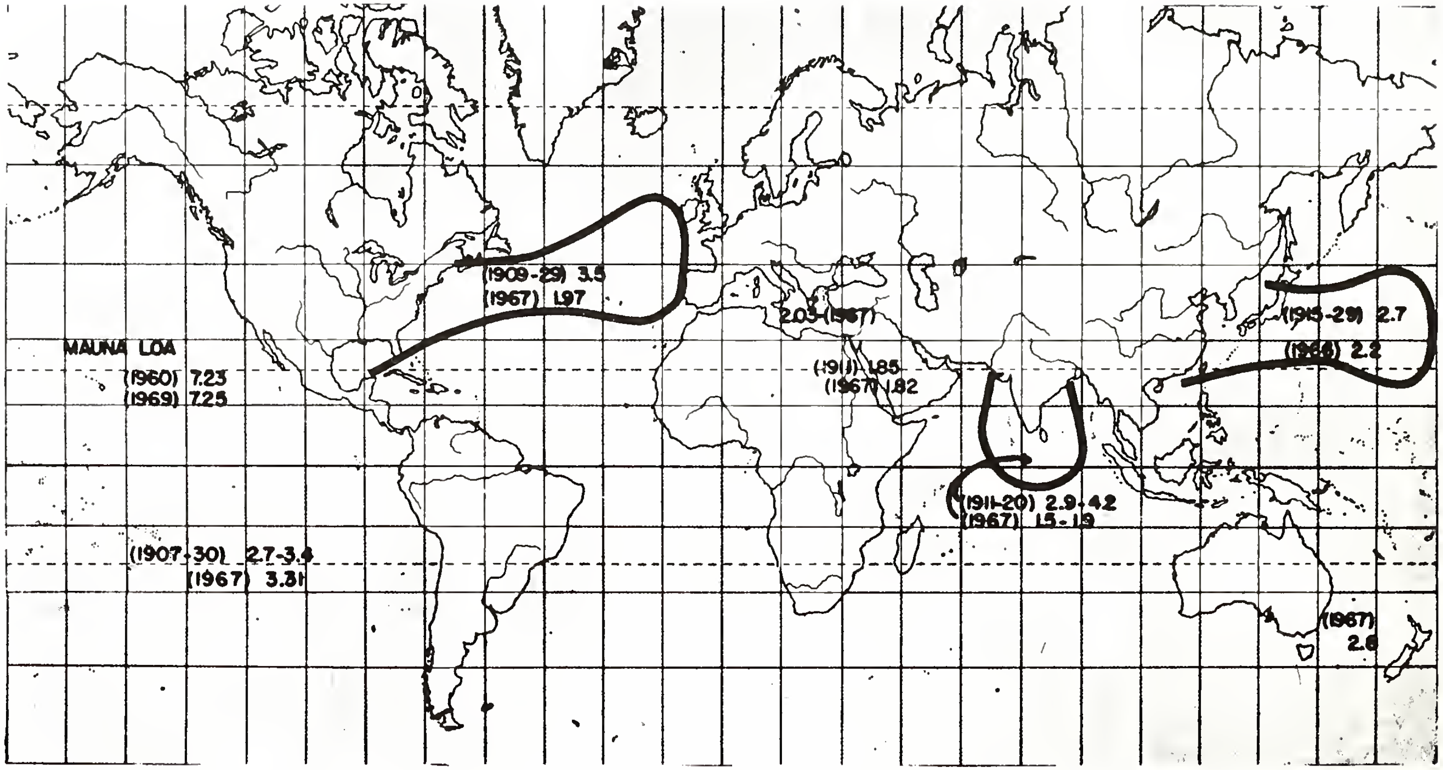

FIG. 2. Oceanic regions of anthropogenic aerosol pollution as indicated by a secular decrease in atmospheric conductivity. Conductivity units are ohms^{-1} m^{-1} × 10^{14}.

area. It is likely that the polar regions should be included with the clean-air ocean environment even though measurements are lacking.

It was indicated by Cobb and Wells (1970) that the unchanged aerosol level in the vast South Pacific trade wind region was partly due to the enhanced processes of aerosol removal. In this report conductivity measurements at Mauna Loa indicate that a similar trendless aerosol condition exists in the Northern Hemisphere trade wind region, at least between 1960 and 1969. It should be noted that measurements at Mauna Loa, on days with no clouds or upslope wind, are representative of the free atmosphere of the mid-Pacific at 3.4 km, well above the trade wind inversion. Ellis and Pueschel (1971), in a report based on solar radiation data at Mauna Loa for the period 1958–70, conclude that human activities have not affected the atmospheric turbidity on a global scale. They also conclude that the 1963 eruption of Mount Agung, a natural phenomena, produced stratospheric aerosols which persisted for 7 years.

The lack of continuous data in the oceanic areas of pollution, shown in Fig. 2, makes it difficult to detect variations of the size and intensity of the regions. It is reasonable to assume, however, that seasonal changes are quite large. In North America, for example, aerosols are more likely to be transported into the stratosphere during the thunderstorm season and as explained earlier, such aerosols will have a much longer atmospheric residence time. Aerosols in the lower troposphere, on the other hand, are largely removed by rainfall, especially the non-shower type precipitation more likely to occur over the western North Atlantic during the winter and spring. Assuming that the production of anthropogenic aerosols in North America is relatively constant throughout the year, the above forces of particle injection and removal suggest that the area of man-made pollution extending over the North Atlantic would be more persistent during the summer and less so in the winter and spring.

Seasonal variations of the oceanic aerosol regions shown in Fig. 2 remain to be proved by observation. The most practical method at this time would appear to lie in the long-term analysis of satellite photography such as the figure shown in a recent paper by Lovelock (1971).

Anthropogenic aerosols are largely produced from the burning of fossil fuels such as coal and oil. The present trend within the world's industrialized urban complexes is toward control of these particulate emissions and an inevitable change to other forms of energy production. Machta (1972) reports that the present growth rate of fossil fuel consumption of 4% per year is expected to fall to 3.5% between 1980 and 2000 as nuclear power comes into wider use. Perhaps it is not too farsighted to predict that the anthropogenic aerosols now detectable in some oceanic regions will begin to decline by the end of the century and that any global climatic changes due to the current increase will be insignificant. Such a prediction is based on the logical assumption that the major sources of anthropogenic aerosols will be reduced and thus the oceanic regions in Fig. 2, which are extensions of the source areas, will also be reduced.

Improved emission control technology, and the change in domestic fuel from coal to oil and gas, have already reduced particulate pollution in major urban areas of the United States as documented by Ludwig *et al.* (1970) of the National Air Pollution Control Administration. Spirtas and Levin (1971) have also documented a mean decrease in particulate levels at 58 U. S. urban centers. Visibility statistics have been analyzed by several investigators, most indicating a decrease in suspended particulates at urban centers (Beebe, 1967; Holzworth, 1962; Freeman, 1968) but with some single-station studies for downtown Los Angeles and New York indicating a secular increase in air pollution (Keith, 1970; McNulty 1968).

This author does not wish to imply that areas of anthropogenic aerosols over the ocean can be ignored. Certainly it is important to monitor the global environment at every opportunity and particularly at sites remote from sources of atmospheric pollution. So long as man continues to produce aerosol pollutants at a rate measured in millions of tons per year, the potential exists for initiating global climatic change. Environmental benchmarks at locations such as Mauna Loa, ocean vessels, the South Pole, and the new geophysical monitoring sites being established by the National Atmospheric and Oceanic Administration at Samoa in the South Pacific and Point Barrow, Alaska, provide the most logical way of detecting secular changes within our global atmosphere.

The reader is reminded that all the measurements of atmospheric electrical conductivity discussed in this paper were made at the surface and are probably not applicable to aerosol conditions in the stratosphere. As discussed in Section 3, aerosols which are carried to the stratosphere have much greater residence times. There may be storage regions over the poles or within the "Junge layer." The existence of aerosol concentrations within the stratosphere, whether natural or anthropogenic, is probably more potentially significant with respect to global climatic change than aerosols in the lower atmosphere.

Aerosol measurements in the stratosphere are scarce and it is hoped that the methods of atmospheric electric measurements used at the surface can be used to detect aerosol levels within the lower stratosphere, either using balloons or high flying aircraft.

REFERENCES

Anderson, R. V., and E. M. Trent, 1962: Atmospheric electricity measurements in the North Atlantic during FALLEX-60. U. S. Naval Research Laboratory, NRL Rept. 5833.

Angenheister, G., 1914: *Nachr. Ges. Wiss., Goettingen, Math.-Phys. Kl.*

Ault, J. P., and S. J. Mauchly, 1925: Atmospheric-electric results obtained aboard the "Carnegie". Washington, D. C., Carnegie Institute Publ. 172, 197–286.

Beebe, R. G., 1967: Changes in visibility restrictions over a 20 year period. *Bull. Amer. Meteor. Soc.*, 48, 348.

Cobb, W. E., 1968a: Ion losses in the Gerdian condenser intake system. *J. Appl. Meteor.*, **7**, 456–458.

——, 1968b: The atmospheric electric climate at Mauna Loa Observatory, Hawaii. *J. Atmos. Sci.*, **25**, 470–480.

——, and B. B. Phillips, 1962: Atmospheric electric measurement results at Mauna Loa Observatory. Tech. Paper No. 46, Weather Bureau, U. S. Department of Commerce, 252 pp.

——, and H. J. Wells, 1970: The electrical conductivity of oceanic air and its correlation to global atmospheric pollution. *J. Atmos. Sci.*, **27**, 814–819.

Ellis, H. T., and R. F. Pueschel, 1971: Solar radiation: Absence of air pollution trends at Mauna Loa. *Science*, **172**, 845–846.

Gunn, R., 1964: The secular increase of the world-wide fine particle pollution. *J. Atmos. Sci.*, **21**, 168–181.

Freeman, M. H., 1968: Visibility statistics for London-Heathrow airport. *Meteor. Mag.*, **97**, 214.

Hidy, G. M., and J. R. Brock, 1970: An assessment of the global sources of tropospheric aerosols. Paper presented at the Second International Clean Air Congress, Washington, D. C.

Holzworth, G. C., 1962: Some effects of air pollution on visibility in and near cities. *Symposium: Air over cities*, Public Health Service, SEC Tech. Rept. A62-5, Taft Sanitary Engineering Center, Cincinnati, Ohio.

Keith, R. W., 1970: Downtown Los Angeles noon visibility trends. Air Quality Rept. 65, Los Angeles Air Pollution Control District.

Libby, W. F., and C. E. Palmer, 1960: Stratospheric mixing from radioactive fallout. *J. Geophys. Res.*, **65**, 3305–3317.

Lovelock, J. E., 1971: Air pollution and climatic change. *Atmos. Environ.*, **5**, 403–411.

Ludwig, J. H., G. B. Morgan and T. B. McMullen, 1970: Trends in urban air quality. *Trans. Amer. Geophys. Union*, **51**, 468–475.

Machta, L., 1972: Mauna Loa and global trends in air quality. *Bull. Amer. Meteor. Soc.*, **53**, 402–420.

McNulty, R. P., 1968: The effects of air pollutants on visibility in fog and haze at New York City. *Atmos. Environ.*, **2**, 625.

Misaki, M., and T. Takeuti, 1970: The extension of air pollution from land over the ocean revealed in the variation of atmospheric electrical conductivity. *J. Meteor. Soc. Japan*, **48**, 263–270.

Morita, Y., 1971: The diurnal and latitudinal variation of electric field and electric conductivity in the atmosphere over the Pacific Ocean. *J. Meteor. Soc. Japan*, 49, 56–58.

Prospero, J. M., and T. N. Carlson, 1972: Vertical and areal distribution of Saharan dust over the western equatorial North Atlantic Ocean. *J. Geophys. Res.*, **77**, 5255–5265.

Robinson, E., and R. C. Robbins, 1970: Gaseous sulphur pollutants from urban and natural sources. *J. Air Pollut. Control Assoc.*, **20**, 233–235.

——, and ——, 1970: Gaseous nitrogen compound pollutants from urban and natural sources. *J. Air Pollut. Control Assoc.*, **20**, 303–306.

Selezneva, E. S., 1966: *Atmospheric Aerosols.* Leningrad, Gidometeorologicheskoi Izdatel'stvo, (Translated by the Indian National Scientific Documentation Centre, New Delhi, 1970).

Spirtas, R., and H. J. Levin, 1971: Patterns and trends in levels of suspended particulate matter. *J. Air Pollut. Control Assoc.*, **21**, 329–333.

Squires, P., 1966: An estimate of the anthropogenic production of cloud nuclei. *J. Rech. Atmos.*, **2**, 297–308.

Torreson, D. W., W. D. Parkinson, O. H. Gish and G. R. Wait, 1946: Scientific results of Cruise VII of the "Carnegie", Ocean atmospheric-electric results. Publ. No. 568, Carnegie Inst., Washington, D. C. 1–176.

Wait, G. R., 1946: Some experiments relating to the electrical conductivity of the lower atmosphere. *J. Wash. Acad. Sci.*, **36**, 321–343.

Weickmann, H. K., 1971: Inadvertent weather modification. *Proc. Thirteenth Interagency Conference on Weather Modification*, National Oceanic and Atmospheric Administration, U. S. Department of Commerce.

Reprinted with permission of the Journal of Atmospheric Sciences,
Vol. 30, No. 7, October 1973.

Reply

William E. Cobb
Atmospheric Physics and Chemistry Laboratory, NOAA, Boulder, Colo. 80302

21 May 1973

I agree that measurements which help to describe the concentration, distribution and chronology of our planet's suspended particulate burden are vitally important. Drs. Hogan, Mohnen and Schaefer deserve much credit for their work described above. Their important measurements of cloud condensation (Aitken) nuclei, on a global scale, will do much toward filling a gap in this type of aerosol research which has existed, with a few exceptions, since the tragic end of the sailing vessel *Carnegie*.

Without disparaging the importance of Aitken nuclei measurements, I would like to take this opportunity to emphasize the advantages of using the electrical conductivity for detecting secular changes in global aerosol levels.

1. The conductivity—An absolute measurement procedure since 1905

The sensor devised by Gerdien (1905) provides a nearly absolute method for measuring the conductivity. Credit should also go to Swann (1914) who confirmed Gerdien's work by showing that Gauss' law for the loss of charge from an isolated and electrified spherical conductor in an ionized gas, also applied to conductors of other shapes such as the rod used as the central electrode in the Gerdien cylindrical condensor. The conductivity may be derived from Ohm's and Gauss' laws and expressed quite simply in mks units as

$$\lambda=\epsilon_0\frac{V_e}{CVR}, \tag{1}$$

where λ is the unipolar conductivity ($\Omega^{-1}\ \mathrm{m}^{-1}$), ϵ_0 the space permittivity constant, C the capacitance of the cylindrical condensor, V the potential between the outer cylinder and the central electrode, R the leakage resistance across the condensor (usually a precision resistor of about $10^{11}\ \Omega$), and V_e the voltage resulting from the collected ionic current flowing through R as air is drawn through the cylindrical condensor.

It is readily seen that the positive or negative conductivity may be measured by reversing the polarity of the collecting voltage V. Note also, that for any given system, it is only necessary to measure V_e since C, V and R all become constant. Such errors as exist in (1) are due to determining the value of C which might be off by no more than $\pm10\%$.

2. Sensitivity of the conductivity to both size and number of suspended particulates

Hogan *et al.* have pointed out that the conductivity sensor, unlike the Aitken counter, is sensitive to both the size and number of particulates in the sampled air. It is this dual sensitivity which helps make the conductivity a useful tool in aerosol research, since aerosol pollution might well be defined as being the total volume which particulates occupy in a given space. It is almost exclusively the presence of small ions which makes the air slightly conducting. The small ion concentration and thus the conductivity are largely controlled by the total relatively immobile surface area which particulates provide for the impaction of small ions. As a result, a few larger sized Aitken nuclei can have the same effect on the conductivity as a greater number of smaller nuclei. For reasons not entirely clear, the sensitivity of the conductivity to both size and number of particulates appears to provide a limiting mechanism which reduces the variability of the conductivity measurement as compared to direct nuclei counts. An example of this is given by Ruhnke (1962) who measured both Aitken nuclei and conductivity along a Greenland Ice Cap trek which intercepted a plume of contaminated air from a human settlement. The expected inverse correlation is apparent but the relative increase in nuclei in the polluted air is about three times the corresponding dip in the conductivity.

3. Atmospheric sampling problems

A problem common to all atmospheric devices is that we may disturb, and usually do, the natural existence of elements we wish to investigate. Ocean vessel measurements are particularly difficult because of diesel exhaust, spray from waves striking the ship's hull, even the exhaled human breath which may contain a significant number of nuclei; all are factors which may create an environment not representative of the free atmosphere. In such circumstances, the continuously monitored conductivity is more desirable than manual checks of the Aitken nuclei density since abnormal conditions caused by the ship are easily identified on the recorded conductivity records. The same will be true, of course, for the recording nuclei counters now available.

Misaki *et al.* (1972) recently checked shipboard contamination by mounting identical Gerdien conductivity systems on opposite sides of the research vessel *Ryofu-Maru*. They found that both conductivity systems read the same only when the relative wind direction was 0° with respect to the bow of the ship. As the wind angle changed with respect to the bow, the conductivity value measured at the side furthest downwind was decreased by contamination from the ship—as much as 35% for a 90° crosswind.

It has been my observation that ship-caused pollution can be identified on the recorded conductivity records. Not only do the traces become erratic, but the ratio of the bi-polar conductivities changes as the more mobile negative ions attach themselves to particulates faster than do the positive ions. I would be interested to know in what manner Hogan *et al.* accounted for the possibility of sampling ship-contaminated air with their Aitken counters.

4. Correlation between aerosols, conductivity and meteorological parameters

In their conclusion, Hogan *et al.* imply that the *Oceanographer* conductivity measurements provide no insight into the relationship between aerosols and other meteorological phenomena. They are, of course, correct. Such correlations involving aerosol sources, atmospheric residence times, gas-to-particle conversions, and associated weather phenomena are very complex and require much more information than conductivity, Aitken nuclei and ships weather log observations can supply.

Atmospheric conductivity is, in fact, largely controlled by aerosol conditions and other meteorological phenomena. Such correlations have been studied in detail by Cobb (1968), Dolezalek (1963), and others, particularly scientists of the Carnegie Institution. For the purpose of establishing benchmark observations of the conductivity, these correlations are intentionally avoided by using "clean air" sites such as ships, mountain tops and polar regions, and by using observations obtained only during "fair weather." The 1967 *Oceanographer* data (Cobb and Wells, 1970), for example, were compiled from 24-hr periods or more of continuous fair weather. Days with rain, fog, high winds, etc., were considered typical of the local environment while it was desired to have the conductivity air sample as representative of as large an area as possible. Thus, 75 days of fair-weather data were obtained which were considered typical of fairly large geographical regions. In addition, the ship made frequent mid-ocean "on-station" studies which lasted from 2 to 5 days.

5. Conclusion

The detection of secular changes in globally suspended particulates is admittedly a difficult problem and I may, as Hogan *et al.* have implied, have overemphasized the value of conductivity measurements in drawing conclusions concerning anthropogenic aerosols (Cobb, 1973). I consider the conductivity measurement, however, as possibly the best tool presently available to do the job. Hogan *et al.* admit to a ±30% accuracy in the absolute value of nuclei measurements using portable photoelectric counters. Obviously it becomes difficult, then, to look for secular changes which might amount to a few percent in a decade.

Particle counting is a rapidly improving science, as witnessed by the progress shown at the Second International Workshop on Condensation and Ice Nuclei at Ft. Collins, Colo. As stated earlier, I believe the oceanic measurements of Hogan *et al.* are very important and should be continued. Hopefully they will be able to install a few of the newer, continuously recording Aitken counters or conductivity sensors. An added advantage of measuring both particle density and conductivity is that one may then determine the particle radii (Ruhnke, 1962).

REFERENCES

Cobb, W. E., 1968: The atmospheric electric climate at Mauna Loa Observation, Hawaii. *J. Atmos. Sci.*, **25**, 470–480.

——, 1973: Oceanic aerosol levels deduced from measurements of the electrical conductivity of the atmosphere. *J. Atmos. Sci.*, **30**, 101–106.

——, and H. J. Wells, 1970: The electrical conductivity of oceanic air and its correlation to global atmospheric pollution. *J. Atmos. Sci.*, **27**, 814–819.

Dolezalek, H., 1963: The atmospheric electric fog effect. *Rev. Geophys.*, **1**, 231–282.

Gerdien, H., 1905: Demonstration eines Apparates zur absolution Messung der electrischen Leitfahigkeit der Luft. *Phys. Z.*, **6**, 800–801.

Misaki, M., M. Ikegami and J. Kanazawa, 1972: Atmospheric electrical conductivity measurement in the Pacific Ocean, exploring the background level of global pollution. *J. Meteor. Soc. Japan*, **50**, 497–500.

Swann, W. F. G., 1914: The theory of electrical dispersion into the free atmosphere, with a discussion of the Gerdien conductivity apparatus. *Terr. Magn. Atmos. Elec.*, **19**, pp. 88, 219, 242.

Ruhnke, L. H., 1962: Electrical conductivity of air on the Greenland Ice Cap. *J. Geophys. Res.*, **67**, 2767–2772.

Reprinted with permission of the World Meteorological Organization,

1973.

WORLD METEOROLOGICAL ORGANIZATION

TECHNICAL NOTE No. 128

THE INTERNATIONAL RADIOMETERSONDE INTERCOMPARISON PROGRAMME (1970-1971)

by

J. C. Gille and P. M. Kuhn

IMO-WMO
CENTENARY

WMO - No. 358

Secretariat of the World Meteorological Organization - Geneva - Switzerland
1973

PREFACE

The flux of radiation at the upper and lower boundaries of the atmosphere and the divergence of this flux within the atmosphere represent major energy sources and sinks for atmospheric motions on different time and space scales. Radiation flux measurements and calculations, therefore, could contribute essential information for carrying out the over all scientific objectives of the Global Atmospheric Research Programme (GARP). This was recognized and clearly stated in the GARP Study Conference Report, Stockholm, 1967; further discussed in GARP Publication Series No. 5, Problems of Atmospheric Radiation in GARP; and again in the report on the fifth session of the Joint Organizing Committee, Bombay, 1-5 February, 1971.

Because of the difficulties attending solar radiation observations, most of the past efforts have been concentrated on measurement of the flux of thermal radiation in the atmosphere at wavelengths beyond 4 µm. As a result, several balloon-borne instruments have been developed by scientists in different countries to measure the upward radiation flux in the earth's atmosphere. In order to standardize these instruments in measurement of the radiation field in the atmosphere, and to assist in their improvement, the Radiation Commission of IAMAP, through its Working Group on Radiometersonde Intercomparison, conducted two series of intercomparisons (one in 1963 and one in 1965) of several of the leading types of such instruments. These intercomparisons were supported by WMO and IAMAP funds. On the basis of the field results, steps were taken after each series to modify and improve each of the radiometersonde systems.

In continuance of this over all programme, the Radiation Commission, at its meeting in Bergen, Norway, in August, 1968, endorsed the recommendation of its working group "...that another intercomparison be conducted over a large homogeneous surface, as for example, the sea (with balloon launchings preferably from on board a ship)...." It was also recommended that a theoretical researcher, active in the field of radiative transfer, be added to the working group. The purpose of the latter recommendation was to co-ordinate the observational results with theoretical flux calculations based on vertical temperature and humidity soundings taken simultaneously with the radiometersonde observation, as had been suggested in the GARP, Stockholm, 1967, report. This would provide, in addition to a check on the consistency among the various instruments, comparison between theoretical calculations and observations. Standardization of radiometersondes and the development of a "correct" and "sensitive" radiation model are essential for GARP and many of its sub-programmes (e.g., GATE, etc.). This third radiometersonde intercomparison was supported by ICSU/WMO through the GARP implementation fund and was originally planned to take place in the fall, 1969, over the eastern part of the tropical Pacific.

The intercomparisons were eventually carried out in two phases. Phase I was conducted aboard the NOAA oceanographic research vessel, DISCOVERER, operating from Miami, Florida, through the Gulf of Mexico, Panama Canal, into the Pacific to 8°S latitude and return to Miami. Twenty successful combined flights were conducted between 3 and 21 May, 1970, under a variety of atmospheric conditions. These ascents involved radiometersondes from Japan, Germany (F.R.G.) and the U.S.A.

A discussion of the results took place in Tokyo, Japan, from 24 to 27 March, 1971. At that time Phase II intercomparisons were conducted at Tateno, Japan, with three co-ordinated flights of radiometersondes from Japan, the U.S.A. and the U.S.S.R., thus allowing for an intercomparison of four radiometersonde systems.

This technical report, prepared by Dr. J.C. Gille and Dr. P.M. Kuhn, discusses the results of the complete programme (Phase I and Phase II) including comparison between observed and theoretically calculated results. The main conclusions and recommendations for improvement and standardization of radiometersondes for use in GARP and an assessment of the present differences between instrumental observations and theoretical calculations of radiative flux divergence in the free atmosphere are included at the end of the report in chapters 6 and 7. Description of the different radiometersondes used by the co-operating groups and details of the theoretical calculations are given as Appendices.

The following scientists constituted the Working Group on Radiometersonde Intercomparison, Radiation Commission (IAMAP) and contributed actively to the operation of the programme and to the recommendations at the end of this report.

Dr. Peter M. Kuhn (U.S.A.) Chairman
Dr. H.G. Müller (F.R.G.)
Mr. H. Fimpel (F.R.G.)
Dr. J.C. Gille (U.S.A.)
Dr. M. Shimizu (Japan)
Mr. A. Yata (Japan)
Dr. Y. Sekiguchi (Japan)
Dr. V.I. Schlyakov (U.S.S.R.)
Dr. A. Ph. Kuzenkov (U.S.S.R.)

The Radiation Commission would like to thank NOAA (U.S.A.) and the Japan Meteorological Agency for making their facilities available for the intercomparisons and Dr. M. Yoshitake, former Director of the JMA, for his hospitality. In addition, the assistance of Col. William Barney, NOAA Headquarters, Sgt. J. Blankenship, USAF, M. Pointdexter, NOAA, Lois Stearns, NOAA, the technical staff at the Tateno Aerological Observatory, R. G. Ellingson and P. Bailey, Florida State University and Rose Lee Dacey, University of Colorado, is very gratefully acknowledged.

Julius London
President
Radiation Commission (IAMAP)

CONTENTS

Page

Foreword V

Preface (English, French, Russian, Spanish) VII

Part I: Description of the Intercomparison Program 3
Peter M. Kuhn

1. Phase I Intercomparison Flights 3

2. Phase II Intercomparison Flights 7

Part II: Analysis of Intercomparison Program Results 9
John C. Gille

3. Analysis of the Phase I Intercomparison Measurements 9

4. Analysis of the Phase II Intercomparison Measurements 27

5. Comparison Between Observed and Calculated Fluxes and Heating Rates 37

6. Summary and Conclusions 44

Part III: Recommendations of the IAMAP Working Group on Radiometersonde Intercomparisons 52

References 54

Appendix A. Instrument Descriptions 55

Appendix B. A Brief Description of the Computational Scheme 87

Appendix C. Statistical Results for the 1970-71 Intercomparison Flights 89

Appendix D. Radiometric and Meteorological Data for Individual Intercomparison Flights 106

References for Appendices 126

Reprinted from NOAA Technical Report ERL 269-APCL 28,
124 pages, April 1973.

MINIMAX - A FORTRAN COMPUTER PROGRAM TO ASSEMBLE THE MACHINE CODE FOR THE INTERDATA MODEL 70 MINICOMPUTER ON THE CONTROL-DATA 3800

H. H. Grote

In the course of the development of the Divergence Display System (Grote Plotter) an assembler was needed. There was not enough memory in the present minicomputer system to accomodate the Interdata provided software. With only a teletypewriter available the edit and assembly process would have been quite time consuming. Having a Control Data 3800 facility available with many time saving peripherals it appeared profitable to have a cross assembler. A program was written that inputs from cards and outputs the compiled program on the printer. Having the source program on cards provided the additional convenience of easy program changes and listings. Originally written for the Interdata Model 3, it was later expended for the Model 70

Reprinted with permission of the American Meteorological Society,
Vol. 54, No. 11, November 1973.

types of snowfall

J. E. Jiusto
Atmospheric Sciences Research Center
State University of New York
Albany, N.Y. 12222
and H. K. Weickmann
Atmospheric Physics and Chemistry Laboratory
NOAA
Boulder, Colo. 80302

Abstract

Few would question such doggerel as "no two snow crystals are alike and in infinite variety they fall." Conversely, many might challenge the statement that individual crystals are relatively scarce by comparison with snowflake aggregates, rimed crystals, and irregular forms; but they are. The types of snow occurring in a storm are a function of many variables including updraft strength, temperature, cloud moisture, liquid water content, cloud thickness, and ice nuclei and crystal concentrations. Some of the relationships are obvious, others more obscure, still others unknown. This paper describes ground observations and calculations that attempt to clarify certain snowfall forms in terms of the cloud conditions likely to produce them.

1. Introduction

Regarding the habit of snow crystals occurring in nature, we are accustomed to thinking in terms of symmetric, individual hexagonal forms of planar or prismatic type. These are certainly the basic initial crystallographic forms, as the excellent photographs of Bentley (in Bentley and Humphrey, 1931) and extensive work of Nakaya (1954) show. It is well known that such crystals grow by deposition of water vapor in an ice saturated environment, with a uniform vapor density gradient surrounding each crystal. However, if one expects to commonly observe such perfect crystals in snowstorms, he is quite apt to be disillusioned. Bentley (1902) noted (though the comment is rarely quoted, if remembered) that the symmetric crystals he concentrated on photographing fell mainly from certain (more passive) quadrants and edges of storm systems.

A better known fact is that snow crystals often continue to grow, depending on cloud conditions, by the accretion of supercooled cloud droplets (riming) or by the collection of other crystals (aggregation or snowflaking). Houghton (1950) and Hosler and Hallgren (1961) have inferred that collisional growth can be appreciable. Also, the degree of crystal fragmentation by collisions or other mechanisms is probably underestimated because of the tendency to ignore irregular or amorphous crystal forms.

Over several years, we have observed snowfall type in many locales in mesoscale Great Lakes snowstorms (western New York), synoptic-scale east coast storms, and in Rocky Mountain, European, and Arctic snowfalls. Aided by such observations and hydrometeor growth considerations, it is the intent of this paper to try and put the various growth mechanisms and their related cloud criteria into better perspective.

2. Snow cloud systems

Subsequently we will forget the beauty and dream world of the delicate snowstars and stellar dendrites and ask about the habits of those "workhorse" snow crystals that are responsible for precipitating the moisture which is stored or released in a cloud. Before doing so, we need to define the precipitation systems being dealt with. As the discussion will center on snow crystals, we will generally ignore large graupel, soft hail, and hail, i.e., those solid hydrometeors which precipitate from summer convective cumulus-type clouds. We will, consequently, emphasize winter cumuli and those stratiform cloud systems which fall within Bergeron's (1950) classical definition as consisting of a "releaser" cloud and a "spender" cloud, or—expressed by different synonyms—of a "seeder" cloud and a "feeder" cloud.

Bergeron postulates with these definitions that any stratiform storm system which precipitates effectively requires the production of crystals capable of scavenging the precipitable water that is stored in the lower part of the cloud system. In a normal cyclonic system, the former is the altostratus or cirrostratus cloud, while the latter is the low-level stratus and nimbostratus cloud. The high level cirrostratus or altostratus typically is caused by an upper level trough or by a warm front, while the low-level stratus or nimbostratus results from the storm's low-level vorticity or baroclinicity. Consequently, the cirrostratus or altostratus is the "releaser" cloud, while the low-level stratus or nimbostratus is the "spender" cloud due to its higher liquid water content. We will soon see that these cloud types can occur singly or in combination, with differing precipitation consequences. The Bergeron cloud system concept is supported by the results obtained from radar studies at McGill University (Marshall, 1953; Gunn *et al.*, 1954); namely, that a layer of generating cloud elements at the top of the cloud system is necessary for the formation of precipitation particles.

The elevated convective generating elements provide for water saturation and low temperature, which are necessary for condensation-freezing mechanisms to cause ample ice formation. Down to temperatures of −25C, the generating elements may still consist of water droplets which may subsequently crystallize. Consequently, the generating cloud elements provide three efficient nucleation conditions to provide ice crystals.

> 1) Ice nuclei which are sufficiently large to act as condensation nuclei may produce ice crystals by means of condensation-crystallization mechanism, 2) ice nuclei which are too small for this mechanism (or too hydroprobic) but large enough to nucleate the liquid phase may do so by phoretic or Brownian deposition as contact nuclei, and 3) ice nuclei which are already embedded within a drop but have not yet reached their activation threshold may do so on ascending into colder strata.

Amplifying on the above, it is possible to distinguish three different cloud systems:

> 1) the high-level releaser cloud (altostratus or, in some cases, cirrostratus) alone whose particles nevertheless arrive at the surface,
> 2) the combination of a releaser and spender cloud (a high level altostratus and a lower level stratus), as Bergeron postulated, and,
> 3) a relatively shallow spender cloud (convective stratocumulus to cumulus) alone whose precipitation potential is not always released naturally.

The occurrence of the first cloud system permits us to observe the number concentration of snow crystals which nature produces to effectively scavenge the precipitable water of system #2, or of a deep cyclonic system. The crystals of system #2 often have gone through too many stages of growth by diffusion, riming and aggregation for individual crystals to still be recognized and counted, and the crystals of system #3 are usually subject to the same metamorphosis or are determined only from a small (to non-existent) number when temperatures are comparatively high. In Section 3 we shall refer to these three cloud systems, where possible, in describing corresponding crystal habit and concentrations. The variety of cloud types found prior to or during Great Lakes snowstorms often lends itself to this type of categorization.

a. Great Lakes snowstorm systems

Lake-effect snowstorms that occur to the lee of Lake Erie have been studied in some detail (e.g., McVehil *et al.*, 1967; Weickmann *et al.*, 1970a; Jiusto and Holroyd, 1970; Lavoie *et al.*, 1970; Eadie *et al.*, 1971). Because of their mesoscale band dimensions, transition from lake to land influence, and distinct seasonal changes in cloud microphysics properties, they offer a means of examining the relationship between differing cloud properties and resultant snowfall types. Also they provide a variety of temperature, updraft, and mixed-phase cloud combinations that probably at one time or another are similar to snow clouds in a number of other geographic locales.

Early in the winter season (November and December) when the lake is relatively warm, the vertical fluxes of momentum, heat, and water vapor are pronounced and the frequency of mesoscale secondary troughs in arctic air outbreaks relatively high. The coupling of these events (Peace and Sykes, 1966; Paine, 1971) can lead to intense storm bands. The associated convective clouds that develop over water are characterized by large water-to-ice ratios (i.e., clouds at water saturation); overall average updrafts of the order of 0.5–1.0 m sec^{-1} (3–6 sec^{-1} in vigorous cloud cores—McVehil *et al.*, 1968); and owing to the cold ambient temperatures, small droplets often averaging 10–30 μm diameter. Ice nucleus concentrations typically measure less than 1 l^{-1} at −20C.

3. Snow crystal types and concentrations

a. Releaser and spender clouds

Typical crystals of system #1 (releaser cloud only) are shown in Fig. 1a obtained from cirrus clouds (T = −37C), and in Fig. 1b as sampled at the ground. Their prism habit is in agreement with the Magono-Lee (1966) ice crystal diagram (Fig. 2). With the spender cloud missing, the crystals have little tendency to rime or form flakes and their concentration can be calculated quite accurately by counting the number that fall in, say, 10 seconds on one cm^2 of a black velvet surface (and estimating their fall velocity). A small hand-held microscope helps to determine their habit and link them with the correct cloud system. We found that their concentration ranges quite consistently within the limits of 5 to 40 l^{-1}. Since they fall at nearly 1 m sec^{-1}, approximately 5,000 to 40,000 crystals per second enter each m^2

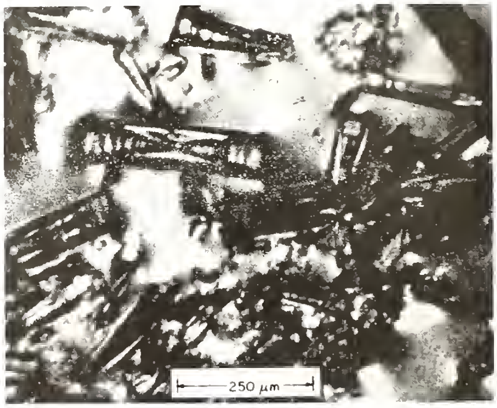

Fig. 1a. Ice crystals in form of prism bundles formed in cirrus cloud at 7500 m and —37C.

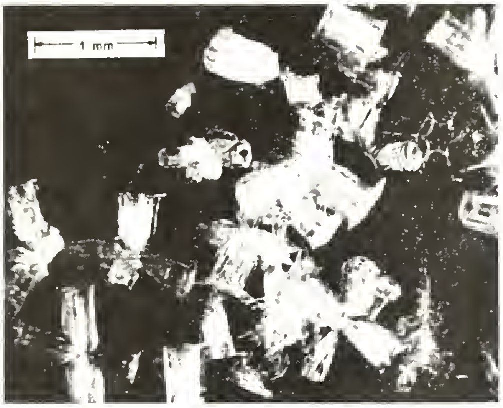

FIG. 1b. Snow crystals in form of prism bundles observed at the surface at a surface temperature of −13.9C.

area. It is interesting to note that the concentration of raindrops which arrive at the surface is about 1,000 m^{-2} sec^{-1}, or roughly an order of magnitude less.

We believe that this is the first time that a realistic concentration of nature's supply of snow crystals from the seeder cloud has been determined, and three conclusions come immediately to mind: 1) in deep cyclonic systems, nature supplies rather too much than too few crystals, 2) crystal aggregation and flake formation prior to melting must be an important process in the determination of certain raindrop spectra, and 3) in precipitating warm clouds the raindrop collision rate is generally considerably greater than accretion and aggregation rates of ice crystals in mixed phase clouds. (Note that cloud droplet concentrations are some three to four orders of magnitude greater than ice crystal concentrations; and the number of respective collisions for a large raindrop and snowflake similarly different.)

The significance of aggregation, however, is as yet still insufficiently explored. In clouds above the freezing level it leads to slowly falling, rotating and tumbling large flakes which efficiently scavenge the cloud droplets; below the freezing level they melt to a few large and fast falling raindrops which are less efficient in raining-out an existing water cloud than a greater number of smaller melt drops (seeding induced) would be (Weickmann, 1957a). We believe, therefore, that conditions for artificial rain augmentation from stratified precipitation systems via the Bergeron-Findeisen process by ice nuclei seeding are most favorable when the spender cloud reaches below the freezing level, so that the increased particle concentration may come to bear. Also, rain makers might well consider that these numbers are an order of magnitude greater than the conventionally assumed one crystal per liter for stimulating precipitation.

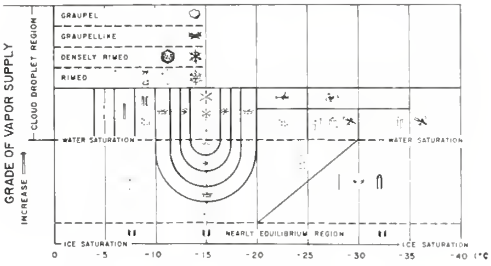

FIG. 2. Temperature and humidity conditions for the growth of natural snow crystals of various types (Magono and Lee, 1968).

Another system #1 example occurred in Buffalo, New York, on 13 February 1971. It was a synoptic scale precipitation system whose center moved northeastward and was located east of the Great Lakes region. Warm air overriding cold air on the back side of the larger depression caused the formation of a deep altostratus layer which continuously discharged very fine snow crystals. A typical radiosonde cross section is shown in Fig. 3. (Using Nakaya's classification, the dominant crystal types observed are shown schematically in Fig. 3 and subsequent figures.) The overriding warm air is clearly shown from the inversion (temperature increase at 900 mb). In the shallow layer below the inversion, clouds could form but no ice crystals as the temperature was not sufficiently cold. Lake Erie, being frozen at that time, did not introduce significant low-level convection. Yet from the homogeneously overcast sky, fine snow fell whose crystals had the depicted shapes typical of low-temperature cirrus and altostratus (Fig. 1a and b). The ice character of the cloud above 600 mb follows from the dewpoint trace which represents ice saturation for the indicated environmental temperatures.

Small flakes of tiny rimed prism bundles (similar to

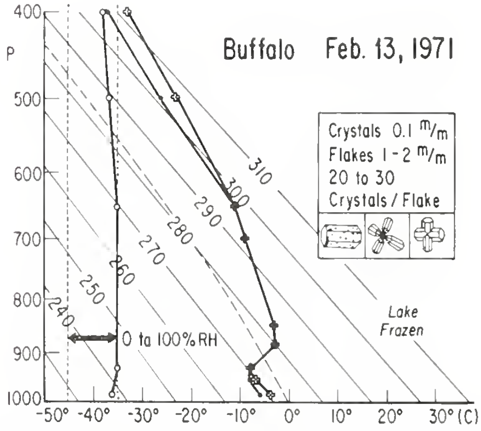

FIG. 3. Radiosonde data (temperature, dewpoint, relative humidity) 13 February 1971, a.m., Buffalo, N.Y., during snowfall from releaser cloud (altostratus) only.

those in Fig. 1b) fell. Individual crystal sizes were about 0.1 mm in diameter making up flakes 1 to 2 mm, with 20 to 30 crystals per flake. Note from Fig. 3 that the occurrence of a thin stratocumulus layer at the inversion is possible, which undoubtedly accounted for the riming and aggregation of the descending high level crystals.

The total snow accumulation in 24 hours in the Buffalo area was light and not more than 2 to 3 inches; in Bergeron's terminology, the snowfall was characterized by the existence of a "releaser cloud" but the quasi-absence of a substantial low-level "spender cloud." Toward the center of the storm, where the latter was present, 12 inches of snow and more accumulated.

This same type system can occur over a great temperature interval. Fig. 4 shows a temperature-humidity profile which occurred during an intensive snowfall over the Denver, Colo., area. The high humidity extended up to the −25C level, which must have been the top of the cloud deck, and probably of the generating cloud elements. Crystals were observed near Boulder, Colo., with a great variety of forms: from small, about 0.1 mm diameter graupel to small unrimed plate assemblies[1] (spatial plate crystals), about 0.1 to 0.2 mm diameter; to large sector dendrites, rimed and unrimed, partly in flakes, partly single. The main forms were spatial plate assemblies, single and aggregated, with 3–5 per flake very similar to the laboratory crystals shown in Fig. 5.

It is noteworthy that on this day we estimated a crystal concentration of 1–2 l^{-1}, or near the lower end of the concentration mentioned above. This may be due to the warmer temperature at which the crystals had formed. The habits as described above persisted throughout the entire day in varying ratios: during periods of heavier snowfall rates, the spatial plate assemblies turned into spatial dendrites, rimed and unrimed, thus displaying nature's great flexibility of adjusting crystal forms to the rate of condensation. (This system was actually bordering on the type 2 classification.)

An example of system #2 (combined releaser and spender clouds) occurred to the lee of Lake Erie on 12 November 1968. The synoptic situation of this system was very similar to the one of 13–14 February 1971 over the Great Lakes region. Again northerly winds prevailed, but we were located closer to the center of the depression. The lakes were warm (Lake Erie temperature of 11C) which increased the tendency for the formation of low level convective clouds. Along the south shore of Lake Erie over a 20-mile stretch adjacent to Buffalo, N.Y., moderate snowfall restricted visibility to less than 1 km. The snow at 1500 EST consisted of several forms: mainly graupel, spatial dendrites, prism bundles with side plates completely and partially rimed.

These forms are consistent with the temperature and humidity profile of this day as noted in the insert of Fig. 6. The warm lake temperature explains the formation of low convective clouds with some graupel formations. The morning radiosonde (Fig. 6) indicated the existence of a deep moist layer which was ice saturated in its upper parts, causing the formation of prismatic crystals; the evening radiosonde showed drying out from

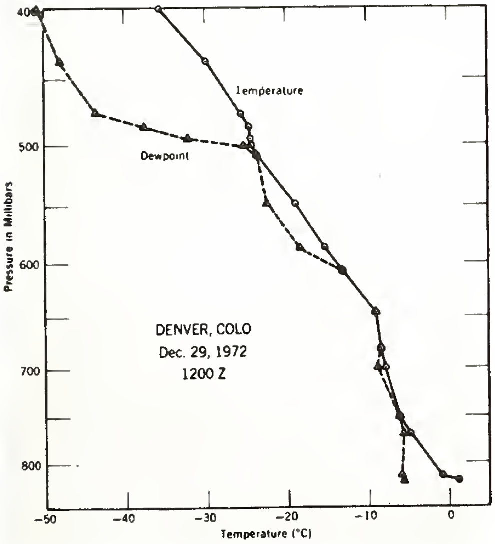

FIG. 4. Radiosonde data (temperature and dewpoint) for Denver, Colo., 29 December 1972, a.m., during intensive snowfall.

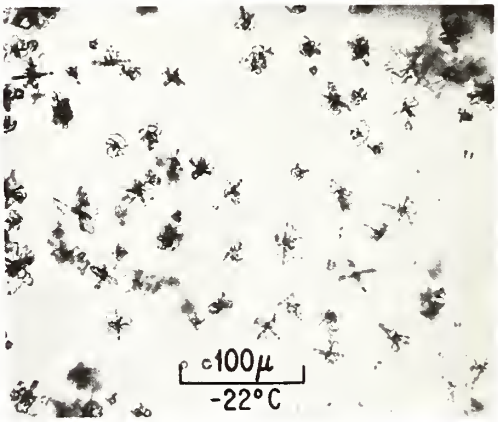

FIG. 5. Spatial dendrite embryos grown in water cloud at −22C in cold chamber after seeding with AgI (aufm Kampe *et al.*, 1951).

---

[1] The term "assembly" is used to typify a single crystal which has grown as an irregular spatial assembly of prisms (also called bundles of bullets), of plates, and branches; in contrast to "snowflake" or "aggregate" which denotes a cluster of individual crystals that have collided with and become attached to one another.

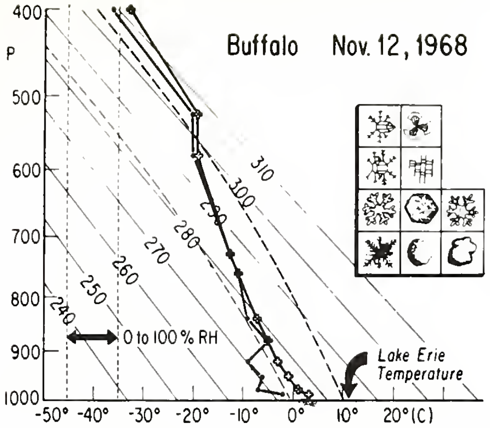

FIG. 6. Radiosonde data (temperature, dewpoint, relative humidity) for Buffalo, N.Y., 12 November 1968, a.m., during snowfall from deep stratiform cloud system.

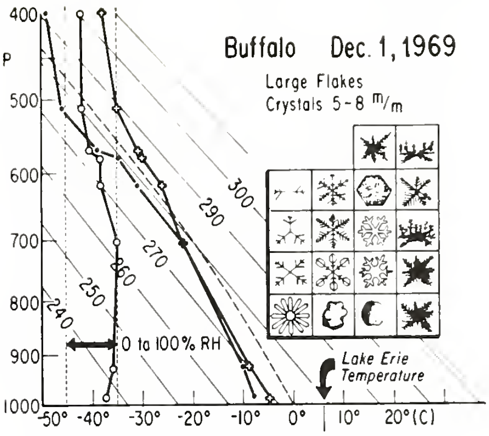

FIG. 7. Radiosonde data (temperature, dewpoint, relative humidity) 1 December 1969. Buffalo, N.Y., a.m., during precipitation from spender cloud (convection stratocumulus).

above, but still saturation up to −20C which accounted for the formation of spatial dendrites. With the presence of a lower spender cloud, the precipitation efficiency was increased compared with the case of system #1, as is evident from the low visibility and presence of many rimed crystal forms.

Crystal concentrations that we measured at the ground in these type 2 systems varied from a few per liter to 50 l^{-1} (approximately 3000–50,000 m^{-2} sec^{-1}). In deeper cyclonic systems of the northeast, maximum concentration values twice as great frequently have been obtained. Gunn (1967) reported that the typical flux of crystals in six Montreal snowstorms was about 10,000 m^{-2} sec^{-1} with a range of 2000–100,000 m^{-2} sec^{-1}—very comparable numbers.

A moderate lake storm which formed over Lake Ontario on 1 December 1969 serves to illustrate system #3 (spender cloud only). The airflow was from the northwest to north and, as the radiosonde plot in Fig. 7 indicates, the lapse rate was nearly moist adiabatic. The lake was still warm (+6C) causing the formation of a convective stratocumulus layer whose tops apparently reached the 700–650 mb level. A survey of the precipitation particles was made from the edge of the band to its center along an east-west direction, driving from downtown Buffalo, where the snowfall began, eastward for about 30 miles. Every 2 to 3 miles, the snow crystals were examined using a hand held microscope. Typical observations were as follows:

> 1705 EST: 36.9 miles from downtown Buffalo. Moderate to heavy snowfall; large rimed dendrites and spatial dendrites in flakes, riming considerable, causing new branches to grow from crystal surfaces. Fall velocity greater than 1 m sec^{-1}.
>
> 1745 EST: 26.4 miles from downtown Buffalo. Heavy snowfall of large flakes (>1 cm) consisting of large dendrites and spatial dendrites, with branches emerging from rimed droplets, all moderately rimed, sizes of individual crystals 5–7 mm diameter. The flakes are loosely aggregated causing a very moderate fall velocity.

The precipitation process that was active in this cloud system is no longer compatible with the Bergeron mechanism of a spender and releaser cloud. Apparently here the higher releaser cloud is missing and the generation of precipitation has to be accomplished by the spender cloud. While the precipitation intensity is always light when the releaser cloud is present and the spender cloud missing, this is not necessarily true when only the spender cloud is available since the rate of condensation in the convective cloud system can be very high. The ice nuclei activation is then proportional to the updraft strength and the coldest temperatures achieved by the developing cloud. This upward flux ends with an inversion where the cloud spreads in a stratocumulus-cumulogenitus attitude thus preventing the loss of ice crystals through evaporation, as often occurs with cumulus clouds. Therefore, as long as the temperature is low enough and convective activity vigorous, heavy precipitation may fall from even shallow systems.

b. Crystal and snowflake types vs. cloud physics variables

The few observations mentioned above could be supplemented by a great number which have been compiled over the past 25 years. They show that irregular snow crystal habits are those commonly furnished by nature. One tends frequently to ignore these irregular forms in seeking out those more amenable to simpler classification or calculation. While the releaser-spender cloud concept is useful in visualizing winter precipitation mechanisms, one often must look to the cloud dynamics and microphysics variables in attempts to explain the specific type of crystals and snowflakes that occur.

1. Rimed crystals

The snow that falls along the shore plain of Lake Erie in early winter consists mainly of heavily rimed crystals, and spherical graupel averaging 2–4 mm. Highly symmetric graupel cones of the same sizes are not uncommon, the 7 mm cone pictured in Fig. 8a being one of the largest observed. (Graupel in excess of 3–5 mm is occasionally accompanied by lightning discharges.) Fig. 8b illustrates a typical sample of graupel pellets and rimed forms virtually devoid of crystalline structure. Standard collection calculations suggest that a single crystal can accrete thousands of supercooled droplets in its evolution to a graupel pellet.

Somewhat further inland, less heavily rimed crystals of the type shown in Fig. 8c–e are often observed. The transition in degree of riming is attributed to gradual depletion of the cloud water content and weaker updrafts over land, both factors allowing the given cloud humidity to reduce and approach ice saturation.

2. Snowflakes

Snowflake aggregates occur with greater frequency as inland distance increases and soon become dominant. Later in the winter season, as air and water temperatures decrease, aggregates prevail even at the shortline. Rimed crystal forms correspondingly decline, which is consistent with the lower liquid content, the generally reduced convective activity, and the exponential ice-

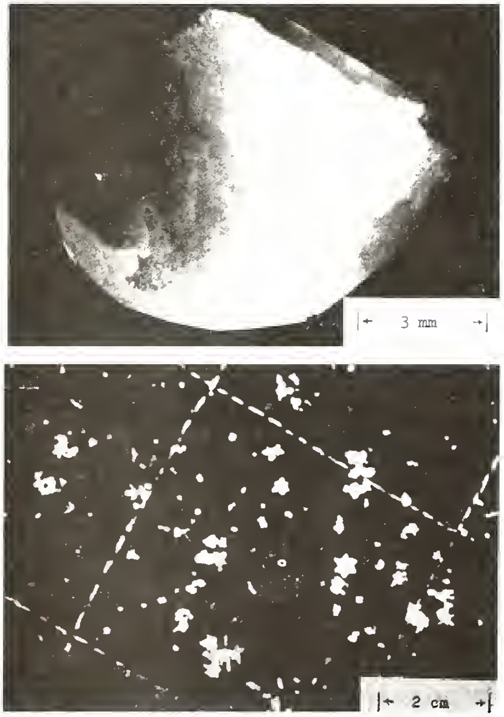

Fig. 8a (top)–b (bottom). Rimed snow crystals.

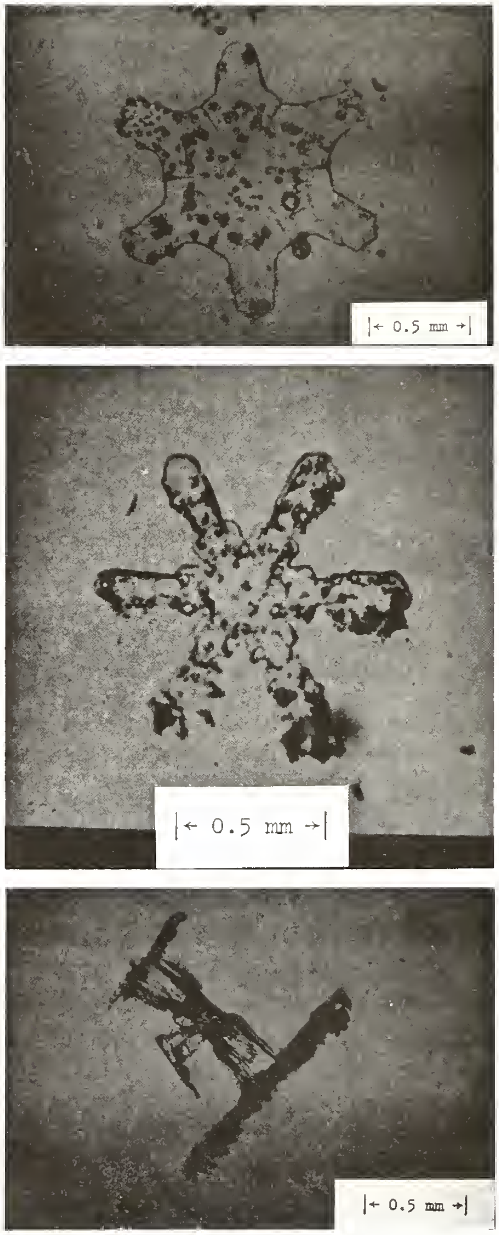

Fig. 8c (top)–e (bottom). Rimed snow crystals.

nucleus concentration increase with falling temperature. In short, colder clouds with weaker updrafts more effectively glaciate, yielding larger concentrations of crystals.

Fig. 9a shows several snowflakes, the largest measuring approximately 2.5 cm. Examining such flakes under higher magnification as in Figs. 9b–c, it is evident that they usually consist of loosely packed dendritic crystals and some thin plates. Data, though not plentiful, support the contention that dendritic crystals favor the aggregation of crystals. Clearly, they should possess a higher aerodynamic collection efficiency than compact crystals (Weickmann, 1957). Additionally, they form at near water-saturated conditions (note Fig. 2) where supercooled droplets are present. If droplets are accreted by the dendrites, then the spectrum of crystal fall velocities and crystal adhesion properties are likely to increase. Both factors are capable of enhancing the collision-collection mechanism as suggested by a standard crystal mass aggregation expression:

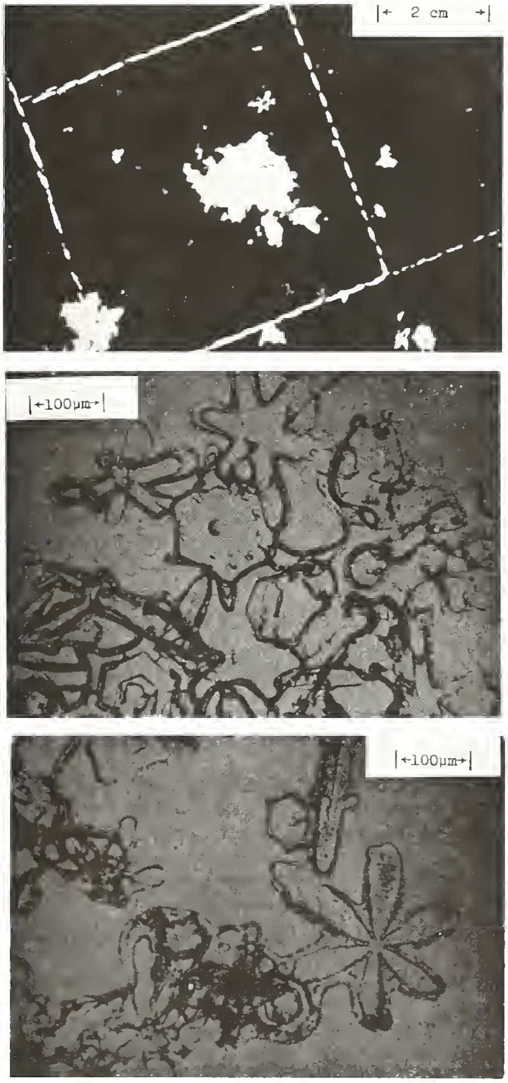

Fig. 9a (top)–c (bottom). Snow crystal aggregates—dendritic.

$$(dm/dt) = \pi r_f^2 E_1 E_2 \omega_i (V_f - V_i),$$

where r_f is the flake radius, E_1 and E_2 the collision and attachment efficiencies, ω_i the cloud ice content, and V_f and V_i the fall velocities of flake and individual crystals respectively. In short, dendritic crystal shape and riming are likely to increase E_1, E_2, and V_f, other factors being equal.

Snowflakes consisting of thick plates and prisms are rather uncommon (Magono, 1953). Figs. 10a and b illustrate dense snowflakes resulting from heavy seeding of a Lake Erie cloud by NOAA and the Cornell Aeronautical Laboratory (Weickmann *et al.*, 1970; Holroyd and Jiusto, 1971). In this case the supercooled cloud was rapidly glaciated by silver iodide concentrations of the order of 1000 l^{-1}. Despite the small size of the competing crystals (about 100 μm) and their compact nature, the high concentrations produced snowflakes with tens to hundreds of crystals per flake.

Collisions amongst snowflakes and between flakes and crystals can cause breakage of branches which subsequently develop into additional irregular crystals and flakes. The process of aggregation is complex and detailed investigations are still rare (Sasyo, 1971). About the only extensive data on snowflake statistics known to us is Dowbrowolski's report of snowflakes vs. temperature which he observed in the Antarctic during the first Polar year, 1897–1899 (Dowbrowolski, 1903). He found a marked temperature dependence of snowflake occurrence as given in Table 1.

The data indicate that surface temperatures warmer than −10C are favorable for aggregation to occur in polar latitudes. This agrees with Magono (1960) who states that snowflakes generally occur at temperatures warmer than −10C. Our lakestorm observations, conversely, suggest that aggregation can occur at colder temperatures; they also indicate that a form dependence exists, as spatial dendrites easily interlock and aggregate.

Interestingly, spatial prism bundles show little tendency to aggregate. Only a few laboratory investigations have dealt with the formation of snowflakes. As pointed

Table 1. Snowflake occurrence.

Temperature	Frequency (%)
+1.0 to − 5.0C	83
−5.1 to −10.0C	9
colder than to −10C	8

out by Hallgren and Hosler (1960) and by Fletcher (1962), the formation of snowflakes is not only a matter of collision but also a matter of adhesion, and as mentioned above, of interlocking of crystals. According to Hallgren and Hosler's observations the adhesion is dependent on the environmental humidity; it is strongly diminished if the crystals collide in a dry environment. At temperatures warmer than −10C adhesion is enhanced by a thin quasi-liquid film which covers the ice surface and whose thickness at −5C is computed to be about 40 Å. This circumstance appears to explain the great tendency of needles to form flakes. The chance for two crystals to collide, on the other hand, is not always proportional to the fall distance, as evidenced by the poor tendency of prism bundles to form flakes; prism bundles formed at the cirrus level have most certainly a long common trajectory and interaction time, but apparently not a sufficiently large concentration or attachment efficiency for significant aggregation.

3. Individual crystals

Fig. 11a somewhat restores faith in the occurrence of symmetric crystals. These unrimed crystals occurred in cold stratiform clouds in Yellowstone Park (Cheng, 1971). Individual unrimed crystals are also the dominant type measured by Grant and Mielke (1967) in the orographic clouds of Climax, Colo. Here the clouds are very cold (typically −20C or lower) and the updrafts a weak 10–15 cm sec^{-1}. We have also observed a higher frequency of simple pristine crystals in shallow arctic clouds over the Greenland Ice Cap. Conversely, winter orographic clouds if sufficiently vigorous can produce rimed crystals and aggregation not unlike lakestorm snow forms, as described earlier. It would appear that conditions favorable for single symmetric crystals are cold thin clouds, low liquid water content, weak updrafts, and adequate but not excessive concentrations of ice nuclei. These conditions are sometimes met in a) upper level trough systems (releaser clouds only), and b) convective cyclonic systems at mid-latitudes, but apparently only along the storm edges (as Bentley observed) or for relatively short periods when cloud cells are just developing or decaying.

Figure 11b, at first glance, is another symmetric crystal. Closer observation, however, reveals a number of irregularities and gaps along its branches. Some distortions may result from nonsymmetrical diffusion patterns about a falling crystal. Yet this dendrite (and several others examined) strongly suggests a crystal fragmentation mechanism, perhaps through collisions with other crystals or supercooled drops. Large numbers of crystal fragments are observed in some lake storms; in one case 80% of the replicated crystals consisted of fragments. The crystal classification system of Magono and Lee (1966) includes several fragment categories, notably broken branches and rimed broken branches suggestive of dendrite collisions.

Fig. 11c (from Fredonia College, a few miles inland from Lake Erie) illustrates that all three mechanisms—diffusion, riming, and aggregation—can and do act simultaneously in the development of some crystals. One would expect the corresponding a priori conditions to be vigorous convective clouds with ample supercooled water and ice crystals.

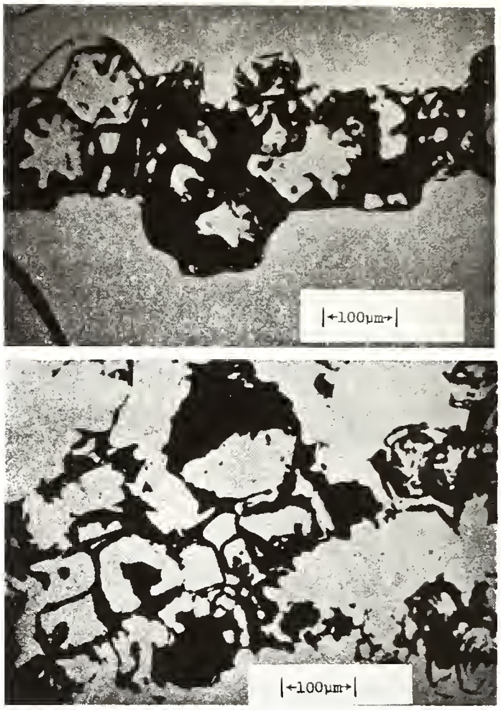

Fig. 10a (top)–b (bottom). Dense snow crystal aggregates from seeded clouds.

4. Double crystals

Double crystals, that is, two parallel planar crystals separated by a frozen droplet, often go unnoticed because of the small dimension of the connecting center. They have been observed in Great Lakes snowstorms on several occasions and in the northern Rockies (Auer, 1970), and have been duplicated in the laboratory (Weickmann *et al.*, 1970). The latter authors have shown that relatively large (15 to 25+ μm) supercooled drops, upon freezing, can initiate the growth of crystals on opposite sides of the drops (Fig. 12a); contact nucleation was dominant in these experiments.

Clearly, vigorous supercooled clouds would be required to form sizable drops and dual crystals. The process should be favored by reasonably strong updrafts, few ice nuclei, and relatively warm temperatures (note that the droplet growth rate by diffusion is approximately twice as great at −10C as at −25C). Polycrystals described in the next section require colder freezing temperatures.

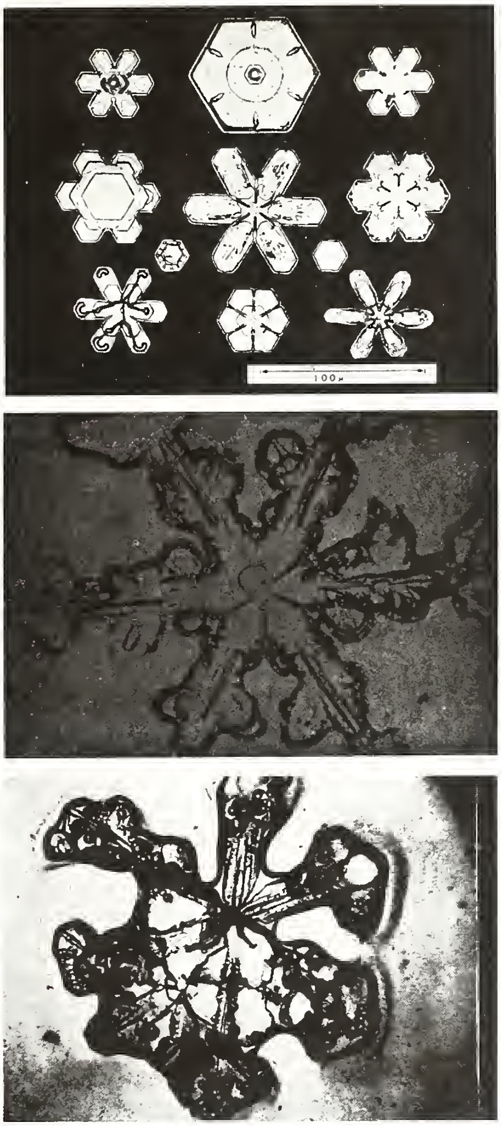

Fig. 11a (top)–c (bottom). Crystals with diffusional growth dominant (progressive irregularities): (a) shallow orographic cloud, Yellowstone National Park; (b, c) convective stratocumulus, Lake Erie, N.Y.

5. Irregular polycrystals and spatial crystals

There are numerous processes leading to irregular three-dimensional habits. Prism bundles emerge from irregular low temperature cirrus crystals; the prisms may display air enclosures, they can be entirely hollow or even open along one prism side in the form of a scroll. It appears that hollow prism forms are a sign of high ice supersaturation (near water saturation). If these crystals fall into a spender cloud at temperatures warmer than −25C and relative humidities near water saturation, their bases develop into end plates, stars, or dendrites. Also prism bundles, which have grown side plates, have been described and received a special category (S3) in the Magono-Lee classification.

Irregular and spatial crystals in water clouds at temperatures warmer than −25C can develop due to "birth defects" from droplet freezing by contact nucleation or by an embedded ice nucleus; alternately, irregular growth can result from defects acquired during the growth phase, particularly in the riming process at low temperatures. (Riming at higher temperatures, above about −10C to −15C, will usually cause the formation of graupel.) Fig. 12b shows laboratory crystals at an early stage of development, whose irregularities we would call "birth defects." Only if the crystal emerges from a frozen droplet can its irregularity be systematized.

Depending on temperature and size, a droplet upon freezing may become a single crystal or polycrystal. For a population of cloud droplets with diameters up to 100 μm, Fig. 13 shows the percentage of single crystals and polycrystals, respectively, as a function of temperature. As the temperature lowers, the formation of polycrystals increases while the formation of single crystals decreases. The data for Fig. 13 have been derived by us from the studies of Magono and Aburakawa (1968). A similar but inverse relationship can be established between polycrystallinity and size, i.e., the larger the drop the more probable is the formation of a polycrystal. This may be, as Brownscombe and Hallett (1967) point out, due to dendritic growth from several nucleating sites in the crystallizing bulk water of the large drop.

Figs. 14a and b illustrate schematically how double stars may form with two parallel crystals and spatial multiple stars from polycrystals (droplet centers). The proximity of the developing crystal branches causes a

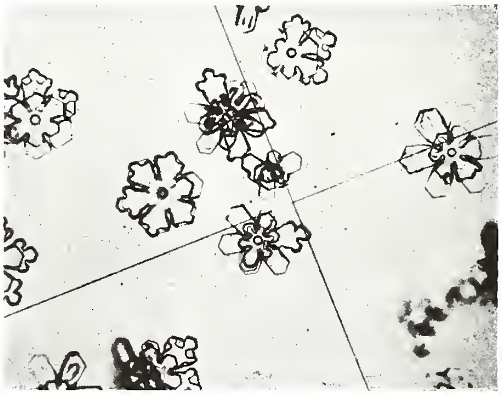

Fig. 12a. Double crystals developed in cold chamber after droplet nucleation by seeding with 2% AgI-Isopropylamine mixture at −17C.

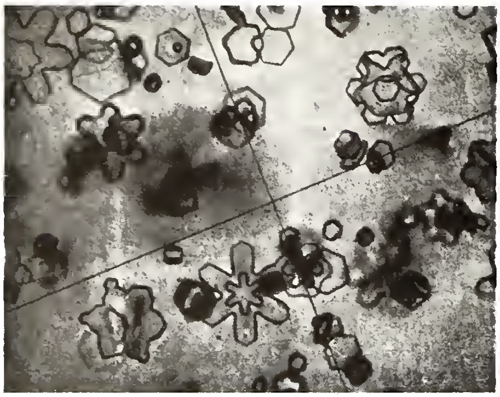

Fig. 12b. Crystals developed in cold chamber after nucleation with dry ice at —17.5C. Note that crystals have irregular forms but no center droplet due to homogeneous nucleation.

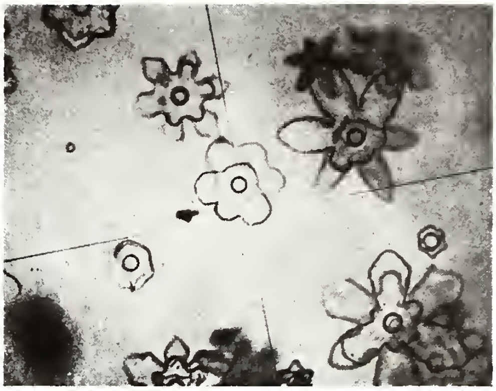

Fig. 12c. Double crystals showing competition for water vapor of upper and lower branches.

competition for the water vapor amongst the twelve rays in the case of the double crystals. The result is that the upper crystal may succeed in developing a certain number of rays which are complemented by the alternate branches of the lower crystal (note Fig. 12c). Some 12-ray stars apparently represent an interesting twinning form of this kind in which the secondary axes of the upper and lower star are rotated by 30°. A corresponding selection takes place in the development of a spatial dendrite from a polycrystal nucleus (Weickmann, 1972). The crystals of Figs. 5 and 12a were the result of contact nucleation of droplets by silver iodide. Homogeneous nucleation after dry ice seeding leads to irregular forms also, as Fig. 12b shows, but the crystals are of course without center drops.

The ventilation of planar and spatial dendrites during descent causes the local concentration of water vapor near the crystal surface to be enhanced (Hallett, 1965). Since most dendrites rotate as they fall, the ventilation factor is again enhanced, having the same effect as an increase in supersaturation. This permits dendritic growth to proceed at higher temperatures (approximately 2C) than without ventilation (Hallett, 1964). A similar vapor enhancement effect is caused by the presence of a water cloud. The water droplets in the proximity of an ice crystal deform the field of vapor diffusion around the crystal in a way that the vapor pressure gradient toward the crystal increases. These conditions have been studied by Marshall and Langleben (1954). They found that for dense clouds, liquid contents >10 gm m^{-3} and large ice particles (diameter about 1 mm), the equivalent supersaturation corresponds to 1.23 times the value at water saturation. Ventilation and the relative motion between crystals and cloud droplets are not considered; both factors will, however, further increase the localized supersaturation. The Marshall and Langleben theory appears to be well confirmed by a series of very interesting, little known experiments by Nakaya *et al.* (1958). While the true relationships are still poorly understood, there can be no question that one is confronted here with a much neglected area in cloud microphysics which enters significantly into the efficiency not only of the Bergeron precipitation process in a stratiform system, but in any precipitation process in convective clouds in

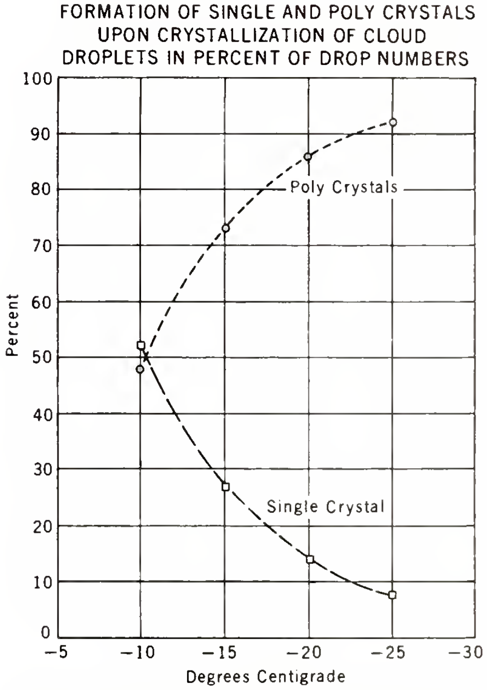

Fig. 13. Formation of single and polycrystals upon crystallization of cloud droplets in percent of drop numbers.

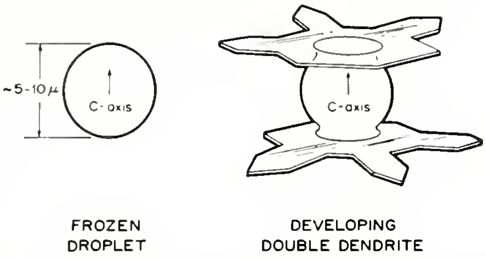

Fig. 14a. Schematic drawing indicating formation of double star on the ends of a droplet frozen into single crystal. Note competition for vapor causes irregular growth of opposing branches of the two crystals.

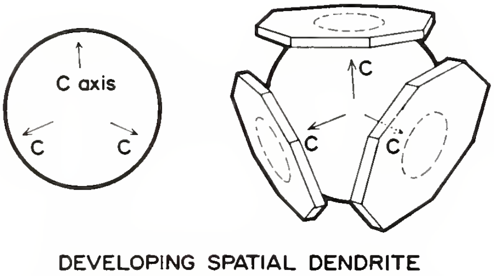

Fig. 14b. Schematic drawing of the crystal development from polycrystal. Crystal habit is spatial dendrite.

which the ice phase plays a role. Further, formidable barriers for analytical as well as numerical solutions still exist. No doubt, the growth rates estimated by Marshall and Langleben will cause growth irregularities and spatial developments due to the highly supersaturated growth condition.

Finally, attention is again called to the very important processes of riming and aggregation. Magono and Lee (1966) devote considerable attention to the formation of secondary branches emerging from collected supercooled cloud droplets, thus forming spatial dendrites. Iwai (1971) shows that a cloud droplet collected and then freezing to the surface of a stellar or plate crystal often causes a new branch to grow which is inclined 70° to the host plane. He shows that such growth can be explained as twin formation of two *c*-axes.

The fundamental significance of all spatial crystal forms lies in the fact that they are excellent scavengers of moisture, via both vapor diffusion as well as by droplet riming. The scavenging efficiency of these crystals is extraordinarily high for several reasons:

1) Nakaya (1957) was the first one to emphasize that air passes not only around a snowflake but also through it. Thus, their riming efficiency is strongly enhanced and not diminished as it is for a solid body of the same size, shape, and fall velocity.

2) Their irregular rotating and tumbling fall attitude likewise helps to collect cloud droplets, and finally

3) These cloud droplets at low temperatures form centers for new branches; at high temperatures near the freezing point, upon crystallization, they easily form needles which again enhance the riming efficiency in the high water contents of the warm spender clouds.

The important point must be made here that these needles are secondary ice formations which originate because large cloud droplets and drizzle drops are collected and crystallize subsequently. Under these conditions giant wet snowflakes form, such as those we observed on 30 April 1973 (2115 LT). The log entry reads: "Heavy snowfall from large flakes, 1/2 to 2 cm diameter, consisting of wet crystals amongst which many long needles (sticks) are conspicuous together with wet and irregular dendritic forms and large frozen drops. Concentration of the large flakes estimated at 15 to 20 per 30 liters of air."

c. Precipitation modification

We realize that all the foregoing processes are designed to increase the snow-out capability of a cloud and to adjust the rate of precipitation to the rate of condensation. Lamellar spatial growth, dendritic branches, enhancement of crystal diffusional growth through ventilation and the proximity of water drops, fall attitude, aggregation and finally riming and aggregation to giant flakes are the milestones in the evolution of snow crystals in the presence of high contents of precipitable water and/or a deficiency of freezing nuclei. It appears that only when nature has exhausted all of these growth processes, and still has not succeeded in scavenging much of the potential moisture, does artificial seeding have prospects of enhancing precipitation. The chances appear more favorable if a deep water (warm or supercooled) cloud lies below the snow cloud. Seeding may, though not always, increase the number of snowflakes; then the greater number of accreting flakes (or coalescing melt raindrops) may increase the precipitation efficiency of the low-level cloud.

4. Cloud microphysics calculations

No entirely satisfactory model of crystal development in a mixed-phase cloud has yet been devised. The vapor deposition process can be handled reasonably well for certain idealized crystal habits (e.g., Koenig, 1971); efforts to incorporate riming effects (Jiusto, 1967; Podzimek, 1969; and Cotton, 1970) have met with some success recognizing the necessity of introducing simplifying assumptions; finally, the consideration of snow crystal aggregation has only been attempted to date by separate calculations divorced from the other two mechanisms (Magono, 1953; Jiusto, 1971; Sasyo, 1971). Nevertheless, these partial formulations provide information useful in interpreting the crystal observations of Section 3.

Fig. 15 illustrates the time dependence of ice crystal type and cloud glaciation on ice nucleus concentrations ($N = 1$–1000 l^{-1}) in a vigorous cloud of 1 m sec^{-1} updraft and temperature of −20C. As described elsewhere (Jiusto, 1971), the conditions simulate active Great Lakes snowstorms in which crystal riming and deposition are occurring. The letter P indicates the onset time of partial riming and R heavy crystal riming; if sufficient crystals are present, a return to strict vapor deposition growth (D) may occur as the cloud glaciates. Crystal size and type are indicated after 30 minutes of growth time.

It is evident that light riming in the model cloud [2] commences in about two minutes almost independently of ice nucleus concentrations (≤ 100 l^{-1}). Heavy riming and graupel formation commences in approximately 12–13 min for $N = 1$ and 10 l^{-1}, with these crystal concentrations not being able to accommodate all the liquid water generated in the 1 m sec^{-1} updraft. Approximately 4 to 5 mm graupel pellets are predicted after a 30-min growth time.

Crystal concentrations of approximately 50 l^{-1} or more are able to prevent heavy riming and succeed in completely glaciating the cloud in times of 15 min or less. It is interesting that some riming is to be expected even with $N = 100$ l^{-1}. Only in the simulated overseeding case of $N = 1000$ l^{-1} was riming completely inhibited. These trends of crystal type, size, and riming were supported by field observations.

Table 2 lists the approximate time and cloud layer thickness required for the formation of graupel of 1 mm radius in model clouds of varying updrafts. Note that the stronger the updraft, the less is the time required for graupel to form. This is due to the corresponding increase in cloud liquid water, and hence, increase in crystal riming rate as the updraft becomes more intense. Of particular interest is the indication that the required cloud layer thickness can be as shallow as about 0.18 km, which occurs with updrafts of 1 m sec^{-1}. Such updraft magnitudes correspond rather closely with the terminal fall velocity of partially rimed crystals so that a growing crystal remains relatively "stationary" with respect to the ground. Because natural crystal concentrations in excess of 50 l^{-1} are rare and average lake storm updrafts of 0.5–1 m sec^{-1} are not, one should not be surprised at the common occurrence of graupel and rimed crystals observed near the shorelines of the Great Lakes.

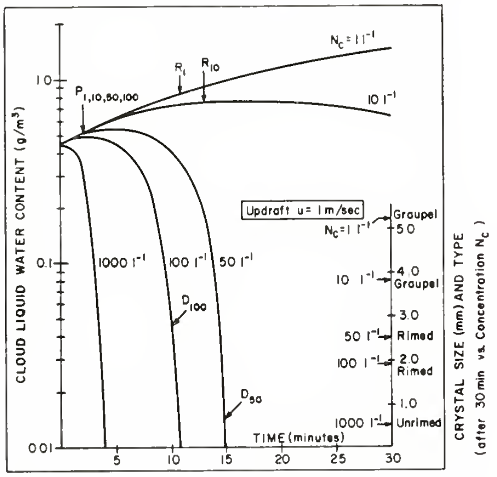

Fig. 15. Cloud liquid water content as used up by various crystal concentrations (N_c).

Snowflake aggregates, as noted earlier, constitute one of, if not the most common form observed in typical snowstorms. The collision rate (dC_o/dt) of a snowflake falling through a population of individual crystals can be expressed as

$$(dC_o/dt) = \pi\, r_f^2\, E\, N_c\, (v_f - v_c),$$

where r_f is the radius of the flake, N_c the concentration of individual ice crystals in the cloud, and v_f and v_c the fall velocity of flake and crystals, respectively.

The terminal fall velocity v_f of snowflakes, and of flake radius r_f as a function of crystal concentration n_c per flake and individual crystal radius r, can be expressed (Jiusto and Holroyd, 1970) as follows:

$$v_f = 150\, r_f^{0.2},$$
$$r_f = 0.25\, n_c^{1/2} r.$$

These equations allow, with some simplifying starting assumptions, an estimation of crystal aggregation rates and the size and velocity changes of falling snowflakes. It was assumed that a three-crystal snowflake initially existed, that $v_c = 30$ cm sec^{-1}, and $E = 1$. The equation set was then solved numerically for various cloud crystal concentrations (N_c) and fixed crystal sizes (r).

The degree of aggregation (number of crystals per flake) can be estimated by such simple first-approximation calculations. A constant population of cloud crystals was assumed and, without a depletion term, aggregation is certainly exaggerated. However, the general trends are

Table 2. Required cloud layer depth (km) and time (min) for graupel (r = 1 mm) formation.

Updraft u (cm/sec)	Ice nucleus concentration N_c (l^{-1})			
	1	10	50	100
	km (min)	km (min)	km (min)	km (min)
5	0.70 (15.2)	0.96 (19.2)	*	*
20	0.51 (14.2)	0.62 (16.0)	*	*
100	0.18 (11.4)	0.18 (11.9)	*	*
300	1.17 (8.7)	1.20 (8.9)	1.30 (9.6)	*

* Graupel does not form.

---

[2] Model cloud: $T = -20$C; $p = 800$ mb; liquid water $\omega = 0.43$ gm m^{-3} initially; water saturation initially.

considered informative. In short, aggregation is slight to nonexistent with crystal concentrations of 1 l^{-1}, and also minimal with $N = 10$ l^{-1} until crystal sizes reach 2 mm or so. Aggregation becomes a dominant growth mechanism for crystal concentrations in excess of about 50 l^{-1}. A simulated overseeding case ($N_c = 1000$ l^{-1}, $r =$ 0.2 mm) indicated, after 30–40 min, aggregation values of several tens to hundreds of crystals per flake; such values are closely comparable with the field observations illustrated in Figs. 10a and b.

How does one explain the common occurrence of snowflakes if crystal concentrations of several tens per liter of air are required? First, as we have mentioned above, in deep systems nature already provides for 5 to 40 crystals per liter. Second, some type of multiplication process appears necessary as numerous investigators have reported (reviews by Mossop, 1970, 1971). The observations of broken crystals and fragments in convective lake storms certainly gives strong evidence of a dendritic fragmentation process, at least in active mixed-phase clouds possessing temperatures of −10 to −20C. An updraft-balance mechanism for concentrating crystals in certain (presumably upper) layers of clouds also offers a possibility. The rupturing of frost fragments (Schaefer and Cheng, 1971) may be operative. Supercooled droplet splintering cannot be ruled out, although laboratory results (Hobbs, 1969; Mossop, 1970) appear inconclusive. It is perhaps prudent to refrain from speculation and merely suggest that the common snowflake aggregation mechanism is deserving of substantial laboratory and field investigation.

5. Summary

Snow crystals grow by the diffusion of water vapor, by droplet riming, and by crystal aggregation. The major growth mechanisms are interrelated and strongly affected by important feedback mechanisms whose effects on the integrated snow crystals growth process is still poorly understood. Each dominant growth mechanism or combination of mechanisms is indicative of certain cloud conditions. Numerical cloud models are thus far too simplistic and observations too spotty to specify in detail the relationship between snow forms and cloud variables. Individual crystals growing strictly by diffusion possess a well-known unique dependence on temperature and humidity (Nakaya, 1954) that undoubtedly cannot be paralleled with more complex snow types and their varying cloud environment. However, certain snowfall signatures at the ground do reveal a good deal about cloud physics processes taking place overhead.

Based on mixed-phase cloud calculations and observations (direct or reported) in several geographically different winter storms, the following points appear applicable:

1) A modified Bergeron-classification of an upper releaser cloud and a lower spender cloud (or each type alone) is often useful in describing the efficiency of precipitation of layered clouds as well as explaining resultant crystal types. An *a priori* condition for heavy snowfall is the presence of a thick convective spender cloud; when such a cloud is too warm to precipitate effectively, artificial seeding of its upper portions or of a higher releaser cloud may stimulate precipitation. Crystal concentrations discharged by releaser clouds range quite consistently between 5 and 40 per liter, in measurements made to date.

2) The most common type of snowfall in mid-latitude vigorous storms consists of snowflake aggregates. Flakes comprised of 10 to 100 or more individual crystals require high crystal concentrations somewhere in the cloud. They often consist of dendrites and thin plates indicative of moist conditions near water saturation; interestingly, flakes consisting of numerous needles occur also. Column and thick-plate aggregates signifying ice-saturated conditions are far less common. The latter can be produced by heavy seeding of supercooled clouds.

3) Rimed crystal forms are common in the beginning or toward the end of the winter season, when ambient temperatures are relatively mild or near large water bodies. In all cases, vigorous convection and a scarcity of ice nuclei to produce water-saturated cloud conditions and a high ratio of water-to-ice are required. Lightning discharges have been observed in the presence of falling graupel over the Great Lakes and in East Coast storms. Rimed crystal forms become far less common during the height of the winter season.

4) Individual symmetric crystals are rather rare in vigorous thick storm systems. They are more apt to be found on the passive edges of major cyclonic and mesoscale lake-storm systems, or in thin orographic clouds. Only weak updrafts can be tolerated in order to minimize cloud liquid water and interaction with droplets; ice crystal concentrations cannot be so great as to promote aggregation. These conditions are often met in shallow Arctic clouds. They have also been reported from orographic clouds in the Rocky Mountains (Grant and Mielke, 1967).

5) Irregular crystal forms—fragments, rimed branches, and unsymmetric segments—are sometimes dominant during periods of convective storms. They suggest that hydrometeor interactions are common, that collisional processes must be considered in realistic cold-cloud models, and that multiplication of crystals by some type of fracturing or riming may be significant.

6) Double crystals, which are often difficult to discern without stereoscopic microscopic inspection, may be more prevalent than the few observations would suggest. Typically forming on supercooled drops, they signify the presence of supercooled clouds and relatively large drops. Polycrystals and spatial dendrites reflect droplet freezing at colder temperatures or of larger droplets, but other formation (collisional) mechanisms not involving droplet centers but accreted cloud droplets appear equally possible. After more definitive study, it is possible that these latter complex crystal forms will serve

as indicators of specific cloud conditions and nucleation mechanisms.

7) Snow crystal investigators should be encouraged not to single out the aesthetic symmetric crystals but to give equal weight to irregular forms and fragments so that:

- a) a better perspective can be gained of the many crystal formations and interaction mechanisms occurring in given clouds and storm types, and
- b) more realistic numerical models of mixed-phase clouds can be developed.

Acknowledgments. Much of the work reported by the first author was sponsored by grants from the National Oceanic and Atmospheric Administration, U.S. Department of Commerce.

References

Auer, A., 1970: Observations of ice crystal nucleation by droplet freezing in natural clouds. *J. Rech. Atmos.*, **4**, 145–160.

Bentley, W. A., 1902: Studies among the snow crystals during the winter of 1901–2, with additional data collected during previous winters. *Mon. Wea. Rev.*, **30**, 607–616.

——, and W. J. Humphrey, 1931: *Snow Crystals.* McGraw-Hill Co., 227 p.

Bergeron, T., 1950: Über der mechanismus der ausgiebigen Niederschläge. *Ber. Deut. Wetterd.*, **12**, 225–232.

Brownscombe, J. L., and J. Hallett, 1967: Experimental and field studies of precipitation particles formed by the freezing of supercooled water. *Q. J. Roy. Met. Soc.*, **93**, 455–473.

Cheng, R., 1971: Eleventh Yellowstone Field Research Expedition, ASRC-SUNYA Pub. No. 141, Albany, N.Y., NSF Grant GA-1112.

Cotton, W. R., 1970: A numerical simulation of precipitation development in supercooled cumuli. Rept. No. 17 to Nat. Sci. Foundation, NSF Grant GA-13818, Dept. of Meteor., Pennsylvania State University, 178 p.

Dobrowolski, A. B., 1903/1904: La neige et le givre. Résultats du voyage de S. Y. "Belgica" en 1897–1898–1899. Rapports Scientifiques 3, *Météorologie*, Pt. 3, 78 pp.

Eadie, W. J., R. J. Pilie, and W. C. Kocmond, 1971: Modification and modeling of lake-effect weather. NOAA Grant E22-39-70(N), Cornell Aeronautical Lab., Rept. No. VC-2898-P-2, 101 p.

Fletcher, N. J., 1962: *The Physics of Rain Clouds.* Cambridge, Cambridge University Press, 386 p.

Grant, L. O., and P. W. Mielke, 1967: A randomized cloud seeding experiment at Climax, Colo., 1960–65. *Proc. Fifth Berkeley Symp. on Math. Statis. and Prob.*, **5**, 115–131.

Gunn, K. L. S., 1967: The number flux of snow crystals at the ground. *Mon. Wea. Rev.*, **95**, 921–924.

——, M. P. Langleben, and A. S. Dennis, 1954: Radar evidence of a generating level of snow. *J. Meteor.*, **11**, 20–26.

Hallett, J., 1964: Experimental studies of the crystallization of supercooled water. *J. Atmos. Sci.*, **21**, 671.

Hallgren, R., and Ch. L. Hosler, 1960: Preliminary results in the aggregation of ice crystals. AGU Geophys. Monogr. #5, *Physics of Precipitation*, H. Weickmann, ed., AGU Publ. No. 746, Baltimore, Waverly Press, 257–263.

Hobbs, P. V., 1969: Ice multiplication in clouds. *J. Atm. Sci.*, **26**, p. 315.

Holroyd, E. W., and J. E. Jiusto, 1971: Snowfall from a heavily seeded cloud. *J. Appl. Met.*, **10**, No. 3, p. 266.

Hosler, C. L., and R. E. Hallgren, 1961: Ice crystal aggregation. *Nubila*, **13**, 249.

Houghton, H. G., 1950: A preliminary quantitative estimate of precipitation mechanisms. *J. Meteor.*, **7**, p. 363.

Iwai, K., 1971; Note on Snow Crystals of Spatial Type. *J. Meteor. Soc. Japan*, **49**, No. 6, 516–519.

Jiusto, J., 1967: Nucleation factors in the development of clouds. Ph.D. Dissertation, Pennsylvania State University, 124 pp.

——, 1971: Crystal development and glaciation of a supercooled cloud. *J. Rech. Atmos.*, **5**, 69–85.

——, and E. W. Holroyd, 1970: Great Lakes snowstorms—Part 1. Cloud physics aspects. ASRC, State University of New York at Albany, ESSA Grant No. E22-49-70, 142 pp.

Koenig, R., 1971: Numerical modeling of ice deposition. *J. Atmos. Sci.*, **28**, 226–237.

Lavoie, R. L., W. R. Cotton, and J. B. Hovermale, 1970: Investigations of Lake-effect storms. Dept. of Meteor., Pennsylvania State University, Final Report, NOAA Contract E22-103-68(N), 127 pp.

Magono, C., 1960: Discussion remarks. AGU Geophysics. Monograph #5, *Physics of Precipitation*, p. 263, H. Weickmann, ed., AGU Publ. #746. Baltimore, Waverly Press.

——, 1953: On the growth of snowflakes and graupel. Sci. Rept., Yokohama Nat. University, Sec. 1, 2, 18–40.

——, and H. Aburakawa, 1968: Experimental studies in snow crystals of plane type with spatial branches. *J. Faculty Sci.*, Hokkaido University, Ser. VII, **3**, 85–97.

——, and C. W. Lee, 1966: Meteorological classification of natural snow crystals. *J. Faculty Sci.*, Hokkaido University, Ser. VII, **2**, 321–335.

Marshall, J. S., 1953: Precipitation trajectories and patterns. *J. Meteor.*, 10, 25–29.

——, and M. P. Langleben, 1954: A theory of snow-crystal habit and growth. *J. Meteor.*, **11**, 104.

McVehil, G. E., J. E. Jiusto, R. A. Brown, and R. L. Peace, 1967: Project Lake Effect. ESSA Contract E22-49-67(N), Cornell Aeronautical Laboratory, Rept. No. VC-2355-P-1, 55 pp.

——, C. W. Rogers, and W. J. Eadie, 1968: The structure and dynamics of Lake-effect snowstorms. ESSA Grant E22-89-69(N), Cornell Aeronautical Laboratory Rept. VC-2559-P-1, 49 pp.

Mossop, S. C., 1970: Concentrations of ice crystals in clouds. *Bull. Amer. Meteor. Soc.*, **51**, p. 474.

——, 1971: The multiplication of ice crystals in clouds. *Intl. Conf. Wea. Mod.*, Canberra, Australia. Amer. Meteor. Soc., p. 1–4.

Nakaya, U., 1957: Physical investigations of snow flakes. *Artificial Stimulation of Rain.* H. Weickmann and W. Smith, ed., 327–331. Pergamon Press, New York.

——, 1954: *Snow crystals natural and artificial.* Harvard University Press, 510 pp.

Nakaya, U., M. Hanajima, and J. Muguruma, 1958: Physical Investigations on the Growth of Snow Crystals. *J. Faculty Sci.*, Hokkaido University, Japan, Ser. II, **V**, 33–118.

Paine, D. A., 1971: The diagnosis and prediction of synoptic-scale influences leading to mesoscale Lake-effect development. Ph.D. Dissertation, Dept. Atmos. Sci., State University of New York, Albany, 95 pp.

Peace, R. L., and R. Sykes, 1966: Mesoscale study of a lake effect snow-storm. *Mon. Wea. Rev.*, **94**, 495–507.

Podzimek, R., 1969: Le modele theorique d'un nuage de precipitation. Ann. 1st Univ. Navale di Napoli, XXXVII, 12 pp.

Sasyo, Y., 1971: Study of the Formation of Precipitation by the Aggregation of Snow Particles and the Accretion of Cloud Droplets in Snowflakes. *Papers in Meteorol. and Geophys.*, **22**, 2, 69–140.

Schaefer, V., and R. Cheng, 1971: The production of ice crystal fragments by sublimation and electrification. *J. Rech. Atmos.*, **5**, 5–10.

Weickmann, H. K., 1957a: Current understanding of the physical processes associated with cloud nucleation. *Beitr. Phys. Atmos.*, **30**, 97–118.

——, 1957: A nomogram for the calculation of collision efficiencies. *Proc. Artificial Stimulation of Rain*. Pergamon Press, p. 161.

——, 1972: Snow crystal forms and their relationship to snowstorms. *J. Rech. Atmos.*, **VI**, Nos. 1–2–3, p. 603–615.

——, J. E. Jiusto, G. E. McVehil, R. J. Pilie, and J. Warburton, 1970a: The Great Lakes Project. *Proc 2nd Nat. Conf. on Wea. Mod.*, p. 34. Amer. Meteor. Soc.

——, N. Katz, and R Steele, 1970: AgI-Sublimation or contact nucleus. Preprint, *2nd Natl. Conf. Wea. Mod.*, p. 177–178, Amer. Meteor. Soc.

Reprinted with permission of the International Conference on Weather Modification, Tashkent, USSR, October 1-7, 1973.

The Effect of Chaff Seeding on Lightning and Electric Fields of Thunderstorms

H.W. Kasemir

Atmospheric Physics and Chemistry Laboratory
National Oceanic and Atmospheric Administration
Boulder, Colorado 80302

Abstract:

Corona discharge appears at the ends of a chaff fiber in an electric field of 30 kV/m or more. If a pound of chaff consisting of about 2 million fibers is released from an airplane ina thunderstorm field of about 60 kV/m, a corona current of about one microampere is generated at the ends of each fiber. The net current of the two million fibers adds up to about 2 ampere and the charge released into the cloud in a time period of 100 seconds would be of the order of 200 Coulomb. The net current as well as the net charge are comparable to the values of an average thunderstorm and will tend to mask or neutralize the thunderstorm field. The application of this concept to modifying lightning or thunderstorm fields encounters two main difficulties. One is the distribution of chaff fibers in the high field areas of the cloud fast enough to be effective in a large enough cloud volume, and the second one is the possibility that ions liberated by corona discharge are trapped by the cloud droplets in the immediate neighborhood of the individual chaff fiber. This could generate a concentrated space charge around the fiber, which may quench the corona discharge before a large amount of charge is released.

To investigate these problems a number of field experiments have been planned to study the effect of chaff seeding on the electric fields and the lightning discharges of thunderstorms. After some preliminary tests in Flagstaff, Arizona, the first of these experiments was carried out in Boulder, Colorado, in 1972. The results seem to indicate that the decay of the electric field underneath a thunderstorm is accelerated by about a factor five by chaff seeding as compared to the natural decay of the field of a not seeded storm. Instrument development, test procedures, and data analysis of this field decay experiment as well as its significance to lightning modification will be discussed.

1. Introduction

The field decay experiment Boulder 1972 may be considered as the first experimental step in lightning suppression by chaff seeding. The physical concept of this method is based on the idea that corona discharge on a large number of chaff fibers releases so many ions into the cloud that the conductivity of the air is increased and consequently the field is decreased. The high field value of about 500 kV/m necessary to ignite lightning discharges may never by reached [1],[2]. This picture is largely oversimplified and many expected ramifications are discussed in [1] and more unexpected difficulties are anticipated.

One of the favorable aspects of chaff seeding is the fact that corona discharge on the chaff fiber will start in an electric field of about 30 kV/m which is more than a factor 10 below the lightning igniting field - and that the corona current (ion production) increases with the square of the field. [3] Therefore the discharging effect of the chaff fibers intensifies with the growth of the thunderstorm field. With respect to the decay-speed of the field after seeding we may expect that high fields on the order of 120 kV/m or more - which is four times the corona onset field - decay fast, that lower fields in the order of 60 kV/m - i.e., twice the corona onset field - decay slow, and that for fields below 30 kV/m there should be no effect from chaff seeding on the normal variation of the thunderstorm field. The objective of the 1972 chaff seeding experiment was to confirm these patterns.

2. Experiments

The chaff is dispersed from an airplane making repeated passes under a thunderstorm. The airplane is equipped with a chaff dispenser, field mills, [4], a corona indicator, and the necessary accessory equipment such as a strip chart and magnetic tape recorder, altitude recorder and so on. The test procedure was to select one growing cumulus cloud which already showed the emergence of light precipitation at the base. The electric field was then monitored during continuous passes back and forth underneath the storm. If the field reached values of the order of about 50 kV/m two consecutive passes were seeded (or not seeded) and the field recording continued until the storm dissipated. The decision to seed or not to seed was based on the requirement that data should be collected of an equal amount of seeded or not seeded storms. With the clear cut physical objective and the necessary monitoring equipment no elaborate randomization process is needed.

The graphs presented in Figures 1 to 3 show the field underneath the storm versus time. For each pass the maximum value of the negative vertical field component was listed with the corresponding time and these peak values are connected in the graph by straight lines. The time interval between consecutive passes ranges from 3 to 9 minutes (with an average of 4 minutes). In Figure 1 the average field of four seeded storms and in Figure 2 of four not seeded storms, is shown in the upper half of the figure. In the lower half of the figure the field of each individual storm is given with a reduced vertical scale. To calculate the average field values the seeded storms have been synchronized with respect to the first seeding run, and the not seeded storms with respect to their maximum field value. Seeding events are marked on the curves by the letter S.

It is evident from a comparison of Figure 1 and 2 that the field decay of the seeded storms after the second seeding run (Fig. 1) is much faster than the field decay of the not seeded storms (Fig. 2). The accelerated field decay of the seeded storm is 6 kV/m/min as compared to the decay of the not seeded storm of 1.2 kV/m/min. If the field in the seeded storm is reduced to 34 kV/m the accelerated decay stops because the corona discharge on the chaff fibers stops, and further decay continues at a rate of 1.5 kV/m/min which is about the value of the not seeded storm.

Storm 4 merits special attention because the field did increase after the first seeding run and started to decrease only after the second seeding run. Furthermore, the field increase before seeding is much faster than in all of the other examples. This means we are dealing here with a rapidly growing charge which was still far before an equilibrium state. Therefore, the first seeding run was not effective enough to reverse the sharp field increase to a field decrease. However, the most significant feature of this test was that seeding was done inside the cloud instead of below the cloud as in all the other cases. One has to expect that a large number of ions liberated by the corona discharge are captured by the cloud droplets, made immobile, and therefore removed from their role of increasing the conductivity of the cloud. From purely theoretical consideration it is not possible to decide if this effect will completely counteract the purpose of chaff seeding or if it is only an insignificant side effect. This one test seems to indicate that chaff seeding causes an increase in conductivity even inside the cloud and consequently a decrease in the field but there may be a delay in the overall process.

Figure 3 shows the field decay caused by chaff seeding of a storm with an extremely high field value of 300 kV/m. The field maintained its high value for about 18 minutes when chaff seeding began. After 4 seeding runs, which required about 5 minutes, a dramatic field decay occurred at the high rate of 58 kV/m/min. The field dropped in about 5 minutes to the low value of 10 kV/m and remained below this value for the rest of the flight. This is about 10 times the decay rate of the previously discussed storms.

The field decay experiment Boulder 1972 has been repeated in 1973 with similar results. The meteorological conditions in 1973 have been somewhat unusual with respect to the thunderstorm activity in Colorad. The storms appeared much later in the season, i.e., in the second half of the summer. They had generally a shorter life time and produced higher fields, which changed more rapidly than during the storms in 1972. The last factor may reduce the average field decay of the not seeded storms somewhat. However, even with the greater field variability in 1973 the decay rate of the seeded storms was always faster than that of the not seeded storms. Ten storms produced fields underneath the base in the range of 100 to about 300 kV/m. This will furnish some high field control storms to the one seeded case discussed above, and also more seeded cases. The exact figures of the decay rate of the seeded and not seeded high field storms have to await the proper evaluation of the data. However the faster decay rate of the high field as compared to the low field seeded storms was already apparent by a preliminary review of the records.

4. The significance of the field decay experiments with regard to lightning suppression

The link between the field decay experiment and lightning suppression is the strong electric field necessary to initiate a lightning discharge. If the generation of high fields of about 500 kV/m in the cloud can be prevented or their time of existence shortened it is a reasonable assumption that lightnings will not occur or that at least the number of lightnings per storm will be very much reduced. The most effective way to achieve lightning suppression would be to seed the regions in the storm where highest fields occur. These maximum fields will occur between two charge center of opposite polarity. Ground discharges should be initiated between the main negative charge center in the base of the cloud and the positive pocket charge in or at the base of the cloud.

The numerous field records obtained during the field decay experiments revealed the fact that the old tripolar thunderstorm model of Simpson, Scarse, and Robinson [5], [6], should be corrected. This well known model has the three charge centers arranged vertically one above the other with the smallest - the positive pocket charge of about 4C - at the base of the cloud, the main negative spherical space charge of about -20C with its center at about 3 km above ground and the spherical positive space charge of about 24C at about 6 km above the ground.

From our flight records it follows that the positive base charge is first of a much larger magnitude - in the average about half of but sometimes even larger than the negative space charge - that its lateral extension is much larger, in the order of several kilometers, and that the positive base charge center is located about 1 km above cloud base. The negative space charge center is 1.5 to 2 km above base and its lateral distance from the positive base charge in the order of 4 km. Therefore it seems that these two opposite base charges are arranged more side by side than on top of each other. This picture conforms much better with the charge arrangement given by Reiter [7]. He also states that the horizontal dimension of the positive base charge is several kilometers and that the maximum lightning activity occurs in the region of the positive base charge. (According to his figure 117, page 276, at the boundary between the positive and negative charge.)

Furthermore our flight records show usually a certain time delay in the growth of the positive base charge. Positive fields - indicating positive charge overhead - appear when the negative charge is already well established, and with time the positive field grows stronger whereas the negative field decays. It happens sometimes that at the end of the storm the positive charge completely dominates in the base of the cloud so that only positive fields are recorded.

In conclusion we may state the following:

(1) The field decay experiments Boulder 1972 and 1973 show that electric fields underneath a thunderstorm decay more rapidly with chaff seeding than without seeding.
(2) The higher the seeded fields the more rapid is the decay.
(3) The seeding took place underneath the cloud in clear air sometimes in rain.
(4) There is some question if seeding inside the cloud has the same or appreciably the same effect on the electric field as it has in clear air. The one in cloud seeding shows also an accelerated field decay after seeding. However this one flight is not enough by far to establish this result as a general fact. More in-cloud seeding flights are needed.
(5) For lightning suppression location and timing of the seeding runs are important. From the analysis of the field records obtained underneath the cloud it seems that the best place to seed would be about 1 km above cloud base between the positive and negative base charges. This area can be determined in time from field records of flights underneath the cloud.

References

[1] Kasemir, H.W., 1973: Lightning suppression by chaff seeding. NOAA-ERL Technical Report.

[2] Holitza, F.J., Kasemir, H.W., 1973: Accelerated decay of thunderstorm electric fields by chaff seeding. J.G.R. (in press).

[3] Chapman, S., 1958: Corona-point-discharge in wind and application to thunderclouds. Recent Advances in Atmospheric Electricity, Pergamon Press (pp. 277-287).

[4] Kasemir, H.W., 1972: The Cylindrical Field Mill. Meteor. Rundschau, 25, 2, pp. 33-38.

[5] Simpson, G.C., Scarse, F.J., 1937: The distribution of electricity in thunderclouds. Proc. Met. Roy. Soc. A, 161, pp. 309-352.

[6] Simpson, G.L. Robinson, G.D., 1940: The distribution of electricity in thunderclouds. Proc. Met. Roy. Soc. A, 177, pp. 281-329.

[7] Reiter, R., 1964: Felder, Ströme und Aerosole in der unteren Troposphare. Dietrich Steinkopt Verlag. Darmstadt (page 276, fig. 117).

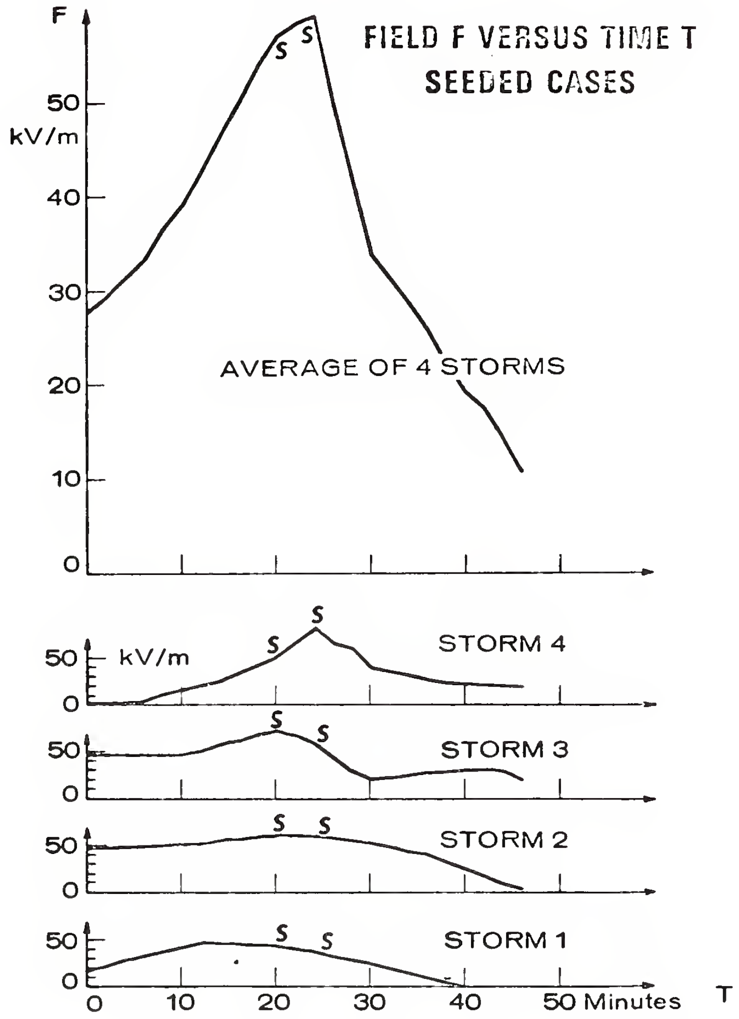

Figure 1. Field F versus time T.
Seeded cases.

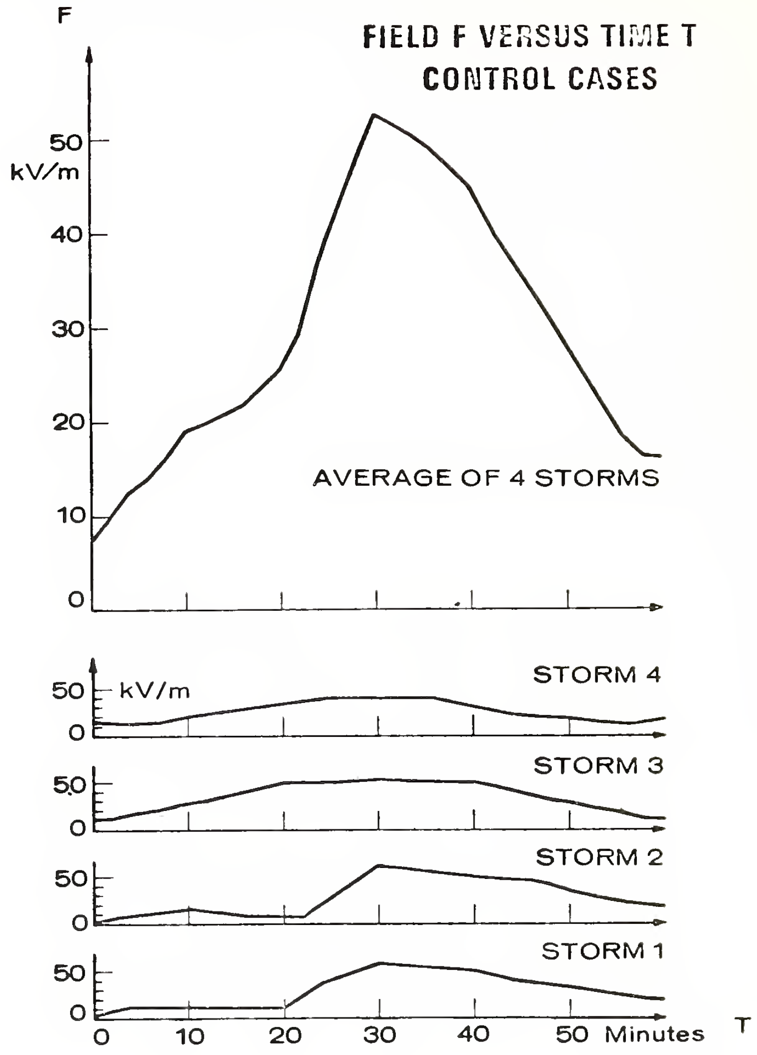

Figure 2. Field F versus time T.
Control cases.

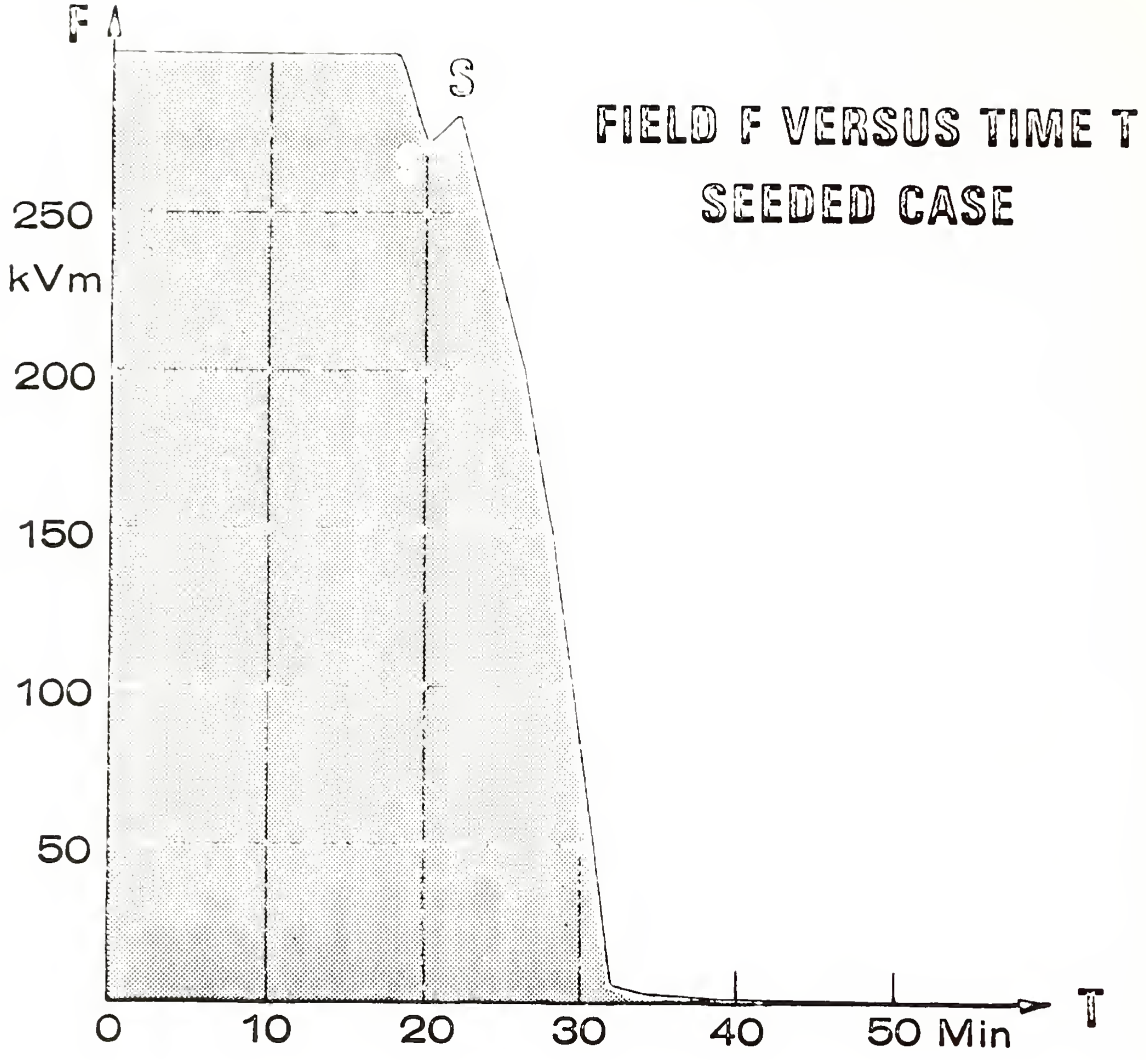

Figure 3. Field F versus time T.
Seeded cases.

Reprinted with permission of the Antarctic Journal,
September-October 1973.

Long wave antarctic radiation budget anomaly

P. M. KUHN *and* L. P. STEARNS

National Oceanic and Atmospheric Administration
Atmospheric Physics and Chemistry Laboratory, Boulder

Vertical profiles of the thermal or infrared radiation budget over South Pole Station were initiated by balloon radiometersondes (Suomi and Kuhn, 1958) during the 1959 austral winter. The radiometersonde or radiation sonde that links the "poor man's" radiometer to the conventional U.S. radiosonde provides independent observations of the upward, downward, and net (upward less downward) radiant flux or irradiance every 150 meters during balloon ascent. The atmospheric cooling (°C. day^{-1}) is derived from the divergence with height of the net radiation. These observations begin at the air-ice interface and continue upward to balloon burst (averaging some 28 kilometers).

An important feature of the research has been the use of the same design and material fabrication of the radiometersonde since its 1959 inception in antarctic research. Therefore, conclusions can be drawn concerning changes with time of atmospheric thermal radiation profiles.

A first conclusion relates to changes in the observed radiative cooling, $\Delta T / \Delta t$ (°C. day^{-1}), a function, as stated, of the divergence with height of the net radiation flux. Since 1963 this quantity noticeably has increased in the mean. One should consider the noise equivalent response of the radiometersonde or the minimum detectable change in the measured cooling due to radiation divergence. This is ± 0.4C. day^{-1} by the expression for radiative cooling derived from the first law of thermodynamics. The mean, winter antarctic (Pole Station) columnar cooling due to radiation from 500 to 100 millibars, increased by 0.25C. per day during 1963 to 1972. Since our standard error ($\delta N^{-1/2}$, where δ is the root mean square error or minimum detectable signal of the radiometersonde, ±0.4C. day^{-1}, and N is the mean number of observations of the same atmospheric layer, equal to approximately 10) is about ±0.3C. day^{-1}, the increase in cooling of 0.25C. day^{-1} statistically is significant.

The second conclusion related to atmospheric monitoring of the profiles of radiant flux and derived parameters over Antarctica, is that calculations and observations of downward directed radiant flux for the same balloon sounding show a decreasing difference (calculated minus observed flux) when the same atmospheric transmission model is employed with the same spectral resolution, 10.0 cm^{-1}, for the data of the 9-year period. In all cases aerosol effects on the downward flux are omitted, but included are mean cloudiness effects when reported for cirrus and altostratus clouds. This is accomplished by introducing a volume absorption coefficient of 1.0 x 10^{-3} cm^{-1} By adjusting this cloud volume absorption coefficient in the radiative transfer equation and assuming a droplet or particle distribution through Mie theory computations, one could conclude approximate figures for the liquid water content. This is being attempted. The question of calculated versus observed radiant flux is a long-standing problem that requires direct observations in the least contaminated atmosphere, presumably the Antarctic, to minimize the number of variables in the transmission model employed.

The inference from both conclusions is that cloud or moisture "contamination" decreased over the Antarctic from 1963 through 1972. Observations and related calculations are planned at least through 1976, in an attempt to validate this apparent change in atmospheric transmission in the infrared above Antarctica.

Reprinted with permission of the Journal of Atmospheric Sciences
Vol. 30, No. 3, April 1973.

Radiometric Observations of Atmospheric Water Vapor Injection by Thunderstorms[1]

P. M. KUHN AND L. P. STEARNS
Atmospheric Physics and Chemistry Laboratory, NOAA, Boulder, Colo. 80302

8 January 1973

1. Introduction

Radiometers have been adapted to high-flying jet aircraft for the measurement of the total water vapor in the upper troposphere and lower stratosphere above the aircraft flight level. McKinnon and Morewood (1970) accomplished the first successful radiometrically inferred water vapor aircraft observations in the stratosphere. Their results were obtained from meridional flight tracks from 70N to 40S over North and South America at aircraft altitudes of 10.7 to 18.3 km. From much lower altitudes (13 km) Kuhn *et al.* (1969) acquired radiometrically inferred water vapor overburden measurements over long traverses across the North American continent from the NASA CV-990 jet aircraft laboratory.

Recently, infrared radiometers sensitive in the 18–23 μm spectral interval have been employed to determine the water vapor budget of the high atmosphere in the vicinity of cumulonimbus clouds. The advantages of a controlled flight track over a balloon platform carrying a direct measuring hygrometer for this type of investigation is obvious. The observations, accomplished with a WB-57F aircraft of the 58th Weather Reconnaissance Squadron, U. S. Air Force, Kirtland Air Force Base, operating for the Los Alamos Scientific Laboratory, were made at specified levels up to 19 km. It is our purpose to report on the preliminary results of this continuing research effort.

2. Method of calculation

The water vapor overburden is computed from direct observations of downward emitted infrared radiation from the column of air above the zenith-directed radiometer. Emission in the 18.0–23.0 μm spectral band is due almost entirely to water vapor. Thus, received power is proportional to the optical mass of the atmospheric slabs in the field of view of the radiometer, multiplied by a weighting function depending upon temperature, pressure and wavelength. The assumption is made that the downward IR signal measured at the aircraft is due to emission from the water vapor overburden (gm cm^{-2}) distributed with a constant mixing ratio (gm gm^{-1}) above flight level.

The radiant power received by the radiometer when observing the zenith sky is given by

$$N{\downarrow}_c\,[\mathrm{W\ cm^{-2}\ sr^{-1}}] = \int_{\nu_1}^{\nu_2}\int_{p}^{p=0.1} \phi(\nu)B[\nu,T(p)]\frac{d}{dp}\tau(\nu,p,\mathrm{H_2O})\,dp\,d\nu, \quad (1)$$

where $B[\nu,T(p)]$ is the Planck function (W cm^{-2} sr^{-1} cm); $T(p)$ is temperature (°K) at pressure p (mb); $\phi(\nu)$ the spectral sensitivity of the radiometer; and $\tau(\nu,p,\mathrm{H_2O})$ the transmission of the atmosphere along a path from p_1 to p_2, a function of the pressure, temperature, water vapor mass, and the spectroscopic data for the 18.0–23.0 μm band.

Of these quantities the only unknown is the water vapor mass which, in principle, can be determined. This further assumes the existence of water vapor trans-

---

[1] This research was supported by the Office of Science and Technology, U. S. Department of Transportation and by the National Oceanic and Atmospheric Administration, U. S. Department of Commerce.

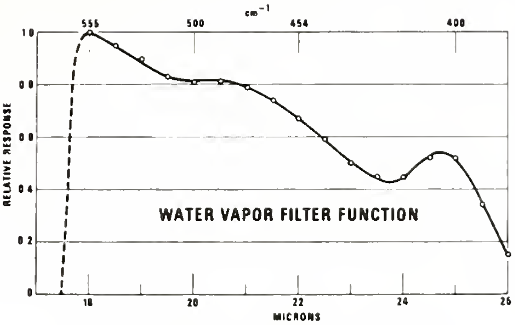

FIG. 1. Detector response function of radiometer.

missivity tables or functions versus water vapor optical mass.

Since the water vapor concentration, H_2O, is inside the integral in (1), no unique description of the variation of vapor density with height can be extracted from the power measurement. However, the calculation is not too sensitive to the form of the vertical water vapor distribution. A smooth and physically reasonable distribution is that of constant water vapor mixing ratio (gm gm^{-1}). Evaluation of the integral then gives a unique value for the overburden (gm cm^{-2}).

Implicit also is the assumption that the temperature profile above the aircraft is known and that it is not seriously disturbed above the thunderstorm cell. The temperature profile is obtained from the nearest sounding stations.

To invert the integral one assumes an initial constant mixing ratio, computes $N\downarrow_c$, and compares this with the observed $N\downarrow_0$. The difference is used to adjust the mixing ratio in that direction to reduce the difference between observed and computed radiance to a small value ϵ, the convergence criterion, i.e.,

$$|N\downarrow_c - N\downarrow_0| \leqslant \epsilon \approx 5.0\times10^{-7}\text{W cm}^{-2}\text{ sr}^{-1}; \tag{2}$$

ϵ is also known as the noise equivalent radiance of the radiometer. In practice this is done using an iterative scheme in an electronic computer. Convergence is rapid for reasonable first guesses based on experience. Tests were made assuming the upward (of the aircraft) temperature profile was in error by ±3.0C to determine errors in the inferred water vapor. It became clear that temperature anomalies in the sounding employed in (1) have much less effect on the calculated radiance do than water vapor mass anomalies, especially when considering the lower concentrations at altitudes above 16 km.

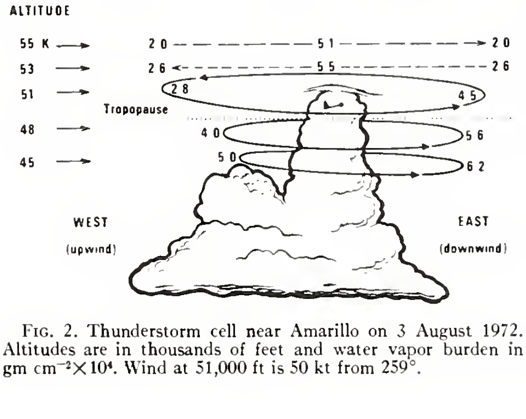

FIG. 2. Thunderstorm cell near Amarillo on 3 August 1972. Altitudes are in thousands of feet and water vapor burden in gm cm$^{-2}\times10^4$. Wind at 51,000 ft is 50 kt from 259°.

3. The instrument

The radiometer is a two-channel, pyroelectric detector bolometer sensing in the spectral bands 18.0–23.0 μm with a noise equivalent radiance of 5×10^{-7} W cm^{-2} sr^{-1}. This corresponds to a maximum water vapor burden resolution of approximately $\pm0.7\times10^{-6}$ gm gm^{-1} or $\pm0.7\times10^{-4}$ gm cm^{-2}. The 10.0–12.0 μm channel will indicate possible cirrus above flight level when its signal increases with the water vapor signal channel. In these instances water vapor inferences would not be valid. The filter spectral sensitivity of the radiometer, $\phi(\nu)$, over the band 18.0–23.0 μm (555–435 cm^{-1}) has an average relative response of 0.55. The response of the detector appears in Fig. 1.

The radiometer sampling rate is 10 sec^{-1} which is then electronically averaged for 1-sec intervals. Thus, the thunderstorm upwind values shown in succeeding figures are averages of some 350 observations.

4. Results

Two typical cases of thunderstorm cells penetrating the lower stratosphere were observed from the WB-57F in the late summer of 1972, one near Amarillo on 3 August and another west of Tucson on 7 September.

Following the calculation methods of Section 2, water vapor burden inferences at various aircraft flight levels provided data for the analyzed results illustrated in Figs. 2 and 3. Flight tracks as shown circumnavigate the cells, and the top of the troposphere is indicated. Altitudes appear to the left and water vapor burdens (gm cm$^{-2}\times10^4$) are indicated at the upwind and downwind legs of the flight tracks. Clearly, the downwind values exceed those upwind except at 53,000 and 55,000 ft (16.1 and 16.8 km). Over the center of the cell at

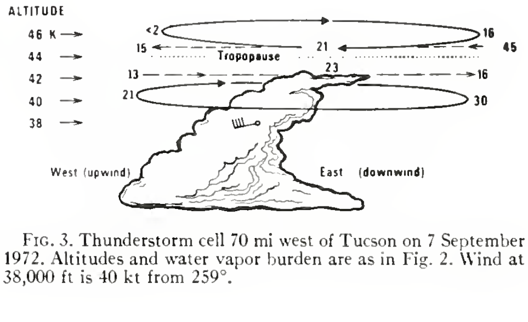

FIG. 3. Thunderstorm cell 70 mi west of Tucson on 7 September 1972. Altitudes and water vapor burden are as in Fig. 2. Wind at 38,000 ft is 40 kt from 259°.

Table 1. Mean mixing ratios (gm gm^{-1}) from the mission of 3 August 1972.

Layer (10^3 ft)	Mean mixing ratio upwind of cell	Mean mixing ratio downwind of cell
51–53	2.4×10^{-6}	18.6×10^{-6}
48–51	2.7×10^{-6}	7.2×10^{-6}
45–48	3.1×10^{-6}	2.9×10^{-6}

Table 2. Comparison of mean mixing ratios (gm gm^{-1}).

Level (ft)	Mean mixing ratio [Mastenbrook]*	Mean mixing ratio [This study]
55,000	2.40×10^{-6}	$2.20\times10^{-6}\pm0.60\times10^{-6}$
53,000	2.45×10^{-6}	$2.40\times10^{-6}\pm0.60\times10^{-6}$
49,000	$2.5\ \times10^{-6}$	$2.70\times10^{-6}\pm0.60\times10^{-6}$
46,000	$2.6\ \times10^{-6}$	$3.1\ \times10^{-6}\pm0.60\times10^{-6}$

* Values extracted from Mastenbrook (1971).

these levels we do have anomalous high values. The mean increase in the observed downwind water vapor overburden from 45,000–55,000 ft (13.7–16.7 km) over that upwind was 27% for the 3 August cell.

For the 7 September cell the downwind values again exceed the upwind at all levels as well as 2000 ft above the cell top level. The mean increase in the observed water vapor overburden from 41,000–46,000 ft (12.5–14.0 km), upwind, over that downwind was 109%. However, if one accepts the possibility of cirrus contamination of the IR signal at 45,000 ft downwind and reduces the 45×10^{-4} gm cm^{-2} overburden to a nominal 16×10^{-4} gm cm^{-2}, the increase becomes 53%. The average increase for the two storms is then 40%. Note that observations covered a total "on-storm" time of only 40 min. Hence, residence times for the water vapor additions to the lower stratosphere are not known. An attempt will be made in the Spring 1973 storm season to determine the residence time of the apparent increase in downstream water vapor by circumnavigating a single thunderstorm cell for 3 hr.

From radiance observations at different aircraft altitudes and corresponding water vapor burden changes, one can calculate the mean layer mixing ratios between flight levels from the expression

$$Q=g\Delta u/\Delta p, \tag{3}$$

where g is the acceleration of gravity, Q the mixing ratio, Δu the water vapor burden, and Δp the differential pressure (dyn cm^{-2}). The results appear in Table 1 for the mission of 3 August.

To place these optical inferences of water vapor mass in perspective, they are compared with direct frost-point hygrometer observations of Mastenbrook (1971). His observations covered a six-year period (1964–69) in the mid-latitude stratosphere and are presented in Table 2. The mean mixing ratios extracted from his results and the mean mixing ratios obtained from (upwind) background data in this study are compared. The differences between the two types of observations can be explained in at least two ways: first, the radiometer maximum resolution is $\pm0.70\times10^{-6}$ gm gm^{-1}, whereas Mastenbrook's maximum resolution is at least $\pm0.20\times10^{-6}$ gm gm^{-1}; second, Mastenbrook's observations were over the southwest United States which could result in differences due to dissimilar high-level flow patterns.

To conclude, it is evident from the limited observations in 1972 and those of 1971 (Kuhn *et al.*) that plains thunderstorms appear to increase downstream water vapor overburden near their tops. The residence time in the lower stratosphere for this increase is not known and must be determined by continuing investigations. The downstream increases, measured out to only 15 n mi from the storm cell, must also be examined at considerably greater distances downstream and at several altitudes from storm top down into the upper troposphere.

REFERENCES

Kuhn, P. M., M. S. Lojko and E. V. Petersen, 1969: Infrared measurements of variations in stratospheric water vapour. *Nature*, **223**, 462–464.

——, ——, and ——, 1971: Water vapor: Stratospheric injection by thunderstorms. *Science*, **174**, 1319–1321.

McKinnon, D., and H. W. Morewood, 1970: Water vapor distribution in the lower stratosphere over North and South America. *J. Atmos. Sci.*, **27**, 483–493.

Mastenbrook, H. J., 1971: The variability of water vapor in the stratosphere. *J. Atmos. Sci.*, **28**, 1495–1501.

Reprinted with permission of the Journal of Applied Meteorology
Vol. 12, No. 1, February 1973.

Reply

P. M. Kuhn and L. P. Stearns
Atmospheric Physics and Chemistry Lab., NOAA, Boulder, Colo. 80302

26 June 1972 and 16 October 1972

to

Comments on "Radiosonde Humidity Retrieval by Simultaneous Radiation Measurements"

D. O. Staley and B. M. Herman

Journal of Applied Meteorology
Volume 12, pp. 229-30

Our analysis of the comments of Drs. Staley and Herman indicates that, basically, they are questioning the following discussions in our publication:

1) References to computed and observed radiant flux.

2) Hygristor errors.

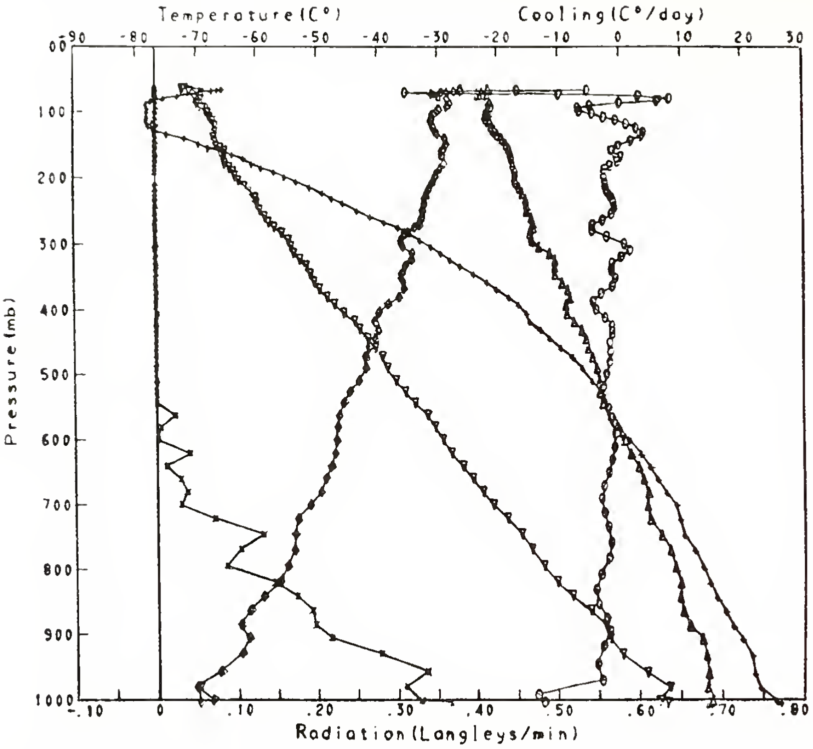

FIG. 1. Radiometersonde run for Barbados, 3 June 1969. Curves and symbols are as follows: ×'s represent humidity (gm kg^{-1}) along lower abscissa, +'s air temperature, △ upward radiant flux, ▽ downward radiant flux, ◇ net radiant flux, and ○'s represent cooling along upper right-hand abscissa.

3) Rapid moisture decreases that could be related to static stability rather than to hygristor error.

4) Reconstruction of the humidity profiles by an "iterative" radiometric method.

5) Contributions of aerosol or haze and other trace gases to the downward radiant flux.

6) Radiative transfer model. (We believe they refer to a model rather than a computer calculation.)

1. Robinson's (1950) measurements and estimates of downward radiant flux referred to *surface* measurements although one might assume that he also implied a measured vs computed *profile* discrepancy. His work took place before the introduction of the radiometersonde (Suomi and Kuhn, 1958). Kuhn and Suomi (1965) detailed this downward radiative flux profile discrepancy between observations and calculations.

2. The problems of the possible hygristor error of the U. S. radiosonde appears to us to be well enough known not to necessitate a literature review or archival listing, and indeed, this was not a study to explicitly define hygristor errors as such. Examples cited in Kuhn and Stearns (1971, 1972), unfortunately not referenced in the original study, clearly indicate that on several occasions during BOMEX the radiosonde hygristor was not functioning properly. A problem does exist and the radiometersonde observations combined with radiative transfer calculations are offered as a possible solution.

3. To assist in answering the questions raised on static stability we reproduce a temperature-moisture-radiation sounding cited as an example of hygristor deficiencies in our publication as Fig. 1. This figure, an ascent of 3 June 1969 at Barbados, does not display a correlation of rapid moisture decrease with static stability changes in the 1000–550 mb layer. Kuhn and Stearns (1971) reported and listed all BOMEX radiative transfer observations and calculations. In the subject report containing 151 temperature-moisture-radiation soundings, 49 cases of rapid moisture decrease with height were noted (32%). Of these only six (12%) could be related to static stability changes.

4. The term "iterative," cited in Section 2, refers to repetitive computer computations of the downward radiant flux by adjusting the amount of water vapor in the successive atmospheric layers until agreement is obtained between the observed and calculated flux. Input consists of three parameters—pressure, temperature, and water vapor mixing ratio. One of the series of

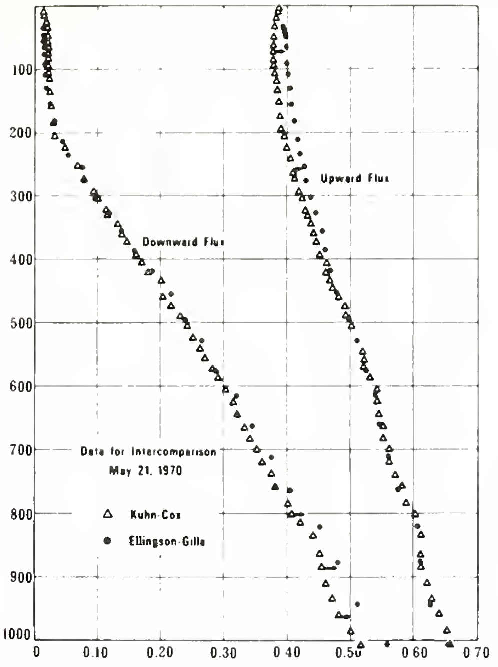

Fig. 2. Comparison of Ellingson-Gille and Kuhn-Cox models for radiative transfer of thermal flux in Canal Zone ascent.

iterations is made with a saturated water vapor profile above a point where the hygristor exhibited a sudden drop or cutoff (Fig. 4 of the original paper). Certainly, saturation would be a maximum estimate, and thus a limiting value to the calculated radiation profile. It also produced, as might be expected, a discontinuity from the original sounding with respect to moisture and hence was not considered the true moisture profile. Having established the minimum (original moisture sounding) and maximum (saturated) boundaries, we repeated the calculations by increasing the moisture using the Smith (1966) power law approximation from the level of rapid moisture decrease. When the difference between calculated and observed flux was within the convergence criterion, the iteration was stopped. As noted above, a moisture profile used as input to the calculations that produced a discontinuity from the original sounding at the level of rapid moisture decrease was disregarded. Only the smooth upward moisture profile was considered the best estimate of the final profile.

Since our publication could not be of text length, we obviously could not detail all information and explanations evidently required by Staley and Herman. These can better be communicated by personal contact. As for the Kuettner and Holland (1969) reference, the authors of the comments misconstrued our purpose in citing this reference. Our reference was to give proper credit to those who supported the BOMEX radiation program and to briefly describe the effort, and not to imply that Kuettner and Holland were comparing radiative transfer calculations and observations.

5. With reference to the capability of Harmattan haze measurements in July to produce radiative divergences in June, the authors of the comments have mistaken our intent. It was stated that island (Barbados) observers reported the haze during the 3 June period. The comment on the July observations of the deep haze layer from the first high altitude aircraft (CV-990) was intended to emphasize the frequent presence and depth of the layer even through July.

During this research effort numerous observations and calculations of the effects of atmospheric haze were made for another project. We will report these conclusions employing mass absorption coefficients (cm^2 gm^{-1}) and volume absorption coefficients (cm^{-1}) for atmospheric cirrus and haze and atmospheric attenuation. However, in the subject publication four references to haze effects on the transfer calculations were made in Section 4.

6. The transmission model employed in the radiative flux calculations is basically the Elsasser (1960) periodic model. The absorption coefficients for water vapor are those of Möller and Raschke (1964), as stated, taken from Yamamoto (1952), covering the 6.3 μm band of water vapor, 1160–2120 cm^{-1}, and the rotational band of water vapor, 200–800 cm^{-1}. The absorption coefficients are listed in the cited reference. They are not the absorption coefficients upon which the Elsasser chart data are based.

In the spectral regions where active absorption bands of two or more absorbers overlap each other, 520–800 cm^{-1} for carbon dioxide and water vapor, and 840–1140 cm^{-1} for ozone and the water vapor window, the multiplicity formulation (Goody, 1964) is employed to determine the total transmissivity. The spectral transmissivity τ is determined by the product of the spectral transmissivities of the individual constituents

$$\tau_\nu = \tau_{\nu_1}\cdot\tau_{\nu_2}\cdot\tau_{\nu_3}\cdots\tau_{\nu_m}, \qquad (1)$$

where the subscripts refer to the specific transmission functions of the n active gasses in the spectral interval ν. We did inadvertently omit the ozone integral in the original publication and it should have been listed in Eq. (1) as

$$\cdots\cdot - \int_0^\infty \int_{\tau=1.0}^{\tau} B(\nu,T)d\tau(u_{O_3})d\nu,$$

where the symbols are listed in the publication, and u_{O_3} refers to the optical mass of gaseous ozone (gm cm^{-2}). In computing the contribution of ozone to the total downward and upward flux we used the data of Walshaw (1957) giving the integrated absorption of the entire 9.6 μm band (840–1140 cm^{-1}).

As for radiative contributions of trace gases neither our model nor the radiometer can bring such a contribution out of the general noise level. The pressure correction for the optical depth employed in the model used was that of Curtis-Godson in the form

$$p_{\mathrm{eff}} = \int p\,du \Big/ \int du, \tag{2}$$

where p is pressure (mb) and u optical mass (gm cm^{-2}).

An error analysis of the calculations may be made by reference to Fig. 3 of the original publication. The calculated downward radiant emittance (CDE) is slightly more than 30% of the measured downward emittance (MDE). In view of the fact that we employ the Curtis-Godson pressure correction we (i) consider gaseous absorption overlap, (ii) do not use the Elsasser chart absorption data, and (iii) calculate emission from ozone; we assume a further error of 10% in our, or for that matter any, radiative transfer calculations. This appears to be one-half of the recovered radiant flux. Aerosol emission could account for one-half of the latter, or 5%. At the worst we could then have recovered 5% of the total flux discrepancy between measured and calibrated radiation and this recovery should be due to water vapor emission. Admittedly, error assessment without an accepted standard is difficult at best. We would suggest continued comparisons between more precise measurements and calculations and certainly serial radiometric profiles.

Finally, we compare two flux calculations employing the same pressure, temperature and water vapor mixing ratio profiles from a radiometersonde ascent of 7 May 1970 in the Caribbean at 12°30′ by 80°00′W (see Fig. 2). The Ellingson-Gille, 57 interval (1972) model follows the approach of Rodgers and Walshaw (1966) while the Kuhn-Cox model (1972)[1] is a modified Elsasser and Culbertson (1960) calculation. Ellingson and Gille included several trace gases in their model while we did not. The agreement is quite good in spite of the basic differences in the calculations. This might emphasize the fact that differences in independent models are less than measured-observed differences.

---

[1] Personal communication.

REFERENCES

Elsasser, W. M., and M. F. Culbertson, 1960: Atmospheric radiation tables. *Meteor. Monogr.*, **4**, No. 23, 43 pp.

Goody, R. M., 1964: *Atmospheric Radiation: Volume I. Theoretical Basis.* London, Clarendon Press, 436 pp.

Kuettner, J. P., and J. Holland, 1969: The BOMEX project. *Bull. Amer. Meteor. Soc.*, **50**, 394–402.

Kuhn, P. M., and L. P. Stearns, 1971: Radiative transfer observations and calculations during BOMEX. NOAA Tech. Rept. ERL 203-APCL 19, 171 pp.

——, and ——, 1972: Radiosonde humidity retrieval by simultaneous radiation measurements. *J. Appl. Meteor.*, **11**, 130–135.

——, and V. E. Suomi, 1965: Airborne radiometer measurements of effects of particulates in terrestrial flux. *J. Appl. Meteor.*, **4**, 246–252.

Möller, F., and E. Raschke, 1964: Evaluation of TIROS III radiation data. NASA Contract Rept. CR-112, University of Munich, Germany, 84 pp.

Robinson, G. D., 1950: Note on the measurement and estimation of atmospheric radiation, 2. *Quart. J. Roy. Meteor. Soc.*, **76**, 37–51.

Rodgers, C. D., and C. D. Walshaw, 1966: The computation of infrared cooling rate in planetary atmospheres. *Quart. J. Roy. Meteor. Soc.*, **92**, 67–92.

Smith, W. L., 1966: Note on the relationship between total precipitable water and surface dew point. *J. Appl. Meteor.*, **5**, 726–727.

Suomi, V. E., and P. M. Kuhn, 1958: An economical net radiometer. *Tellus*, **10**, 160–163.

Walshaw, C. D., 1957: Integrated absorption by the 9.6μ band of ozone. *Quart. J. Roy. Meteor. Soc.*, **83**, 315–321.

Yamamoto, G., 1952: On a radiation chart. *Sci. Rept. Tohoku Univ., Ser. 5*, No. 4, 9–23.

Reprinted from NOAA Technical Report ERL 253-APCL 25,
57 pages, February 1973.

OBSERVATIONS OF THE VERTICAL TRANSPORT OF WATER VAPOR, OZONE, AND AEROSOLS BY THUNDERSTORMS

Peter M. Kuhn[1], Walter D. Komhyr[2], Thomas B. Harris[2],
Paul A. Allee[1], and W. E. Marlatt[3]

The purpose of this field study was to determine the amount of water vapor and particulate matter transported into the stratosphere by thunderstorms in the Plains as well as to investigate the increases in ozone concentration beneath the tropopause in areas of thunderstorm activity. Carbon dioxide measurements were also made to augment information on the mixing process. Measurements of water vapor show an average stratospheric water vapor mass of 9.8×10^{-4} g cm^{-2} to which a typical thunderstorm added 11.2×10^{-4} g cm^{-2} at an altitude of 41,500 feet. Small increases in ozone were observed in areas of thunderstorm activities, corresponding to about a 2-percent change in ozone in a vertical column of the atmosphere above 33,000-feet altitude. The ozone data were, however, inadequate to distinguish between downward transport of ozone from the stratosphere and possible production of ozone by electrical discharges in the clouds. A combination of an ozone high and a carbon dioxide low that occurred during the final flight, not in an area of thunderstorm activity, was interpreted as significant evidence for mixing of stratospheric air into the troposphere. Aitken nuclei counts observed in areas of thunderstorm activity were remarkably high. Maximum concentration measured around the La Crosse, Wis., storm at 40,000 feet of altitude was 7,000 nuclei/cm^3, while typical values around the Grover, Colo., storm at about 42,000 feet of altitude were approximately 20,000 nuclei/cm^3

Reprinted with permission of the Journal of Applied Meteorology
Vol. 12, September 1973.

A Numerical Model of the Effects of Seeding on the Evolution of a Lake-Effect Storm

E. L. Magaziner

Atmospheric Physics and Chemistry Laboratory, NOAA, Boulder, Colo. 80302

(Manuscript received 13 February 1973, in revised form 24 May 1973)

ABSTRACT

The simulation of crystal growth by diffusion and by accretion of cloud droplets is incorporated into the Lavoie mesoscale numerical model for lake-effect storms. The model also allows simulation of seeding and its effect on changing the precipitation growth mode from riming to diffusion. Precipitation particle trajectories are computed so that the effects of seeding on snowfall distribution can be simulated. The model's predictions agree well with observations of nonseeded cases and, in terms of computer time, the model is sufficiently practical to allow experimentation with various seeding strategies under various meteorological conditions. Numerical seeding experiments with the model indicate that optimum seeding strategies can shift the characteristic localized heavy snowfalls to areas where their effect will be less damaging.

1. Introduction

Heavy localized accumulation of snowfall on the lee shores of Lake Erie, caused by lake-effect snowstorms, has prompted weather modification efforts since at least 1965 (McVehil and Peace, 1965, 1966; McVehil *et al.*, 1967, 1968). These efforts have been primarily directed at modifying the distribution of snowfall by seeding with ice nuclei. The underlying concept is to decrease the fall velocity of precipitation particles. Horizontal advection would then distribute the snowfall more widely (Eadie *et al.*, 1971). Experiments in 1968–69 demonstrated that seeding increased the number of elementary snow crystals and decreased or eliminated riming (Layton, 1969; Warburton and Owens, 1969; Eadie, 1970; Jiusto and Holroyd, 1970; Lavoie *et al.*, 1970). No experiments have yet been performed where the snowfall distribution of an intense snowstorm was modified.

The intensity and snowfall distribution of a lake-effect snowstorm is the result of a complex interaction between local (in addition to synoptic scale) meteorological factors, such as lake-air temperature difference, prevailing wind speed and direction, and topographical features. Successful numerical experiments with the single-layer Lavoie model (Davis *et al.*, 1968) of mesoscale effect on the cold airflow over Lake Erie revealed subtle and unexpected perturbations of the wind field over the lake which indicate that a simple upwind seeding strategy is unsatisfactory for snowfall redistribution attempts. The design of an effective lake-effect snowfall redistribution project would be greatly enhanced by a numerical model in which various prevailing conditions and seeding methods can be combined and simulated. Such a numerical model must 1) emphasize the horizontal mesoscale dimension, the domain where the seeding is to eventually have an effect; 2) incorporate a physical model of snowfall production with both accretional and diffusional growth, so that seeding can be simulated; 3) be capable of simulating dispersal and advection of seeding material; 4) include computation of precipitation trajectories consistent with particle fall velocities and horizontal advection, since these are primary determinants of the snowfall distribution; and 5) be *practical* in terms of computer requirements and cost to allow fairly unrestricted experimentation with various seeding strategies. This paper describes a model that attempts to meet these five requirements.

The computer programs for the model were implemented to operate in an interactive graphics mode. The numerical experimenter worked at an interactive computer terminal containing a keyboard on which he could specify a seeding method. The computer's response would appear in a few tens of seconds as graphical output on a CRT display showing the snowfall distribution or any other desired model parameters.

2. Modeling the mesoscale disturbance

The well-known lake-effect numerical model developed by Lavoie (Davis *et al.*, 1968; Lavoie, 1972) is well suited for the numerical experiment. Details of this model cannot be discussed here, but an excerpt from the abstract to the Lavoie paper provides the background:

> The atmospheric structure upwind of the Great Lakes during arctic air outbreaks is represented by three layers: a lower con-

> stant flux layer in contact with the ground, a well-mixed planetary boundary layer surmounted by an inversion, and a deep stratum of overlying stable air. The set of primitive equations is averaged through the depth of the mixed layer to yield predictive equations for the horizontal components of velocity, potential temperature, and specific humidity in the layer and the height of the inversion. Interactions between the well-mixed convective layer and both the underlying and overlying layers are parameterized so that time-dependent calculations can be limited to a single layer. Precipitation from cumulus clouds within the layer is represented in terms of the mesoscale variables and latent heat is included.
>
> The equation set has been solved numerically for a 2,000 point grid mesh centered on Lake Erie. Grid separation was 6 km in the cross-lake direction and 12 km along the lake axis. Initial conditions were specified to be balanced and everywhere uniform. Terrain influences, surface roughness and temperature variations, and moisture fluxes were then allowed to perturb the mixed layer until the resulting mesoscale disturbance approached a steady state.

In this model, the practicality criterion is met by limiting time-dependent calculations to a single well-mixed layer whose interactions with its surroundings are parameterized. Thus, this model lacks vertical structure, but it does contain the necessary horizontal detail in the form of forcing functions that include the effects of topography and surface fluxes of momentum, heat and moisture. The specific humidity calculations and the parameterization of convective clouds and precipitation used by Lavoie are replaced by a new moisture and precipitation scheme. This scheme adds predictive equations for mixing ratio and liquid water content, diagnostic equations for lifting condensation level (cloud base height) and precipitation, and parameterized expressions for temperature lapse rate and natural ice nucleus concentration. Source terms for release of latent heat are added to the potential temperature equation.

3. Incorporation of moisture and precipitation processes

a. Basic concept

The simulation of precipitation growth in cold clouds is a very complex problem, especially because of the multitude of growth habits of ice crystals, as influenced by temperature, liquid water content, and updraft structure. Lavoie *et al.* (1970) have developed models attempting to account for this complexity by computing the growth of ice crystals as they fall through a highly structured cloud. This approach is impractical in the present context. The moisture and precipitation calculations in this paper modify and extend the work of Eadie *et al.* (1971), in which crystal growth equations are integrated over the mesoscale model's layer at each time step during the integration of the primitive equations.

b. Conservation of moisture

Moisture in the model is allowed to take one of three forms: water vapor, liquid cloud water, and frozen precipitation. Water vapor content is represented by r, the height-average mixing ratio for the layer. Liquid water content is measured by Q, the total mass of cloud water in a unit column of the layer. Precipitation is measured in terms of the precipitation rate per unit horizontal area.

Precipitation and evaporation from the lake surface comprise the sink and source of moisture for the layer; thus, moisture mass conservation in a unit column of the layer takes the form

$$\frac{d}{dt}(r\bar{\rho}h+Q)=\text{Evaporation}-\text{Precipitation},$$

where

$$\frac{d}{dt}\equiv\frac{\partial}{\partial t}+\mathbf{v}\cdot\nabla,$$

and $\bar{\rho}$, h and $\mathbf{v}$ are mean density, height of the column (inversion height), and horizontal velocity respectively. Condensation is introduced to separate vapor from liquid water (the terms Evaporation, Condensation, and Precipitation are fluxes when capitalized):

$$\frac{d}{dt}(r\bar{\rho}h)+\frac{d}{dt}Q=\text{Evaporation}-\text{Condensation}+\text{Condensation}-\text{Precipitation}.$$

This yields two equations

$$\frac{d}{dt}(r\bar{\rho}h)=\text{Evaporation}-\text{Condensation},$$

$$\frac{d}{dt}Q=\text{Condensation}-\text{Precipitation}.$$

Implicit in these relations are the following assumptions.

1. The sole source of water vapor is evaporation from the lake surface. Estimation of the evaporation of cloud water and sublimation of precipitation particles are not explicitly considered.

2. The sole sink of water vapor is condensation, which occurs as moist parcels are lifted by mesoscale updrafts. Crystal growth by diffusion is allowed, but we assume that the moisture source for this growth is the evaporation of the liquid cloud water, and not the available water vapor. This is consistent with the first assumption because evaporation of water is not computed. We only assume that precipitation particles grow at the expense of available liquid water.

3. Precipitation is the only sink for liquid water. As stated in No. 2, an intermediate vapor stage may exist, but the vapor produced is entirely dedicated to forming precipitation.

4. The condensation produced by lifting is the only source of liquid water. Melting of precipitation is not

considered because the lake storms in question are too cold for this to occur.

5. In the absence of liquid water, the precipitation rate cannot exceed the rate at which condensation and advection supply liquid water. This is a necessary corollary of moisture conservation and the previous assumptions.

Evaporation from the lake measured as a flux is parameterized using the bulk aerodynamic method also used by Lavoie (1972) and Eadie *et al.* (1971):

$$\text{Evaporation} = \begin{cases} C_E |\mathbf{v}| \bar{\rho}(r_s - r), & \text{over the lake} \\ 0, & \text{over the land} \end{cases}$$

where C_E is a dimensionless drag coefficient equal to the drag coefficients for heat and momentum used in the Lavoie model, $|\mathbf{v}|$ the wind speed, and r_s the saturation mixing ratio at lake surface temperature.

The condensation mechanism is considered as a process in which moist parcels are lifted by the mesoscale updrafts. Upon reaching cloud base c (the lifting condensation level computed from the mixing ratio r and the potential temperature), the vapor in the parcels begins to condense. The standard computations of the condensation rate based on updraft velocity and the derivative of saturation mixing ratio with height were found to underestimate condensation. Eadie *et al.* (1971) also found that this approach yields much smaller precipitation amounts than those observed. The approach taken here is to consider a unit column of the cloud deck $c \leqslant z \leqslant h$ as a water vapor condensor. The condensation efficiency, CE, should increase with the thickness of the cloud deck and should be enhanced by mixing in the model's layer. The parameterization chosen for CE is

$$CE = \frac{h^2 - c^2}{h^2},$$

which simultaneously takes into account cloud deck thickness and the decrease of mixing with height. For example, a deck 2 km thick with its top at 4 km has an efficiency of 0.75. The condensation rate is then the product of vertical transport of water vapor mass and condensation efficiency, i.e.,

$$\text{Condensation} = \begin{cases} r\bar{\rho}\bar{w}\dfrac{h^2 - c^2}{h^2} \\ 0, \quad \text{when } \bar{w} < 0 \text{ or } h \leqslant c \end{cases}$$

where $\bar{\rho}$ and $\bar{w}$ are mean density and updraft. The equation for conservation of potential temperature contains a term to account for the latent heat released in this condensation process.

c. Modeling of precipitation

The precipitation modeling employs growth equations for individual precipitation particles. Two processes are considered: the mass growth of falling crystals by accretion of supercooled cloud droplets, and the mass growth of ice crystals by diffusion of water vapor.

The equations used for this mass growth are (Jiusto, 1971)

$$\frac{dm}{dt} = \pi R^2 E l v, \quad \text{for accretion,} \tag{1}$$

$$\frac{dm}{dt} = 8RGS_i\rho_i, \quad \text{for diffusion (planar unrimed).} \tag{2}$$

In the accretion equation, m is the mass of the growing crystal, R its radius, E the collection efficiency (assumed to be unity), l the liquid water content, and v the fall velocity of the crystal relative to the cloud droplets. In the diffusion equation, the crystal habit is assumed to be planar unrimed, G is a temperature-dependent thermodynamic quantity accounting for latent heat and vapor diffusivity (see Fletcher, 1966), S_i the supersaturation with respect to ice, and ρ_i the density of ice.

The quantities involved in these growth equations are expressed in terms of those predicted by the model, using the following relations (all quantities are in cgs units):

$$l = \frac{Q}{h - c} \tag{3}$$

$$v = \begin{cases} 210R^{0.3}, & \text{for accretion [McVehil } et\ al.\text{, 1967]} \\ 30, & \text{for diffusion [Nakaya, 1954]} \end{cases} \tag{4}$$

$$m = \begin{cases} 0.52R^3, & \text{for accretion} \\ 0.00152R^2, & \text{for diffusion} \\ & \text{[Nakaya and Terada, 1935]} \end{cases} \tag{5}$$

$$G = G(\text{temperature}) \text{ [Fletcher, 1966].} \tag{6}$$

The supersaturation S_i is computed from the ratio

$$\frac{e_{sw}}{e_{si}} = \frac{\text{saturation vapor pressure over water}}{\text{saturation vapor pressure over ice}},$$

using values of e_{sw} and e_{si} vs temperature from the *Smithsonian Meteorological Tables* (List, 1966). The relation

$$S_i(T) = -0.010417\ T$$

is a very good approximation for T in the range 0 to −30C. This relation, combined with the result (Jiusto, 1971) that the supersaturation drops very rapidly to 1–2.5% (depending on the updraft velocity) in the absence of liquid water (see Fig. 1), result in the following computation for S_i:

$$S_i = \begin{cases} -0.010417T, & \text{when } Q > 0 \\ -0.0058\bar{w}^2 + 0.0258\bar{w}, & \text{when } Q = 0 \end{cases} \tag{7}$$

where $\bar{w}$ is the average updraft in the cloud deck (m sec^{-1}) and T is in degrees Celsius. The temperature is computed in terms of the potential temperature predicted by the model and a lapse rate whose somewhat involved derivation appears later.

Substitution of Eqs. (3)–(7) into (1) and (2), and replacement of v by dz/dt, allows each of the two growth equations to be written in the form

$$dM = f dz,$$

where f is some function of the quantities already predicted by the model, and M is the total mass of crystals at level z given by $M = mn$; n is the crystal number density (the determination of n must be discussed later, since it depends on the temperature). The integration over appropriate portions of the model's layer can now be performed as follows. In the absence of liquid water, accretional growth does not occur, and the diffusional growth equation is integrated from h to c, the entire cloud deck. This will be called the D process and M_D' will denote the precipitation mass density at cloud base resulting from this process. In the presence of cloud droplets, diffusional growth is allowed to occur from h to $(h+c)/2$, and from this point down to c, the accretional growth mode is also allowed to operate. This will be referred to as the A process and M_A' will denote the precipitation mass density at cloud base resulting from the accretion process. The integrated mass growth for the D process reveals that the mass at $(h+c)/2$ is $\frac{1}{4}M_D'$; hence, the actual precipitation mass densities M_A and M_D resulting from the competition of the A and D processes are computed as

$$M_A = M_A', \quad M_D = \begin{cases} \dfrac{1}{1+3M_A'/M_D'} M_D', & \text{for } M_A' \leqslant M_D' \\ \frac{1}{4} M_D', & \text{for } M_A' > M_D' \end{cases}$$

This describes either process when its occurring alone and provides a smooth transition from process D to process A, as the liquid water content increases from zero. Finally, precipitation is computed as

$$\text{Precipitation} = M_A V_A + M_D V_D,$$

where V_A and V_D are the respective fall velocities of particles as they reach cloud base. Because of this layer-integrated calculation of precipitation, the calculation of horizontal advection begins as the particles fall out at cloud base. Now they no longer interact with any of the processes, and their trajectories from cloud base to the surface are computed in terms of the mesoscale wind field and fall velocities. The effect of snowflake aggregation on the fall velocity of crystals grown by diffusion is accounted for by using the results of the model by Jiusto (1971). These results are in the form of graphs of the number of crystals per snowflake as a function of cloud crystal concentration and the size of individual crystals, quantities that are known in the model. Jiusto also provides an empirical relation for converting this information into terminal fall velocities.

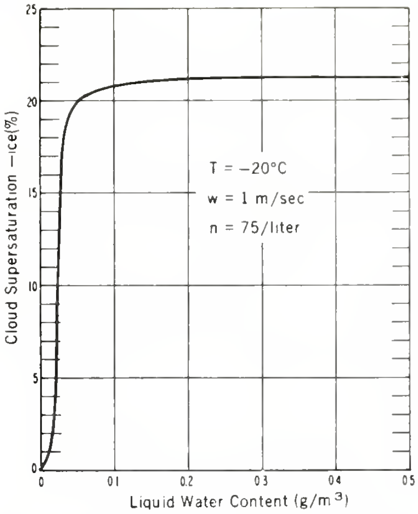

FIG. 1. Typical liquid water-supersaturation relationship, computed from Jiusto's (1971) results: T is temperature, w updraft speed, and n crystal concentration.

d. Modeling of seeding

Now we develop an expression for n, the crystal number concentration. The expression

$$n_a = 10^{-5} e^{-0.6T},$$

is given by Flectcher (1966) for the number of natural ice nuclei per liter active at temperature T (°C). The number n_s of artificial nuclei at a point on the mesoscale grid of the model depends on the nuclei introduced by seeding at that point and also on the advection of nuclei from seeded regions upwind. The standard advection expression

$$\mathbf{v} \cdot \nabla n_s$$

cannot be used in the model because the coarseness of the finite-difference grid (6 km×12 km) does not allow realistic dispension of seeding material and produces severe artificial diffusion. Instead, the seeding nuclei are introduced at exactly the desired points, each of which is then translated by the wind field, and a radial diffusion of 1.5 m sec^{-1} (Weickmann, 1957) is allowed to occur in the translating coordinate system of each seeded point. The crystal number concentration is then assumed to be

$$n = n_a + n_s.$$

e. Derivation of temperature lapse rate

We must finally develop an expression for the temperature at each level z in terms of the potential

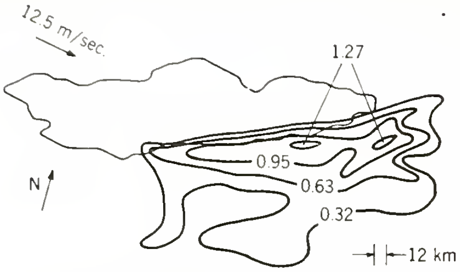

Fig. 2. Observed average precipitation rate (mm hr^{-1}, melted) for 1–2 December 1966. (From Lavoie, 1972.)

temperature predicted by the model. A constant temperature lapse rate is assumed at each point of the mesoscale grid; however, this lapse rate is allowed to vary from point to point in the grid, and at each grid point it is allowed to vary with time. A prerequisite of the mesoscale model is that its moist layer be well mixed; hence, the lapse rate must be between dry and moist adiabatic, and in the calculations it is initialized to 7.5C km^{-1}. Heating of the layer at a point of the grid is caused by advection of heat, flux of heat from the lake surface, and release of latent heat during condensation and precipitation formation. The most intense heating effect is the release of latent heat and, in fact, numerical experiments with a fixed lapse rate led to computational instability: the release of latent heat by precipitation formation lifts the cloud tops into colder regions, increasing the number of naturally active ice nuclei, which in turn accelerate precipitation and heat release, and so on.

The instability is controlled by using a variable lapse rate of temperature. The physical motivation is in the observation that warming by latent heat is not uniform throughout the layer but occurs in the upper portions of the cloud deck; this, therefore, has the effect of decreasing the lapse rate by an amount proportional to the rate of heat release. The following formulation models the phenomenon that latent heat released in the upper portions of the layer cannot instantaneously mix throughout the entire layer. It is assumed that the lapse rate $\gamma_0=7.5\text{C km}^{-1}$ is modified by a quantity ϵ, i.e.,

$$\gamma=\gamma_0-\epsilon,$$

which is determined by a conservation of heat calculation. Let $\Delta\theta$ be the increase in potential temperature of a unit column of the layer after complete mixing. The conservation of heat is expressed as

$$h\bar{\rho}k\Delta\theta=\int_0^h \bar{\rho}k\epsilon z dz,$$

where h is the depth of the layer, $\bar{\rho}$ its mean density, k a heat capacity constant, and the heating is linearly distributed in the column, being zero at its base and maximum at its top. Integration with constant mean density and heat capacity yields

$$\epsilon=\frac{2\Delta\theta}{h}.$$

The resulting expression used for the lapse rate γ is

$$\gamma=\gamma_0-\frac{2\dfrac{d\theta}{dt}\Delta t}{h},$$

where $d\theta/dt$ is the rate of potential temperature increase caused by latent heat release, and Δt is the time step used in the integration of the primitive equations.

4. Example of a numerical seeding experiment

The following example uses the model to illustrate a numerical experiment aimed at determining a seeding strategy for alleviating heavy snowfall at Buffalo, N. Y., on the east end of Lake Erie.

The initial values of the model's parameters are taken, with a few modifications, from the well-documented severe lake-effect storm of 1 and 2 December 1966, which remained in nearly steady state for 30 hr. The information was obtained from Lavoie (1972), who used this case for comparison to his numerical predictions. The observed precipitation pattern is illustrated in Fig. 2, which depicts the average precipitation rate during the 30-hr storm. The most important parameters, those with high positive correlation to the intensity of a lake-effect disturbance (Wiggins, 1950), are slightly modified to obtain a precipitation maximum over Buffalo, N. Y.: 1) an air-lake temperature differ-

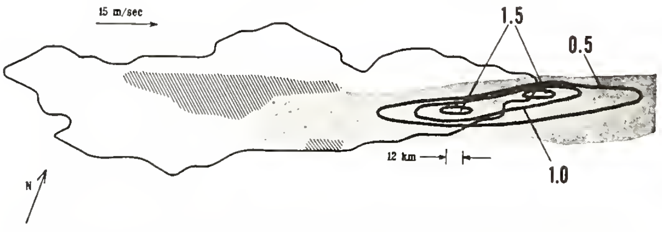

Fig. 3. Predicted precipitation (mm hr^{-1}, melted). Cross-hatched areas indicate primarily diffusional crystal growth, screened areas primarily riming growth.

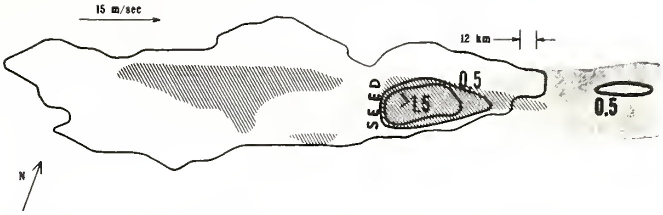

Fig. 4. Predicted precipitation (mm hr^{-1}, melted) after seeding for 1 hr with maximum concentration of 100 nuclei liter^{-1}. Dominant growth mode is indicated as in Fig. 3.

ence of 12C; 2) a maximum length of wind fetch over open water, that is, along the long axis of the lake; and 3) a low-level wind speed of 15 m sec^{-1}.

The model equations were integrated for 6 hr of meteorological time using a 200-sec time step after which the disturbance reached a steady configuration. Fig. 3 shows the precipitation pattern for the steady-state solution. The precipitation rate contours agree well with those of Fig. 2 when the modifications (different wind direction, higher wind speed, and fetch over open water) are considered. The total snowfall area is divided into the two types of snowfall production incorporated into the model; the cross-hatched areas indicate primarily diffusional growth, screened areas primarily accretional growth. The two cross-hatched regions in Fig. 3 are caused by very shallow cloud decks, whose low condensation efficiency cannot produce enough liquid water to support accretional growth.

The numerical integration is then continued for an additional hour of meteorological time during which seeding is simulated. Nuclei are dispersed at an initial concentration of 100 nuclei liter^{-1} for 1 hr along the line segment covered by the letters "SEED" in Fig. 4.

The snowfall pattern after the hour of seeding appears in Fig. 4. This particular seeding location was chosen after experimentation in an attempt to meet the following criteria. First, the snowfall maximum at Buffalo must be eliminated. Second, the snowfall rate about 30 km or more downwind should *not* be affected, so that the ski industry would not be endangered. Finally, the domestic and industrial water supply should be enhanced by piecipitating as much moisure as possible back into the lake.

An examination of Fig. 4 reveals that, at least theoretically, this type of selective modification is possible. Immediately downwind of the seeded line, the crystal growth mode is changed from riming to diffusion. The seeding materials disperse quickly as they are advected downwind, but due to the considerable horizontal convergence (see Fig. 5) the effect is channeled into a "tongue" reaching the lake shore. The precipitation rate 10–15 km downwind from the seeded line seems to be limited only by the number of freezing nuclei, because the rapid and convergent wind channels considerable moisture into that region. This feature appears to conflict with the original concept mentioned in the Introduction, in which seeding eliminates heavy rimed particles in favor of flakes that drift further inland. The parameterization of crystal fall velocities and the inability to trace the trajectories of crystals until they reach cloud base may explain the discrepancy. The snowfall rate on Buffalo is reduced to less than 0.15 mm hr^{-1}. The snowfall type and rate 30 km inland and beyond is essentially unchanged. It appears that the mesoscale geographical features are sufficiently structured and influential to allow this type of control over precipitation distribution.

How lasting is the effect of such seeding? The integration was continued for several more meteorological hours with no more seeding. Fig. 6 shows the precipitation pattern 1 hr after cessation of seeding. The storm has not yet returned to its previous steady-state configuration, especially with respect to the snowfall rate on Buffalo, which is still less than one third of its original value. An additional hour is required before the steady-state features are recovered.

5. Conclusions

It appears possible to incorporate the essential features of snowfall redistribution by seeding into a mesoscale model. The resulting model was used to predict precipitation patterns that agreed well with several documented cases. A hypothetical case indicates that the model may be successfully used to perform nu-

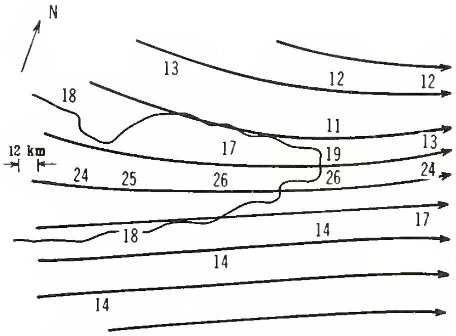

Fig. 5. Wind speed and streamlines (m sec^{-1}).

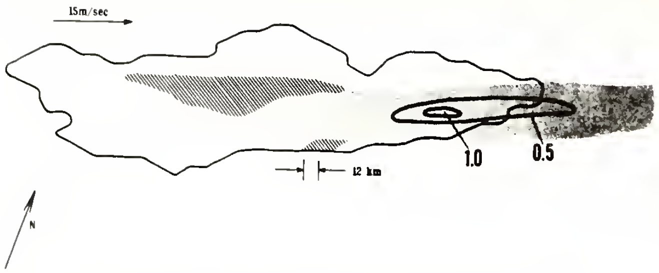

FIG. 6. Predicted precipitation (mm hr^{-1}) 1 hr after seeding has stopped. Dominant growth mode is indicated as in Fig. 3.

merical seeding experiments under any prevailing meteorological conditions. The results of such experiments can lead to optimum seeding strategies, perhaps not too accurate in terms of seeding rates, but useful in terms of the locations at which seeding should be performed.

Improvement of the model can best be achieved when it is used with an actual seeding program. Some of the model's parameterizations (especially the computation of the fall velocities and the trajectory starting points for crystals) can probably be significantly improved by empirical means, leading to an acceptably accurate and very useful tool. Since this type of model is applicable not only to Lake Erie but also to other areas of the Great Lakes Basin, it may be a valuable asset to a precipitation modification program in that area.

REFERENCES

Davis, L. G., R. L. Lavoie, J. I. Kelly and C. L. Hosler, 1968: Lake-effect studies. Final Report, Contract E22-80-67(N), Dept. of Meteorology, Pennsylvania State University.

Eadie, W. J., 1970 The experimental modification of lake-effect weather. Final Report, Contract E22-7-69(N), Cornell Aeronautical Laboratory, Inc., Buffalo, N.Y.

——, R. J. Pilié and W. C. Kocmond, 1971: Modification and modeling of lake-effect weather. Final Report, Contract E22-39-70(N), Cornell Aeronautical Laboratory, Inc., Buffalo, N.Y.

Fletcher, N. H., 1966: *The Physics of Rainclouds*. Cambridge University Press.

Jiusto, J. E., 1971: Crystal development and glaciation of a supercooled cloud. *J. Rech. Atmos.*, **5**, No. 2, 69–85.

——, and E. W. Holroyd, 1970: Great lakes snowstorms, Part 1. Cloud physics aspects. Report, Grant E22-49-70, Atmospheric Sciences Research Center, State University of New York at Albany.

Lavoie, R. L., 1972: A mesoscale numerical model of the lake-effect storm. *J. Atmos. Sci.*, **29**, 1025–1049.

——, W. R. Cotton and J. B. Hovermale, 1970: Investigations of lake-effect storms. Final Report, Contract E22-103-68(N), Dept. of Meteorology, Pennsylvania State University.

Layton, R. G., 1969: Lake effect snow: A study of snow crystals in great lakes snowstorms. Final Report, Subcontract 24-6002-A, State University College of New York at Fredonia, N.Y.

List, R. J., 1966: *Smithsonian Meteorological Tables*, 6th ed. Smithsonian Institution, Washingron, D.C.

McVehil, G. E., and R. L. Peace, Jr., 1965: Project lake effect—A study of the interactions between the Great Lakes and the atmosphere. Final Report, Contract DA-28-043-AMC-00306(E), Cornell Aeronautical Laboratory, Inc., Buffalo, N.Y.

——, and ——, 1966: Project lake effect—A study of lake effect snowstorms. Final Report, Contract CWB-11231, Cornell Aeronautical Laboratory, Inc., Buffalo, N.Y.

——, J. E. Jiusto, R. A. Brown and R. L. Peace, Jr., 1967: Project lake effect—A study of lake-effect snowstorms. Final Report, Contract E22-49-67(N), Cornell Aeronautical Laboratory, Inc., Buffalo, N.Y.

——, C. W. C. Rogers and W. J. Eadie, 1968: The structure and dynamics of lake-effect snowstorms. Final Report, Contract E22-89-68(N), Cornell Aeronautical Laboratory, Inc., Buffalo, N.Y.

Nakya, U., 1954: *Snow Crystals: Natural and Artificial*. Harvard University Press, Cambridge, Mass.

—, and T. Terada, 1935: Simultaneous observations of mass, falling velocity and form of individual snow crystals. *J. Fac. Sci., Hokkaido Univ.*, Ser. 2, **1**, 191–200.

Warburton, J. A., and M. S. Owens, 1969: Silver analysis in lake-effect studies—Lake Erie Experiments, 1968. Final Report, Contract E22-9-69(N), Desert Research Institute, University of Nevada, Reno.

Weickmann, H., 1957: Current understanding of the physical processes associated with cloud nucleation. *Beit. Phys. Atmos.*, **30**, 97–118.

Wiggin, B. L., 1950: Great snows of the Great Lakes. *Weatherwise*, **3**, 123–126.

Reprinted with permission of the Journal of Atmospheric Sciences
Vol. 30, No. 2, March 1973.

The Effect of Hailswath Structure on Hail Suppression Experiments

E. L. Magaziner and H. K. Weickmann
Environmental Research Laboratories, NOAA, Boulder, Colo. 80302

17 July 1972 and 1 December 1972

ABSTRACT

The mesoscale, individual-hailstreak structure of hailswaths can markedly affect the analysis of hail suppression experiments that are based on protecting a given area from approaching hailswaths. Calculations reveal that such an experiment may (depending on the size of the protected area and on hailstreak length) be counted as a success even when the hail suppressing activity is ineffective. This phenomenon may have contributed to serious errors in the evaluation of the pilot test program in hail suppression conducted in the Soviet Union during 1961–63, on which consequent programs were based.

1. Introduction

Considerable information has become available about the Operational Hail Suppression Experiments in the Soviet Union, specifically in the Caucasus. Several books and/or reports have been written by Prof. Sulakvelidze (1965, 1968a) and exchange visits between Russian, American, and Canadian scientists have taken place with fruitful discussions of the subject matter. Yet it has not been possible to obtain a clear appraisal of the validity of the results.

It appears that three efforts are underway in the Soviet Union. One is carried out through the Academy of Sciences of the Georgian SSR and the Central Aerological Observatory. These experiments are conducted in the Alazanskaya Valley in the Caucasus, and the research is connected with the names I. I. Gaivoronskii, Jr., A. Seregin and G. S. Voronov. Another effort by the same Academy of Sciences through its Institute of Geophysics in Tbilisi, USSR, is carried out by A. I. Kartsivadze and his collaborators. Finally, what appears to be the largest effort is carried out by the High Altitude Institute of the Hydrometeorological Service in Nalchik, USSR, under the direction of G. K. Sulakvelidze and his co-workers.

All experiments appear to be designed in similar fashion: a hail forecast, a radar analysis and identification of the hail spawning area in the cloud, and the delivery of the seeding agent into the hailcloud. The delivery is different among the three groups—rockets are being used by the former two, grenades and guns by the latter. The forecasting skill was developed so that special experiments could be carried out to *prevent* the development of impending hail formation.

Other experiments were carried out to *stop* hail that was falling. Russian scientists (Federov, 1967) state that in 1966 more than one million hectares (10,000 km^2) were protected. Hail damage in the protected area was reported to be three to five times less than in the unprotected area; therefore, the cost for the protection amounts to barely 2–3% of the value of the crops protected (Federov, 1967). [Figures for reduction of hail damage quoted by Sulakvelidze (1968a) are more nearly 4–6:1.] For 1966 the total expenditure for protection was 620–980 thousand rubles, and the computed economic effect was a saving of 24 million rubles (Sulakvelidze, 1967a). Hail protection using rockets in 1967 in the Alazanskaya Valley in the Caucasus allowed damage over only 551 hectares for 100,000 hectares of protected area, while the natural hail damage amounted to 4784 hectares in the 100,000 hectares surrounding the protected crop (Gaivoronskii *et al.*, 1968).

In spite of these impressive figures, enough uncertainty remains to make a realistic assessment of the hail suppression technique very difficult. It appears that the inherent great complexity of the field experiments provides much latitude for interpretation as long as the experiments are not strictly randomized. This circumstance may have led to errors in the analysis phase of a series of feasibility experiments during the initial period 1961–63.

Another great handicap for western observers is the unknown type of storms. Damage paths of several to hundreds of kilometers and hailstorm cells "in the rear part of the cloud relative to the direction of motion" have been reported (Gaivoronskii *et al.*, 1968). The period of a hail-cell development cycle is said to average 15 min and rarely exceeds 30 min. This agrees well with these authors' visual observations in northeast Colorado. Therefore, one can only assume that the storms are not of the kind that occur in the heart of the Great Plains of the United States., but rather are similar to those that occur along the periphery in the west and north, i.e., in Colorado, Nebraska, Wyoming, and the Dakotas.

As reported by Sulakvelidze (1968b), before 1961 research in the mechanism of the hail process yielded a design for a hail suppression experiment. This experiment was carried out in 1961–63 over an area of 30,000–50,000 hectares. The area was instrumented with 400 hail collectors and pluviographs. He reports that "in the period of 1961–1963 75 experiments were carried out, of which 19 were performed to stop the hail falling and 56 were preventive ones. All the experiments yielded positive results. The hail did not fall over the protected area." After this test had "yielded positive results over a small territory, it was decided to apply the method . . . for the protection of large territories" [Sulakvelidze, 1968b, p. 799; similar quotations are in Sulakvelidze (1967a)].

2. The probability of obtaining positive results by chance

If this experiment was, as it seems to have been, the basic field test to decide operational applicability of the method, then we must realize that the void of statistical design subjects the evaluation of the results of this experiment to possible gross errors. The following calculations are intended to illustrate that evaluation procedures for hail suppression experiments that are based on protecting a given area from approaching hailswaths must be very carefully designed.

Consider an experiment in which a circular area of radius r_1 is to be protected from hailswaths that threaten to enter it. Assume that all hailswaths within a ring of outer radius r_2, concentric to the protected area but not including it, are considered (Fig. 1).

Assume also for simplicity that the width of a hailstreak is small compared with its length, and that the origin within the ring as well as the direction of motion (a straight line) occurs at random. The probability that a hailstreak of length l, whose direction of motion is such that if it continues it will enter the protected area, may be computed as follows:

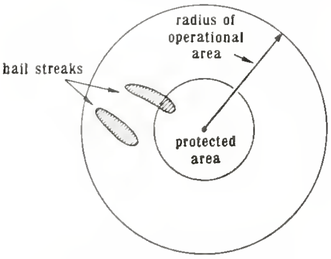

FIG. 1. Schematic of protected area.

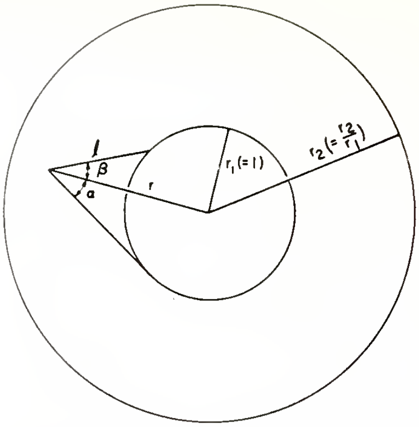

FIG. 2. Diagram illustrating the meanings of the symbols used in the computations.

For normalization purposes, let $r_1=1$. The ring with outer radius r_2 may be divided into three sections:

1. $1 \leqslant r \leqslant (l^2+1)^{\frac{1}{2}}$
2. $(l^2+1)^{\frac{1}{2}} \leqslant r \leqslant l+1$
3. $l+1 \leqslant r \leqslant r_2.$

By simple geometry, it is seen that a hailstreak with origin in Section 1 which threatens the protected area will indeed intersect it and we assign to this section the probability $p(r)=1$. In Section 2, $p(r)$ may be computed as the ratio of two angles α and β. From the diagram (Fig. 2) one can see that $\sin\alpha=1/r$ and $\cos\beta=[1-(r^2+l^2)]/2rl$. Hence in Section 2 we have

$$p(r)=\frac{\cos^{-1}\left[\dfrac{1-(r^2+l^2)}{2rl}\right]}{\sin^{-1}(1/r)}.$$

In Section 3 it is obvious that $p(r)=0$. Now, if A_0 is the area of the total ring, the desired probability $p(l,r_2)$ is a function of l and r_2 and is given by

$$\begin{aligned}p(l,r_2)&=\int_1^{r_2} p(r)\frac{2\pi r dr}{A_0}=\int_1^{(l^2+1)^{\frac{1}{2}}} p(r)\frac{2\pi r dr}{A_0}\\&\quad+\int_{(l^2+1)^{\frac{1}{2}}}^{l+1} p(r)\frac{2\pi r dr}{A_0}=\int_{l+1}^{r_2} p(r)\frac{2\pi r dr}{A_0}\\&=\frac{l^2}{r_2^2-1}+\int_{(l^2+1)^{\frac{1}{2}}}^{l+1} p(r)\frac{2\pi r dr}{A_0}+0.\end{aligned}$$

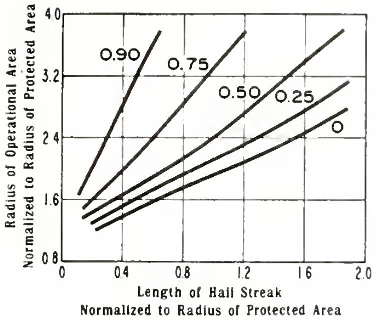

FIG. 3. A plot of $1-p(l,r_2)$ vs l and r_2

Now, given a distribution of hailstreak lengths, characterized by the probability function $q(l)$, the probability $Q(r_2)$ that a hailswath originating in the ring will actually intersect the protected area is given by

$$Q(r_2)=\int_l p(l,r_2)q(l)dl.$$

Fig. 3 is a plot of $1-p(l,r_2)$ vs l and r_2, that is, it yields, for each l and r_2, the probability that a threatening hailswath will terminate from natural causes without entering (i.e., can either stop short or bypass) the protected area.

Let us now relate these calculations to Sulakvelidze's experiment. According to Sulakvelidze (1967a), the size of the protected area in the pilot test case mentioned above was 30,000–50,000 hectares, and the guns that fire the seeding shells had an effective range of about 12 km. Sulakvelidze does not provide any information on the size of the operational area or the placement of the guns, so let us assume that he positioned the guns in the most advantageous fashion possible. This would locate the guns at $(r_1+r_2)/2$, a position that maximizes his opportunity to fire at oncoming hailswaths. This gives, for convenience in our example, a protected area of radius about 9.8–12.6 km, and normalized for an average protected radius of 11.2 km, $r_2=35.2/11.2=3.15$. Sulakvelidze provides no data on the size of l, so let us assume that his conditions were similar to those Changnon (1968) found in Illinois where the average hailstreak length was 16.3 km. This gives the normalized value $l=16.3/11.2=1.46$. If, for simplicity, we assume that all of the hailstreaks were of this length, Fig. 3 gives a probability of about 0.50. This means that about one-half of the threatening hailstreaks would have terminated from natural causes before entering the protected area. This, of course, means that if in the experiment the non-entering of a threatening swath was counted as a success, then the experiment would have been declared a success even if the seeding treatment had no effect.

For another example that has longer hailstreaks, we may use Changnon's (1968) report from South Dakota, where the average streak length was 24.4 km. This yields a normalized value $l=24.4/11.2=2.18$, and we obtain from Fig. 3 a probability close to 0. This means that practically none of the threatening hailswaths would terminate from natural causes before entering the protected area, rendering the claim of success more acceptable. The important features of Fig. 3 may be summarized as follows:

The probability of obtaining positive results by chance is increased by 1) decreasing the radius of the protected area, 2) decreasing the hailstreak length, or 3) increasing the radius of the operational area.

3. Concluding remarks

It must be mentioned that this critical state of affairs creeps into the experiments only if hail does not fall as a continuous swath, but as intermittent streaks. The streak character of hailfall should be considered in the evaluation of these experiments. We feel it is quite possible that an error of this type has continued to propagate into the subsequently conducted large-scale experiments in the Caucasus, because apparently only "a part of the area on both the protected and comparison plots . . . was evaluated" (Sulakvelidze, 1968b).

REFERENCES

Changnon, J. A., 1968: Summary of 1967 hail research in Illinois. Res. Rept. No. 39, Crop-Hail Insurance Actuarial Association, Chicago, Ill., 35 pp.

Fedorov, E. K., 1967: The artificial modification of meteorological processes. Report for the World Meteorological Congress, 5th Congress, Geneva, Cg-V/Doc. 63, Appendix C.

Gaivoronskii, I. I., J. A. Seregin and G. S. Voronov, 1968: Investigations of hail processes and their artificial modifications in flat region of the USSR. *Proc. Intern. Conf. Cloud Physics*, Toronto, Canada, 760–767.

Sulakvelidze, G. K., 1967a: On the principles of hail control method and the results of the hail prevention research. Manuscript of lecture at General Assembly, IUGG, Lucerne, Switzerland.

——, 1967b: Findings of the Caucasus antihail expedition (1965). National Science Foundation, Washington, D. C., 60 pp.

——, 1968a: *Rainstorms and Hail*. Jerusalem, Israel Program for Sci. Transl. (NTIC, Springfield, Va., TT68-50466).

——, 1968b: On the principles of hail control method applying in the USSR. *Proc. Intern. Conf. Cloud Physics*, Toronto, Canada, 796–803.

——, N. Sh. Bibilashvili and V. F. Lapcheva, 1967: Formation of precipitation and modification of hail processes. National Science Foundation, Washington, D. C., 208 pp.

Reprinted with permission of the Journal of Applied Meteorology
Vol. 12, No. 3, April 1973.

Electron-Microscopic Study of Silver Iodide as Contact or Sublimation Nuclei[1]

FARN P. PARUNGO
Environmental Research Laboratories, NOAA, Boulder, Colo. 80302

(Manuscript received 18 September 1972, in revised form 4 December 1972)

ABSTRACT

Experiments of ice nucleation by silver iodide were conducted in a cold chamber at various temperatures. The seeded ice crystals were replicated and an examination of the position of AgI nuclei in individual ice crystals was made using an electron microscope. The mechanism of ice nucleation is discussed.

1. Introduction

In cloud seeding experiments silver iodide is widely used as an ice nucleation agent, yet the mechanism by which it acts as a nucleating agent is still not well understood. There are four different roles which ice nuclei can play to initiate the ice phase (Gokhale, 1969): 1) at ice supersaturation AgI can act as a sublimation nucleus by converting water vapor to ice; 2) at water supersaturation AgI can serve as a freezing nucleus by condensation of water on its surface, followed by crystallization; 3) it is embedded in a droplet acting as bulk freezing nucleus; and 4) it can play a role as a contact nucleus by the crystallization process upon contact of an AgI particle with the supercooled droplet. The relative importance of these mechanisms at different conditions have been studied by Cwilong (1949), Schaefer (1954), Birstein (1955), Mossop (1956), Edwards and Evans (1960), and Balabanova and Zhigalovskaya (1962).

Silver iodide is a hydrophobic substance. It can serve as a condensation-freezing nucleus if it contains hydrophilic impurities, such as sodium iodide. Also, silver iodide can act as a bulk-freezing nucleus if it is prewetted. When pure and dry AgI aerosols are used as ice nuclei, the major mechanism should be considered as either contact or sublimation nucleation. Weickmann *et al.* (1970) suggested that crystals with a center circle could be traced back to their origin from a frozen droplet and that AgI particles acted as contact nuclei rather than sublimation nuclei even at temperatures as low as −17C. To add credence to the understanding of contact nucleation, it is the purpose of this study to search for evidence of coalescence between an AgI particle and a supercooled droplet followed by initiation of freezing and subsequent ice-crystal growth.

If an AgI particle acts as a contact nucleus, it collides with a supercooled drop and initiates ice-crystal growth (Gokhale and Lewinter, 1971). Thus, an AgI particle should be at the boundary of the drop and would be found anywhere in the projected-center frozen droplet in the replica. If condensation-freezing or bulk-freezing nucleation is the case, the nucleus could also be located anywhere within the droplet. However, in this case, the AgI particle could dissolve either partly or completely in the embedded droplet, depending on the size of the particle, to yield an AgI solution. When such an ice crystal sublimes during the process of replication, the initial droplet would leave a dark center circle of AgI residue in the replica. If AgI serves as a sublimation nucleus, it should be at the *c* axis of the nucleated ice crystal and should be found at the center of the symmetry of the ice crystal. Therefore, by examination of an individual AgI nucleus in relation to an individual ice crystal, one may clarify their mode of origin. To accomplish this, it is necessary to study ice crystal replicas with an electron microscope.

2. Experiment

Silver iodide aerosol was produced by electrically heating an AgI coated nichrome wire (Sax, 1970) and was stored in an aluminized Mylar bag. The concentration of the aerosol was approximately 20,000 liter^{-1}. Their size distribution was obtained from an electron microscopic analysis of thermal precipitator samples. Approximately 90% of all the particles were less than 0.1 μm and 50% were less than 0.01 μm in diameter. Seeding experiments were carried out in a cold chamber whose temperature could be controlled within ±2C. A cloud was formed by introduction of moisture into the chamber from an atomizer. When the condition in the cold chamber had stabilized, silver iodide aerosol which was freshly prepared in the bag was introduced into the chamber to produce ice crystals. Moisture was supplied continuously during the experiment to keep it in water supersaturation except in one case which was specified.

---

[1] Part of this study was presented at the Third Conference on Weather Modification at Rapid City, S. D., on 16 June 1972.

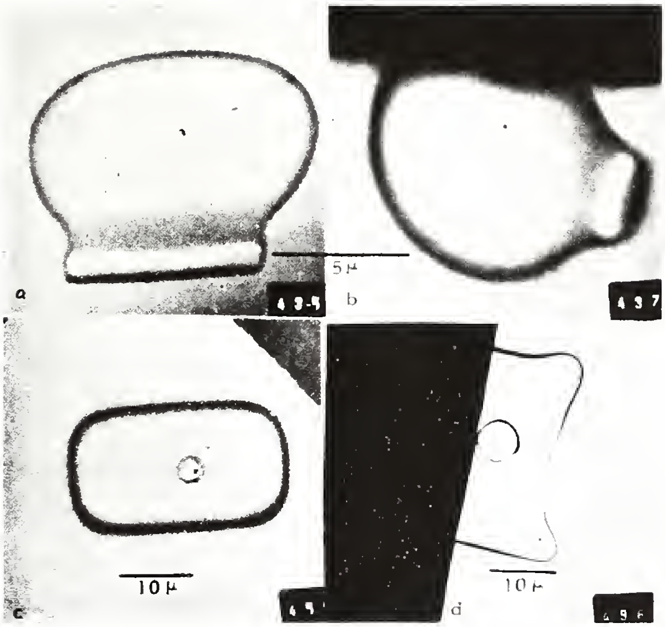

FIG. 1. Silver iodide seeded ice crystals obtained at −8C: (a) and (b) frozen drops; (c) and (d) columns.

In order to obtain an ice-crystal replica which can illustrate its detailed structure and also be thin enough to allow passage of an electron microscope beam, a technique developed by Schaefer[2] was adopted as follows: The sampling screens (200 mesh) were coated with 1% collodion solution in amylacetate and set on a slide. The slide with the screens on it was then dipped in a 0.25% Formvar solution in ethylene dichloride and allowed to dry. This doubly coated slide was placed on the bottom of the cold chamber to receive the AgI seeded snow crystals. A 50-ml beaker with chloroform-wetted filter paper at the bottom was then cooled below 0C and used to cover the sampling slide for 30 sec. Thus, a cold chloroform vapor was generated in the beaker to dissolve the top layer of Formvar on the screens, causing the Formvar to migrate over the ice crystals and replicate them on the supporting collodion film. Precautions which were taken to prevent any possible movement of an AgI nucleus during the replication are as follows: The slide with replicas remained in the cold chamber for at least 4 hr to allow the completion of ice-crystal sublimation; and before the slide was removed from the cold chamber, a warm slide was used to cover the replicated slide in order to avoid the condensation of moisture on the replicas and thus possibly move the nuclei. After warming up to room temperature, the screens were removed from the slide and were ready for examination by the electron microscope.

TABLE 1. Percentage of ice crystals at various temperatures.

	Temperature ±2C					
Type of crystals examined	−8	−12	−16	−20	−24	−18*
	40	112	50	150	200	64
Plate with a nucleus in the center circle	—	70	80	90	30	20
Plate with a center nucleus	—	—	—	10	15	70
Solid column	50	20	20	—	10	10
Hollowed column	30	10	—		30	—
Bullet	—	—	—	—	10	—
Needle	20	—	—	—	5	—

* At ice supersaturation.

3. Results and discussion

The experimental results are summarized in Table 1. For each experimental temperature, 10 sampling screens were used to collect the AgI-seeded ice crystals. The replication method yielded a fine and detailed structure for a thin or small crystal. However, a large column whose thickness could retard the flow of Formvar solution over the whole crystal usually produced a poor replica. The crystal habit of the seeded ice crystals generally followed Nakaya's diagram. At temperatures above −10C there were frozen drops, needles and columns. Four selected electron micrographs are shown in Fig. 1: (a) and (b) are frozen drops with an enclosed particle which subsequently grew to an

---

[2] Private communication, 1967.

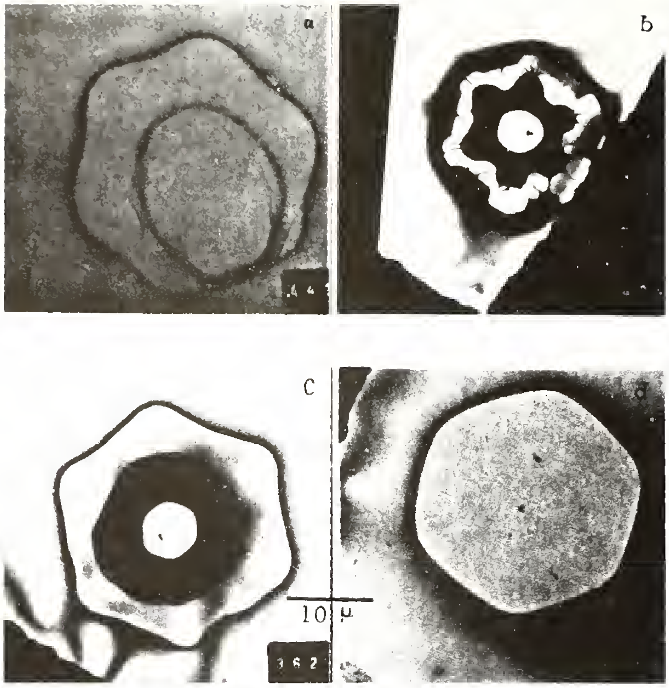

Fig. 2. Ice crystals obtained at (a) −12C, (b) −16C, (c) −20C, (d) −20C.

ice crystal, while (c) and (d) are column ice crystals with a center circle containing a particle. It appears that the crystallization origin depends on the collision and coalescence of a supercooled water drop and an AgI nucleus. When the temperature was between −10 and −20C, the majority of ice crystals observed were hexagonal plates as shown in Fig. 2: (a) at −12C, (b) at −16C, (c) at −20C. In each of these crystals, there was a center circle with a particle in it. It again shows that contact nucleation is the dominant mechanism. However, at −20C, 10% of the observed crystals did not have a circle but possessed a nucleus at their center of symmetry as shown in Fig. 2(d). This gives the impression that the AgI particle acted as a sublimation nucleus. Indeed, when an experiment was carried out at −16 to −20C, at ice supersaturation produced by discontinuing the supply of moisture after excess seeding by AgI aerosol, 70% of the ice crystals received did not possess a center drop as shown in Fig. 3. The AgI nucleus was at the center of the hexagonal symmetry indicating the role of sublimation nucleation. However, when the experiment was attempted at a temperature between −10 and −14C, no ice crystals were obtained after the moisture supply was cut off. This suggests that sublimation nucleation was not active at temperatures > −14C.

Ice crystals formed at temperatures of −24 to −26C are shown in Fig. 4: (a) and (b) are examples of hexagonal plates with a center circle. They contribute approximately 30% of the total ice crystals observed; the nucleus is not at the center of the crystal but in the boundary of the projected center frozen drop. Fig. 4(c) shows a solid column crystal with a circle along its *c* axis and with an AgI particle in the circle (10%). Crystals shown in Figs. 4(a)–(c) can be identified as contact ice nucleation origin. Fig. 4(d) is a hexagonal plate with a nucleus at the center of the crystal symmetry but without a center circle (15%). It may trace back to sublimation nucleation origin. Figs. 4(e) and 4(f) show two hollowed columns (30%). One can observe that they contain a frozen drop in the center of the column and contact nucleation plays a role in nucleation of the ice phase. Figs. 4(g) and 4(h)

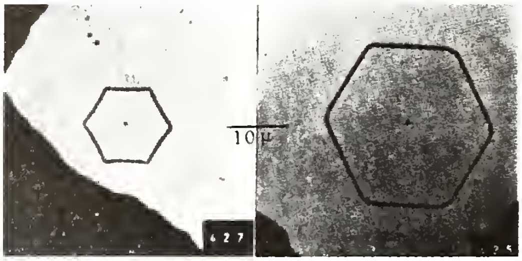

Fig. 3. Ice crystals obtained at −18C at ice supersaturation.

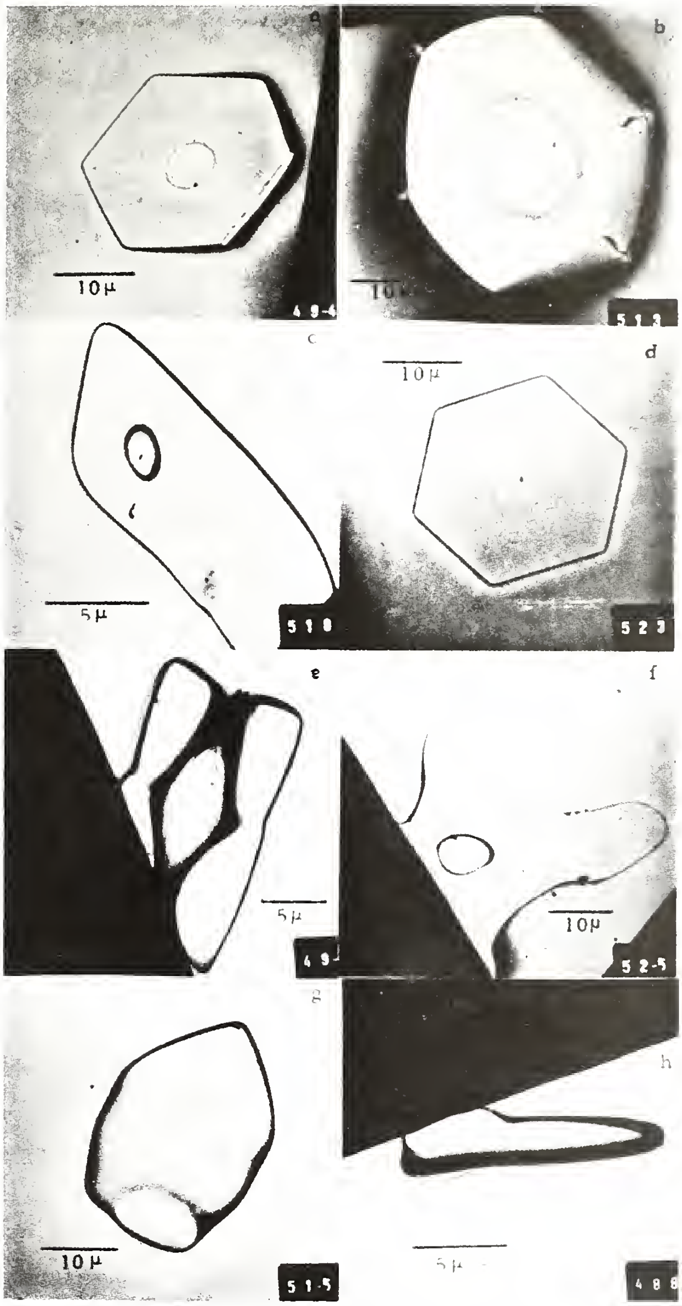

FIG. 4. Ice crystals obtained at −24C. See text for explanation.

are bullet crystals. The oval-shaped shadow at the end of the crystal might be the imprint of a droplet which may have been the initiate of the crystal growth. However, a particle found at the tip of the bullet shown in Fig. 4(g) leads one to believe that the crystal formed from the tip (10%). When this crystal fell on the sampling film, the tip of the bullet lay over the film for a distance of half of the bullet width. It would

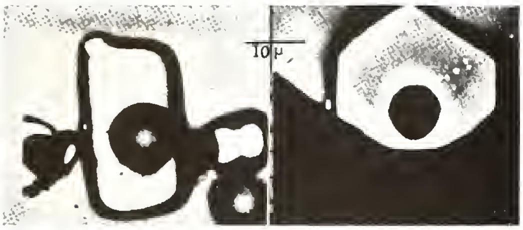

Fig. 5. Ice crystals with clouded circles: (a) obtained at −8C, (b) at −24C.

be difficult to produce a detailed replica of this portion. This may be the reason why no frozen drops can be observed at the tip.

In very rare cases, ice crystals possessed a clouded circle as shown in Fig. 5. It appeared that the original droplet dissolved either an AgI nucleus or other impurity before the crystallization to leave such an opacity circle. Therefore, the nucleus might be considered as condensation-freezing nucleus.

4. Conclusion

Experiments of ice nucleation by silver iodide were conducted in a cold chamber at various temperatures. An electron microscope was used to examine the ice crystal replicas. When the temperatures were above −20C and at water supersaturations, the majority of the ice crystals possessed a center circle containing an AgI particle. It was evident that contact nucleation was a dominant mechanism. However, when the temperature was lower than −16C and the humidity decreased to ice supersaturation, a large portion of the ice crystals did not show a center circle and the AgI nucleus was always found at the crystal's center of symmetry. This indicates that sublimation nucleation took place. Based upon the electron-microscopic study of the seeded ice crystal replicas, one may distinguish the modes of origin of ice nucleation.

Acknowledgments. This study was directed by Dr. Helmut Weickmann. The author would like to express her appreciation to Dr. Jan Rosinski of NCAR for the use of NCAR's electron microscope and Mr. Clarence Nagamoto for his assistance on electron-microscopic techniques.

REFERENCES

Balabanova, V. N., and T. N. Zhigalovskaya, 1962: On the use of silver iodide in the crystallization of supercooled water. *Izv. Akad. Nauk SSSR, Ser. Geofiz.*, 904–906.

Birstein, S. J., 1955: The role of absorption in heterogeneous nucleation. *J. Meteor.*, **12**, 324–331.

Cwilong, B. M., 1949: Sublimation in out-door air and seeded sublimation. *Nature*, **163**, 727–728.

Edwards, G. R., and L. F. Evans, 1960: Ice nucleation by silver iodide: Freezing vs sublimation. *J. Meteor.*, **17**, 627–634.

Gokhale, N. R., 1969: The mechanics of ice nucleation induced by AgI particles in a supercooled cloud. *Proc. 7th Intern. Conf. Condensation and Ice Nuclei*, Prague and Vienna, Publ. House Czech. Acad. Sci., 200–205.

——, and O. Lewinter, 1971: Microcinematographic studies of contact nucleation. *J. Appl. Meteor.*, **10**, 469–473.

Mossop, S. C., 1956: Sublimation nuclei. *Proc. Phys. Soc.*, **B69**, 161–164.

Sax, R. I., 1970: Drop freezing by Brownian contact nucleation. Ph.D. thesis, University of London.

Schaefer, V. J., 1954: Silver and lead iodide as ice crystal nuclei. *J. Meteor.*, **11**, 417–419.

Weickmann, H. K., U. Katz and R. Steele, 1970: AgI—Sublimation or contact nucleus? *Preprints. Second Conf. Weather Modification*, Santa Barbara, Calif., Amer. Meteor. Soc., 332–336.

Reprinted with permission of the International Conference on Nucleation,
Leningrad, USSR, September 23-29, 1973.

Elemental Identification of Natural and Artificial Ice Nuclei

Farn P. Parungo and Rudolf F. Pueschel
National Oceanic and Atmospheric Administration
Atmospheric Physics and Chemistry Laboratory
Boulder, Colorado 80302

Introduction: Atmospheric aerosols can act as heterogeneous nuclei to initiate precipitation and thus effect the weather. Man's contribution to the atmospheric aerosol budget has been unintentional as well as intentional. Not only has he used artificial ice nuclei for modifying the weather, but also his activities have inadvertently contributed 10% of the total global aerosols. For an accurate evaluation of the effects of nucleating materials and air pollutants on the weather, a quantitative relationship must be established between the precipitation elements (rain and snow) and the elemental composition of the nuclei upon which they develop.

To characterize the particulates by their sizes, shapes, and chemical compositions in the precipitation in order to determine their origins, there is the need to obtain maximum information from a large number of individual particles in the minimum amount of time. An optical microscope is a useful technique for identifying particles larger than a few microns. A transmission electron microscope can provide a resolution less than 10Å, but the use of electron diffraction as an identification technique is suitable only for crystalline particles and is of limited use when studying with complete unknowns. A scanning electron microscope (SEM) interfaced with an X-ray energy spectrometer (XES) can visualize a particle less than 250Å and analyze all elements it contains. A collimated field emission electron beam strikes the specimen. The beam scans in a raster pattern across the specimen's surface; it is synchronized with a cathode-ray tube that maps the surface onto the display screen. Simultaneously, the incident electron beam generates characteristic X-ray protons that enter a Si (Li) detector which measures the X-ray energy directly. A spectrum of counts versus energy in keV is displayed on the screen. Since this technique is simple, rapid, and accurate, it is well suited for analyzing particulates within the precipitation.

Specimen preparation: For collection of natural crystals, a piece of black velvet was laid out in an open field. The crystals of interest were transferred (with a toothpick) from the velvet onto a dry SEM specimen stud (diameter 18 mm) which had been coated with 2% Formvar in ethylene dichloride and cooled below freezing. Then a beaker with chloroform-wetted filter paper at the bottom was inverted over the stud for 30 seconds. Thus the chloroform vapor dissolved the Formvar on the stud and replicated the ice crystals on it. The specimen was left in a cold enclosed environment for 4 hours; this allowed the snowcrystals to sublime slowly and completely so that all the particles in the ice crystal would remain in the same position.

For collection of artificial ice crystals, silver iodide (AgI) was used to seed clouds in a cloud chamber. The Formvar coated studs were placed at the bottom of the chamber and received the ice crystals directly. The replication process was identical to that for the natural snowcrystals. The stud with ice crystal replica was then inserted in the SEM specimen chamber for examination and X-ray analysis.

Results and Discussion: Figure 1a shows the SEM image of an AgI seeded ice crystal that originated from a droplet. Figure 1b is the XES focused on the particle that is visable in the center droplet. The peak at 3 keV indicates the presence of silver; the peak at 4 keV indicates iodine. Figure 1c shows an SEM image of another AgI seeded ice crystal. No particle is visible in the center droplet; however, when the electron beam scaned the droplet area, it gave a spectrum (Figure 1d) indicating that AgI particle was enclosed in the center droplet. The expanded spectrum resolves the silver peak at 3 keV as a combination of L line ($L_\alpha = 2.978$, $L\beta = 3.151$) and iodine is indicated by a series of peaks near 4 keV. ($L_\alpha = 3.93$, $L\beta_1 = 4.22$, $L\beta_2 = 4.51$). These results show that the SEM combined with XES can identify AgI as an ice nucleus in an artificial nucleation experiment. Figure 2a shows an example of natural snowcrystals collected on 24 March 1973. Its nucleus gives the X-ray energy spectrum shown in Figure 2b. The particle contains multi-elements (Na, Mg, Al, Si, S, and Cl) and is possibly of marine origin.

Conclusion: Since the XES can detect a particle with a mass as low as 10^{-17} gram and the SEM resolution is 250Å, the combination of these two techniques is suitable for the following studies:

1. Inventorying natural nuclei and their origins.
2. Identifying modes of nucleation (deposition, condensation freezing, or contact).
3. Studying the scavenging efficiency of precipitation (snowcrystal or raindrop).
4. Determining — during a cloud seeding experiment, — whether the precipitation in the target area is actually caused by the seeding material.

Our laboratory is engaging in this research.

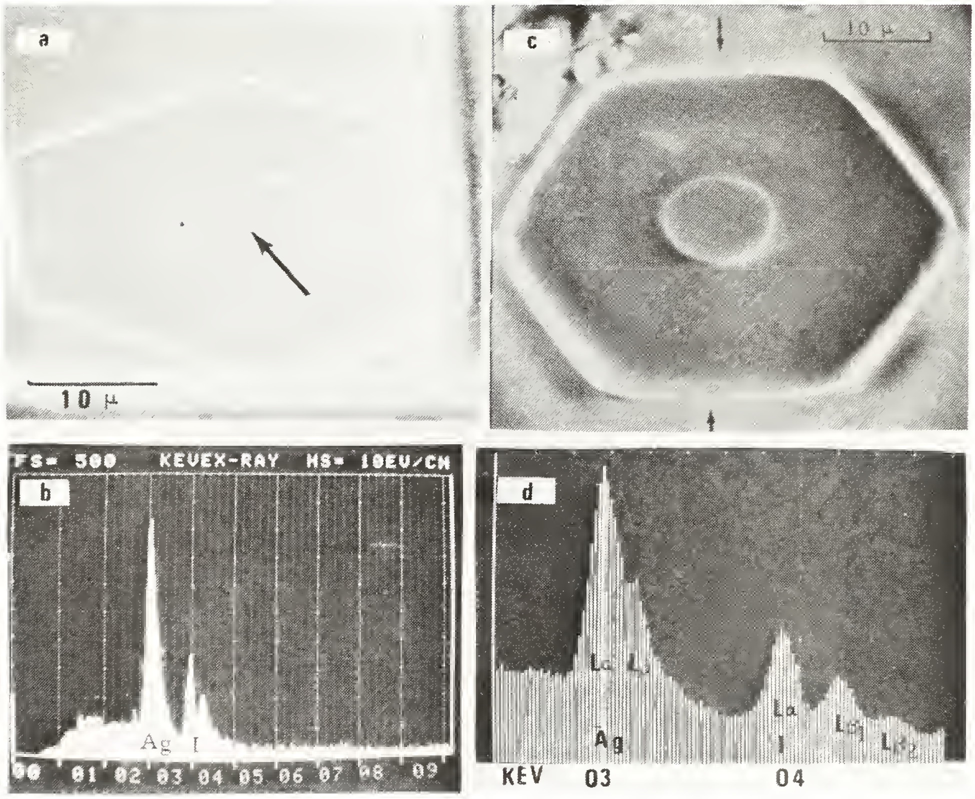

Figure 1. Electron micrographs of AgI seeded ice crystals (a and c) and the X-ray spectra of their nuclei (b and d).

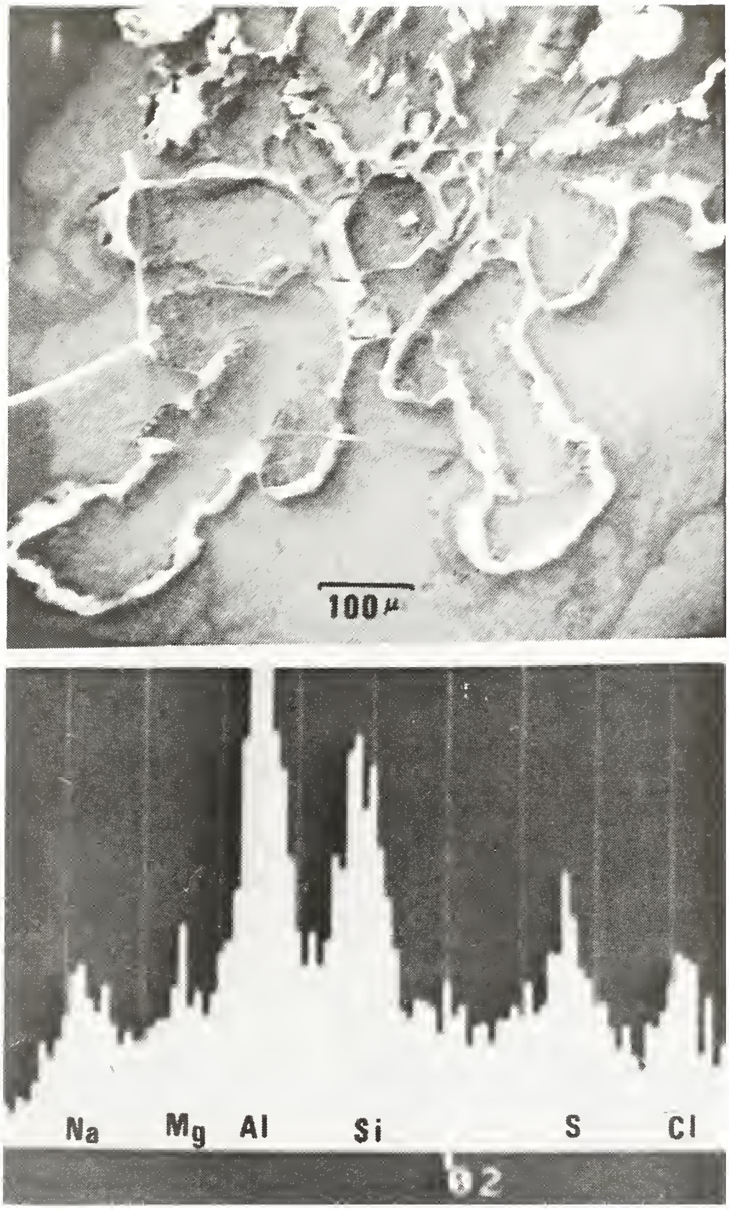

Figure 2. Electron micrographs of a natural snowcrystal and the X-ray spectrum of its nucleus.

Reprinted with permission of Science Vol. 180, June 1973.

Reprinted from
8 June 1973, volume 180, pages 1057-1058

SCIENCE

Ice Nucleation: Elemental Identification of Particles in Snow Crystals

Abstract. *A scanning field-emission electron microscope combined with an x-ray analyzer is used to locate the ice nucleus within a three-dimensional image of a snow crystal and determine the chemical composition of the nucleus. This makes it possible to better understand the effect of nuclei in cloud seeding.*

Information about the elemental composition of atmospheric nuclei is necessary for a quantitative evaluation of deliberate and inadvertent weather modification. In seeding experiments on supercooled clouds, AgI is most often used as the seeding agent. Because the presence of silver in seeded snow can be due to nucleation, scavenging, or sedimentation, analyzing the silver concentration in the snow provides information about the spatial and temporal distribution of AgI in a particular seeding area. However, this method provides little information about the effectiveness of the seeding agent in any weather modification attempt. Only by examining individual AgI particles in relation to individual snow crystals and identifying AgI as the nucleus is it possible to make an objective analysis of seeding experiments.

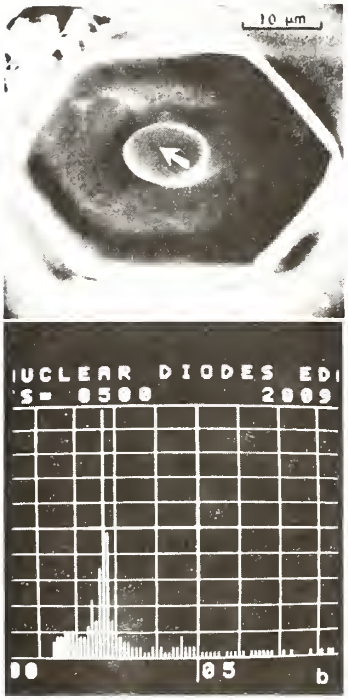

Fig. 1. (a) Image of an ice crystal seeded with AgI and (b) energy-dispersive x-ray spectrum of a particle (arrow) in its center.

Using the principle that a particle can act as a nucleus in its own supersaturated solution, Parungo and Rhea (*1*) developed a technique for growing AgI crystals smaller than a micrometer but large enough to be analyzed with an optical microscope and thereby identified as ice nuclei. However, this method is tedious and its accuracy is limited.

A transmission electron microscope can easily detect ice nuclei smaller than a micrometer (*2*). However, it cannot be used to determine the elemental composition of the nuclei or to isolate the artificial ice nuclei from those provided by nature in a seeding operation in the field. This means that a transmission electron microscope cannot be used to determine the actual seeding effect.

It is possible to use a scanning electron microscope (SEM) to visualize directly the replicas of ice crystals at high magnifications. If the SEM utilizes field emisssion as the electron source, combining the high intensity of the electron beam with excellent spatial resolution, it is possible to locate nuclei of submicrometer sizes in relation to the crystal. Since the SEM operates by bombarding the specimen with a beam of electrons, characteristic x-rays are generated at the point of impact and can be used to determine the elemental composition of nuclei within the ice crystal. Therefore, by combining an

Copyright © 1973 by the American Association for the Advancement of Science

energy-dispersive x-ray analyzer with the SEM it is possible to obtain data about the shape of an ice crystal and the exact location and chemical composition of potential nuclei within the crystal in one operation. With this information, it is possible to evaluate quantitatively the effect AgI has on ice nucleation.

In a cold chamber, ice crystals seeded with AgI were collected on sampling studs coated with 3 percent Formvar in ethylene dichloride. Chloroform vapor was applied to replicate the ice crystals. The replicas were then studied with a Coates & Welter field-emission scanning electron microscope, with a magnification of 10 to 88,000 (*3*). The rapidly scanning electron beam produced an image of the surface of the ice crystal. Particles enclosed in the replica were detected by the appearance of changes in surface features. When a particular feature was of interest the electron beam was focused on it, and a complete analysis of the elements was obtained by using a Nuclear Diodes energy-dispersive x-ray analyzer (*4*). Within minutes, the analyzer produced a spectrum of counts as a function of energy between 0 and 8 kev corresponding to all the major and minor elements at that feature.

Figure 1a shows the SEM image of an ice crystal that originated from the droplet in its center. The spectrum obtained with the x-ray analyzer (Fig. 1b) identifies the chemical composition of a particle (arrow) enclosed in the droplet. In Fig. 2, the spectrum is from the particle (arrow) located off center inside the ice crystal. The long lines in column 02 in both spectra correspond to the $K\beta$ transition of silver and show that the element is present; the short lines in column 04 indicate iodine through its $L\gamma$ transition. Although both elements are equimolar in AgI, the heights of the intensity peaks are not a direct measure of their concentrations because the elements are not excited with the same efficiency. (The peaks in column 01 correspond to the composition of the sampling stud.) For a quantitative analysis, the spectrum for the sample is compared with the spectra for a set of standards of the pure elements. Masses as low as 10^{-17} and 10^{-18} g can be detected.

The field-emission scanning electron microscope coupled with the x-ray analyzer provides a simple and accurate way to identify AgI in seeded snow crystals. This method can also be used for elemental analysis of natural ice nuclei and condensation nuclei. Figure 2 shows two particles at the left edge of the ice crystal; they contain silicon (not documented) and may be quartz (SiO_2) that has been scavenged by the ice crystal. The low ice-forming ability of SiO_2 compared to AgI eliminates these particles as competitive nuclei in initiating the ice phase in our experiment. This method of analyzing ice crystals will provide a way to study many scavenging problems occurring in precipitation.

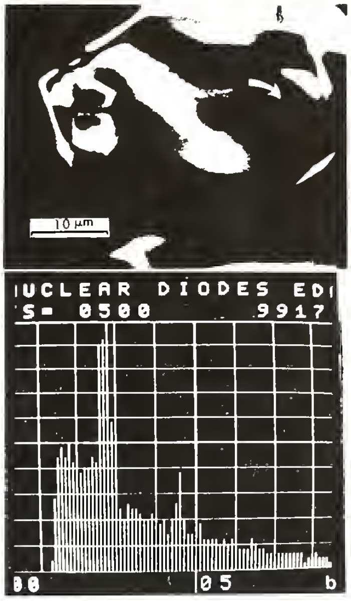

Fig. 2. (a) Image of an ice crystal seeded with AgI and (b) energy-dispersive x-ray spectrum of a particle (arrow) off center.

FARN P. PARUNGO
RUDOLF F. PUESCHEL
Atmospheric Physics and Chemistry Laboratory, National Oceanic and Atmospheric Administration, Environmental Research Laboratories, Boulder, Colorado 80302

References and Notes

1. F. P. Parungo and J. O. Rhea, *J. Appl. Meteorol.* 9, 651 (1970).
2. F. P. Parungo, *ibid.*, in press.
3. CWIKSCAN, Coates & Welter Instruments, Sunnyvale, California.
4. EDAX, Nuclear Diodes, Inc., Prairie View, Illinois.
5. We thank T. E. Brickman and W. Roth of Coates & Welter Instruments for their valuable assistance during this investigation, and Dr. H. K. Weickmann, Environmental Research Laboratories, Boulder, Colorado, and Dr. J. P. Lodge, Jr., National Center for Atmospheric Research, Boulder, Colorado, for their helpful comments.

12 February 1973; revised 16 March 1973

Reprinted with permission of Beitrage zur
Physik der Atmosphare, Vol. 46. Band, 1973.

Growth of Ice Crystals from Frozen Cloud Droplets

Das Wachstum von Kristallen aus gefrorenen Tröpfchen

Farn P. Parungo and Helmut K. Weickmann

National Oceanic and Atmospheric Administration, Environmental Research Laboratories, Atmospheric Physics and Chemistry Laboratory, Boulder, Colorado, U.S.A.

Received May 4, 1973

Summary: An electron microscope was used to study the initial growth process of snowcrystals from frozen cloud droplets. Ice crystals, nucleated by using silver iodide in a cold chamber, were collected and replicated for the examination. The electron micrographs of the observations depicted many growth stages of the spherical frozen droplets developing into different ice crystalline habits. Their growth processes are discussed.

Zusammenfassung: Das Anfangswachstum von Schneekristallen, die ihren Ursprung in gefrorenen Wolkentröpfchen haben, wurde mit einem Elektronenmikroskop untersucht. Eiskristalle, die durch Impfen mit Silberjodid in einer Kältekammer entstanden, sind in Formvar nachgebildet und im Elektronenmikroskop untersucht worden. Die dabei beobachteten verschiedenen Formen beim Übergang vom kugelförmigen gefrorenen Tröpfchen in Kristalle werden diskutiert.

Résumé: On a utilisé un microscope électronique pour étudier la croissance initiale de cristaux de neige à partir de gouttelettes congelées de nuage.
Des cristaux de glace, engendrés en chambre froide par nucléation à l'aide d'iodure d'argent, ont été captés et on en a fait des répliques (Formvar) pour examen au microscope électronique. On discute les diverses formes observées lors de la transformation en cristaux des gouttelettes congelées sphériques.

1. Introduction

There are two major mechanisms to cause the growth of ice crystals upon ice nuclei. The first is deposition nucleation; water vapor deposits on a nucleus either at water supersaturation or at ice supersaturation and grows into an ice crystal. Thus, the ice nucleus is in the center of the ice crystals. The second is droplet freezing nucleation; the nucleus is either embedded in a droplet or contacts a droplet to initiate crystallization that subsequently grows into an ice crystal. Thus, a frozen droplet is in the center of the ice crystal. However, the nucleus need not be in the center of the crystal, but can be located anywhere inside the frozen droplet.

BENTLEY's (1924) early photographic studies of snowcrystals showed that at least one-half of the crystals had a tiny circular figure at its center of the structure, and he concluded that such crystals grew around frozen cloud droplets. NAKAYA et al. (1936), WEICKMANN (1947), and AUER's (1970) observations of snowcrystals caused them to reach a similar conclusion, i. e., frozen cloud droplets play a major role in forming natural snow.

This paper discusses the growth processes of the spherical frozen droplets as they develop into different ice crystal habits. The study is based on photogrammetric observations with an electron microscope.

2. The Formation of Frozen Droplets

To study the initial growth of ice crystals from frozen droplets, it is important to know whether the original frozen droplet is a monocrystal or a polycrystal under the nucleation conditions. Therefore, two sets of experiments were conducted.

2.1. Experiment A

An open drum 40 cm in diameter and 1.2 m tall was placed in a temperature controlled cold room (2.5 × 3 × 2 m). A hand-squeezed nebulizer, filled with distilled water of 0 °C delivered water droplets. These drops froze and fell inside the drum onto glass slides sitting on the bottom of the drum. Many liquid drops in various sizes were observed on the slides. Some evaporated during the microscopic observation; others froze on the slide to yield flat crystals. They were discarded from further examination. Only the drops that froze in the air were examined with a polarization microscope to determine whether they were mono- or polycrystals.

2.2. Experiment B

The same procedure as for experiment A, except that silver iodide (AgI) aerosol, which was produced by electrically heating an AgI coated nichrone wire, was introduced into the drum before the delivery of water drops. No liquid drops were found on the slides.

Fig. 1 shows the percentage of mono- and polycrystallized drops determined in both experiments A and B. At all the experimental temperatures, the drops yielded higher portions of monocrystals in experiment B (with AgI) than in experiment A (without AgI). This can be explained; water drops collide with the AgI particles and crystallize before they have time to cool to ambient temperature. Therefore, the temperature has less effect on the ratio between mono- and polycrystals in experiment B than it does in experiment A. This effect is therefore strictly caused by the experimental conditions.

A comparison of these values with the results of PITTER (1972), MAGONO and ABURAKAWA (1968), and BROWNSCOMBE and HALLETT (1967) is given in Fig. 2. Because of the differences of the experimental methods used, the results vary. However, a qualitative relationship is apparent; at certain temperatures the smaller drops yield monocrystals while the larger ones freeze as polycrystals. Furthermore, in a given size range, drops that freeze as monocrystals at warmer temperatures will give polycrystals at colder temperatures.

These experimental results indicate that polycrystals are formed at a temperature where crystallization proceeds so fast that a regular crystal habit cannot develop and dendritic growth in the supercooled drop occurs. The increase of rate of crystallization with decreasing temperature (PRUPPACHAR, 1967) explains why large droplets develop into polycrystal at high temperatures and small ones at lower temperatures.

3. Ice Crystals Grown from Monocrystallized Droplets

The crystal structure of ice is a hexagonal space lattice with three equal axes (a_1, a_2, a_3) coplanar at 120°, and a principal axis (c) at right angles to them (Fig. 3a). The spherical droplets frozen in monocrystalline habit then adsorb water molecules according to their lattice and grow into a polyhedron (Fig. 3b) with two basal faces and six prismatic faces. Since the relative rates of growth along the two axes, "a" and "c", depend on temperature and humidity, two sets of experiments were carried out to investigate the growth processes.

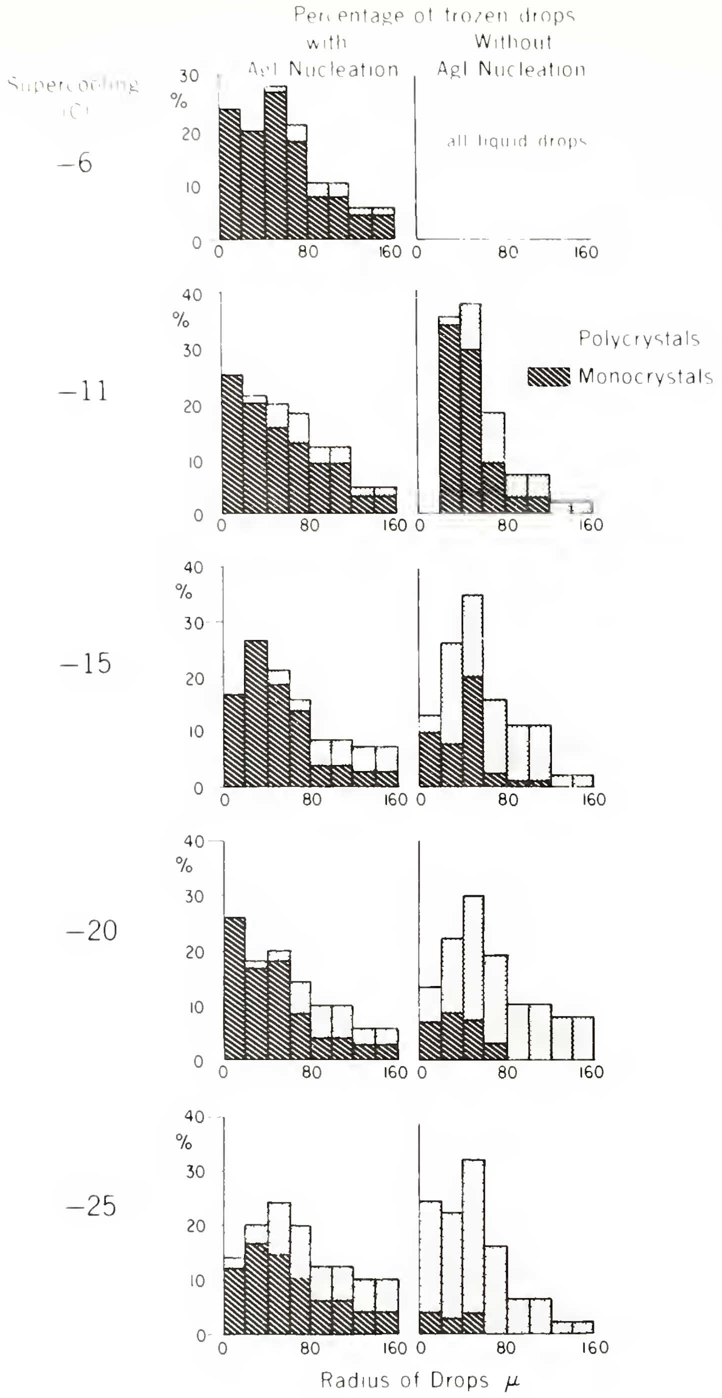

● **Figure 1.** Distribution between monocrystals and polycrystals of frozen drops

● **Bild 1.** Größenverteilung von Ein- und Mehrkristallen gefrorener Tropfen

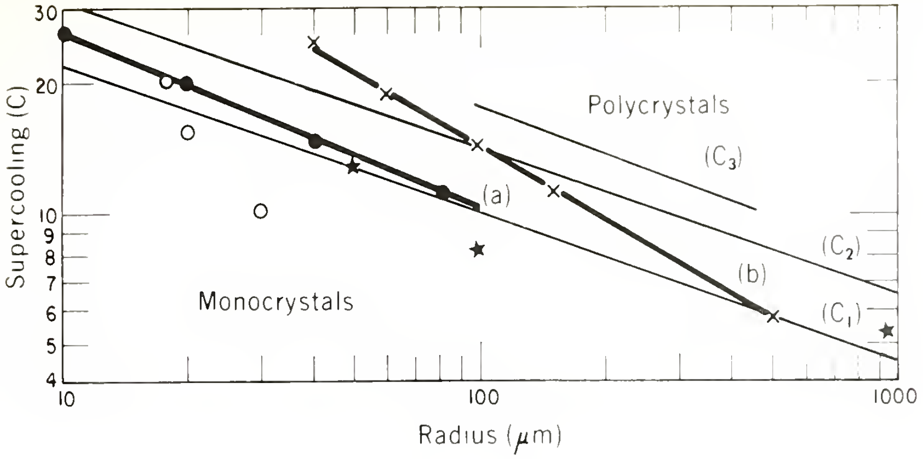

- **Figure 2.** Empirical thresholds for the formation of mono- and polycrystals of frozen drops. (a) without AgI seeding; (b) with AgI seeding; (c) Pitter's (1972) results: c_1 on ice, c_2 in oil, c_3 in the air; (o) Magono and Aburakawa's (1968) values; (*) Brownscombe and Hallett's (1967) values

- **Bild 2.** Empirische Schwelle für die Bildung von Ein- oder Mehrkristallen gefrorener Tropfen (a) Ohne AgI Impfung; (b) mit AgI Impfung; (c) Pitter's (1972) Ergebnisse: c_1 auf Eis, c_2 in Oel, c_3 im Luft; (o) Magono und Aburakawa's (1968) Ergebnisse; (*) Hallett's (1964) Ergenisse

3.1. Experiments with Varied Temperatures

Experiments were conducted at various temperatures under water supersaturation in a cold chamber. Silver iodide aerosol was used to seed a cloud that was produced continuously with an atomizer. The ice crystals were collected on sampling screens and replicated for examination with an electron microscope. The details of this procedure have been described previously (PARUNGO, 1973). The ice crystal habits found at different temperatures are listed in Table 1.

- **Table 1.** Ice crystals obtained from various temperatures at water supersaturation

- **Tabelle 1.** Eiskristalle die bei verschiedenen Temperaturen und konstanter Übersättigung gewonnen wurden

Temperature (± 2 °C)	Plates with a Center Droplet (%)	Columns (%)	Plates with a Center Nucleus (%)	Other (%)
- 8	–	80	–	20
- 12	70	30	–	–
- 16	90	10	–	–
- 20	90	–	10	–
- 24	30	40	15	15

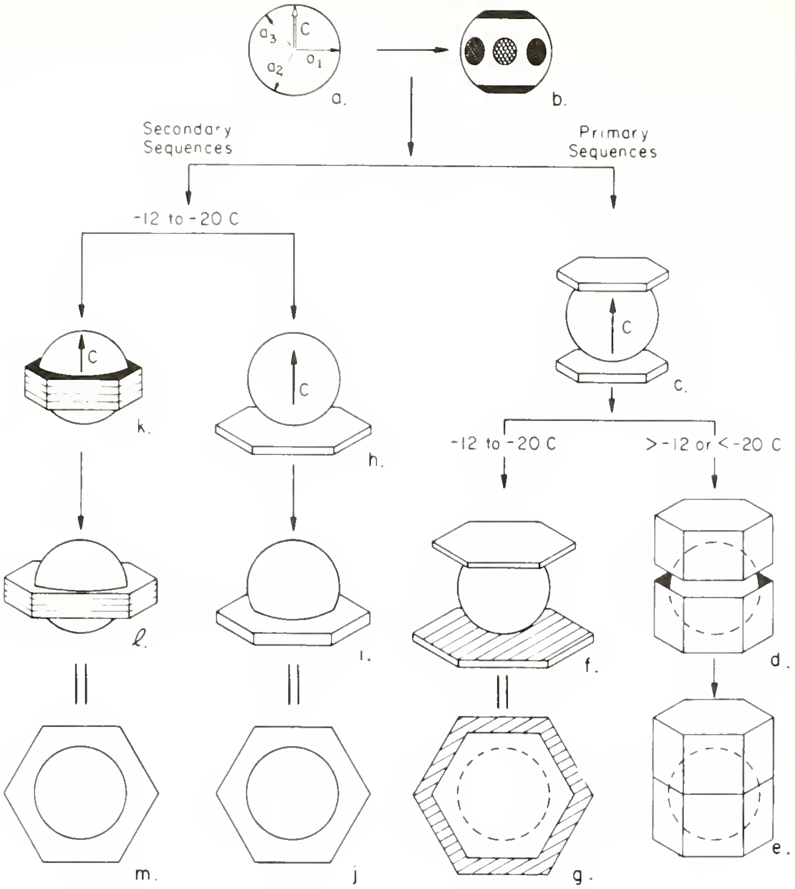

● **Figure 3.** Sketch of growth developments from a monocrystallized droplet to various crystal habits

● **Bild 3.** Skizze der Größenentwicklung verschiedener Kristallformen aus einkristallinen Tropfen

When the temperature is warmer than -12 °C or colder than -20 °C, ice crystals generally form hexagonal columns. Growth apparently favors the direction along the "c" axis to form two basal faces (0001) and $(000\bar{1})$, as shown in Fig. 3c. The subsequent growth on these faces caused them to join together and to form one column. If a defect in the lattice occurs at the junction, which is very likely, the process would leave a line in the middle of the column. However, a perfect reunion of the two sides will build a continuous lattice and no line should be observed. Fig. 3 ($c \rightarrow d \rightarrow e$) shows a sketch of this development. The photogrammetric evidence (Fig. 4) for the growing stages was obtained at -20 to -24 °C from AgI seeded ice crystals; Fig. 4f shows a natural snowcrystal for comparison.

At temperature between -12 to -20 °C, crystal growth favors the direction along the "a" axes. The two basal faces (Fig. 3c) will grow to two hexagonal plates with the mutual axes and will be joined by the common initial droplet. Because of competition for the available moisture, the two plates may not develop identically (Fig. 3f). In many cases, one plate grows at the expense of the other and, thus, retards the other from full development (Fig. 3g). These double-plate crystals were first noticed by

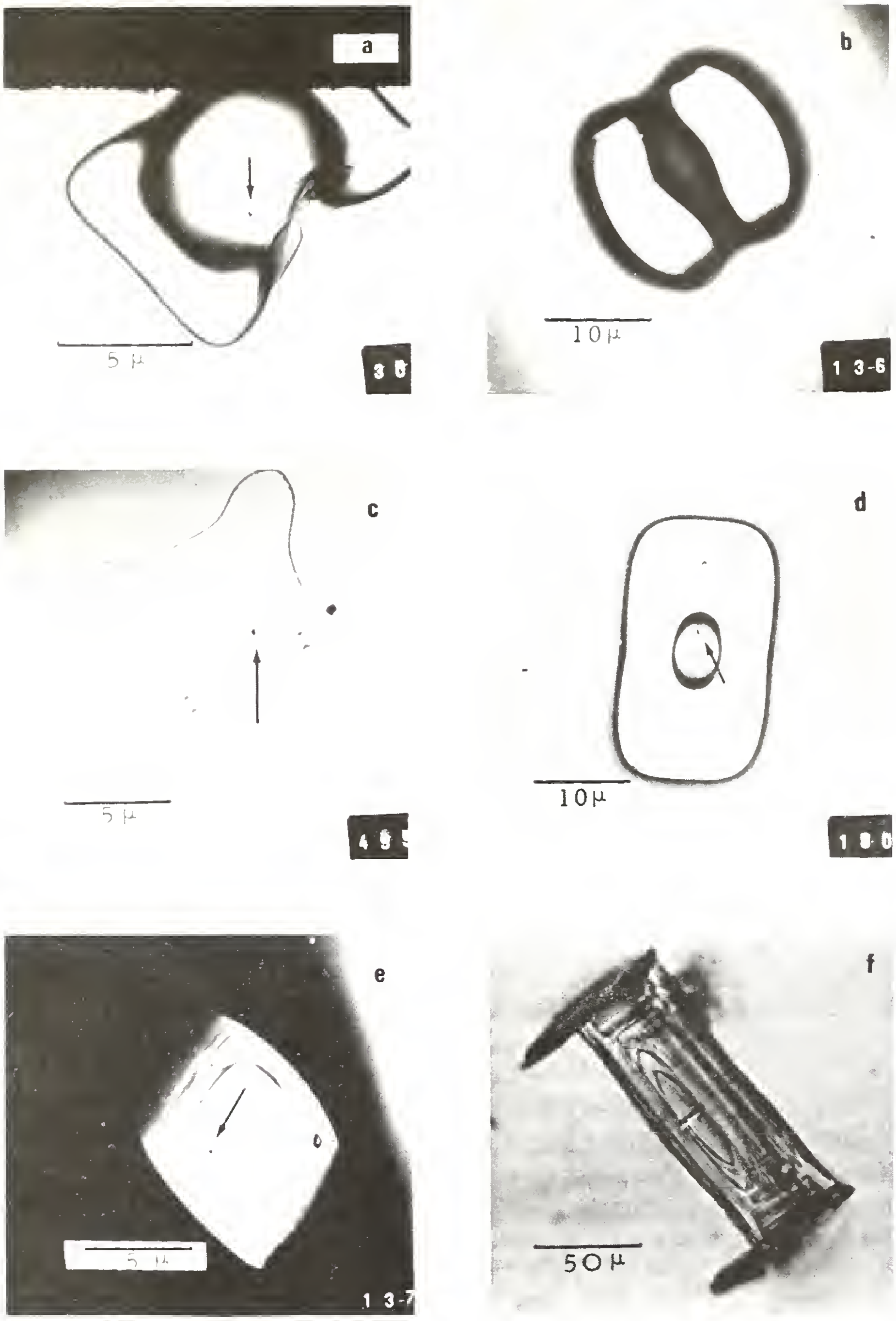

- **Figure 4.** (a–e) Electron micrographs of AgI seeded ice crystals obtained at - 20 to - 24 °C; (f) optical micrograph of a natural ice crystal

- **Bild 4.** (a–e) Elektronenmikroskopische Aufnahmen AgI geimpfter Kristalle im Temperaturbereich von - 20 °C bis - 24 °C; (f) lichtmikroskopische Aufnahme eines natürlichen Eiskristalls

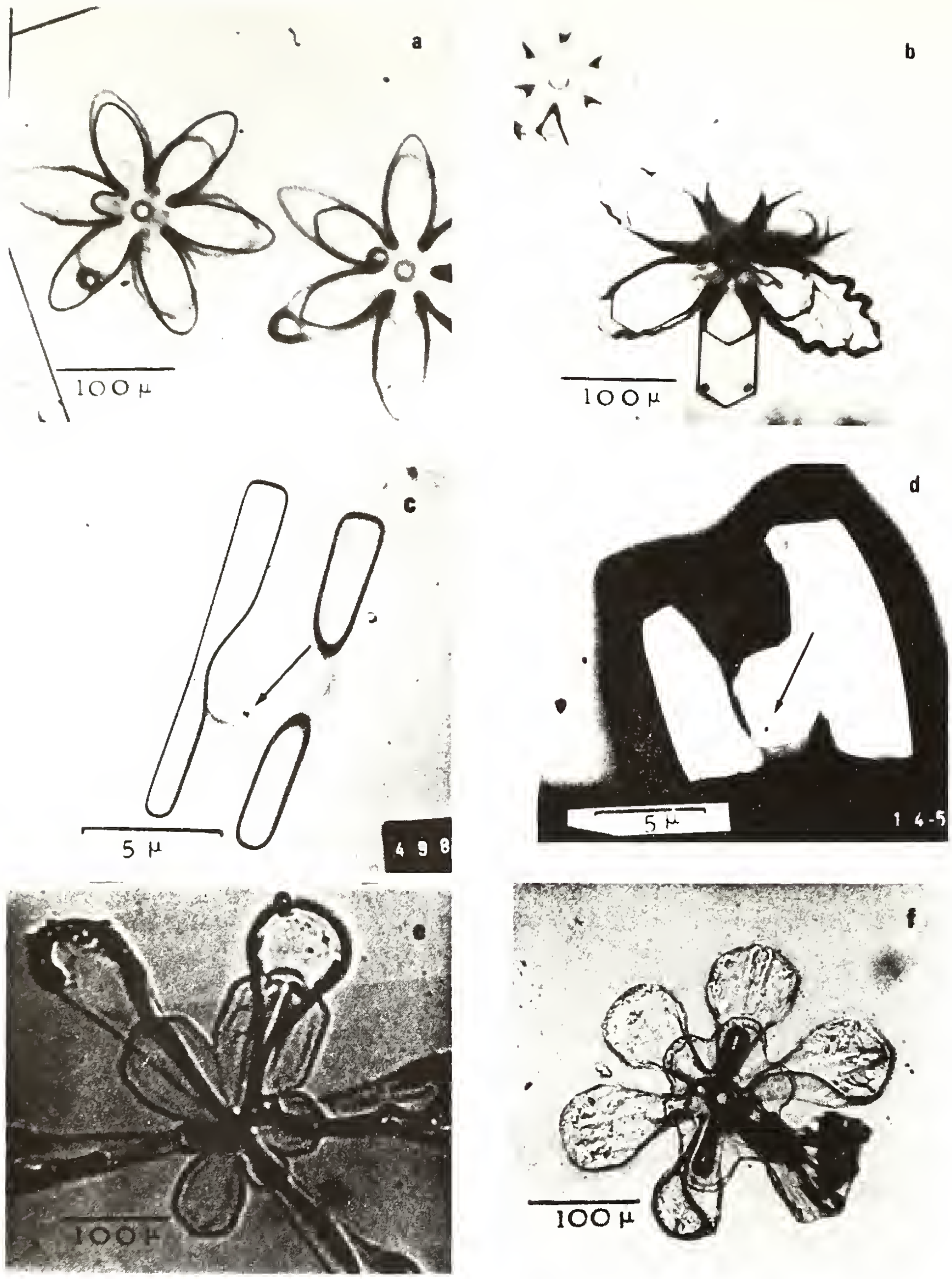

- **Figure 5.** (a–b) Micrographs of AgI seeded ice crystals obtained at - 15 °C; (c–d) electron micrographs of AgI seeded ice crystals (side view) obtained between - 16 and - 20 °C; (e–f) micrographs of natural snowcrystals

- **Bild 5.** (a–b) Aufnahmen AgI geimpfter Eiskristalle bei - 15 °C; (c–d) Eiskristalle im Temperaturbereich von - 16 °C bis - 20 °C; (e) und (f) Aufnahmen natürlicher Schneekristalle

NAKAYA et al. (1936) in natural snow while the correct explanation of the formation of their habit was given by one of us (WEICKMANN, 1947). Later they were produced in the laboratory by AUFM KAMPE et al. (1951). AUER (1970) found them abundant in the natural clouds. Fig. 5 (a and b) shows the double-plate crystals obtained through contact nucleation in AgI nucleation experiments at − 15 °C (WEICKMANN et al., 1970). Fig. 5 (c and d) are electron micrographs showing the side views of this type crystals. Fig. 5 (e and f) shows natural snowcrystals composed of double plates.

Hexagonal columns and double hexagonal plates are found as major portions in natural and artificial snowcrystals, and both develop from the two basal faces of a monocrystalline droplet (Fig. 3c). Thus their developments are considered as primary sequences of habit forming.

When only one of the two basal faces develops on a monocrystallized droplet (Fig. 3h), this grows into a single hexagonal plate with a center circle (Fig. 3i and j). Fig. 6 depicts the growth of such crystals.

In another observed case, crystals grow on the prismatic faces (Fig. 3k) and develop into single hexagonal plates with a frozen droplet in the middle (Fig. 3*l* and m). Fig. 7 depicts electron micrographs of such icecrystal growth at different stages. These crystals were obtained at temperatures from − 12 to − 20 °C.

The formations of these single hexagonal plates are found as minor contributions to natural and artificial snowcrystals; thus they are considered as secondary sequences of habit forming.

In all the AgI seeding experiments at water supersaturation, the ice nuclei, which are detectable (arrow) in electron micrographs (Figs. 4, 5, 6, and 7), are off the center of the ice crystals but within the center frozen droplets. This indication confirms that these ice crystals originated by droplet freezing nucleation.

3.2. Experiments with Varied Humidity

Experiments were carried out at a constant temperature (− 15 ± 1 °C) but with various humidities. Moisture was provided by a beaker of water that was warmed to a desired temperature (T_W). The beaker (400 m*l* with 50 cm^2 surface exposure) was at the bottom of the cold chamber. Because of lack of ventilation in the cold chamber (300 *l*), the humidity provided by the warm water could not reach an equilibrium state; thus, a local gradient of water vapor pressure existed. The supersaturation inside the chamber could not be measured; the temperature of the water represented a qualitative indication of the humidity.

Silver iodide, the seeding agent, was used in two sets of experiments; one set was underseeded and the other was overseeded. Ice crystals formed were collected and replicated. The results are listed in Table 2.

In the underseeding experiments, a limited amount of AgI aerosol being introduced into a very humid cloud, generated by 50 °C water, the nucleated frozen droplets had sufficient water vapor to grow into large plates and sectors, as shown in Fig. 8 (a and b). Some hexagonal plates grew branches, or whiskers, at their corners, showing they were developing into dendrites (Fig. 8 c and d). Ice nuclei are often found just outside of the center circle as shown in Fig. 8e (arrow); the explanation is that the original droplet is partially covered by the growing ice crystal and is actually larger than the size of the center circle. Therefore the nucleus is inside of the original frozen droplet. In Fig. 8 (d and f), the AgI nucleus is visible off the center of the original droplet, the location of these ice nuclei indicates that they originated from droplet freezing nucleation.

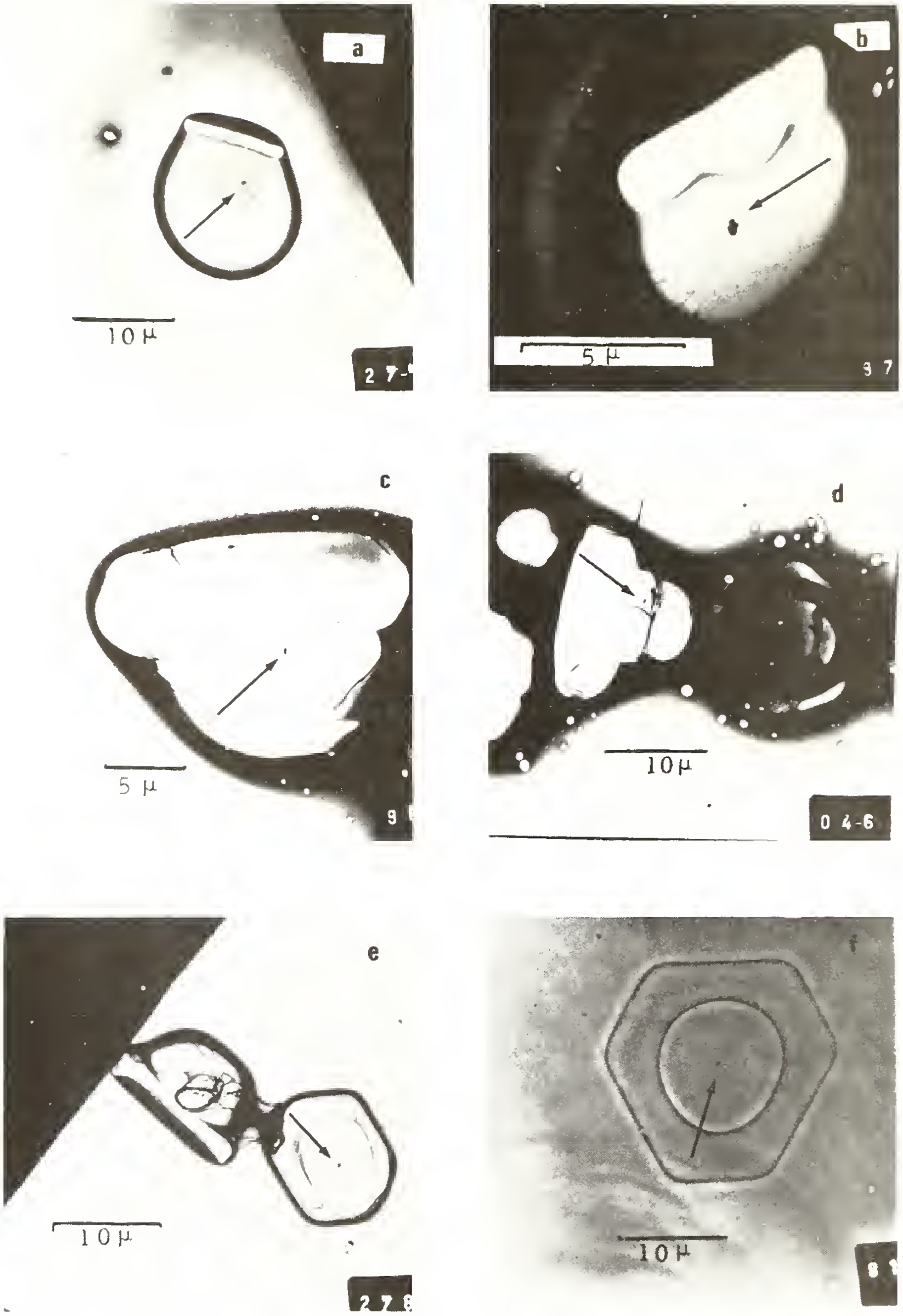

● **Figure 6.** Electron micrographs of AgI seeded ice crystals obtained at - 20 °C

● **Bild 6.** Elektronenmikroskopische Aufnahmen AgI geimpfter Eiskristalle die bei - 20 °C gebildet wurden

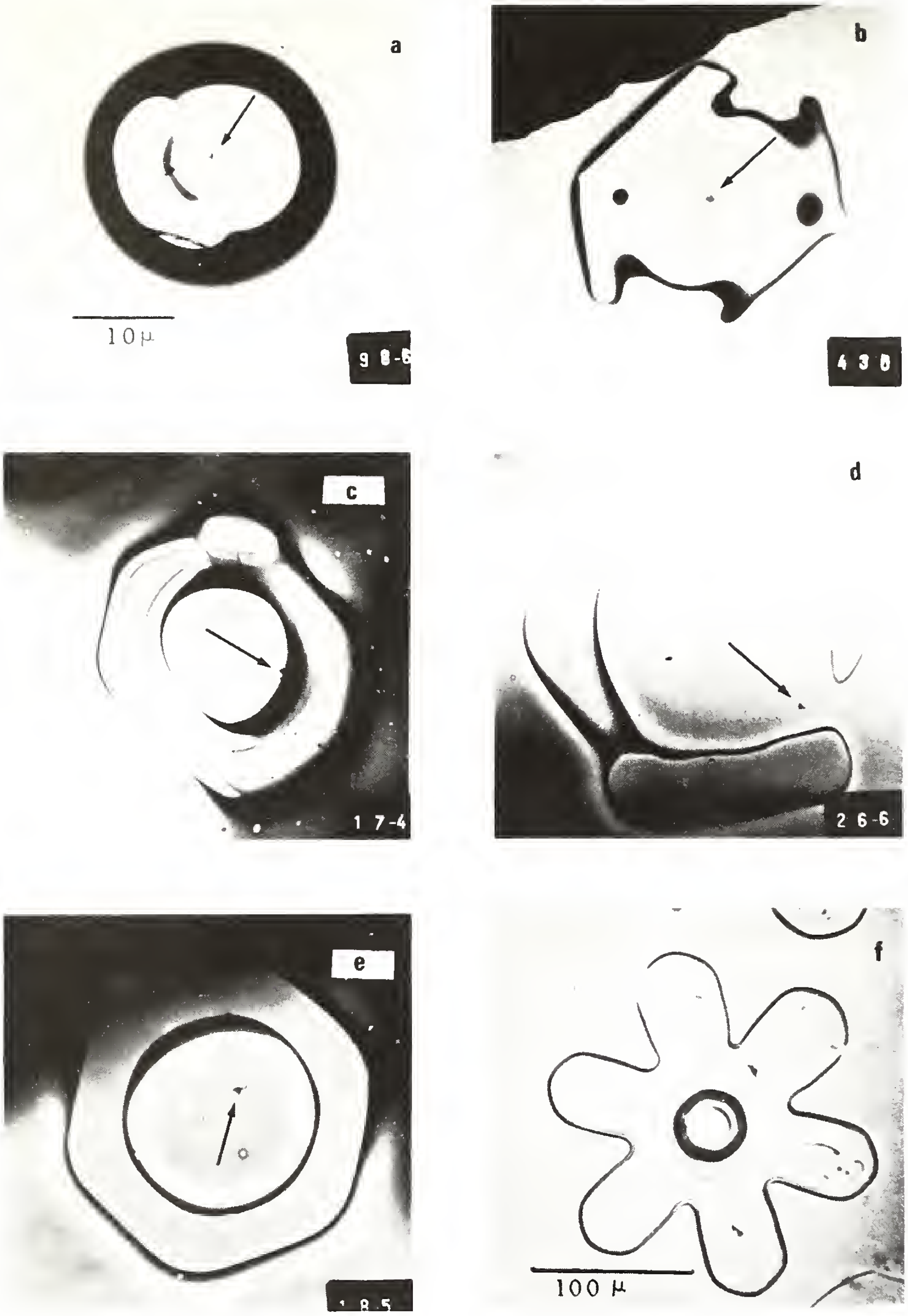

● **Figure 7.** AgI seeded crystals obtained between – 12 °C and – 20 °C. (a–e) electron micrographs (magnification 1620 x); (f) optical micrograph

● **Bild 7.** AgI geimpfte Kristalle, entstanden im Temperaturbereich von – 12 °C bis – 20 °C; (a–e) elektronenmikroskopische Aufnahmen (Vergrößerung 1620 x); (f) lichtmikroskopische Aufnahme

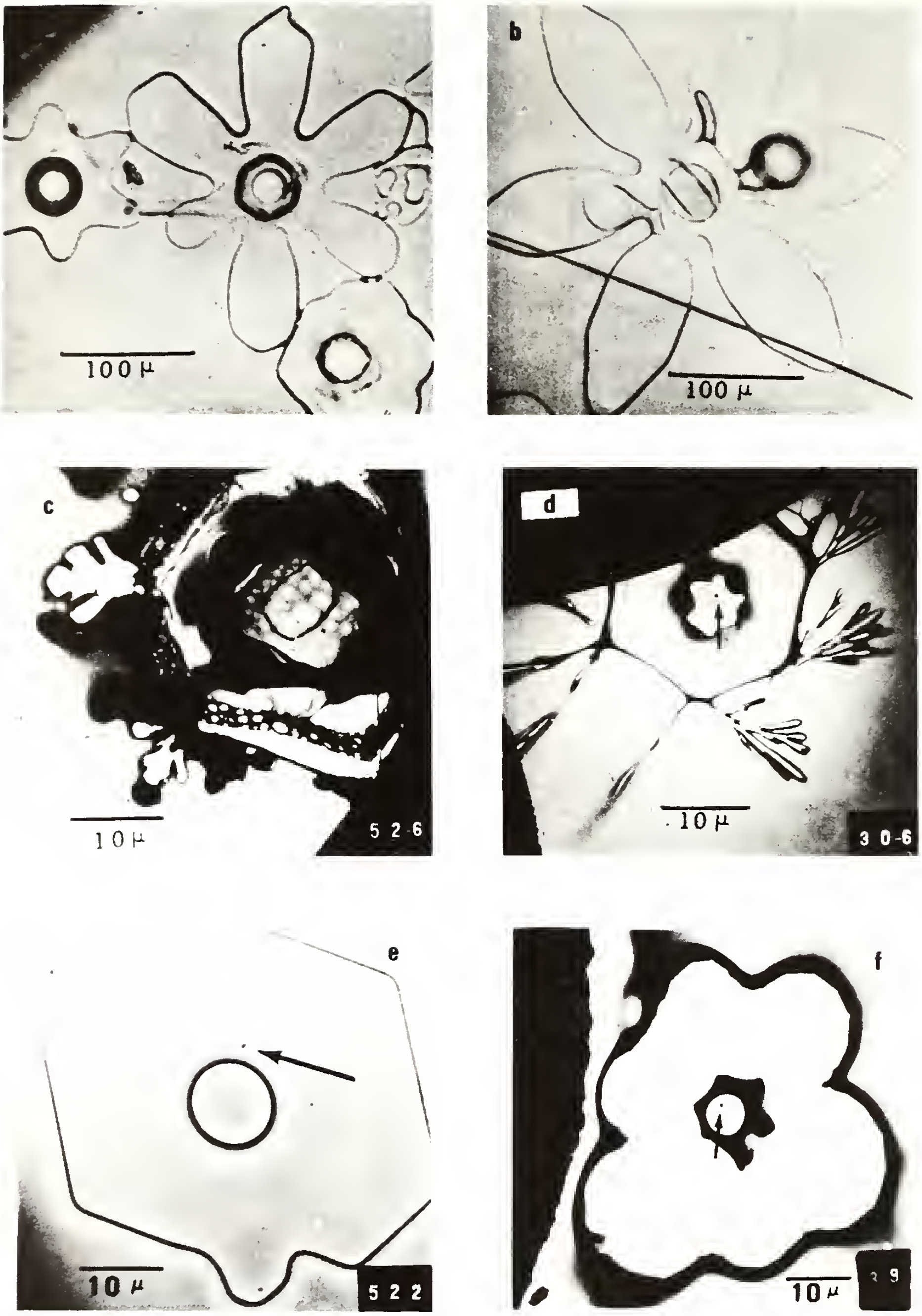

- **Figure 8.** Ice crystals obtained at - 15 °C with high water vapor supply; (a–b) micrographs; (c–f) electron micrographs

- **Bild 8.** Eiskristalle die bei - 15 °C unter reichlicher Wasserdampfzufuhr gebildet wurden; (a–b) lichtmikroskopische Aufnahmen; (e–f) elektronenmikroskopische Aufnahmen

■ **Table 2.** Ice crystals obtained at – 15 °C at various humidities

■ **Tabelle 2.** Eiskristalle die bei verschiedenen Feuchten und – 15 °C gewonnen wurden

Water temperature T_W (°C) (Moisture supply)	Plates with a center droplet (%)	Columns (%)	Plates with a center nucleus (%)	Size range (μm)
	Underseeded with AgI			
50	99	1	–	50–250
35	90	5	5	20–100
20	80	10	10	10–50
5	–	–	–	–
	Overseeded with AgI			
50	85	5	10	10–60
35	80	10	10	10–50
20	40	30	30	10–30
5	–	–	–	–

As the supersaturation was reduced by lowering T_W to 35 °C or 20 °C, the size of the ice crystals produced also decreased (Table 2). Five to ten % of the hexagonal plates did not contain a center droplet, instead an AgI nucleus was found at the center of the symmetry (Fig. 9 e and f); this indicates these crystals originated by deposition nucleation. In addition, 5 to 10 % of the ice crystals were columns. At T_W of 5 °C, no ice crystals were obtained.

In the overseeding experiments, the excess AgI nuclei compete for the available moisture and reduce the vapor supply. The ice crystals obtained were small (10 to 60 μm) even at T_W of 50 °C. As we decreased the moisture supply further by reducing the T_W to 20 °C, the percentage of columns and plates with a center nucleus increased significantly. According to NAKAYA (1954), KOBAYASHI (1958), and MAGONO and LEE (1966), at – 15 °C, the ice-crystal habit changes from dendrites to sectors, to plates, and then to columns as the rate of water vapor supply decreases. Our experiments at – 15 °C, agreed with their statement that the percentage of columns increased with decreasing humidity (Table 2).

4. Ice Crystals Grown From Polycrystallized Droplets

When a frozen droplet in polycrystal form (Fig. 10a) starts to grow, all the component monocrystals will compete for available water molecules and adsorb them according to their individual lattices. Fig. 11 (a to c) shows the initial growing stages. When the ambient temperature and water vapor supply favor growth along the "a" axes, a polycrystallized droplet will develop into spatial plates or spatial dendrites (Fig. 10, a → b → c) (WEICKMANN, 1972). However, if the conditions favor growth along the "c" axis, then the droplet will develop into a combination of bullets or combination of columns (Fig. 10, a → b → d). Occasionally, the components in the spatial plates or in the combination of columns appear in a certain symmetry. This is probably caused by the original polycrystallized droplets being built of two or more homogeneous portions of the same crystal species in juxtaposition.

In a study of natural snowcrystals, WEICKMANN (1947) observed that combinations of columns (Fig. 11d) form in cirrus clouds at temperature below – 25 °C where they originated through deposition of water on the different sides of a nucleus without a transition through the droplet phase. The crystal growth along the "c" axis is at a temperature higher than – 12 °C or lower than – 20 °C. Since cloud droplets seldom crystallize as polycrystals when warmer than – 12 °C and deposition nucleation becomes the important process when colder than – 25 °C, the formation of a combination of columns detoured via polycrystallized droplets does not frequently occur in nature.

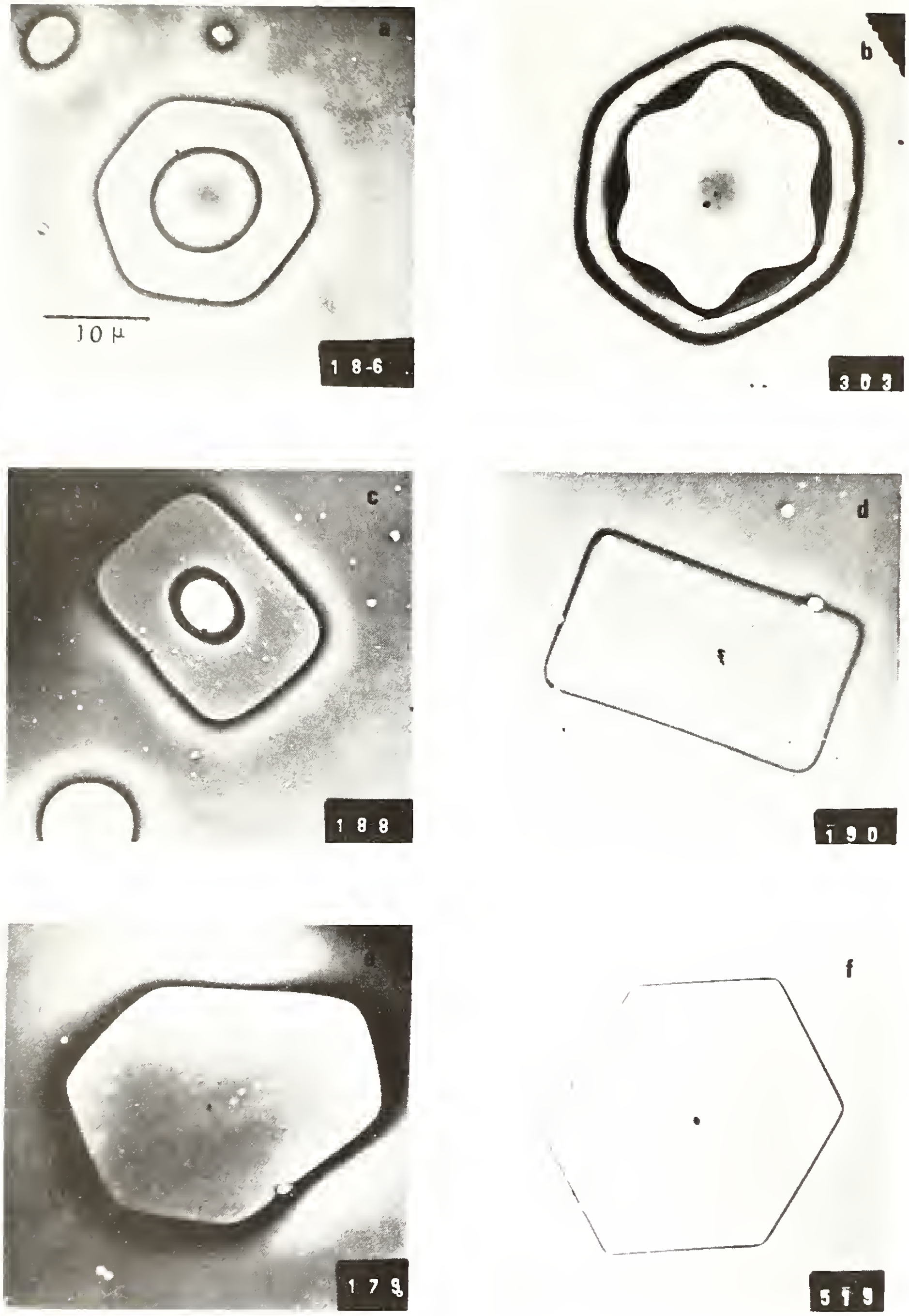

- **Figure 9.** Electron micrographs (1620 x) of ice crystals obtained at - 15 °C with low water vapor supply. (a–d) from frozen droplets; (e–f) from deposition

- **Bild 9.** Elektronenmikroskopische Aufnahmen (1620 x) von Eiskristallen die bei - 15 °C unter knapper Wasserdampfzufuhr gebildet wurden. (a–d) aus gefrorenen Tropfen; (e) und (f) durch Sublimierung

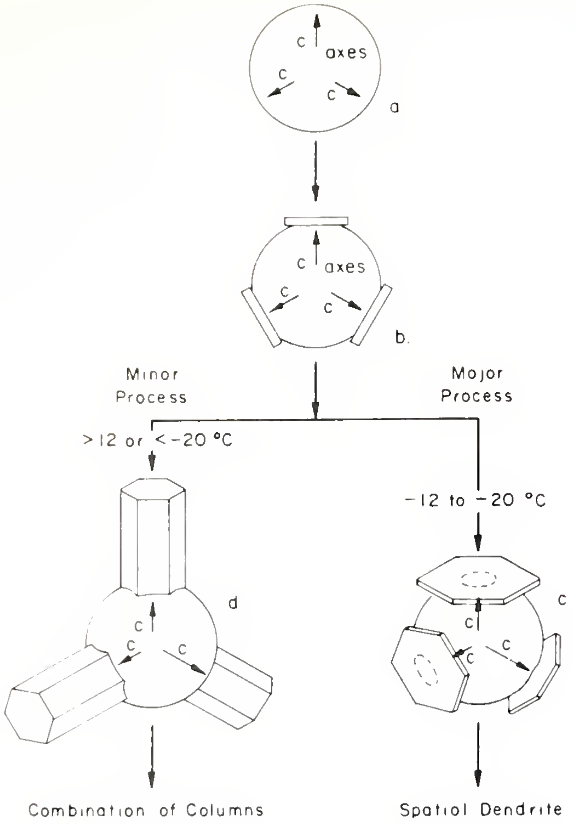

- **Figure 10**
  Sketch of growth development from a polycrystallized droplet
- **Bild 10**
  Skizze der Größenentwicklung verschiedener Kristallformen aus mehrkristallinen Tropfen

NAKAYA (1954) classified spatial dendrites into two types. The radiating type has dendritic branches growing from the center (Fig. 11e). The other type has a hexagonal dendritic crystal at its base and many dendritic extensions growing from various points on each branch (Fig. 11f). He proposed that secondary branches were formed from ice nuclei (frozen droplets) collected by the main crystal. HALLETT (1964) later confirmed that they developed from cloud droplets frozen on the crystal. These ideas can explain only the latter type of spatial dendrite. For the radiating type, all the branches form simultaneously at the initial stage, either from a deposition nucleus or from a polycrystallized droplet.

5. Conclusion

Photogrammetric observations with an electron microscope were made of artificial ice crystals. Emphasis was placed on the growth process of snowcrystals from frozen water droplets. Many growth stages were photographed and compared with micrographs of natural snowcrystals. We observed that a spherical monocrystallized frozen droplet could develop into various crystal habits, such as plate, double plates, and column; these habits depend upon supercooling and supersaturation. The observations also suggested that spatial dendrites and combinations of columns could originate from polycrystallized frozen water droplets.

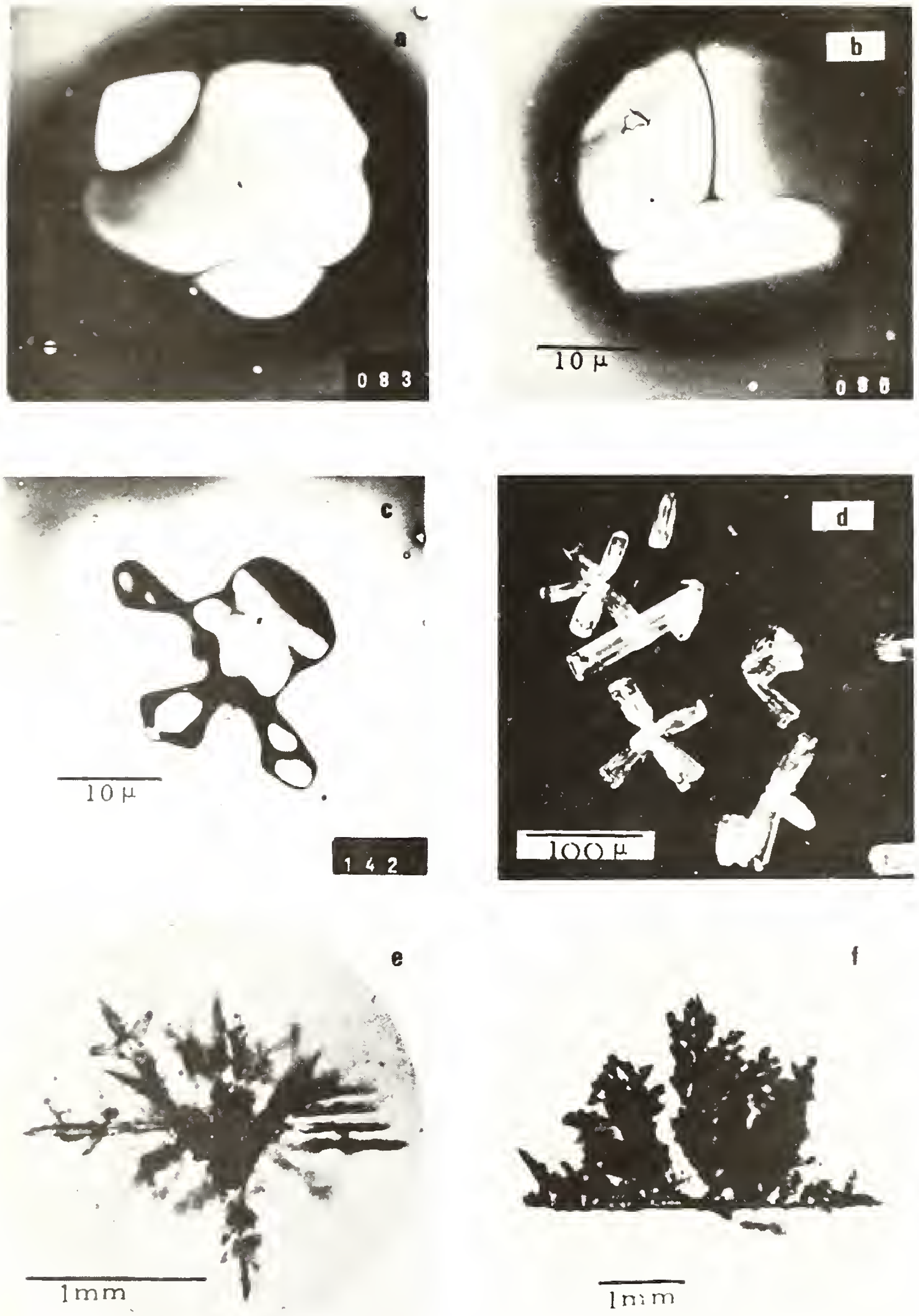

- **Figure 11.** (a–c) Electron micrographs of initial growth of polycrystallized droplets obtained at - 30 °C; (d) natural combination of columns; (e–f) natural spatial dendrites photographed by Nakaya et al. (1943)

- **Bild 11.** Elektronenmikroskopische Aufnahme des Anfangswachstums mehrkristalliner Tropfen bei - 30 °C. (d) Vereinigung natürlicher Säulen; (e) und (f) natürliche dreidimensionale Dendriten aufgenommen von Nakaya et al. (1943)

6. Acknowledgement

The authors express their thanks to Jan Rosinski of National Center for Atmospheric Research for arranging for them to use NCAR's electron microscope and his helpful discussions.

References

AUER, A. H., Jr., 1970: Observation of ice crystal nucleation by droplet freezing in natural clouds. *J. Rech. Atmos.*, 4, 145–160.

AUFM KAMPE, H. J., H. K. WEICKMANN and J. J. KELLY, 1951: The influence of temperature on the shape of ice crystals growing at water supersaturation. *J. Meteo.*, 8, 168–174.

BENTLEY, W. A., 1924: Forty years' study of snow crystals. *Mon. Wea. Rev.*, **52**, 530–532.

BROWNSCOMBE, J. L., and J. HALLETT, 1967: Experimental and field studies of precipitation particles formed by the freezing of supercooled water. *Quart. J. Roy. Met. Soc.*, 93, 455–473.

HALLETT, J., 1964: Experimental studies on the crystallization of supercooled water. *J. Atmos. Soc.*, **21**, 671–682.

KOBAYASHI, T., 1958: On the habit of snow crystals artificially produced at low pressure. *J. Met. Soc., Japan*, 36, 193–208.

MAGONO, C., and H. ABURAKAWA, 1968: Experimental studies on snow crystals of plane type with spatial branches. *J. Fac. Sci.*, Hokkaido Univ., 3, 85–97.

MAGONO, C., and C. W. LEE, 1966: Meteorological classification of natural snow crystals. *J. Fac. Sci.*, Hakkaido Univ., Ser. VII, **2**, 321–362.

NAKAYA, U., 1954: Snow crystals. Harvard Univ. Press, 510 pp.

NAKAYA, U., Y. SIKODO and M. TADA, 1936: Notes on irregular snow crystals and snow pellets. *J. Fac. Sci.*, Hokkaido Univ., Ser. II, **1**, 215.

NAKAYA, U., Y. SEKIDO and M. TADA, 1943: Bemerkungen über unregelmäßige Schneekristalle und Graupeln. *Mitteilungen der Deutschen Akademie der Luftfahrtforschung.* Kommissionsverlag von R. Oldenbourg, München und Berlin, 162 pp.

PARUNGO, F. P., 1973: Electron-microscope study of silver iodide as contact or sublimation nucleus. *J. Appl. Meteo* **12**, 517–521.

PITTER, R. L., 1972: A wind tunnel investigation of the crystalline structure of small, frozen drops falling at terminal velocity in air. Preprints of papers. The International Cloud Physics Conference, London, 62–63.

PRUPPACHER, H. R., 1967: Growth modes of ice crystals in supercooled water and aqueous solution. *J. Glacialogy* 6, 651–662.

WEICKMANN, H. K., 1947: The ice phase in the atmosphere. Ministry of Supply, London, 154 pp.

WEICKMANN, H. K., U. KATZ and R. STEELLE, 1970: AgI-sublimation or contact nucleus? Preprints. Second Conf. Weather Modification, Santa Barbara, Calif., *Amer. Meteor. Soc.*, 332–336.

WEICKMANN, H. K., 1972: Snow crystal forms and their relationship to snow storms, *J. Rech. Atmos. Dessens Memorial Issue* 6, 603–615.

Reprinted with permission of the eighth International Conference on Nucleation, Leningrad, USSR, September 1973.

Ice Nucleation and Crystal Growth Studied by Electron Microscopy

Farn P. Parungo and Helmut K. Weickmann
National Oceanic and Atmospheric Administration
Atmospheric Physics and Chemistry Laboratory
Boulder, Colorado 80302

To study the mechanism of ice nucleation and crystal growth processes, we replicated ice crystals and observed them photogrammetrically with an electron microscope.

By examining the position of the ice nucleus within the crystal, we can determine which of the two major mechanisms caused the heterogeneous nucleation: (1) For deposition nucleation, water vapor may deposit on a nucleus within the range from ice saturation to water saturation, and grows into an ice crystal. Therefore, the nucleus must be in the center of the ice crystal (Figure 1a). (2) For droplet freezing nucleation, a nucleus is either imbedded in a droplet or contacts one. This initiates crystallation and growth into an ice crystal. Thus the nucleus can be anywhere inside the frozen droplet and need not be at its center (Figure 1b).

In laboratory experiments, we used silver iodide to nucleate ice crystals. We then traced the origin of the crystals--either deposition nucleation or droplet freezing nucleation--and found that in an existing water cloud, droplet freezing nucleation was the major mechanism, even at temperatures as cold as -24°C. However, with no water cloud present (ice supersaturation) and temperatures < -18°C, ice crystals formed via deposition nucleation (Table 1).

Since nucleation by droplet freezing plays a major role, it is important in the study of growth process of ice crystals to know whether the nucleated droplets crystallize as monocrystals or polycrystals. We used a polarization microscope to determine the crystallography of droplets that froze at different temperatures. Our experimental results and the results of Pitter (1972), Magono and Aburakawa (1968), and Brownscombe and Hallet (1967) are shown in Figure 2.

These results indicate that polycrystals are formed at a temperature where crystallization proceeds so fast that a regular crystal habit cannot develop and dendritic growth in the supercooled drop occurs. The increase in the rate of crystallization with decreasing temperature explains why large droplets develop into polycrystal at high temperatures and small ones at lower temperatures.

We studied growth processes of ice crystals from spherical frozen droplets. Figure 3 shows a sketch of development of a monocrystallized droplet and Figure 4 of a polycrystallized droplet. When a monocrystallized droplet begins to grow, it adsorbs water molecules according to hexagonal lattice and develops into a polyhedron (Figure 3b) with two basal faces and six prismatic faces. The relative rates of growth along "a" and "c" axes depend on temperature and humidity. The photographic observations of the developments are shown in Figure 5. At water supersaturations when the temperature is > -12°C or < -20°C, the two basal faces of the polyhedron grow along "c" axis to form a hexagonal column (Figure 5a and b). When temperature is between -12°C and -20°C, the growth favors "a" axis direction; double hexagonal plates (Figure 5c and d) and single hexagonal plates (Figure 5e to h) are major products. However, if the humidity reduces to ice supersaturation, the fraction of column crystals increases.

When a frozen droplet in polycrystal form (Figure 4a) starts to grow, all the component monocrystals will compete for available water molecules and adsorb them according to their individual lattices. Figure 6(a to c) shows the initial growing stages. When the temperature is > -12°C or < -20°C, the conditions favor growth along the "c" axis, the droplet will develop into a combination of columns (Figure 4, a→b→d). Since cloud droplets seldom crystallize as polycrystals at > -12°C and deposition nucleation becomes the important at low temperature, the formation of a combination of columns detoured via polycrystallized droplets does not frequently occur in nature. When the temperature is -12°C to -20°C and at water supersaturation, the conditions favor growth along the "a" axes; therefore, a polycrystallized droplet will develop into spatial dendrites (Figure 4, a→b→c). Figure 6e is a radiating spatial dendrite developed via a polycrystalline droplet. Another type of spatial dendrites (Figure 6f) has a hexagonal plate with many branches are from various points. Nakaya (1954) explained that secondary branches formed from frozen droplets collected by the main crystals.

For comparison, Dry Ice was used for homogeneous ice nucleation. The resulting crystals contain no foreign particles. Beside hexagonal plates and columns, we found 20% of the ice crystals were trigonal, V-shaped, and spatial plates (Figure 1c and d). These crystals were formed by the quick local cooling which does not give the water molecules enough time to arrange themselves into the most thermodynamically stable lattice.

References

Brownscombe, J. L., and J. Hallet, 1967: Experimental and field studies of precipitation particles formed by the freezing of supercooled water. *Quart. J. Roy. Met. Soc.*, 93, 455-473.

Magono, C., and H. Aburakawa, 1968: Experimental studies on snow crystals of plane type with spatial branches. *J. Fac. Sci.*, Hokkaido Univ., 3, 85-97.

Nakaya, U., 1954: Snow crystals. Harvard Univ. Press, 510 pp.

Pitter, R. L., 1972: A wind tunnel investigation of the crystalline structure of small, frozen drops falling at terminal velocity in air. Preprints of papers, The International Cloud Physics Conference, London, 62-63.

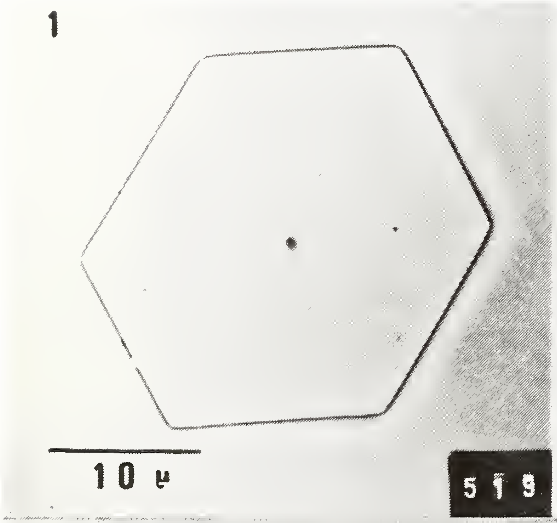

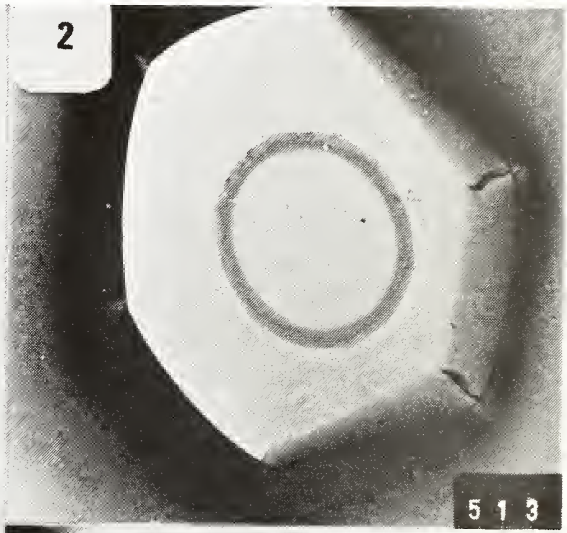

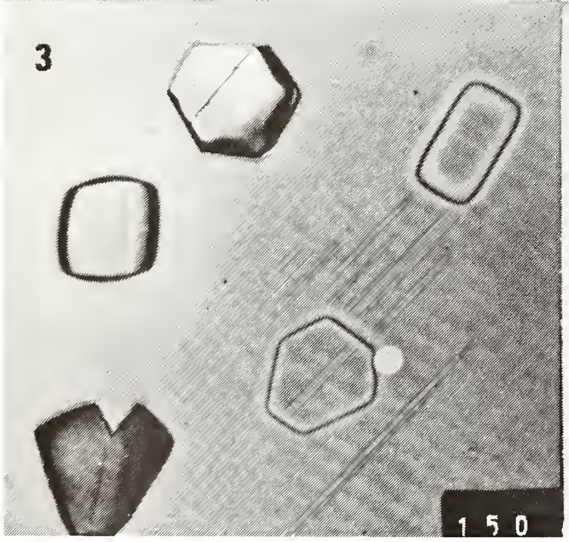

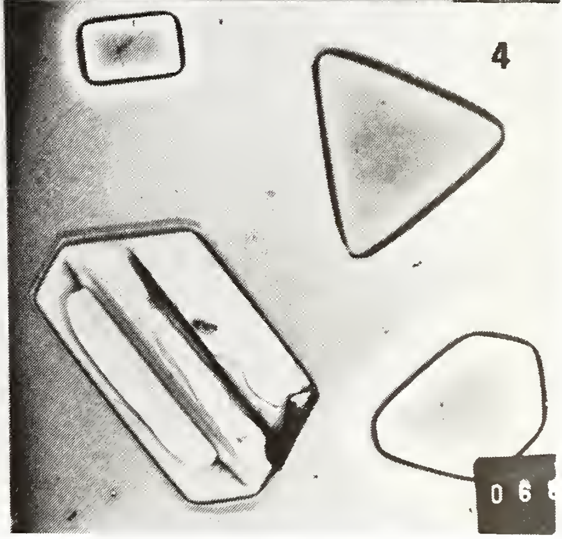

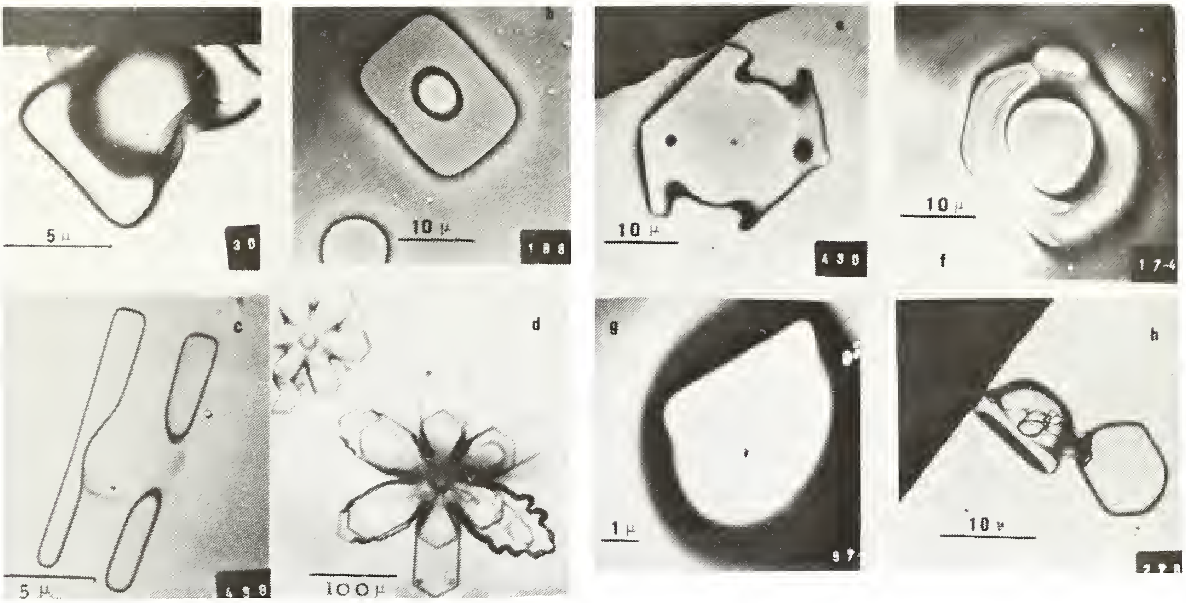

Figure 5. Ice crystals grown from monocrystals.

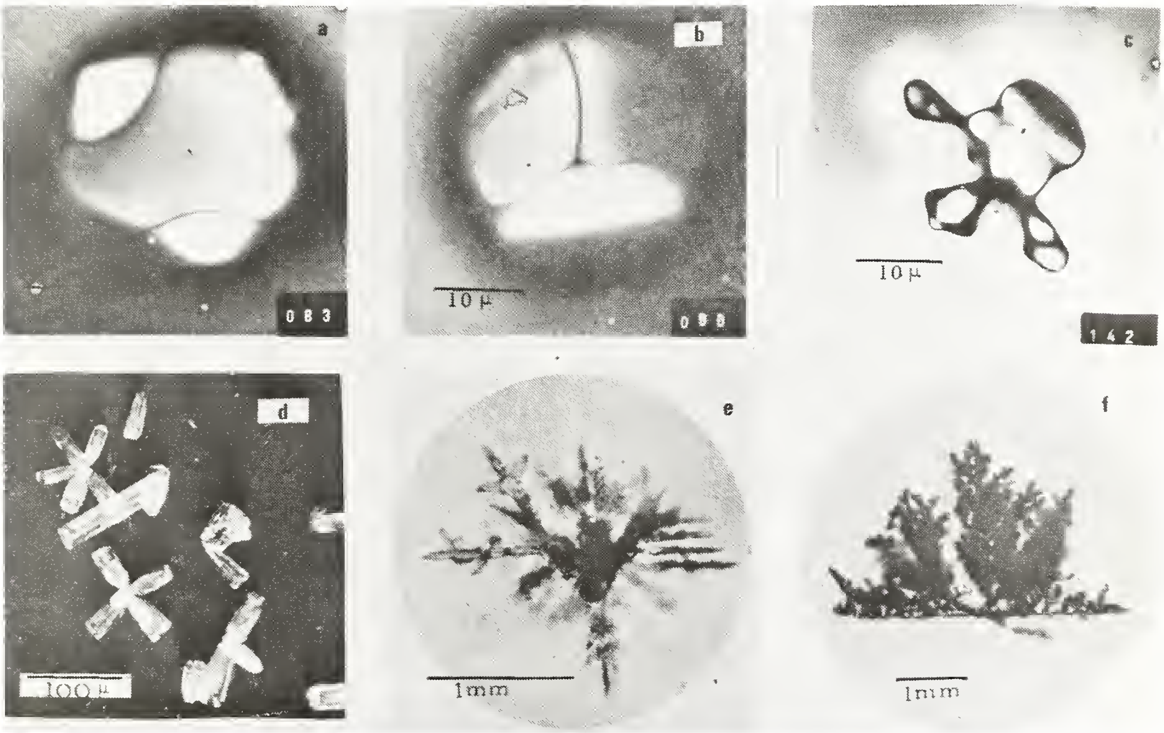

Figure 6. Ice crystals grown from polycrystals.

Reprinted with permission of the Journal of Applied
Meteorology Vol. 12, No. 3, December 1973.

Precipitation Characteristics of a Sheared, Moderate Intensity, Supercell-Type Colorado Thunderstorm

BYRON B. PHILLIPS

Atmospheric Physics and Chemistry Laboratory, NOAA, Boulder, Colo. 80302

(Manuscript received 15 June 1973, in revised form 15 September 1973)

ABSTRACT

A dense 450-station network of hail and rain gages in 2025 km^2 of northeastern Colorado has provided surface precipitation data from a moderate intensity thunderstorm that crossed the network on 22 July 1972. The storm, which existed in an environmental vertical wind shear of 6×10^{-3} sec^{-1} for over 4 hr, exhibited characteristics of the supercell-type storm including a well-defined and continuing weak echo region, a deviate motion to the right of the local winds, a precipitation wall advancing toward the region of strongest inflow, and a forward overhang of high reflectivity as far as 10 km and more ahead of the precipitation wall. The surface precipitation network results from the storm are analyzed and correlated with other measurements obtained from precision radar, instrumented aircraft, multiple high-altitude released dropsondes, rawinsondes, and surface observations. Hail recorded at 12 network stations was associated with two inflow regions that existed simultaneously and moved in divergent directions. Hailfalls correlated with regions of high radar reflectivity gradient. Hailfalls that comprised a principal hailswath were precisely located with respect to the weak echo region of the primary updraft. Four distinct rainfall maxima occurred within the network, each regularly spaced 13 km apart at 15-min intervals. A description of the storm processes is given.

1. Introduction

During the past two years a dense network of rain and hail sensors was established and operated in northeastern Colorado to support the National Hail Research Experiment (NHRE). This summertime NHRE field investigation incorporated multiple measurement and analysis programs that included instrumented aircraft capable of measuring inflow, outflow and updraft variables during flights about the storm and flights penetrating the storm core; precision pencil-beam dual wavelength radars; a four-station rawinsonde array; multiple high-altitude release dropsondes for measuring the vertical wind structure within storms; and a surface mesoscale network having a dense array of precipitation stations interspersed with two north-south rows of meteorological stations.

A coordinated set of measurements was successfully accomplished on a thunderstorm of moderate intensity, which passed across the NHRE operational area during the afternoon of 22 July 1972. Despite the description of "moderate intensity" this storm exhibited many of the characteristics of a "supercell storm" (Browning, 1964, 1965; Marwitz, 1972a). Details of the storm as revealed by the data are given in associated reports (Bushnell, 1973; Eccles, 1973; Foote and Fankhauser, 1973; Modahl, 1973; Musil *et al.*, 1973). This paper describes in detail the characteristics of the precipitation as observed by the surface gage and hail sensor network and their relation to the other associated measurements.

2. The NHRE surface precipitation network

The surface precipitation network of 452 stations covering 2025 km^2 is shown in Fig. 1. The primary target, or "Protected Area," of the experiment (outlined) was near 25 by 25 statute miles square ($\sim$1600 km^2) and contained the greatest density of gages. Within the network, 112 major stations were equipped with a recording weighing rain gage, a recording hail momentum-rate gage, a hail-rain separating gage, and hailpad; 160 stations were equipped with a hail separating gage and hailpad; and 180 stations were equipped with a non-recording total-precipitation gage and hailpad. All hail-rain separating gages, non-recording total precipitation gages and hailpads were serviced each evening when a storm had occurred within the network during the operational day.

The hail-rain separating gage, designed by NHRE and placed into operation in the network during 1972, mechanically separated the rain and hail by means of sloping screens. This gage had a receiving area of 0.125 m^2 and measured the total rain and the total hail for the day. The hailpad sensor was a 0.11 m^2 styrofoam board covered with aluminum foil. It recorded the incidence of hail and the distribution of hailstone size (and with certain assumptions, the hail energy and momentum). The essentially mechanical recording hail momentum-rate gage (Phillips *et al.*, 1973)[1] was elec-

---

[1] In preparation.

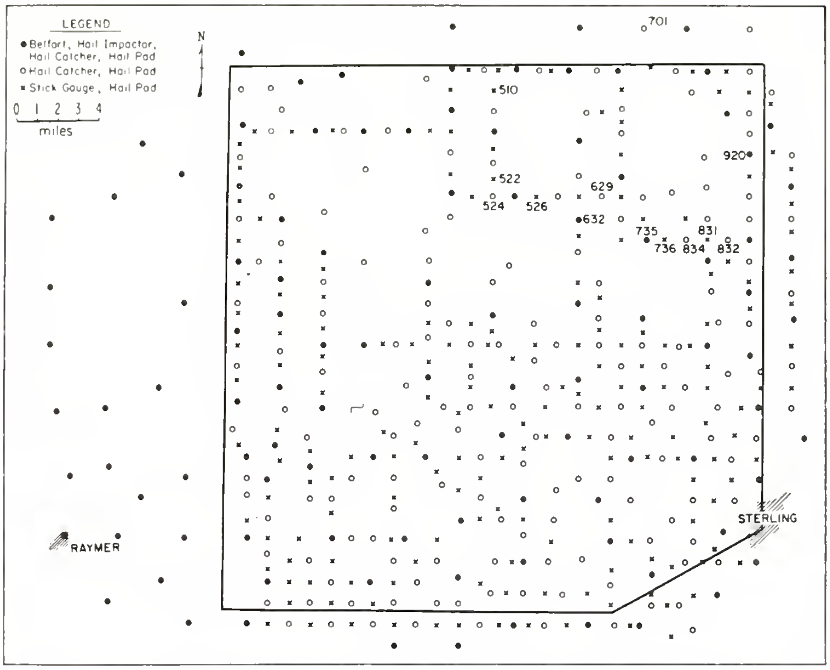

Fig. 1. National Hail Research Experiment (NHRE) 1972 surface precipitation station location map.

trically activated upon hailstone impact. Once operating, the recorder ran continuously until ~100 sec after the last hailstone impact. Given a second or third hailfall, etc., the system restarted, recording the time and momentum of the hailfall. The receiving screen was near 0.1 m^2 and the mechanism was damped to resolve three stone impacts per second. The total-precipitation recording and non-recording gages were each standard 8-inch diameter gages (324 cm^2 receiving area).

3. Storm history

The synoptic situation for 22 July 1972 has been described by Modahl (1973) and Foote and Fankhauser (1973). In northeastern Colorado, the 500-mb winds were from 240° at 20–25 m sec^{-1}. A marked increase in moisture existed west to east through the NHRE area. Winds in the lower 1–2 km were light (<10 m sec^{-1}) and showed easterly components such as to advect moisture into the region. A small shower developed over the extreme northern portion of the network, and moved eastward from 1440 to 1530 (all times MDT) along the northern boundary of the Protected Area. From cloud base the environmental wind speeds increased sharply with altitude; at 200 mb speeds were over 50 m sec^{-1}. Based on the several NHRE upper air soundings obtained during the storm, the environmental vertical wind shear was from 5×10^{-3} to more than 6×10^{-3} sec^{-1} at all cloud levels.

The major storm of 22 July 1972 originated around 1400 to 1430 some 130 km west of the NHRE operational area in the vicinity of Fort Collins, Colo. Its track has been traced for a period of more than 4 hr and a distance greater than 200 km (Eccles, 1973; Foote and Fankhauser, 1973). These authors used continuous tracking data from the National Weather Service WSR-57 radar located at Limon, Colo., some 180 km south of the storm track.

From 1430 to 1600, the storm motion was from 245° at 12.5 m sec^{-1} closely in the direction of, and at one-half the speed of, the environmental mean winds at cloud level. The storm passed over the NHRE project headquarters at Grover, Colo., 44 km west of the northwestern corner of the Protected Area, and produced pea-sized hail there about 1545. After 1600, the track deviated to the right of the environmental winds, traveling in a direction from 275° and averaging 15 m sec^{-1} across the northern half of the NHRE network, passing eastward from this area after 1745.

Radar surveillance by the NHRE Cloud Physics 2 (CP-2) precision radar (10 cm wavelength, 1° pencil beam) located at Grover began as soon as the storm was east of the radar site. Beginning shortly after 1600 this provided detailed data of the radar reflectivity factor Z, contoured at 10-dBZ intervals from 25 dBZ until after 1820 MDT when the storm was well east of the NHRE area (Eccles, 1973).

As shown by the CP-2 radar, the deviation to the right

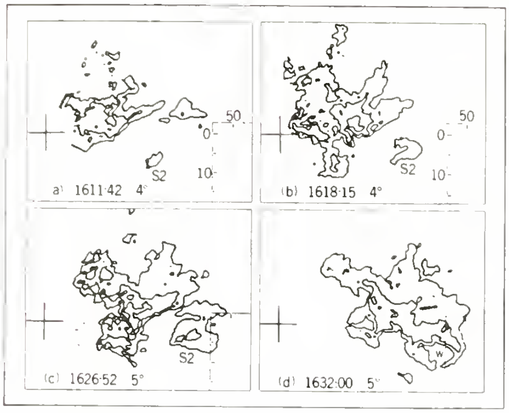

FIG. 2. New cell (S2) development and merger with continuing storm resulting in a weak echo updraft region W in the southeastern part of the storm. Radar contours are for 25, 35 and 45 dBZ. A cross marks the location of the NHRE precision radar at Grover, Colo. Scan elevations and time are as shown. Tick marks on the Protected Area (dotted area) indicate range in kilometers east and south from the Grover radar.

of the mean environmental flow was closely associated with the rapid development of a new storm cell 15 km southeast of the existing storm (Fig. 2). This new cell was first detected as a small echo (S2) at 1612 when the cell height already extended to 8.5 km MSL; the echo was showing considerable tilt to the east with increased elevation above the 4.0 km MSL cloud base. For the first half-hour, movement of this cell (240° at 11 m sec^{-1}) was again approximately with the mean winds. By 1632 the growth of the new cell was such that the 35-dBZ contours of the two storms at and above 4 km MSL were joined, the high reflectivity "center of gravity" shifting southeastward to the new storm. A pronounced and readily identifiable weak-echo region had developed along the southern and eastern echo contours of the storm astraddle the western boundary of the instrumented NHRE Protected Area (see W, Fig. 2d). The observed deviation of the storm reflectivity center to the right of the mean wind that occurred at about 1600 was clearly the result of the strong development of the new cell, i.e., a shift of the storm center. Its deviation to the right thereafter resulted from intensified growth on the southern side of the storm following the merger of these two cells; the vector addition of the intensified storm propagating southward and translating eastward produced the continuing storm track to the right of the mean wind.

From this time until the storm passed eastward from the network, the radar contours on the southeastern edge of the storm showed 1) a consistent pattern with characteristic weak echo region (WER) or bounded weak echo region (BWER) at mid-cloud elevation indicating strong inflow; 2) a steep reflectivity gradient with contours oriented southwest-northeast at low elevation indicating a precipitation wall advancing eastward with the storm; and 3) a forward-extended middle and upper level zone of radar reflectivity indicating the presence of appreciable hydrometeor overhang to the east out to distances of 10 km and more from the wall. Although Eccles has documented a discontinuous movement of the BWER at about 1650, the above primary storm features clearly identify with the quasi-steady, right-deviating severe storm (SR-storm) type. However, the storm's limited precipitation output, low maximum reflectivity factor (near 55 dBZ), and absence of associated severe storm phenomena, led us to subjectively classify the 22 July storm as of moderate intensity rather than a severe storm. This classification is further justified by the aircraft and dropsonde data obtained.

4. Network measurement results

Figs. 3–6 show the measurements from the surface precipitation network for 22 July from 1600 until the storm passed out of the NHRE Protected Area at 1800. During this period 158 network stations recorded precipitation in excess of a trace. The isohyetal analysis of the total precipitation, rain plus hail, and the areas of hailfall are shown in Fig. 3. Precipitation amounts are in millimeters. The dashed lines indicate the precipitation beginning times for quarter-hour intervals. Precipitation from the primary storm fell over the northern half of the network; smaller amounts, as judged from the isohyet patterns and radar, fell north of the network. The light rainfall ($\leqslant 2$ mm) that fell in the southern part of the network was associated with a series of small shower cells that developed independently along a southwest-northeast line after 1720. Despite the quasi-steady nature of the radar echo structure, Fig. 3 shows that the resulting precipitation pattern is decidedly cellular. The precipitation maximum (20 mm) occurred in the eastern part of the network; a minimum was observed 60–63 km east of the Grover CP-2 radar.

Hail incidence and the hail size distribution as recorded by the hailpad array is given in Table 1. Hail fell at only 12 stations. The amount of hail is given in equivalent rainfall as computed from the stone size and number incident on the hailpads. As seen, the amount of hail was a negligible part of the total precipitation. Hail having a diameter large enough to activate the hail rate-momentum gage (~ 1 cm) occurred only at station 632. The 2-min hailfall (1711–1712) recorded clearly indicated that the hail immediately preceded a 9-min period of heavy rain ($R = 54$ mm hr^{-1}) which began at 1713.

Of the 158 stations receiving rain, 51 were major stations that provided rain rate R and time resolution. From these 51 stations, the maximum rainfall rates (mm hr^{-1} for 2 min or longer) are shown in Fig. 4 together with the regions of hailfall (stipled areas). Dashed curves show the beginning times for precipita-

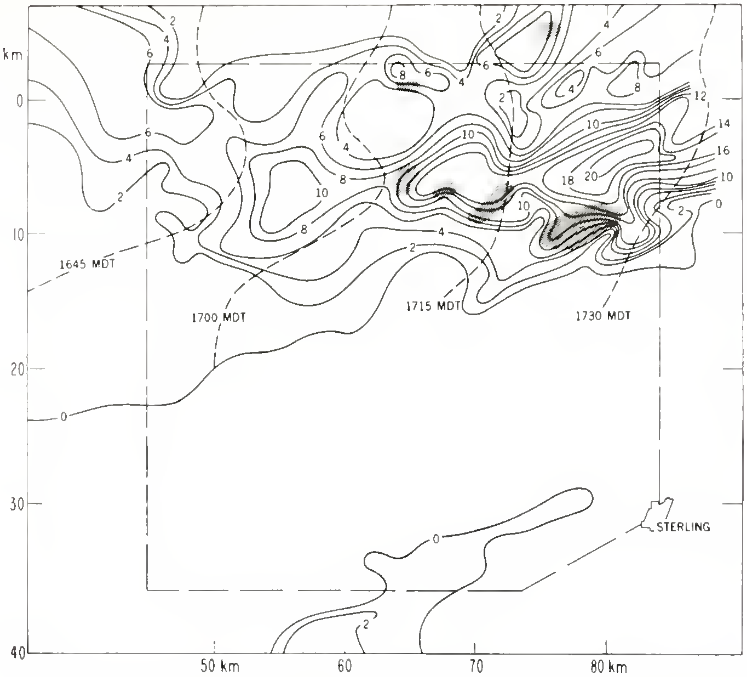

Fig. 3. Isohyets of total precipitation (mm) and areas of hail (shaded) for 1600–1800 MDT 22 July 1972. Dashed curves indicate precipitation onset times. Tick marks indicate range in kilometers east and south from the Grover radar.

tion rates exceeding $R=25$ mm hr^{-1}. Numbers on the hailfall regions are estimated periods of hailfall. The maximum rates are large. For example, rates over 100 mm hr^{-1} occurred in the eastern part of the network. These high rates were of short duration, 2 to 5 min. If we use the Z-R approximation $Z=200R^{1.6}$, then $R=100$ mm hr^{-1} corresponds to 10 log $Z=55$. With a storm motion of 15 m sec^{-1}, the width of such a precipitation burst is 2–4 km. Inspection of low elevation scans shows that narrow (1–2 km) north-south 55-dBZ echo contour peaks did occur over this region of maximum R during 1722 to 1735, which agrees with the given Z-R relation.

Figs. 5 and 6 show the duration of rain rate R greater than 25 mm hr^{-1} and 6 mm hr^{-1}, respectively. Based

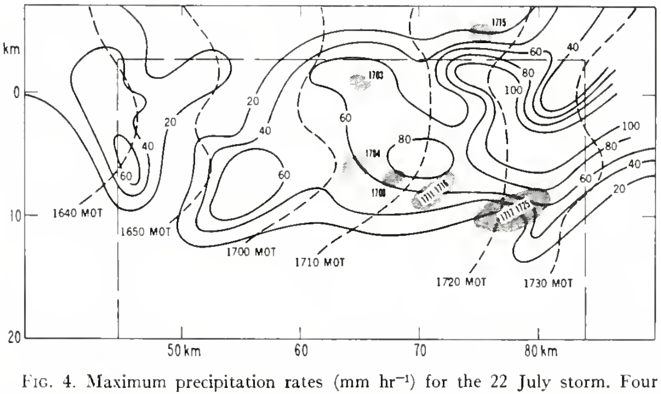

Fig. 4. Maximum precipitation rates (mm hr^{-1}) for the 22 July storm. Four hailstreaks, shown shaded to the south of the region of maximum precipitation rates, form a hailswath associated with the primary updraft. Two northern hailstreaks are associated with a weaker, secondary updraft.

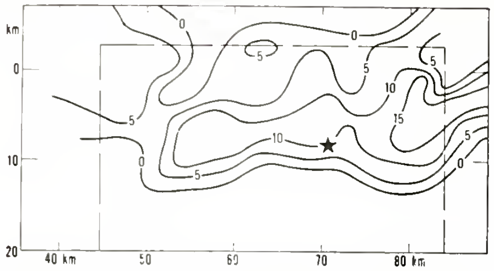

FIG. 5. Durations in minutes of rain rates >25 mm hr^{-1}. The star locates the timed hailfall at 1711–1712.

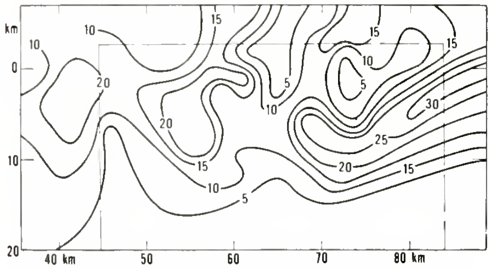

FIG. 6. Duration in minutes of rain rates >6 mm hr^{-1}.

on the above Z-R relationship, these R correlate closely with the radar contours of 45 and 35 dBZ. The two patterns of rainfall duration are approximately correlated. Starting times for the plotted rainfall rate >25 mm hr^{-1} are shown as dashed curves in Fig. 5. The star locates the measured hailfall that occurred from 1711 to 1712. In the eastern part of the network, a few stations recorded two or more rain bursts that summed to the longer durations and greater total precipitation. For example, at station 920 (see Fig. 1) a steady rain of approximately $R=50$ mm hr^{-1} began at 1725 and lasted for 16 min. After a 3-min lull, a 2-min gush began at 1744 and had a rainfall rate of $R=114$ mm hr^{-1}.

TABLE 1. Data from stations receiving hail in the 22 July storm.

Station	Number of stones (per 0.1 m^2)	Largest stone diameter (mm)	Amount of hail (mm)	Total precipitation (mm)
510	28	11	0.06	3.5
522	57	14	0.25	11.7
524	76	11	0.16	11.2
526	17	11	0.05	10.0
629	25	6	0.02	4.3
632	29	10	0.10	10.0
701	258	8	0.21	8.9
735	10	5	0.01	10.0
736	87	5	0.03	7.7
831	16	8	0.10	12.3
832	71	5	0.08	3.8
834	28	5	0.02	8.1

A cellular structure of the precipitation regime is evident in the pattern of the lower rain rates shown in Fig. 6.

5. Correlation of results

a. Hailfall

Table 1 and Figs. 3 and 4 clearly show that the hailfall from the 22 July storm was not co-located with the region of maximum rainfall or maximum rain rate. Hail fell in the eastern half of the network while the storm

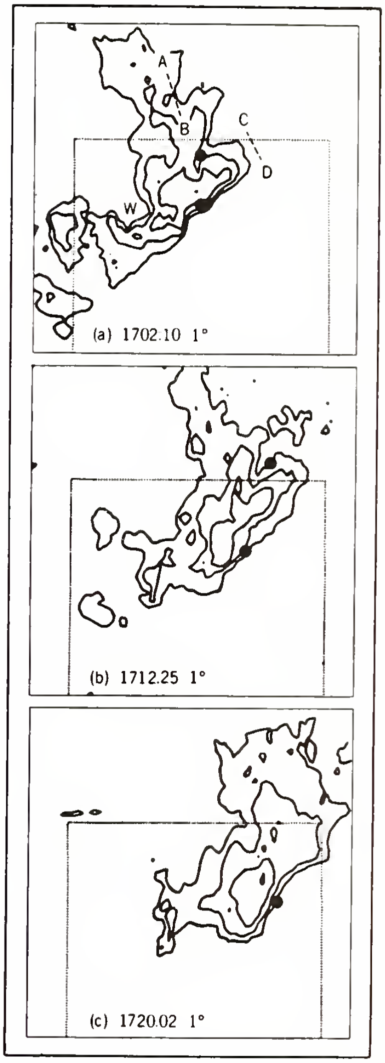

FIG. 7. Low elevation (1°) scan radar contours and associated hailfalls (shaded) for 1702:10, 1712:25 and 1720:02. Radar contours are for 25, 35, 45 and 55 dBZ. Line AB shows the release line of dropsondes at 13 km MSL altitude, while CD shows the surface impact of the sondes.

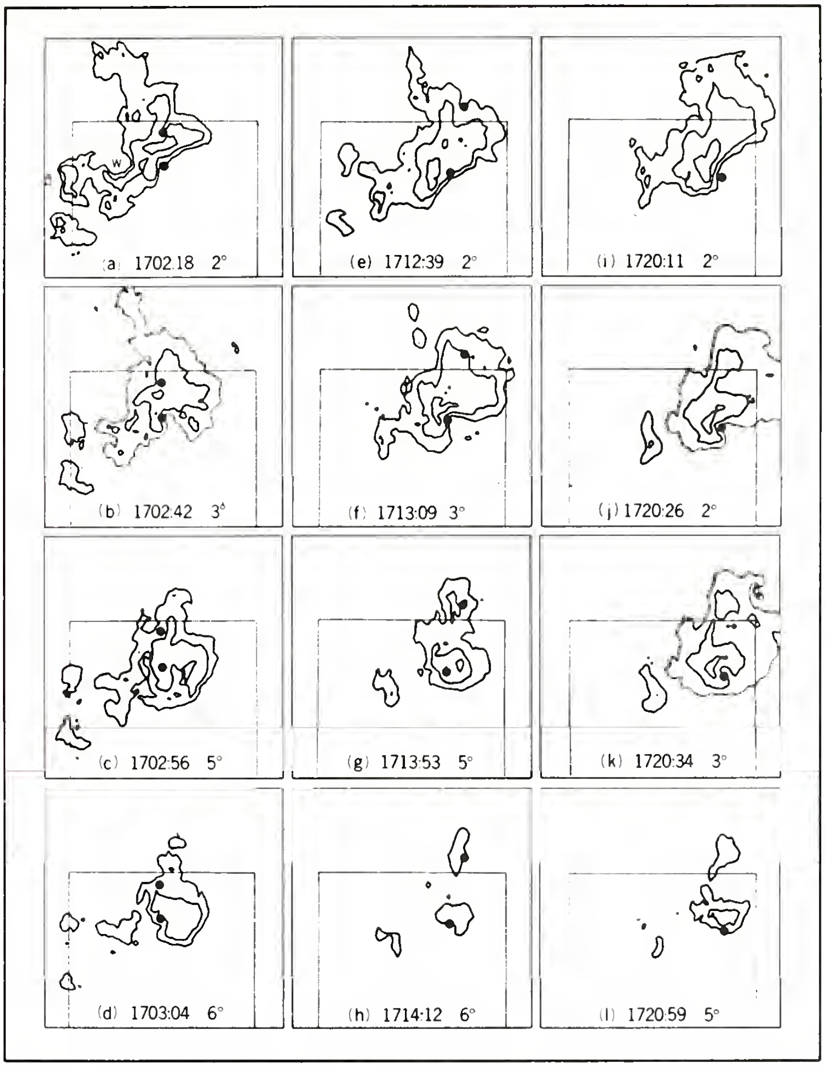

FIG. 8. Correlation of hailfall positions and storm radar structure at scan elevations from 2° to near cloud top for the 1703 and 1704 hailfalls (a–d), the 1712 and 1715 hailfalls (e–h), and the 1720–1721 hailfall (i–l). Hail areas are shaded, and radar contours are for 25, 35 and 45 dBZ.

was apparently intensifying, as judged by the eastern position of the precipitation maximum. The largest hailstones (diameter ~1 cm) fell early in this period. The small hailfalls at 1704, 1708, 1711–1716 and 1717–1725 were oriented to the right, or south, of the maxima of both the rainfall rate and the total precipitation. A line through the center of these hailfalls was approximately parallel to the storm path. The regularly spaced hailstreaks constitute a hailswath as described by Changnon (1970). They appeared as discrete falls well separated in time and space despite the steady-state radar structure of the cloud system.

Fig. 7 shows the 1° elevation CP-2 radar contours (10-dBZ contours beginning with 25 dBZ) for 1702:10, 1712:25, and 1720:02. The location of hailfall that occurred at the ground approximately 1 min later is indicated by the markers on the respective scans. Fig. 7b shows that the leading edge of the precipitation wall had just crossed the known point of hailfall at station 632. Above the 1° elevation scan, the correlations of hailfall position and the storm radar structure are striking, as can be seen in Fig. 8. Figs. 8e–h show the surface hailfall point plotted with the 2°, 3°, 5°, and 6° CP-2 scan data (corresponding approximately to 4, 5.2, 7.6 and 8.8 km MSL cloud levels) obtained between 1712 and 1714:12. At 2° elevation (which was essentially cloud base), the hailfall position relative to the radar structure had not changed appreciably. As in the 1° scan, the precipitation wall had little major detail, although the narrow 25 and 35 dBZ contour spacing does suggest a region of inflow stretching southwest-northeast along a cloud front nearly 20 km long. However, at 3° elevation angle, the location of the surface hailfall was near the apex of a well-defined U-shaped indentation in the forward precipitation echo structure. This relationship was accurately repeated at the 4° elevation scan (not shown). At the 5° and 6° elevation scans, the maximum reflectivities occurred east and north of the position of the surface hailfall; at the lower levels the maximum reflectivities occurred west and north. This analysis makes it clear that the southeastern region along the precipitation wall was indeed a region of strongest inflow. The primary updraft area was clearly defined by the WER existing at the 5 to 7 km levels (3° and 4° scan elevations). In the upper cloud ($\geqslant 8$ km) the region of maximum precipitation loading shifted across to the north of the surface hailfall position.

The surface hailfall was associated with the forward, advancing region of maximum reflectivity gradient through at least the level of 7 km MSL, and to a lesser extent, it was associated with the border of the high reflectivity zone through upper storm levels. The surface hailfalls did, in fact, occur beneath regions of maximum reflectivity gradient, which extended vertically upward through the storm.

The same detailed features of the storm radar structure and point of hailfall also occurred for the 1704 and 1717–1725 hailstreaks, as can be seen in Figs. 8a–d and 8i–l. Here again, the position of the surface hailfall was exactly along the border and near the apex of a well-defined WER at the 3° and 4° elevations. Surface hail was measured only for 1711–1712; however, it is evident that the repeated hailstreaks occurred along the zone of maximum reflectivity gradient existing between the WER of high updraft velocity and the adjacent region of maximum precipitation loading. The radar echo structure shows that the strongest updraft in the southeastern front of the storm rose steeply along and in front of the advancing semi-circular enclosure of the precipitation bounding the WER at middle cloud levels. With the loss of thermal buoyancy and the increased precipitation loading at upper storm levels, the updraft flow exhausted northward and eastward as the combined resultant of the inflow momentum and upper level shear.

The two northern hailfalls at 1703 and 1715 (Fig. 4) appeared at first glance to be isolated events. However, their time and location showed they were identically positioned with respect to the V-shaped indentation on the northeastern portion of the storm echo. This is shown in Figs. 7a and 7b where the 1703 hailfall is positioned with respect to the 1701:55 CP-2 display, and the 1715 hailfall with the 1712:25 display, respectively, both at 1° elevation. This suggested strongly that the northern indentation was also a WER region with well-organized low-level inflow. Further evidence in support of this interpretation was obtained through Fig. 8. The positions of the 1703 and 1715 hailfalls are indicated by the northern markers at the 64- and 76-km ranges (from Grover), respectively. The consistent V-shaped inflow contours are equally evident on the 2° elevation scans (~ 5 km MSL); at 3° a broad maximum is adjacent to the surface hailfall location; at 5° and 6° elevations (near 9 km) north-south oriented maximum areas are apparent. For the earlier period, the upper maximum was displaced eastward from the point of hailfall. By the time of the later period, the east side of this northern maximum echo region was nearly directly above the point of surface hailfall despite the strong shear; this indicates that a more intense updraft was occurring during this period. Under the strong shear conditions, the north-south extension of the upper level maximum can only be interpreted as the upper level outflow region. The picture presented is that of a low-level inflow from the northeast; the updraft, which still possessed appreciable southwesterly horizontal velocity near cloud base (1° and 2° scans), became nearly vertical at mid-cloud level (3° scan), produced a small amount of hail, and finally reached its maximum height along a north-south line at elevations of 7–9 km MSL (5° and 6° scans).

We are fortunate to be able to verify these features of the flow by studying dropsonde trajectories obtained concurrently with the 1703 hail (Bushnell, 1973). At 1659 MDT, 10 dropsondes were released at 500 m intervals from the NHRE Sabreliner aircraft flying at 13 km altitude above cloud tops along the line AB in Fig. 8a. Nine sondes arrived at the surface approximately 10 min later falling along the line CD. Bushnell reported that the initial sonde drift above cloud tops was easterly; drift at upper cloud levels (8500–7000 m) was northerly, and at lower cloud levels, southerly. As seen, the dropsonde trajectories straddled the region of interest around 1703. Sonde No. 6 remained aloft approximately 75 sec longer as a result of interception by more intense updraft with maximum vertical velocity of 13 m sec^{-1} at 7–9 km elevation, and arrived at the surface north of its expected point of impact along CD.

Study of the radar returns showed that from 1645 to 1720 the northeasterly inflow was a persistent feature of the storm. This inflow region moved east-northeastward (from 240°), perhaps as the result of its differing propagation direction while the primary storm, as evaluated from the rainfall contours, moved east (from 270°). The small areas of precipitation maxima along the northern boundary of the Protected Area were doubtlessly associated with the northern updraft system. The divergent motion of the respective updraft and cell areas suggests that the two updrafts constituted an incipient splitting storm which, perhaps because of the limited buoyancy (energy) that existed on this day, failed to develop into two separate steady-state systems. The basic storm-splitting mechanism is believed by the author to originate with the inflow orientations evident here.

The existence of the second well-developed updraft verifies the conclusion of Musil *et al.* (1973) that targeting of seeding material simultaneously into more than one region of the cloud is a requirement for effective hail suppression. An examination of Fig. 7a and Figs. 8a–d shows that very possibly a moderately well-developed updraft occurred at 1702 in the region (W on Fig. 7a) on the rear side of the storm. This feature was not evident 10 min later (Fig. 7b and Figs. 8e–h); however, it emphasizes the complexity of a storm's organization with time and space. Given the primary continuing inflow-updraft regime on the southeastern side of the storm, significant secondary and tertiary flow fields to the storm may exist simultaneously. Operation controllers engaged in field seeding programs must be especially skilled in recognizing the pattern of updraft regimes within the radar echo structure of storms.

b. Rainfall

The pattern of total precipitation (Fig. 3) is decidedly cellular despite the quasi-steady storm structure evidenced by radar. The rainfall isohyetal contours show the regions of maximum and minimum rain were regularly spaced across the network. Table 2 lists the positions of maxima and minima (in kilometers east from Grover) and the distances that separate them. The spatial regularity was also reflected in the isochrones of precipitation onset, shown as broken lines in Fig. 3. The precipitation minima occurred approximately along the curves of 1645, 1700, 1715 and 1730 MDT.

Similar variations have been reported (Stall *et al.*, 1971) from dense precipitation networks in Ohio and in Illinois. This suggests that pulsed precipitation is a property of quasi-steady state storms regardless of their geographical and meteorological environment.

c. Aircraft measurements

The 22 July storm was penetrated twice by the armored T-28 aircraft (Musil *et al.*, 1973). The final penetration was made from northwest to southeast through the region of highest reflectivity; the plane exited the storm through the region of the WER and forward overhang. Hail estimated from pea size to 2 cm diameter was encountered near the edges of the updraft, implying the region of hail growth. Errors in aircraft and radar positioning preclude a definite conclusion about whether the hail observed at flight level (5–6 km) occurred in the region of high reflectivity gradient or that of highest reflectivity. On the basis of the network and radar analysis given here (position errors are small), the conclusion that the hail was encountered within the region of maximum reflectivity gradient appears warranted.

Table 2. Locations and distances of separation of rain maxima and minima (km).

Location of maximum	Distance between maxima	Location of minimum	Distance between minima
43	13	50	12
56	13	62	12
69	13	74	13
82		87	

6. Summary and description of the sheared, moderate-intensity thunderstorm

The 22 July storm occurred in an environment of moderate to strong shear (6×10^{-3} sec^{-1}) and, throughout the more than 1-hr period of transit across the precipitation network, evidenced a well-defined and persistent WER along its southeastern flank. The storm's motion was nearly from the west, to the right of the 240° environmental winds. A well-defined precipitation wall oriented southwest–northeast and 15–20 km long was evident from the low-level radar echo. The WER region was most pronounced at 4–6 km MSL and generally oriented to form an inverted U-shaped region with its apex toward the northwest. A steep reflectivity gradient existed within the wall at cloud base and below and bordered the WER to the west and north at lower-to-middle cloud levels. The observed hailfalls, which were recorded south of the regions of precipitation maximum, appear to be precisely located along the northwestern extremity of the WER and at the leading edge of the precipitation wall. At the point of surface hailfall, the line or arc of maximum reflectivity gradient rose nearly vertically to mid-cloud levels which was approximately the region of −15C cloud temperature. Only in this WER area did the storm have this height of vertical wall separating the precipitation and WER. Above this, the WER was capped by increased hydrometeor loading which, at still higher cloud levels, spread north and east.

During this same period, one additional updraft zone was persistent in the northeastern storm quadrant. This was initially deduced from observed surface hailstreaks and the storm's radar reflectivity pattern and confirmed by dropsonde vertical wind profiles. The WER here was less well-developed and was capped by a hydrometeor distribution at a lower elevation, indicating a less intense updraft than that existing in the southern storm cell. The horizontal motion of these two systems was divergent; however, the northern branch died before storm splitting. The high-level outflow from the second updraft region was such as to cause the north-south oriented high-level radar echo (Figs. 8c–d and 8g–h), despite a near 50 m sec^{-1} environmental crosswind (from 240°) at the cloud top.

The timed hailfall observed at the surface during this storm provides the basis for an analysis of the precipitation and hail mechanisms. On the southeastern storm flank, the relative orientation of the WER and the position of the reflectivity maximum show that the low-level inflow was from the southeast. The lateral extent of the precipitation wall at cloud base indicates enough inflow to develop precipitation all along the wall, but the existence of the WER shows that horizontal convergence occurred along the central region ahead of the wall near or below cloud base. The WER was the region of maximum updraft; however, the presence of the continuing reflectivity maximum arc adjacent to the WER (at low and mid cloud level) can only mean that a major part of the hydrometeor growth occurred within the vertical sheath defined by the maximum reflectivity gradient. Here the existing precipitation distribution acts to capture the cloud water, increasing the precipitation along the forward surface of the reflectivity core. This continues until the loading within this sheath causes negative buoyancy and the region contributes to the precipitation downdraft of the storm. Even with adiabatic cloud water contents, this growth by capture is comparatively rapid (Phillips, 1969; Iribarne and De Pena, 1962).

In accordance with the equations of motion and continuity, such an increase in the precipitation loading is accompanied by a decrease in vertical cloud updraft velocity with time. This necessarily results in a divergent forward flow of cloud and precipitation particles from the vertical reflectivity sheath toward the maximum updraft velocity region within the WER. This provides for a new sheath region of growing particles which grow to load an adjacent sheath. The process is repeated and repeated, in a continuous manner, the net result being that the region of high reflectivity (precipitation) continuously propagates forward into the WER which is, in turn, forced backward before the storm.

Such a near vertical sheath region of high horizontal shear is clearly an ideal region for hail growth. Once the WER attains updraft velocities greater than hailstone terminal speeds, then somewhere in the shear zone between downdraft and maximum updraft, the proper updraft velocities exist for hail growth. Hail embryos are provided from the precipitation capping the WER, perhaps having been developed in the forward overhang, and either can grow in one continuous path along the forward edge of the vertical and overhanging precipitation wall or can grow as they are circulated and tumbled about in the divergent flow regimes originating with the continuous hydrometeor loading within the wall. In the latter case, the growing stone can be carried forward again into higher velocity updrafts where it may circle about in new growth environments and repeat the growth cycles.

The hailstreaks observed beside the region of the maximum precipitation in the 22 July storm require only a slightly more complex growth analysis. These growth mechanisms that operate within the region of large horizontal gradients in the vertical updraft velocity are believed to be the principal hail-producing mechanisms operating in most storms. Dependent, as they are, on the horizontal divergence arising from the loss of buoyancy with precipitation growth, hail development is largely independent of such factors as updraft slope and maximum updraft velocities.

On another point, Kitschfeld (1959) has suggested that the ability of a storm system to remain upright in the presence of severe wind shear occurs because the winds erode the cloud and precipitation sheath from around updraft cores. This erosion prevents the cores from becoming surrounded by large concentrations of precipitation which would cause the updraft to become negatively buoyant. Marwitz (1972a) further proposed that the shear acts to erode the precipitation from around a given side of the core; this allows the large WER to persist. From the analysis of the 22 July storm, slightly simpler arguments seem adequate. First, though the northern precipitation-inflow areas neither were "well-defined" as to WER, nor were of long-term persistence (as specified by Marwitz), it is clear that this regime, which did exist for some 30 min, was almost entirely shielded from the environmental flow by the blocking cloud structure upwind. No erosion by the local wind was therefore possible. Second, the flow regime in the southeastern quadrant itself prevented the development of precipitation along the southeastern border of the WER. The inflow air motion to the cell was from the southeast; it passed partially through the region of high reflectivity gradient where it lost appreciable cloud water through hydrometeor capture. The remainder of the cloud water (perhaps 50–75%) was carried upward through the WER. The precipitation load that formed at high cloud level, capping the WER, was diverted by the 240° windflow there and was carried northeast. From inflow at cloud base, the wind veered with height executing approximately a 90° curve by the time of outflow from the updraft. In the northern cell, the radar structure suggests that there the wind veered as much as 150° with height and exited north or perhaps north–south at high levels. For this northern system, one can speculate that the limited lifetime of this cell resulted from the more nearly 180° veering with height and resulting precipitation loading of the updraft flow. In contrast, the removal of the precipitation at the high cloud level in a specified direction, such as occurs in the southern system, prevents precipitation loading along the outer boundary of the WER and therefore allows the continuing updraft and WER to backstep before the storm.

Acknowledgments. The author especially acknowledges the work of H. J. Wells whose supervision of the precipitation network contributed immeasurably toward the quality of the precipitation data, and also the generous support and leadership of Dr. H. K. Weickmann, Director of NOAA's Atmospheric Physics and Chemistry Laboratory, Dr. W. Swinbank, Director of the National Hail Suppression Experiment, and the many other fellow scientists involved in the NHRE program.

REFERENCES

Browning, K. A., 1964: Airflow and precipitation trajectories within severe local storms which travel to the right of winds. *J. Atmos. Sci.*, **21**, 634–639.

——, 1965: A family outbreak of severe local storms—A comprehensive study of the storms in Oklahoma on 26 May 1963, Part 1. Spec. Rept. 32, AFCRL-65-695 (1), 346 pp.

Bushnell, R. H., 1973: Dropsonde measurements of vertical winds in the Colorado thunderstorm of 22 July 1972. *J. Appl. Meteor.*, **30**, 1371–1374.

Changnon, S. A., 1970: Hailstreaks. *J. Atmos. Sci.*, **27**, 109–125.

Eccles, P. J., 1973: Two discontinuous movements of a severely sheared storm. NHRE Tech. Rept. No. 73/1, NCAR.

Foote, G. B., and J. C. Fankhauser, 1973: Airflow and moisture budget beneath a northeast Colorado hailstorm. *J. Appl. Meteor.*, **12**, 1330–1353.

Hitschfeld, W., 1959: The motion and erosion of convective storms in severe vertical wind shear. Sci. Rept. MW-29, Stormy Weather Group, McGill University, Montreal, 48 pp.

Iribarne, J. V., and R. G. De Pena, 1962: The influence of particle concentration on the evolution of hailstones. *Nubila*, **5**, No. 1, 7–30.

Marwitz, J. D., 1972a: The structure and motion of severe hailstorms, Part I: Supercell storms. *J. Appl. Meteor.*, **11**, 166–180.

——, 1972b: The structure and motion of severe hailstorms, Part III: Severely sheared storms. *J. Appl. Meteor.*, **11**, 189–201.

Modahl, A. C., 1973: Meso-scale surface flow features on 22 July 1972. *Preprints 8th Severe Local Storms Conf.*, Denver, Colo., Amer. Meteor. Soc., 149–154.

Musil, D. J., W. R. Sand and R. A. Schleusener, 1973: Analysis of data from T-28 aircraft penetrations of a Colorado hailstorm. *J. Appl. Meteor.*, **12**, 1364–1370.

Phillips, B. B., 1969: Water load in convective storms and its influence on storm kinetics. ESSA Tech. Memo. ERL TM-APCL 6, 55 pp.

Stall, J. B., F. Asce and F. A. Huff, 1971: The structure of thunderstorm rainfall. Preprint 1330, Amer. Soc. Civil Engineers National Water Resources Engineering Meeting, Phoenix, 30 pp.

Reprinted with permission of the workshop on Inadvertent Weather
Modification, State University, Logan, Utah, August 1973.

Recent Developments in Chemical Aerosol Analysis

Rudolf F. Pueschel
Atmospheric Physics and Chemistry Laboratory
National Oceanic and Atmospheric Administration
Boulder, Colorado 80302

Presented at the Workshop on Inadvertent Weather Modification
13-31 August, 1973, Utah State University, Logan, Utah

1. Introduction

The growing number of publications dealing with the environmental crisis are ample proof of an existing concern about man's activities having detrimental effects on the global climate and the local weather. Our involvement over the past decade in weather modification research and environmental monitoring permits the following conclusions:

The atmosphere over remote areas of the globe, such as the mid-Pacific, is still unpolluted. Although the turbidity at such locations is affected by occasional volcanic eruptions, no trend is apparent which could be attributed to industrial growth during the past 15 years (Ellis and Pueschel, 1971). The visibility still approaches the 350 km Rayleigh limit, and precision conductivity measurements between 1960 and 1968 showed no change in the aerosol content of the atmosphere (Cobb, 1973).

The situation is different near population centers. There we find evidence of a deterioriated environmental quality that is in direct proportion to the density of anthropogenic pollution sources. Smoke stacks from metal foundries are prolific sources of freezing and condensation nuclei (Barret et al., 1970). During our research in the Great Lakes Basin, we frequently observed strong glaciation in supercooled stratus downwind from industrial plumes. Even at remote locations we find examples of trends in the atmospheric aerosol concentration; Figure 1 shows the vertical Aitken nuclei profiles in such locations from 1955, 1961, and 1972 (Weickmann, 1957; Junge, 1961; and Allee, 1973). The atmospheric changes shown in these observations make it necessary to find better qualitative and quantitative means to evaluate the atmospheric nuclei budget.

2. Approach

A knowledge of the Aitken nuclei population alone does not permit a proper evaluation of possible effects of aerosols on weather and/or climate. These particles are generally too small to scatter light enough to have consequences on the radiation budget, and the high supersaturation at which they are detected permits little if any conclusions about their behavior in natural clouds. This is illustrated in Figure 2 by a series of measurements on 8 June, 1973 in Denver, Colorado, of Aitken nuclei, cloud condensation nuclei, ice nuclei, and the atmospheric light scattering coefficient. From the start of the measurements at 0830 MDT until about 0930 MDT, the instruments were located downwind from the city. A wind shift then positioned them directly upwind.

Focusing attention first on the Aitken nuclei profile, note that the wind shift caused a decrease in the atmospheric Aitken nuclei population. This could mean either a decrease in the total number of particles or a decline of the number of smaller particles that have been converted to larger ones by coagulation. The increase in light scattering simultaneous with a decrease in Aitken particles shows that the latter was indeed the case. Most important in regard to inadvertent weather modification is the simultaneous increase in both cloud and freezing nuclei. The increase in cloud nuclei can be explained by the presence of larger particles that through their appreciably larger surface area provide a greater number of sites of least Gibbs free energy for water molecules. An explanation of the greater number of ice nuclei, however, requires additional information about the ice forming property of a particle, such as, epitaxi and/or chemical composition.

The data shown in Figure 1 were acquired with instruments installed in a mobile laboratory that consisted of the following components:

(1) A recording Aitken Nucleus Counter (Environment/One, 1970),
(2) A recording Cloud Condensation Nucleus Counter (Radke and Hobbs, 1969),
(3) A NCAR Acoustic Ice Nucleus Counter (Langer, 1973),
(4) An integrating Nephelometer (Ahlquist and Charlson, (1967).

Although these commercially available instruments provide valuable information about existing nuclei populations, they do not permit much information about the chemical composition of individual particles. Yet it is the aerosol chemistry that determines in connection with size and shape their scattering/absorption and nucleation capability. Therefore, a laser spectroscopic particle analyser has been developed and elemental analysis is performed using a combination of scanning electron microscopy--energy dispersive X-ray analysis. These last two methods, because of their novelty, are the subject of discussion in this paper.

3. Chemical Aerosol Analysis

3.1 Spectroscopic Laser Particle Analyser

The principles of spectroscopic aerosol analysis are shown in Figure 3 (Pueschel, 1969). Individual aerosol particles are exposed to an environment whose energy density is high enough to vaporize the particles and excite the atoms and molecules of the vapor. While conventional flames and arcs can be used, the instrument we used was a 50 W CO_2 laser that gives, through proper focusing, an energy density of 10^6 W/cm^2. This has the advantages of providing a truly dark background for the short wavelength-sensitive photomultiplier, and avoids the formation of refractory oxides and carbides, which greatly reduce the lower detectability limit of the element. The spectral light emission from the particles is detected by a photomultiplier, with a narrow-band interference filter to select the desired wavelengths. The electric pulses from the photomultiplier are analyzed by a pulse height analyzer. This is a special-purpose digital computer with ferrite core memory. The device sorts the incoming pulses in each energy band or memory location to produce a complete energy spectrum of the light flashes emitted as individual aerosol particles pass through the sensing volume.

Figures 4 and 5 demonstrate the type of information that results from this analyzer. Figure 4 shows, as function of wavelength, the maximum energy emitted from particles in the exhaust from an internal combustion engine burning premium (upper curve) and regular gasoline (lower curve). Clearly, premium gas produces aerosol particles that emit a greater amount of energy. This is equivalent to stating that the exhaust particles produced by the combustion of premium gas contain a larger amount of specific elements and absorb more of visible light. Noteworthy also is the enhanced emission at wavelengths coinciding with emission lines (arrows). The laser particle analyzer can provide qualitative and quantitative information about the chemical composition of aerosols.

Figure 5 shows as function of channel number, which is proportional to the intensity of light pulses emitted from individual particles, the number of emissions for a series of 1-hour tests in Denver, Colorado, on 8 June 1973. The solid dots in Figure 5 are running means over 100 channels from a 1024-channel pulse height analyzer. The stars below the dots represent the corresponding standard deviations from the means. Note that the latter approach the measuring values when the sampling population is low. In the majority of cases, however, the mean exceeds the standard deviations to a statistically significant degree. The ratio between arithmetic mean and standard deviation can be further increased by a longer sampling time.

The operating conditions of the apparatus and pertinent weather observations are listed in Table 1: Column one identifies the sampling runs for the time intervals given in column two. Column 3 shows the wavelengths intervals at which the particle emissions were measured. These were determined by interference type light filters mounted in front of the photomultiplier tube. The fourth column gives the area under each curve, corrected for filter transmissivity and spectral S-11 characteristic of the photomultiplier tube. These values are proportional to the total aerosol emissivity in the particular wavelength intervals.

The following conclusions can be drawn from the data in Figure 5 and Table 1:

(1) The increase in counts during the morning demonstrates the addition to the atmosphere of anthropogenic aerosols. This is most conclusively shown by a comparison of runs number 2 and 3 which are operationally identical. The aerosols emissivity-absorptivity within a wavelength interval centered around a lead emission line at 405.8 nm increased fivefold during the morning rush hour. Lead from automobile exhaust is the probable cause for this increase. Run No. 7 shows that later in the day, after the temperature inversion breakup dilutes the aerosols, absorptivity reduces to the value observed before the early morning traffic.

(2) The change of aerosol emissivity during this same time at a wavelength band centered around 484 nm, which does not contain a lead emission line, is considerably smaller.

We conclude, that the anthropogenic city aerosol contains an appreciable amount of lead which is detectable with the laser particle analyzer.

Hence, this instrument provides two important types of information. First, as is well known from climatic models, an increased atmospheric aerosol burden can warm or cool the earth's surface; this depends on the scattering-to-absorption ratio of the added particles. Scattering can be measured quite reliably with existing instruments; but aerosol absorptivity is less amenable to measurements. Now, the area under the curves of Figure 5 is proportional to the emissivity of the aerosol that has been investigated with the laser particle analyzer. Once the coupling of laser energy with particulate matter is understood, application of Kirchhoff's radiation law will permit us to interpret this analyzer output in terms of the aerosol absorption coefficient. Second, the detection of emission of radiation at lines and bands that correspond to specific elements and molecules, respectively, results in a chemical analysis of individual aerosol particles. This chemical makeup of the particles, in turn, determines their capability to act as heterogeneous nucleation centers for transforming water vapor into droplets or crystals. Both types of information can be obtained *in situ* and on a real-time basis.

3.2 Scanning Electron Microscopy and Energy-Dispersive X-ray Analysis

Size, shape, and chemical composition of aerosol particles are all vital information for evaluating their nucleation capability and their effects on the radiation budget. A scanning electron microscope (SEM) interfaced with an energy dispersive X-ray analyzer can provide all three types of information. Because secondary electrons are emitted from the specimen's surface, the scanning electron microscope enables the user to visualize directly the surface of particles at large magnifications. This instrument is thus quite different from the conventional light microscope, which has a very limited depth of field at high magnifications (e.g., 1000 max) and a resolution limit that can hardly be pushed beyond 0.5 μm; and also from the conventional transmission electron microscope, which has great depth of field and resolution but cannot work directly with solid surfaces. Since the SEM operated by bombarding the specimen with electrons, X-rays that are characteristic of particular elements are generated at the point of impact and can be used to determine the elemental composition of the specimen. The general construction of the scanning electron microscope (Figure 6) includes an electron gun, lenses to produce a fine beam of electrons at the specimen, and deflection coils to scan the beam over the specimen's surface. Usually, the beam current employed in any SEM is too weak to be used for X-ray excitation. A breakthrough was recently achieved by employing field emission principles in commercial SEM's. Although the beam intensity is still weaker than in a conventional microprobe analyzer, this disadvantage is compensated for by the SEM's better focusing capability, which results in an improved resolution of about 200 Å. As the name implies, the energy dispersive spectrometer measures X-ray energy directly, producing a spectrum of counts versus energy in keV. As each X-ray quantum enters the detector (Figure 6), it produces a shower of photoelectrons that strike the silicon atoms and raise bound electrons to the conduction band. Each such event requires exactly 3.8 eV of energy, so that the total number of electrons freed is linearly proportional to the energy of the entering X-ray. The charge is collected by an applied bias voltage before the next X-ray enters the detector. To prevent losing the electrons during this collection process, it is necessary to fill up any imperfections or dislocations in the silicon lattice which would trap electrons. This is done by diffusing in lithium atoms. Because the device is operated at liquid nitrogen temperatures this reduces the dark current and permits these very low currents to be measured accurately.

The charge collected from the detector is amplified by a field effect transistor preamplifier, whose output is a stairstep of voltage; the height of each step is proportional to the X-ray energy. Further amplification, filtering to reduce noise, and differentiating of the signal produce a train of pulses. Again, each pulse has a height proportional to the energy of the X-ray that produced it. A special-purpose computer called a pulse height analyzer measures and stores these pulses in a spectrum. It operated by using each pulse to charge up a small capacitor and then discharges it with a constant current. During this process, a high-frequency crystal controlled clock measures the time required; again this is a linear measure of the X-ray energy. The resulting time is used as an address to store a count in the spectrum memory. The resulting spectrum can either be displayed with a suitable scale for interpretation or be transferred to a computer for further processing.

The information resulting from this operation is illustrated in Figures 7 through 9. Figure 7 (bottom) shows the formvar replica of an ice crystal that has been grown on an AgI nucleus (Parungo and Pueschel, 1973). The inhomogeneity that is apparent in the right of the crystal was investigated at 80,000 X magnification; the resulting X-ray spectrum (Figure 7, top) shows Ag at 3 keV and I at 4.5 keV. An examination of the inhomogeneity to the left of the crystal showed Si as the constituent; it is probably a quartz particle that was scavenged while the crystal was airborne. This latter particle — in competition with AgI — can be excluded as the ice nucleus on which the crystal developed.

The mechanism of ice nucleation is of considerable importance in weather modification. The position and composition of the ice nucleus within the ice crystal indicates by what mechanism it was formed. The nucleus being off center in the crystal indicates the crystal developed by a contact freezing process (Weickmann, 1970). Other possible nucleation mechanisms include deposition freezing, which would locate the nucleus in the center of the crystal, and droplet freezing by which the condensation nucleus acts as the nucleating center. If contact nucleation is the prevalant nucleation process, small nuclei must be produced for weather modification experiments, which would mean a considerable saving of nucleating material.

Figures 8 and 9 show (top to bottom) replicas of snowcrystals that have grown on natural nuclei, the nuclei dimensions, shape, and chemical composition. The nucleus in Figure 8 contains considerable amounts of Al and Si; it probably was kaolinite, an efficient freezing nucleating material. On the other hand, the nucleus in Figure 9 contains iodine, suggesting it has a marine origin.

Experiments are underway to establish the atmospheric distribution of natural and man-made freezing nuclei and their origin, by using this equipment.

4. Summary and Conclusions

The stability of cloud systems is determined by the size distribution of the cloud droplets that, in turn, is affected by the physical and chemical properties of the nuclei on which they have developed. At present, little information is available about what properties in the continental aerosols determine their efficiency in condensing and freezing water vapor. The techniques described in section 3 are being applied to regional field investigations of the atmospheric aerosols. This research will study the existing nuclei budget and provide important information for evaluating the advertant and inadvertant impact of man's activities on weather and climate. Our method of determining the elemental composition of individual aerosol particles enables us to identify man-made aerosols; thus, we can correlate changes in nuclei concentrations with man's activities.

A second area for applying our analytic techniques is a study of the transformation of initially inert particles into potential freezing nuclei when trace substances change their surfaces. For example, during the increased nuclei activity in Denver on 8 June 1973 (see Figure 2), we found that the bulk chemical property of the aerosols did not change significantly. However, we did discover that during this time there was an increased nucleating capability because the mineral dust was coated with heavy metals such as Pb and Ni. Such a surface coating in conjunction with possible photochemical reactions can apparently enhance the nucleating capability of otherwise inert dust particles. Another example of this kind is the property of Los Angeles smog to deactivate ice nucleation. Our involvement in nuclei inventory studies in Hawaii indicated a similar neutralizing effect on the ice nucleating capability of gases emitted by Kilauea Volcano.

Of considerable interest, from both the conceptual and the practical point of view, is the mechanism by which a freezing nucleus converts water vapor into ice. Our capability to determine the locale of the nucleus within the crystal enables us to determine the extent contact nucleation occurs in nature; therefore during cloudseeding, we can assess the effectiveness of the experiments. The considerable amount of nucleating material that could be saved by triggering contact nucleation in comparison with deposition nucleation has been mentioned.

An important unknown in climatic models is the absorptivity of aerosols for shortwave and longwave radiation. This determines whether an increased particulate loading of the atmosphere would lead to a warming or a cooling of the earth's surface. This parameter will be amenable to a quantitative evaluation once the coupling of laser energy with atmospheric particulate matter is understood. However, the present capability of the laser particle analyzer to provide on a real-time basis (1) signatures of aerosols that can be used to classify the aerosol content of a particular region and (2) information about the elemental composition of the aerosol, is already of great value in our attempt to learn about sources, sinks, and atmospheric residence times of aerosols in general, as well as condensation and freezing nuclei in particular.

Acknowledgements:

It is a pleasure to acknowledge the valuable contributions to this phase of the work, of Dr. Helmut Weickmann, whose interest, encouragement and support made the achievements possible; of Dr. Farn Parungo, who aided in the acquisition and interpretation of the energy-dispersive X-ray spectra; and of Richard Proulx and Charles Van Valin, who helped in instrument development and data acquisition.

REFERENCES:

Ahlquist, N. C., and R. J. Charlson, 1967: A New Instrument for the Evaluation of the Visual Quality of Air, J. Air Poll. Contr. Assoc. 17, 4, 7-470.

Allee, P. A., 1973: Personal Communication.

Barrett, E. W., R. F. Pueschel, H. K. Weickmann, P. M. Kuhn, 1970: Inadvertent Modification of Weather and Climate by Atmospheric Pollutants, ESSA Technical Report, ERL 185-APCL 15.

Cobb, W. E., 1973: Oceanic Aerosol Levels deduced from Measurements of the Electrical Conductivity of the Atmosphere, J. Atm. Sciences 30, 100-105.

Ellis, H. T., and R. F. Pueschel, 1971: Solar Radiation: Absence of Air Pollution Trends at Mauna Loa, Science 172, 945-84.

Environment/One Corporation, 1970: Instruction Manual for Condensation Nuclei Monitor Cat. # E-1033A-001.

Junge, C. E., 1961: Vertical Profiles of Condensation Nuclei in the Stratosphere, J. Meteorol. 18, 501-50.

Langer, G., 1973: Evaluation of the NCAR Ice Nucleus Counter, J. Appl. Meteor., Sept. 1973.

Parungo, F. P., and R. F. Pueschel, 1973: Ice Nucleation: Elemental Identification of Particles in Snow Crystals, Science 180, 1057-1058.

Pueschel, R. F., 1969: Principles and Applications of the Flame Scintillation Spectral Analysis, PhD Dissertation, University of Washington.

Radke, L. F., and P. V. Hobbs, 1969: An Automatic Cloud Condensation Nuclei Counter, J. Appl. Meteor. 8, 105-109.

Weickmann, H. K., 1957: Recent Measurements of the Vertical Distribution of Aitken Nuclei. In Artificial Stimulation of Rain, H. Weickmann and W. Smith, ed. Pergamon Press, London, p. 81.

Weickmann, H. K., 1970: AgI-Sublimation or Contact Nucleus? Proceedings 2nd National Conference on Weather Modification, Santa Barbara, 1970, p. 332.

Table 1. Laser particle analyzer operating conditions.
Denver, Colorado, 8 June 1973

Run No.	Sampling Period (MDT)	Wavelengths (nm)	$\int_0^c \frac{\Delta N}{\Delta c}\,dc$	T	T_s	Wind Direction	Wind Speed
1	0437-0537	450.0 ± 150	0.62	57	37	18	04
2	0555-0655	405.8 ± 25	1.75	60	41	18	08
3	0700-0800	405.8 ± 25	9.17	68	45	18	10
4	0812-0912	485.0 ± 25	6.38	74	48	24	04
5	0922-1022	589.0 ± 25	18.37	80	37	12	08
6	1030-1130	484.0 ± 25	3.57	82	39	09	12
7	1140-1240	405.8 ± 25	1.88	83	40	10	12

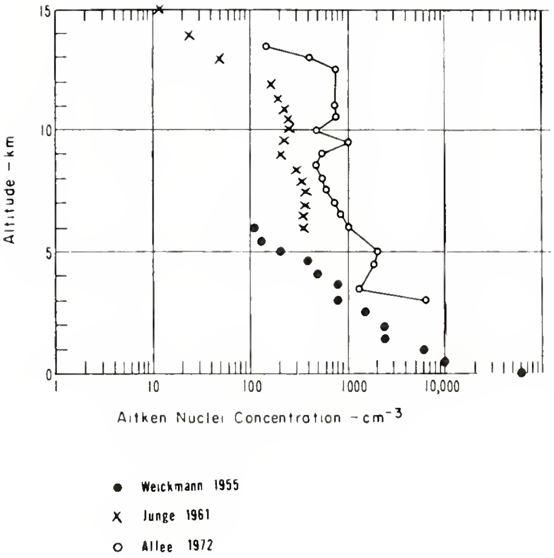

Figure 1. Vertical Aitken nuclei profiles over the north American continent from 1955, 1961, and 1972.

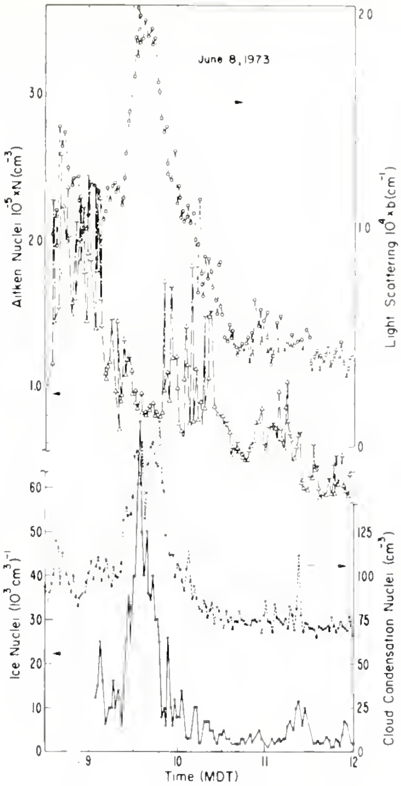

Figure 2. Temporal variation of Aitken nuclei, cloud condensation nuclei, ice nuclei, and light scatter during an air pollution episode in Denver, Colorado.

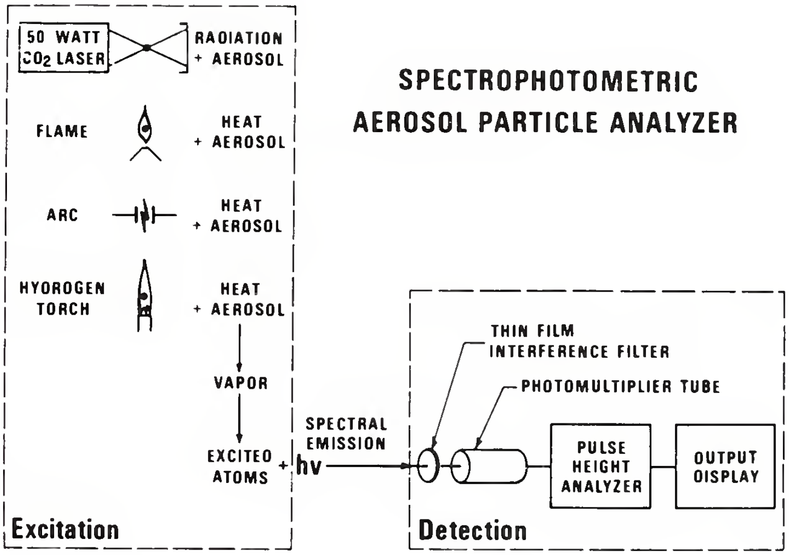

Figure 3. Principles of aerosol detection and analysis with a spectrophoto metric particle counter.

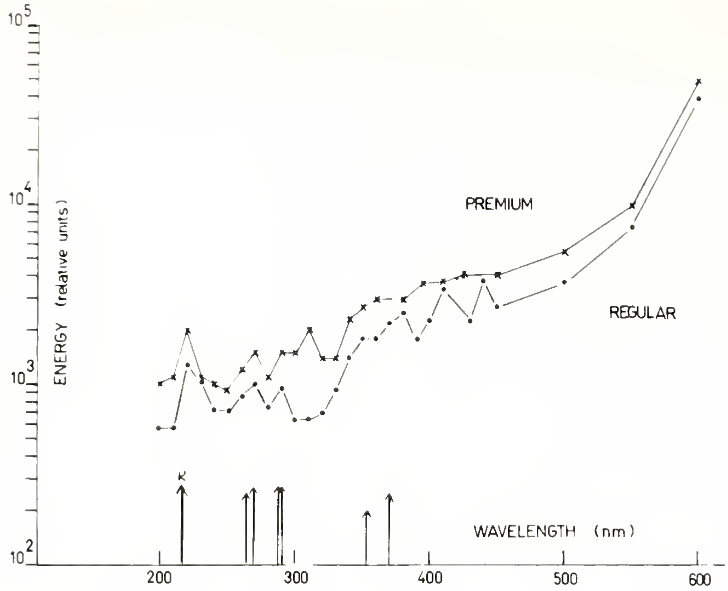

Figure 4. Wavelength response of the laser particle analyzer to exhaust aerosol from an internal combustion engine burning regular and premium gasoline.

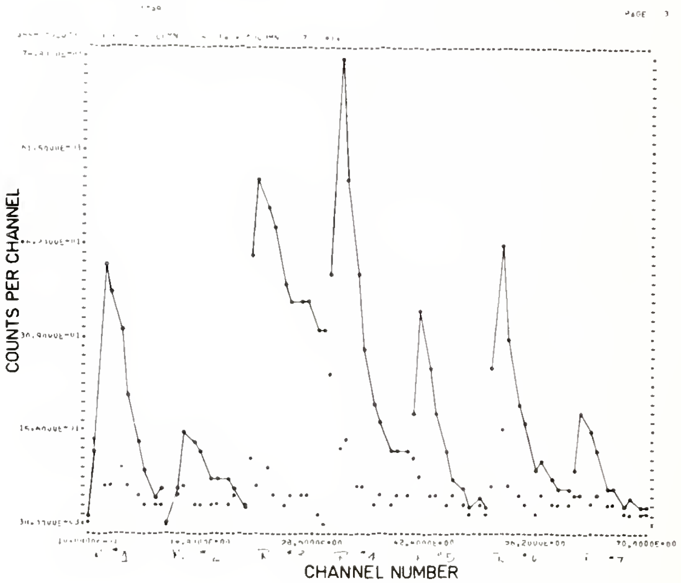

Figure 5. Relationship between aerosol concentration and emissivity as function of time and wavelength during an air pollution episode in Denver, Colorado.

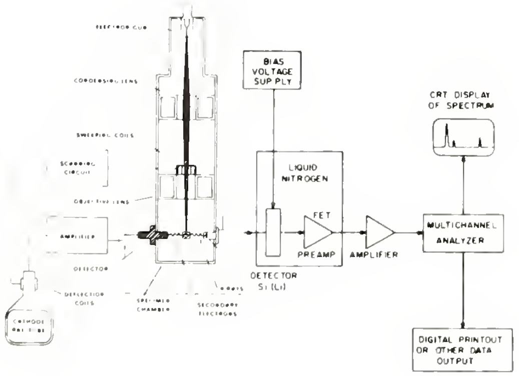

Figure 6. Schematic of scanning electron microscopy and energy dispersive X-ray analyzing system.

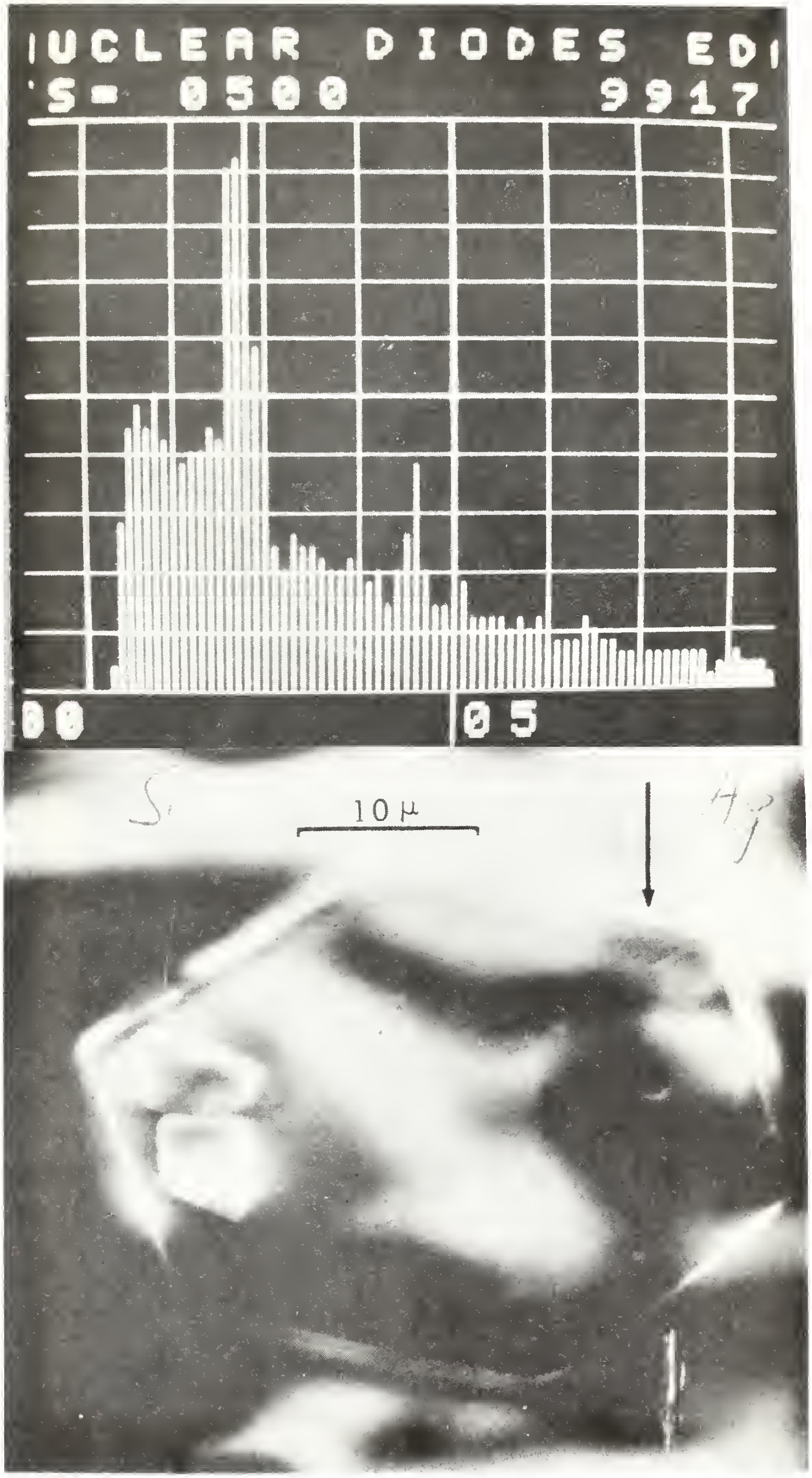

Figure 7. AgI seeded ice crystal and chemical composition of its nucleus.

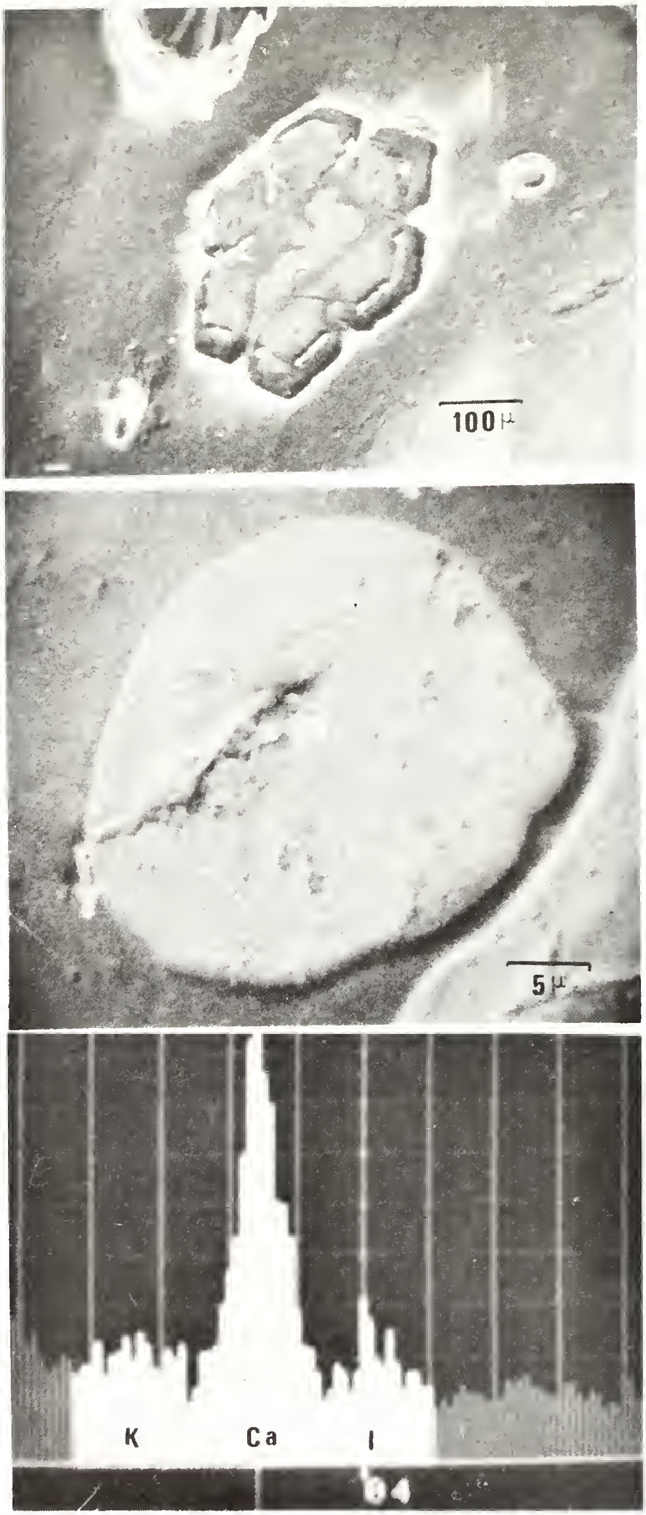

Figure 8. Replica of a natural snowflake, shape and elemental composition of its nucleus, collected in Boulder, Colorado.

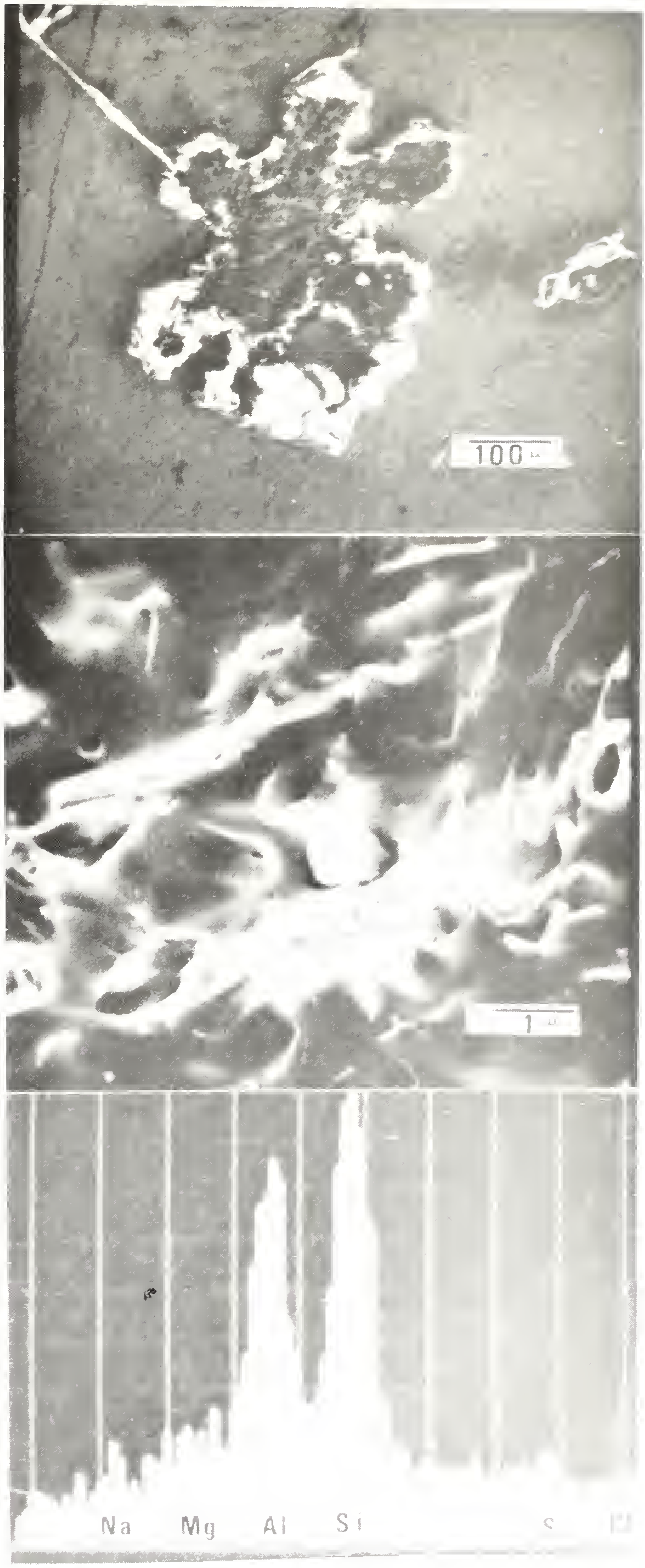

Figure 9. Replica of a natural snowflake, shape, and elemental composition of its nucleus.

Reprinted with permission of the Journal of Applied Meteorology
Vol. 12, No. 3, April 1973.

Sugar Cane Fires as a Source of Ice Nuclei in Hawaii

Rudolf F. Pueschel
Atmospheric Physics and Chemistry Laboratory, NOAA, Boulder, Colo. 80302

and Gerhard Langer
National Center for Atmospheric Research[1]*, Boulder, Colo. 80302*

2 November 1972 and 9 January 1973

Evidence of the existence of predominantly terrestrial sources of ice nuclei on the island of Hawaii has accumulated recently through studies by Mendonca and Pueschel (1972), Kline (1972), Hobbs *et al.* (1971), and Price and Pales (1964). This evidence contradicts the views of Bigg (1968) and Droessler and Hefferman (1965) who have reported evidence in Hawaii for support of Bowen's (1953) hypothesis of an extraterrestrial source of ice nuclei. Several field experiments with NCAR counters[2] and an improved membrane filter method during 1971–72 identified the burning of leaves during sugar cane harvesting as the most prolific source of ice nuclei on Hawaii. Previously, cane smoke had been studied only as a source of cloud condensation nuclei (Warner, 1967). Hobbs and Locatelli (1969) had observed ice nuclei from forest fires. The lowest nucleus concentration was found in the effluents of Mauna Ulu, a vent of Kilauea Volcano which was active during the latter part of the measurement period. Other sources investigated were automobile traffic in Hilo and ocean spray, both of which were determined to be minor sources of ice nuclei.

For the field tests, an NCAR counter was installed in an instrument trailer along with a continuous Aitken nucleus counter[3] and an integrating nephelometer[4]; the latter measures the total light scattering coefficient of the aerosol samples.

The data from one experiment at the Puna Sugar Co., 8 km south of Hilo, are shown in Fig. 1. (Similar results were obtained at a plantation 5 km northwest of Hilo.)

---

[1] The National Center for Atmospheric Research is sponsored by the National Science Foundation.

[2] NCAR-Bollay Ice Nucleus Counter, Model 103, Bollay Assoc., Boulder, Colo. (now E. E. & G., Albuquerque, N. M.).

[3] Condensation Nuclei Monitor, Model Rich 100, Environment One Corp., Latham, N. Y.

[4] Integrating Nephelometer, Model 550, Meteorology Research Inc., Altadena, Calif.

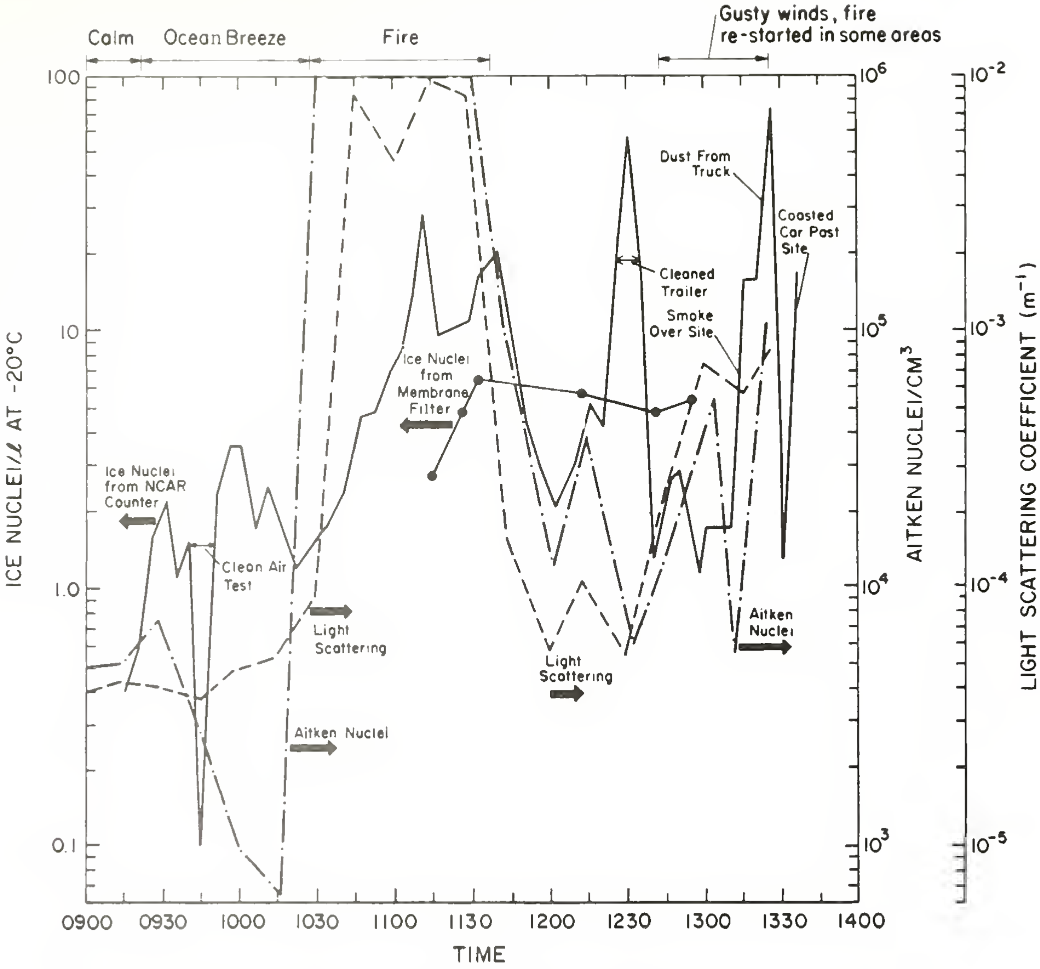

FIG. 1. Ice nucleus concentration (solid line), Aitken nucleus concentration (dot-dashed line), and light scattering coefficient (dashed line) variations with time in the vicinity of a sugar cane fire.

The figure shows ice nucleus concentrations from the NCAR counter and filter membranes, the light scattering coefficient, and Aitken nucleus data, all plotted as a function of time. Sampling was conducted for several hours prior to the start of the fires at 1000 LST at a distance of 100 m upwind. Under calm conditions before 0920, typical values of the measured parameters were as follows: 1) ice nucleus population of the order of 5×10^{-1} liter^{-1} at -20C, 2) Aitken nucleus concentration about 5×10^{3} cm^{-3}, and 3) the light scattering coefficient about 5×10^{-5} m^{-1}. The onset of an ocean breeze causes only a slight increase in atmospheric light scattering, accompanied by a significant decrease in Aitken counts due to the small aerosol concentration in maritime air. It also brings a marked increase in freezing nucleus concentration. More striking, however, is the marked increase of all three parameters after the start of the fire at 1030, and their positive correlation thereafter.

A full contribution of the cane fires to the ice nucleus inventory of the mid-Pacific area and their potential for inadvertent weather modification can be evaluated only by a continuous spatial survey during the overall harvesting period which usually lasts 10 months, i.e., February through November. Air sampling flights during May and June, 1972, showed ice nucleus concentrations to be between 0.3 and 1.0 liter^{-1} at -20C when membrane filters were partially exposed to the narrow smoke plumes between 100 and 300 m altitude. The pilot was unable to stay in the smoke plume at all times.

In laboratory tests, soil samples from Hawaii and from Colorado were dispersed separately into an NCAR counter; the samples of Hawaiian soil showed a ten

Table 1. Typical values of ice nucleus concentrations near potential sources in Hawaii.

Source	Ice nucleus concentration per liter at −20C	Method of detection
Upper tropospheric air	0.1	NCAR counter
Active volcanism at rim of volcano	0.1	Membrane filter
Volcanic fumes at rim of volcano	0.5	NCAR counter
Volcanic fumes at rim of volcano	0.5	Membrane filter
Hilo traffic at University of Hawaii campus	1.	NCAR counter
Maritime air 400 m from surf	1.	NCAR counter
Maritime air 400 m from surf	2.	Membrane filter
Cane fires, ground sample 30 to 300 m downwind from fire	10.	NCAR counter
Cane fires, ground sample 30 to 300 m downwind from fire	5.	Membrane filter
Cane fires*, 100 m above ground	1.	Membrane filter
Cane fires*, 300 m above ground	0.3	Membrane filter

* Flight along smoke plume.

times higher ice nucleus content. Apparently, the continuous accumulation of ash particles makes the Hawaiian soil rich in ice nuclei.

Cane leaves ripe for harvesting were burned in the laboratory and the smoke was aspirated through an NCAR counter at −21C. The leaves were supported so that the basic leaf structure remained intact during combustion. The count from the smoke alone was relatively low, but as soon as the ash skeleton disintegrated to produce a fine dust, the counts increased by an order of magnitude. This observation suggests that the noncombustible inorganic content of the leaves which are rich in copper and zinc provide the material that is active in ice forming nuclei.

In Table 1 the ice nucleus counts downwind from sugar cane fires are compared to other potential sources of nuclei on the island of Hawaii. Clearly, sugar cane fires are the most prolific single source of ice nuclei on the island of Hawaii.

REFERENCES

Bigg, E. K., 1968: Ice nucleus concentrations in Hawaii. *J. Appl. Meteor.*, **7**, 951–952.

Bowen, E. G., 1953: The influence of meteoritic dust on rainfall. *Australian J. Phys.*, **6**, 490–497.

Droessler, E. G., and K. J. Hefferman, 1965: Ice nucleus measurements in Hawaii. *J. Appl. Meteor.*, **4**, 442–445.

Hobbs, P. V., and J. D. Locatelli, 1969: Ice nuclei from a natural forest fire. *J. Appl. Meteor.*, **8**, 833–834.

——, C. M. Fullerton and G. C. Bluhm, 1971: Ice nucleus storms in Hawaii. *Nature*, **230**, 90–91.

Kline, D. B., 1972: Measurement of ice nuclei and associated chloride particle concentrations at Mauna Loa Observatory. *J. Appl. Meteor.*, **11**, 684–687.

Mendonca, B. G., and R. F. Pueschel, 1972: Ice nuclei, total aerosol and climatology at Mauna Loa, Hawaii. *J. Appl. Meteor.*, **12**, 156–160.

Price, S., and J. C. Pales, 1964: Ice nucleus counts and variations at 3.4 km and near sea level in Hawaii. *Mon. Wea. Rev.*, **92**, 207–221.

Warner, J., 1967: The production of cloud nuclei by cane fires and the effect on cloud droplet concentration. *J. Atmos. Sci.*, **24**, 704–706.

Reprinted with permission of the Journal of Applied Meteorology
Vol. 12, No. 8, December 1973.

Ozone and Water Vapor Injected into the Stratosphere from Two Isolated Thunderstorms

A. Shlanta[1] and P. M. Kuhn

Atmospheric Physics and Chemistry Laboratory, NOAA, Boulder, Colo. 80302

(Manuscript received 18 January 1972, in revised form 14 August 1973)

ABSTRACT

The local ozone concentration and water vapor overburden were measured from a WB-57F aircraft near thunderstorms that reached or penetrated the tropopause. Two storms were studied extensively: one that penetrated 800 m above the tropopause and another that reached to about the tropopause level. In both cases, water vapor overburdens above and downwind averaged some 40% higher than those upwind of the storms. The water vapor overburdens directly above the higher storm were about 2.4 times that of those background measurements upwind and at the same levels; directly above the weaker storm the water vapor was about 1.8 times as great as the background measurements. The spatial distribution of ozone around the two storms was similar to that of the water vapor: downwind concentrations exceeded those upwind at all levels. An excess in ozone of about 25% was observed in circumnavigations above the storm tops when compared with fair-weather values at the same levels away from the storm. Ozone concentrations directly above the higher storm, however, were observed to be about 40% more than those concentrations away from the storm, while those directly above the weaker storm were about 20% less than in undisturbed air. It thus appears that thunderstorms do inject substantial amounts of water vapor into the stratosphere and that growing, electrically active storms also generate ozone at their tops.

1. Introduction

In support of the U. S. Department of Transportation's Climatic Impact Assessment Program (CIAP), we are conducting a number of airborne surveys to determine the strengths of various natural sources and sinks of stratospheric trace constituents whose abundances might be affected by SST operations. Part of our program includes the study of transports of water vapor and ozone into the stratosphere by mesoscale convective circulation systems with instrumentation flown aboard a WB-57F aircraft. In this paper, we limit ourselves to a discussion of the data obtained in August and September, 1972, from two isolated thunderstorms that penetrated or reached the tropopause in the southwestern United States. These flights were flown by personnel of the 58th Weather Reconnaissance Squadron and were made out of Kirtland AFB, Albuquerque, N. M.

The first storm, 40 mi north of Amarillo, Tex., on the afternoon of 3 August 1972, was very active and reached a peak altitude of 15.5 km, which was about 800 m above the tropopause. Four overflights and five circumnavigations (boxes) were executed near this storm. Fig. 1 was taken from the aircraft at 16.8 km.

The second storm, 70 mi west of Tucson, Ariz., on 7 September 1972, was less massive and not as tall as the first. It was difficult to determine whether this storm penetrated the tropopause; the cloud reached 13 km, but the tropopause was indistinct and could be placed anywhere between 12.5 and 13.7 km. We considered this storm to be weakly penetrating in

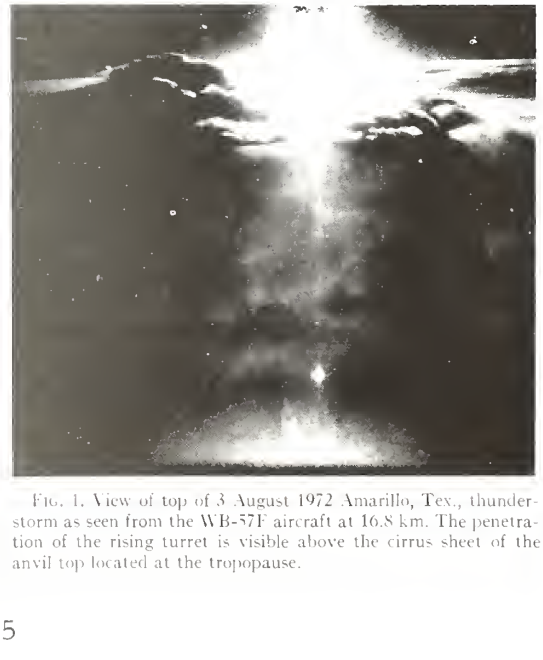

Fig. 1. View of top of 3 August 1972 Amarillo, Tex., thunderstorm as seen from the WB-57F aircraft at 16.8 km. The penetration of the rising turret is visible above the cirrus sheet of the anvil top located at the tropopause.

---

[1] Present affiliation: Michelson Laboratory, Naval Weapons Center, China Lake, Calif.

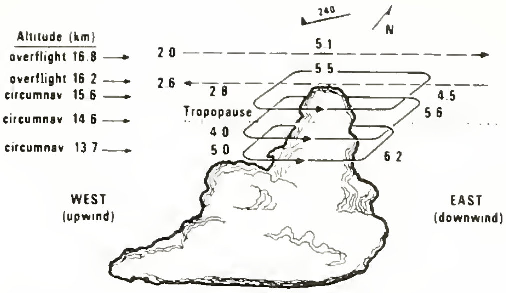

FIG. 2. Water vapor overburden values (gm cm$^{-2}\times10^4$) along flight tracks at descending altitudes in the vicinity of the Amarillo, Tex., thunderstorm. Note the overburdens downwind are greater than those upwind of the storm.

comparison with the first. Two overflights and two circumnavigations were flown near this storm which had already reached its peak height when first encountered by the aircraft. The storm declined noticeably during the rest of the mission.

2. Experimental instrumentation

The total mass of water vapor above flight level was measured by the infrared radiometric technique developed by Kuhn *et al.* (1969, 1971). For the measurements discussed here, a prototype upward-looking chopper bolometer radiometer with a filter spectral sensitivity in the band 18–23 μm was installed in the nose section of the WB-57F aircraft. To guard against interference from substances other than water vapor, such as aerosols or cloud particles, a second channel in which water vapor emission is negligibly small (from 10–12 μm) was also used. This water-vapor radiometer measures the *overburden* of water vapor (gm cm$^{-2}\times10^{-4}$), i.e., the water vapor for the entire atmosphere above flight level. This instrument has a response time constant of about 1 sec to a sudden change in overhead water vapor.

The ozone measuring instrument was an electrochemical concentration cell device (Kohmyr, 1969) using a wet chemical potassium iodide-iodine method for measuring ozone. This instrument measures *in-situ* values of the ozone concentration and has a response time constant of 20 sec to a sudden change in *local* ozone concentration. When this instrument was operating, ambient air together with any ozone was fed to the ozone monitor mounted in the bomb bay. To prevent contamination of this ozone monitor before and during takeoff, a barometric pressure switch was installed on the monitor to activate the instrument at altitudes above 3 km mean sea level (MSL).

To normalize the effects of the wide range of atmospheric pressures encountered in this study, the concentration units used for ozone are those of a volume mixing ratio, i.e., the number of ozone molecules per hundred million air molecules (pphmv). An ozone-air mixing ratio of 1 pphmv is equivalent at standard conditions to an ozone concentration of 2.69×10^{17} molecules or 21.4 μg, both per cubic meter of air. For a comprehensive discussion of various ozone units see Sticksel (1966).

3. Results of measurements

a. Water vapor

Fig. 2 gives water vapor overburdens for the 3 August storm where simplified flight tracks for three of the circumnavigations are shown in perspective; the downward crossings were located at about 10 km from the cloud. Water vapor overburdens are plotted upwind and directly above the storm top for the overflights but for the circumnavigations the data are plotted on the upwind and downwind cross-tracks.

The water vapor overburdens on the circumnavigations in Fig. 2 show that the values *downwind exceed those upwind* on an average of about 40%. On the overflights, the water vapor overburdens directly above the storm top were 2.4 times that of the background measurements upwind of the storm and at the same levels.

For the second storm on 7 September, the downwind water vapor values again exceeded those upwind at all flight levels, even at 700 m above the cloud top. The mean excess of downwind water vapor overburden in the layer 12.5–14 km was about 50%, a slightly higher figure than for the earlier storm. The water vapor overburdens directly above the top of this weaker storm were about 1.8 times greater than the background measurements upwind of the storm and at the same levels.

b. Ozone

The ozone data from the mission of 3 August are displayed in Fig. 3 as a function of altitude. These data show that the ozone concentrations averaged about 40% *higher* directly above the top of the storm than at the same levels away from the storm. Circumnavigations of the storm top showed an average excess of about 25% above the tropopause. On the other hand, the mean values measured during the circumnavigations of the cloud at or below the tropopause averaged about 15% *lower* than the measurements in undisturbed air at the same levels.

Fig. 4 gives the spatial distribution of ozone mixing ratio around the storm. The distribution in each of the circumnavigations is quite similar to that of the water vapor (Fig. 2); *downwind concentrations exceed* those upwind at all levels.

Fig. 5 shows the distribution of ozone concentration with altitude and the background sounding away from the storm for the mission of 7 September. As mentioned earlier, the region of high static stability was question-

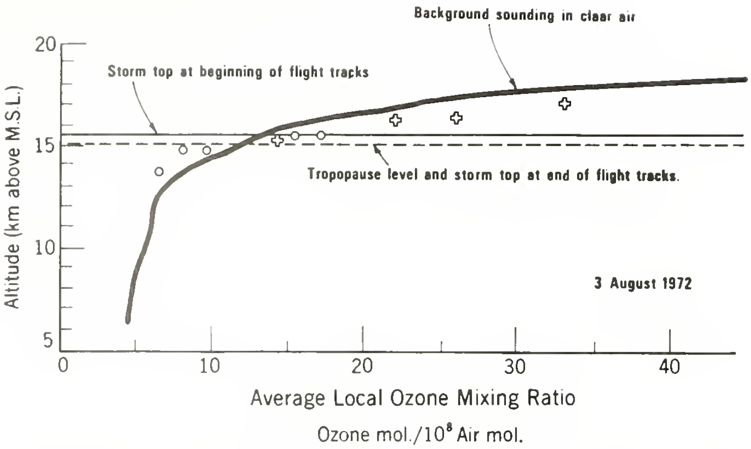

Fig. 3. The ozone concentration measured around the Amarillo, Tex., thunderstorm. The continuous line from 6 to 18 km is the background sounding made in clear air. The crosses are ozone concentrations measured directly above the storm during aircraft overflights. The small circles are the mean ozone concentrations measured during circumnavigations of the thunderstorm.

able, and the tropopause plotted in the figure is approximate. The most significant difference between these data and those of Fig. 3 is that the ozone concentrations directly above the cloud top averaged about 20% *less* than the fair-weather values at the same heights. The average concentrations measured during the circumnavigations above the storm are, however, *higher* by 30% than the fair-weather values (as was also found for the storm of 3 August). On the circumnavigations of the 7 September storm, the downwind concentrations of ozone once again exceeded those upwind.

The preceding discussion implies that on a broad scale a positive correlation exists between deviations (from the background values) of ozone and water vapor near the tops of high rising thunderstorms. To test this correlation on a shorter term basis, we statistically analyzed one circumnavigation just above the cloud top from the mission of 3 August. The results, shown in Fig. 6 as a pair of time series, yield a zero-lag correlation coefficient of 0.67.

4. Discussion

Williamson and Houghton (1965) and Mastenbrook (1968) reported, on the basis of balloon measurements to about 25 km in fair weather, that the normal stratospheric water mixing ratio profiles are very nearly constant with height. Consequently, thunderstorms injecting a substantial amount of water vapor into the stratosphere could be significant. Kuhn *et al.* (1971), using infrared radiometric measurements aboard a CV-990 aircraft, reported results similar to those presented here for water vapor measurements around thunderstorms. Near the tops of plains thunderstorms

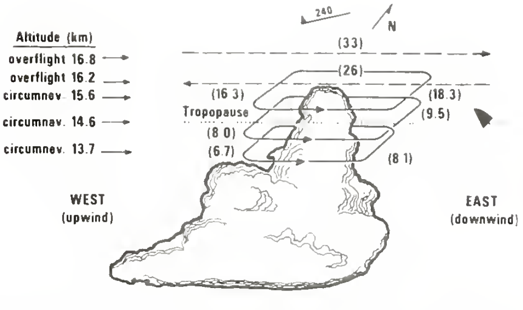

Fig. 4. Local ozone concentration values (O_3 molecules per 10^8 air molecules) along the flight tracks at descending altitudes around the Amarillo, Tex., thunderstorm. Note the local ozone concentration values are similar to the water vapor overburdens along the circumnavigations, i.e., the concentrations downwind are greater than those upwind of the storm.

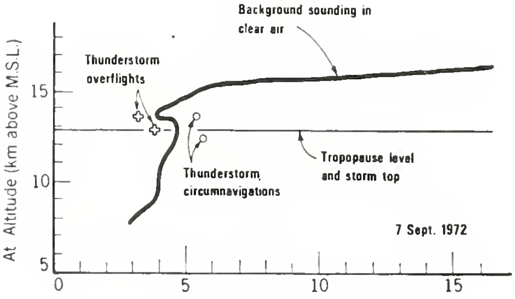

Fig. 5. Ozone concentrations measured near the Tucson, Ariz., thunderstorm.

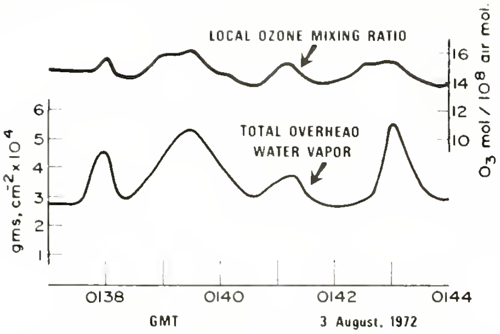

FIG. 6. Total overhead water vapor and local ozone concentration measured while circumnavigating at 15.6 km, and just above the thunderstorm located near Amarillo, Tex., on 3 August 1972.

in the United States, they observed that downwind water vapor overburdens exceeded those upwind and found an average threefold increase over the fair weather background in the mass of water injected into the lower stratosphere and upper troposphere. They estimated further that a significant fraction of thunderstorms do penetrate the tropopause to deposit water vapor in the stratosphere. Kuhn *et al.* (1971) computed that thunderstorms transport 1.6×10^9 gm of water vapor per day into the Oklahoma stratosphere. From the observations reported here and the measurements of Kuhn *et al.* (1971), it appears that *significant amounts of water vapor are deposited in the stratosphere by thunderstorms.*

While the data we have gathered show that a stratosphere-penetrating thunderstorm contributes positively to the stratospheric water vapor budget, they do not yet permit us to answer with any certainty the question: How much do they contribute? To answer this, we must be able to compute the flux through a closed surface around and above storms. This was not possible on these missions because the aircraft position as a function of time was known only from voice recordings made by the navigator-observer; this method is too imprecise to permit a detailed reconstruction.

We were also unable to determine the "residence fractions" for the water vapor supplied by the storm, i.e., what percentage of the water vapor delivered to the region above the tropopause remains there after the storm has subsided. To determine this in the future, we must precisely know the aircraft's position and it must remain in the vicinity of one storm for at least 3 hr.

The WB-57F aircraft has recently been equipped with an inertial navigation system. We are therefore hopeful that data from future studies of thunderstorms will enable us to present some quantitative figures on water vapor fluxes to the stratosphere, and to determine residence fractions for this trace constituent.

The ozone perturbation in the vicinity of a thunderstorm is a more complex matter than the water vapor perturbation. The first storm, which penetrated strongly into the stratosphere, exhibited an ozone excess directly over the top, but the second (weak or non-penetrating) showed a deficit there. On the other hand, circumnavigations around both storms above cloud heights measured ozone excesses. For the strongly penetrating storm, ozone deficits were found on circumnavigations below the tropopause. No such circumnavigations were made for the second storm.

The small sample size and the lack of data on other parameters related to the ozone concentration near and in the tops of the two thunderstorms precludes the drawing of conclusions about the sources of the observed ozone perturbations and how they affect the stratospheric ozone budget.

5. Summary

In the study of two thunderstorms—one penetrating the other near-penetrating the tropopause—ozone and water vapor increases were measured above and near the storm tops. In addition, a positive correlation was found between concentrations of ozone and overburdens of water vapor near the tops of these thunderstorms. More aircraft overflights are required to see if these observations are repeatable in nature.

Acknowledgments. This work has been supported by the Department of Transportation under Contract DOT-AS-20038 and by the Office of Naval Research.

The help of Dr. Earl W. Barrett and Charles H. Johnson at NOAA-APCL and Prof. C. B. Moore at New Mexico Institute of Mining and Technology is greatly appreciated. We also appreciate the efforts of Col. Click D. Smith and his WB-57F flight crews at the 58th Weather Reconnaissance Squadron, and are grateful to Paul R. Guthals and Capt. Russell T. Glenn of the Los Alamos Scientific Laboratory for their logistics support. In addition, we would like to thank George T. Gregg and his staff at the National Weather Service forecast center at Albuquerque, N. M., for their assistance with the thunderstorm forecasts.

REFERENCES

Komhyr, W. D., 1969: Electrochemical concentration cells for gas analysis. *Ann. Geophys.*, **25**, 203–210.

Kuhn, P. M., M. S. Lojko and E. V. Petersen, 1969: Infrared measurements of variations in stratospheric water vapour. *Nature*, **223**, 462–464.

——, —— and ——, 1971: Water vapor: Stratospheric injection by thunderstorms. *Science*, **174**, 1319–1321.

Mastenbrook, H. J., 1968: Water vapor distribution in the stratosphere and high troposphere, *J. Atmos. Sci.*, **25**, 299–311.

Sticksel, P. R., 1966: The vertical distribution of ozone over Tallahassee, Florida, Ph. D. dissertation, Florida State University.

Williamson, E. J., and J. T. Houghton, 1965: Radiometric measurements of emission from stratospheric water vapor. *Quart. J. Roy. Meteor. Soc.*, **91**, 330–338.

Reprinted with permission of the American Meteorological
Society Bulletin, Vol. 54, No. 2, February 1973.

International Cloud Physics Conference
London, United Kingdom
September, 1972

Welcoming speech to the participants

Helmut K. Weickmann, *President, International Commission on Cloud Physics; National Oceanic and Atmospheric Administration, Boulder, Colo. 80302*

It is a privilege to be here in these venerable halls of the Royal Society that have seen centuries of research activities, thus providing a most fitting background for our discussions during the International Cloud Physics Conference. My friends from East and West and North and South, it is a privilege to welcome you to this conference on behalf of the International Commission on Cloud Physics.

Clouds are most fitting objects of international conferences as they themselves are international messengers: the moisture supply of the clouds over this city today may stem from the Gulf Stream and may therefore have originated in the Gulf of Mexico, while their population of freezing nuclei may have been injected by air originating in the Sahara Desert. Clouds and precipitation therefore know no national boundaries and nobody can claim ownership to them. This, we realize, can be both a blessing and a curse. A *blessing* because they invite us scientists to conduct joint projects across national boundaries and stimulate us to meet regularly and to exchange views about them. A *curse* because they may become political objects with undesirable feedbacks into our joint endeavors. For instance, in times of drought and fresh water shortage, clouds may be considered as a natural resource that can be "mined for water," as ore is "mined for minerals." Then, as an American proverb goes: Apostle Peter may claim that he is robbed by Apostle Paul. Much research along the lines of precipitation enhancement is going on in the semi-arid regions of the U.S.A., the U.S.S.R., and Australia. Europa Felix, watered by moist air from both the warm Gulf Stream and the warm Mediterranean, has few such problems. Therefore, weather modification is a "low-key" item in this conference. This will however not prove to be a disadvantage—both Professor Mason's universal knowledge of the *physical principles of cloud physics* and his Program Committee's well-balanced selection of invited and contributed papers will convey to us an overview of the entire field of cloud physics and help us also to see more clearly the potential of weather modification.

In the discussions we will find a new *freedom*, one in which what counts is what is true, not how well we can manipulate nature and the data of our work—a freedom in which we will not have to hide the complexity of nature's ways.

In the atmosphere of spiritual freedom which marks the scientific minds of those who lectured and debated here before us, we will neither fall victim to become *"des terribles simplificateurs"* nor the narrowly educated, vastly creative, yet irresponsible "*ignorants*," which the Spanish philosopher Ortega y Gassett sees as the scientist's fate due to ever-progressing scientific specialization.

On the contrary: We will find ourselves closer to the answers of thousands-of-years-old queries as we read them in the Book of Books, such as: Can anyone understand the spreading of the clouds, the thunderings of the firmament? *(Job 38: 29)*. Have you entered the storehouses of the snow, or have you seen the storehouses of the hail? *(Job 38: 22)*.

Finally after conquering and harnessing atomic energy, the sound barrier, and space, we may find that we are about to conquer the clouds by finding in modesty and truth the answer to the same age-old source of penetrating question:

> Can you lift up your voice to the clouds, that a flood of water may cover you?
> Can you send forth lightnings, that they may go and say to you "Here we are"? *(Job 38: 34–35)*.

Sometimes, we can—and we will understand in modesty why!

Reprinted with permission of the American Meteorological Society,
Vol. 54, No. 2, February 1973.

International Cloud Physics Conference
London, United Kingdom
September 1972

Closing remarks by Dr. Weickmann, 26 August

It is a privilege to make some closing remarks at the end of this very stimulating conference and to inform you in a preliminary manner of the deliberation which the ICCP has been engaged in during the last days. Let me first express my thanks to the organizers of this conference who have succeeded in shaping an extraordinarily well-conducted and smoothly run meeting. I would like to mention particularly the efforts of the Organizing Committee and its Chairman, Dr. Mason, and Dr. Goldsmith and his able assistants at the conference desk. Secondly, I would like to thank all of the contributors, the speakers, the discussion speakers, and all participants who have made contributions. The Organizing Committee has succeeded in making an excellent selection of scientific contributions. I would like to come back to the motto of the Royal Society, *nullius in verba*, which has a very specific double meaning in this conference. The first meaning could be characterized by a more eloquently expressed verse by Horatius *"O, si tacuisses philosophus mansisses!"* "Had you remained silent, you would have been a philosopher!" I am happy to say that none of the papers fall in this category. The second meaning of the motto could be expressed by the Latin phrase *totum scribendum* meaning "put everything in written form." I would like to express my hope that many authors will do so and publish their papers in available journals.[1]

Now comes the schedule of future conferences. For the next *International Conference on Cloud Physics,* I am happy to announce that we have an invitation for 1976 in Boulder, Colo., U.S.A., jointly by the National Center for Atmospheric Research and the National Oceanic and Atmospheric Administration. This meeting will be sponsored, as the present one is, by IAMAP as an International ICCP Conference. As a consequence of the interesting papers that we have heard in the past week, I would like to express my personal hope that the 1976 conference will have many contributions of measurements inside and outside of clouds and in the cloud environment in order to supply necessary data for improving numerical models. An attempt will be made to coordinate this conference with the next *International Weather Modification Conference* in the series sponsored by the Australian Academy of Science and the American Meteorological Society which is also planned for 1976 in Boulder, Colo.

The *Nucleation Conference* in Leningrad is tentatively planned for September 20 to 30. I request that any inquiries with respect to this conference be directed to the Chairman, Nucleation Committee, Prof. H.-W. Georgii, Institut für Meteorologie und Geophysik, Johann Wolfgang Goethe-Universität, Frankfurt a.M.-1.

IAMAP Conference in Melbourne, January 1974. The Commission has decided to propose for this meeting contributions to the problem of cloud physics and radiation. The form of these contributions will be suggested in further circulars.

The next *General IUGG Assembly* is planned for Paris in 1975. I would like to call your attention to the fact that at this Assembly new ICCP officers will be elected, and that the Assembly is essentially a business meeting, open however, for ICCP contributions.

Nuclear Workshop. The need has been expressed for convening a small study group on the fundamentals of ice nucleation under strictly controlled conditions of nuclear properties, temperature, and humidity, as it is believed that the very large discrepancies among the measurements of the last Nuclear Workshop are very much due to fundamental problems in the ice nucleation process which are not entirely clear and which consequently cannot as yet be incorporated in ice nucleus counters. More detailed plans for this study group will be available in due time through the Chairman, Nucleation Committee, Prof. Dr. H.-W. Georgii.

I have just received word from the distinguished member of the Soviet delegation, Prof. Khrguian, that his country would give favorable consideration to an ICCP recommendation for holding an *International Conference on Weather Modification* in his country at an early date. While we have not been able to discuss this possibility in connection with the calendar of international conferences, I will give very serious consideration to this desirable scientific conference and will keep the cloud physics community informed through the scientific journals. Presently, I would like to thank the Soviet delegation for their initiative in this matter.

Finally, I would like to thank you all for a very stimulating conference.

---

[1] The real meaning of the motto is, of course, a much more penetrating one; probably an abbreviated form of Horatius' verse: *"Nullius addictus jurare in verba magistri,"* meaning "Pledged not to speak out in the words of any master." This meaning, put into the context of its time, must be considered as one of the significant turning points in the evolution of the European mind.

Reprinted from NOAA Technical Memorandum ERL APCL-16,
34 pages, December 1973.

CLOUD PHYSICS PROGRAM IN SUPPORT OF GATE

(H. K. Weickmann Coordinator)

1. INTRODUCTION

As the program for GATE emerges from the general uncertainty into subprograms, flight plans and scale interrelationships, the need for a cloud physics program which reaches down to the D scale becomes increasingly apparent. Subsequently, a review is given of the cloud physics program as it stands today composed from bits and pieces; also a proposed supplementary program is discussed which the reader will find to be well justified. It is to be carried out within the convective subprogram and as far as possible on the flight program which is currently planned.

GATE Report #1 states under the heading "Other Sub-programmes": "...as soon as the number and type of platforms to be contributed by the participating nations are known, these programmes must be formulated without delay. For example, the *cloud physics* programme could contribute to the Central Programme by a cloud census (for the parameterization of convection) and by the measurement of liquid water content in clouds and precipitation as a function of height and time (for the energy cycle of B- and C-scale phenomena). However, the complete cloud physics programme will be more complex and remains to be determined."

It also postulates: "All the bulk properties of cumulus ensembles ...must be verified by direct sampling from research aircraft, especially on the C- and D-scales."

Report #1 suggests that these data are obtained from averaged profiles of wind, temperature and moisture, and averaged precipitation at different heights where "averaging covers areas comparable in size to a considerable part of the B-scale area and times of the order of hours or even a day."

Since averages are being made up from a number of individual measurements and individual times steps, the need for sampling on the D-scale in order to obtain meaningful averages on the C- and B-scales is obvious.

Reprinted from NOAA Technical Report ERL 265-APCL 26,
103 pages, January 1973.

THE MODIFICATION OF GREAT LAKES WINTER STORMS

Helmut K. Weickmann
Atmospheric Physics and Chemistry Laboratory
Environmental Research Laboratories
National Oceanic and Atmospheric Administration
Boulder, Colorado 80302

ABSTRACT

In the Great Lakes region of the U.S.A., shallow but intensive winter storms form through a combination of cold continental air moving over large still-unfrozen and even warm water surfaces. These storms, depending on their trajectories over the lakes and their persistence, may precipitate large amounts of snow onto the downwind shorelines of the Great Lakes. Natural freezing nuclei-concentration causes heavily rimed crystals to form; seeding increases their number, and prevents riming, which in turn causes smaller crystal fall velocities. Consequently, these smaller velocities mean a longer transport of snow downwind and away from the urban and industrial centers near the shores. The experiment is designed around a mesoscale numerical model and a microphysical model of snowcrystal formation. The great variability of the cloud systems prevents a clear definition of a homogeneous sample of comparable experiments and, therefore, makes a clear statistical design impossible. The execution involves seeding from the ground and air, tracking the seeding agent through the cloud system with an airborne freezing nucleus counter, and analyzing AgI nuclei in the precipitated snowcrystals. The analysis includes radar, surface and airborne observations. Results indicate that snowfall can be affected in the desired manner. However, there is a strong dependence on the cloud top temperature, which indicates that snowfall can be initiated, redistributed, or not be affected at all. The reader will notice a certain evolution of the thesis. Through application of interrelated and comparative snowcrystal analysis, the plausibility that the Great Lakes winter storms belong to a more general category of shallow winter storms for which boundary layer flow constitutes an important origin is examined. This storm type is shown to occur frequently not only in large-scale orogenic precipitation but also in large-scale cyclonic warmfront type snowstorms.

Reprinted with permission of the International Conference on Weather Modification, Tashkent, USSR, October 1-7, 1973.

Snowfall Enhancement

H. Weickmann

Atmospheric Physics and Chemistry Laboratory
National Oceanic and Atmospheric Administration
Boulder, Colorado 80302

The problem of snowfall enhancement is closely related to the more general problem of precipitation enhancement or rainmaking. We know that the proof for effective precipitation enhancement is for most projects based on statistical evidence. This evidence while often convincing to mathematicians as often fails to convince physicists. However, only in the past years has evidence become available which permits a physical assessment. It is particularly the insight into the interrelationship between several parameters - some of them are mesoscale, some microscale - in nature which has brought the understanding of the snow process into sharper focus. The most important mesoscale parameter is the rate of condensation which determines the amount of moisture released for precipitation. The most important microphysical parameter is the concentration of snow crystals furnished by nature.

1. Concentration of snow crystals

Apparently this parameter depends on two factors: 1) the concentration of freezing nuclei and 2) the rate of upward flux of freezing nuclei. When the rate of updraft doubles from say 5 cm/sec to 10 cm/sec at a certain atmospheric level, characterized by the threshold temperature of freezing nuclei, twice as many nuclei will become active and twice as many crystals will form. As the rate of condensation also depends on the updraft velocity, one has here an interesting self-regulating mechanisum: the more precipitable water is liberated by the rate of condensation which is related to the large scale cyclonic mechanism, the more crystals to form to snow-out the water. Since the rate of condensation and the rate of precipitation are related, it is not surprising that - in general - proportionality exists between the latter and the snow crystal flux. This important relationship follows from the research of Gunn [1]. He studied the number of individual snow crystals by carefully separating those which were aggregated in a snowflake, then he melted them and determined from the size of the resulting droplets an average mass $\bar{m}$ of an individual crystal. At the same time he determined the rate of precipitation R and was able to compute the flux of snow crystals $R/\bar{m}$ per cm and sec^{2}as a function of r.

$$R/\bar{m}\ (m^{-2}\ sec^{-}\ ) = 1.5R^{1.0}$$

Figure 1 shows the results of 6 storms and 84 individual measurements. If we assume an average fall velocity of the snow crystals of 1 m/sec, then the figure says that at a rate of precipitation of 1 mm/hr, an average concentration of about 20 crystals per liter exists with a variation from 6 to 40; the concentration increases to about 50/1 for a rate of precipitation of 3 mm/hr. Gunn points out that in individual snowfalls the variability of the particle flux may vary within a factor or 4. The graph clearly indicates the proportionality between snow crystal concentration and rate of precipitation. Looking at the graphs of the individual snowfalls, however, which are given by the author, a marked inverse proportionality between snow crystal concentration and the average mass for a snow crystal is apparent also. In two cases the compensation is practically complete: While the rate of precipitation remains almost constant, variations of the particle flux are compensated by inverse variations of the average particle mass. This permits the important conclusion that nature compensates for the small scale variability of nuclei concentrations by adjusting the crystal size. This observation makes it highly plausible that, in general, nature does a pretty good job in stratiform snow producing systems to snow out very effectively the water which is furnished by the rate of condensation Unprecipitated water is stored in the cloud as liquid water, and it is well known from measurements in the USSR as well as in the USA that this amount is small indeed and hardly worth the effort of artificially inducing its precipitation.

We were able to confirm Gunn's basic numbers of particle flux by a somewhat different approach. We based our studies on the Bergeron [2] concept of the mechanism of plentiful precipitation. Bergeron defines a "releaser" or "seeder" cloud and a "spender" or "feeder" cloud. The former produces the ice crystals which subsequently snow out the latter. The releaser cloud is usually a Cirro or Altostratus in which the particles grow by diffusion while the spender cloud is a low level Stratus where growth proceeds by diffusion, riming and aggregation. Both cloud systems occur independently as well. The releaser cloud crystals are typically prism bundles which deform in the spender cloud through growth of end-plates and branches as well as additional irregularities through riming. These crystals easily aggregate, and it requires Gunn's tedious procedure to separate them. If, however, the spender cloud does not exist, they fall as single crystals and can easily be counted. In such cases we found concentrations of 5 to 40 per liter in good agreement with Gunn's values (Weickmann [3] and Jiusto and Weickmann [4]).

It appears that these concentrations are perfectly capable of supporting considerable rates of stratiform precipitation. Figure 1 indicates that a flux of 3-5 cm^{-2} sec^{-1} supports a rate of precipitation pf 4 mm/hr, which can be easily anything from a 4 to 8 cm snowfall per hour.

The concentration of crystals, the rate of condensation and the temperature at which crystals form determine other important parameters such as: the growth habit, regular or irregular, affecting the rate of diffusional growth; the fall altitude, oscillating, rotating, tumbling affecting the ventilation factor in the diffusional growth equation; the riming efficiency depending on crystal habit, fall velocity and attitude and affecting in various ways the rate of crystal growth; and finally the aggregation of crystals into flakes depending on crystal concentration and attachment factors, and affecting the riming efficiency.

It is not yet possible to assess all of these parameters in their relationship and importance to precipitation efficiency, but we would like to mention a few examples. In cases where the crystal concentration is lacking, special growth habits are developed which appear to compensate the deficiencies. We would like to quote one typical case from our log on snowfalls. On November 2, 1969, a convective Stratocumulus layer about 2500 m thick with tops at -25°C precipitated rimed flakes made up of rimed spatial plate crystals. Suddenly, the snowfall changed to very large flakes. The large flakes consisted of rimed large spatial dendrites of about the same concentration as the small spatial plate crystals before. Apparently, a sudden abundance of the water supply or an increase of the rate of condensation has caused a habit change from rimed spatial plate crystals to rimed large spatial dendrites thus increasing effectively the scavenging ability of the precipitation particles. Likewise, if riming occurs in the temperature range between about -5°C and the freezing level, the collected droplets tend to crystallize into fast growing needles which in turn increase the collection efficiency of the crystal ensemble.

It appears that overabundance of freezing nuclei and consequently of ice crystals does not lead to overseeding and loss of precipitation, but to much increased efficiency in aggregation of the crystals to large snowflakes. This follows clearly from our seeding experiment near Buffalo on 21 November 1969 (Weickmann [3]). On this day multiple cloud lines formed formed over Lake Erie in a NW-SE direction and produced snowshowers over the southern shores of the lake. The cloud base was at 600 m and -10°C while the tops were at 2400 m and -18°C. The structure of the cloud system was convective, consisting of Cumulus clouds which were topped by a Stratocumulus layer, penetrated on isolated locations by the Cumulus clouds. The precipitation consequently was of shower character. From 11.57 to 12.23 local time, seeding was carried out at 800 m with pyrotechnic flares releasing a total amount of 2400 g AgI. After one hour a cloud volume of about 2000 km^2 had become modified and was made visible from the aircraft flying above the cloud tops by an intensive undersun forming downwind of the seeding track over a cloud area of 28 x 40 km. The seeding rate at homogeneous distribution of nuclei throughout the cloud system would have produced a crystal concentration of about 50 to 60/ℓ. Homogeneous distribution, however, seldom occurs; therefore, some areas will have received more and others less. From 13.30 to 13.54 a mobile ground observer unit observed the composition of a heavy snowshower which apparently had received an abundance of nuclei (Figure 2). The normal precipitation consisted of a broad distribution of particle sizes made up of mixed dendrites and graupel. This particle characteristic changed to great numbers of tiny crystal forms most of which were unreconizable, the others consisted of plates, stars, needles and columns. They were aggregated in great numbers to large flakes. Some flakes contained from 100 to 1000 individual crystals according to the observer's log. Qualitatively it appeared that the shower became intensified during the snowflake stage. Figure 3 shows on the right the natural particle characteristics and on the left the flakes made up of the many tiny crystals. This important observation which was made repeatedly points strongly to the fact that overseeding is not the problem in snow enhancement; the problem is underseeding. Any seeding project should always tend to produce at least as many crystals as the natural process does, or at least 10 to 50 crystals/ℓ.

2. Rate of condensation and cloud thickness

We mentioned above that precipitable water in a cloud appears in two forms: 1) as liquid water stored in the cloud and 2) as water released by the rate of updraft in the condensation process, shortly be the rate of condensation. The water storage in stratiform clouds is with few exceptions very small, mostly less than .3 g/m³. The total precipitable water in a cloud 1000 m thick is therefore only of the order of 0.3 mm - hardly enough to reach the ground and produces only one shower, then the cloud has to be reformed. Contrary to this storage, the rate of condensation is a process which may proceed over many hours and produces little precipitable water per hour but much over the entire time. The amount of water R_W liberated in mm/hour by an updraft of 1 m/sec is given by the relationship:

$$R_W = \frac{780}{T} \frac{de_W}{dT} \gamma_W - 2665 \frac{e_W}{T^2}$$

where e_W is saturation vapor pressure over water (mb)

T is temperature (°K)

γ_W is saturated pseudo adiabatic lapse rate (°C/100gpm)

For a 1000 m thick layer, seeding from roughly 950 mb to 850 mb and a range of base and top temperatures, Table 1 gives R_W in mm/hr for various updraft velocities:

Table 1

Base & Top Temp	0 to -10°C	-5 to -15°C	-10 to -20°C	-15 to -25°C
Updraft				
1 m/sec	1.45 mm/hr	1.18 mm/hr	.93 mm/hr	.70 mm/hr
.5 m/sec	.73 mm/hr	.59 mm/hr	.47 mm/hr	.35 mm/hr
.1 m/sec	.15 mm/hr	.12 mm/hr	.09 mm/hr	.07 mm/hr

Precipitable water R_w in mm/hr released in a cloud 1000 m thick as function of updraft velocity and base and top temperature.

Table 1 shows clearly that 1000 m is indeed a minimum thickness for which cloud seeding should be attempted as only for updraft velocities larger than 5 m/sec and top temperatures warmer than -20°C are noteworthy amounts of precipitable water being released. Of course, at a top temperature of -20°C the natural release of precipitation is already quite effective; furthermore, it may be possible that the snow-out efficiency is less than 100%. Effective snowfall enhancement under such conditions requires either a thicker cloud deck or a higher updraft velocity.

3. Snowfall enhancement opportunities

The previous discussion indicates that snowfall enhancement opportunities may present themselves through the microscale mechanism of snow formation as well as through the mesoscale flux parameters of cloud systems. Chappell [5] in studying natural and artificial snowfall in unpolluted air from orographic winter clouds over the Rocky Mountains derives somewhat schematized physical conditions for snowfall enhancement opportunities. Observation indicated that in these orographic snowfalls most snow crystals had grown by diffusion only and not through riming or aggregation. For this to occur model considerations of the air flow over the mountains suggested an updraft velocity of 11.0 cm/sec. It was assumed that the cloud tops were at about the 500 mb level; then, the observational data was permitted contruction of a diagram (Figure 4) which has as abscissa the 500 mb level temperature from -35 to -10°C and as ordinate the water equivalent per precipitation day. In the diagram two parameters are plotted: the average rate of condensation (solid curve) and the average diffusional growth rate of ice crystals for a 460 mb of cloud top and the natural ice nuclei spectrum (dashed curve). The author also plots values of observed precipitation averaged over the number of observational days. While for temperatures below -20°C these values follow the curve for the average rate of condensation, for temperatures warmer than -20°C the precipitation no longer is proportional to the rate of condensation but follows the diffusional growth rate--thus exhibiting a precipitation deficiency. Of course, then water storage should occur in the cloud and why is it not that nature invokes other growth processes for compensation, such as riming and the formation of secondary dendritic branches, etc? Figure 5 which is self-explanatory shows how seeding was able to bring the rate of precipitation back to agree with the rate of condensation. Seeding in this experiment was carried out by surface generators. This somewhat idealized definition of existing seeding opportunities for temperatures of the (assumed) cloud tops warmer than -20°C postulates that no releaser or seeder cloud exists or that for temperatures colder than -20°C no spender of feeder cloud exists--which of course is an obvious condition when the target area is already at about the 700 mb level and the entire cloud thickness is not more than 200 mb. Indeed, such cloud layers exist also in the flatlands more frequently than generally assumed.

4. Winter cloud systems with seeding potential

4.1 The convective Stratocumulus systems.

Shallow convective Stratocumulus systems with top temperatures warmer than -20°C have been observed and described for the Pacific NW territories in the USA (Hall [6]) in the Great Lakes region of the USA (Lavoie [7]); they furnish the snowfall in Hokkaido, Japan (Magono [8]); satellite observations show them over the Caspian Sea (Bugaev [9]); they are known to occur in the Mediterranean and we believe that they are the cloud systems which furnish water for the effective rain making experiments in Israel. All they systems have one thing in common: they are related to relatively shallow layers of cold air within the planetary boundary layer moving over warn bodies of water--be it the Gulf of Alaska nd its southern regions, the Great Lakes, the Japan Sea, the Mediterranean Sea, or the Black and Caspian Seas. These cloud systems are highly convective and may locally also have high water contents of the order of 1 g/m^3. Updraft velocities have been measured by means of a doppler radar (McVehil, et al. [10]) which would reach several meters, thus producing an effective rate of condensation. Snow crystals falling from them have been described by Magono [8], Jiusto and Holroyd [11], Weickmann [3]; they are typically dendrites, rimed and in flakes. A useful numerical model for these cloud systems has been developed by Lavoie [12].

4.2 The upslope Statrocumulus systems.

Figure 6 shows a satellite picture of the western USA (note the Pacific coast line) with a cloud system in the center. Denver, Colorado is located at about the cross mark in the center of the picture. This system was caused by an Anticyclone located north of Denver which moved the air from east to west upslope against the Rocky Mountains. This causes the air to ascend more than 1000 m, so that condensation is eventually reached. The Denver Radiosonde shows the thickness of the cloud system and a temperature humidity profile which was highly favorable for artificial precipitation having a cloud top temperature of only -10°C. Slope and wind component perpendicular to the slope determine the rate of condensation which is in most cases near 10 cm/sec. A climatological study of the frequency of such systems in the High Plains over the past 10 years (Whiteman [13]) has shown that per year about one dozen seedable cases occur (Figure 7.). Such cloud systems also occur frequently over the Bavarian High Plains in Germany. The special feature of these cloud systems is that precipitation can be released over a large area and not just from single cumulus clouds.

Typical shallow cloud systems also occur within the large winter anticyclone over the USSR, but it appears that these layers are usually shallow (about 300 m thick) and formed due to radiation processes which makes for a low rate of condensation. They have, therefore, a poor artificial precipitation potential (Leskov [14]; Kondratova [15]).

4.3 Cyclonic shallow cloud systems.

Shallow cloud systems also occur in connection with warm fronts and may constitute a true and so far unexploited seeding potential (Grunow [16]; Weickmann [17] [3]).

5. Geometry of precipitation zone (target area determination)

The geometry of the precipitation zone or the determination of the target area has been the subject of studies by Elliott [18], Grant [19], and more thoroughly by Soviet scientists (e.g. Leskov [20]). Elliott discusses the movement of the seeding agent which was dispersed from a single ground generator and which affected atmospheric layers subjected to wind shear. He moves the plume first with the low level wind vectors and then with the upper level vectors. Grant [19] studies the effect of orography and finds preferred propagation along mountain passes. Soviet scientists (Leskov [20]) eliminate one-half of this difficult problem by seeding from aircraft and so do we (Weickmann [3]). The problem is presented in Figures 8a-f. Figure 8a is taken from Leskov [21] and shows the difference of target location if an average wind vector from the surface to cloud top is used, compared to taking into special consideration the wind below the cloud layer separate from an average wind in the cloud layer. Airborne seeding takes place along line A-B. Leskov could explain why in two special cases the target area with the Leonov method was incorrectly forecast to be inside the network area (dashed line parallelograms). The correctness of his argument is reflected in Figure 8b which shows how the true precipitation is located within the area forecase by his method. Note, however, that the shear in this case is only in speed and not in direction. The conditions for shear in direction are discussed by Leskov [21] by means of Figure 8c. Leskov suggests consideration of the low level and upper level drifts of the seeding line. Of course, since there will always be a transition zone between these two vectors, the entire area AA_1 B_1 A_2B_2B will be affected by the seeding agent. This follows clearly from our experiment on December 3, 1969 (Figures 8d-f). On this day we seeded a cloud line with AgI over the south shore of Lake Erie. A considerable shear in speed and direction existed within the convective Stratocumulus layer, base temperature at 900 m (2700 feet) was -4°C, top temperature -18°C at 2750 m (8300 feet). The seeding level was at 1000 m, wind was NNW 15 kts while at the top of the layer it was WNW 30 kts. Figure 8d shows the aircraft flight path during seeding and thereafter as well as low level streamlines while Figure 8e shows the same information with the addition of the upper level streamlines. The shaded area gives boundaries of the cloud volume into which the AgI will have diffused if an effective vertical exchange exists within the cloud layer. Figure 8f confirms this circumstance by indicating the analysis flight path during which the concentration of the ice nuclei was measured. In the entire area diamond dust was observed and regions of high nuclei concentration. Of particular interest is the series of high counts in the western half of the flight path. They were measured at a flight level of 1200 m (4000 ft) and it is clear that they could have arrived there only by means of the upper level winds. Especially high counts of ice nuclei are marked along the flight path by large dots or emphasis of the line. During summer in convective atmospheric conditions airborne seeding near the cloud bases as was done in Whitetop may result in different target areas, as diffusion throughout a deep atmospheric layer reaching from the surface to some level above the flight level needs to be taken into account. Whitetip used two different diffusion plumes: the so-called "Chicago plume" which took into account the most divergent winds between flight level and 4200 m (16,000 ft), and the "Missouri plume" defined by the winds at seeding level (Braham [22]). We feel that both approaches are incorrect as the 4200 m top level is quite arbitrarily selected and as the plume has not been extended to the ground surface.

6. Seeding technique

During airborne seeding operations the experimenter has a number of options, such as: one-dimensional line seeding at cloud base or cloud tops and two-dimensional "curtain" seeding from the cloud tops. Figure 9 shows the effect in one and the same cloud deck of line seeding with an aircraft AgI generator at cloud base, and of Dry Ice "curtain" seeding from the cloud tops (Weickmann [3]). Curtain seeding was accomplished by a seeding rate of 10 lbs/mile using pea to walnut sized Dry Ice particles. In both cases strong seeding effects developed in the cloud deck which were observed by radar (Figure 10a and b). The echo areas were carefully planimetered and the growth of the affected area plotted in Figure 9. While the Dry Ice grows linearly from the beginning, the AgI area requires about 20 minutes delay before its spreading rate parallels that of Dry Ice. It shall be mentioned in this connection that the nuclei concentration in the Dry Ice area was a factor of about 3 larger than in the AgI area. Corresponding data are obtained when the rate of linear spreading perpendicular to the seeded line is plotted. The irregularity of the diffusion mechanism causes the rate of lateral spreading to scatter considerably, but Figure 11 shows that the Dry Ice effect spreads out twice as fast as the AgI effect. Again, however, Dry Ice produced more nuclei than AgI by about a factor of 10. This is an entire order of magnitude and could cause internal eddies in the cloud deck. In this case, both agents were introduced about 150 m beneath the cloud tops; the rate of spreading was measured by repeatedly passing over the seeded areas. The absolute numbers of nuclei produced in these cases were as follows: left side of Figure 11- Dry Ice 3.5×10^{14} nuclei/mile, AgI + NaI 0.32×10^{14} nuclei/mile. Right side of Figure 11: line 1: 4×10^{13} nuclei/mile; line 2: 2×10^{13}nuclei/mile;

line 3: 12×10^{13} nuclei/mile. From this work it follows that the lateral spreading of the seeding effect throughout the cloud layer depends on the seeding intensity and the seeding mode. Curtain seeding will apparently enhance the spreading velocity by roughly a factor or two. The results are in good agreement with earlier data (Weickmann [23]) Figure 12. These data are based on curtain seeding with Dry Ice only. On the average the line did spread within about 30 minutes 1 1/2 miles to either side, or a total of about 5 km. If consequently parallel lines are seeded 3 miles to either side, or a total of about 5 km. If consequently parallel lines are seeded 3 miles (5 km) apart, then after 30 minutes they should have joined. This brings us to the problem of the most advantageous seeding pattern for modification of large areas.

Seeding pattern. In most cases of snowfall enhancement from Stratus clouds, it is desirable to affect the entire deck downwind of the seeding track. There exists an infinity of seeding patterns, depending on cloud conditions, seeding technique, size of seeding pattern, aircraft speed and wind speed. It is always assumed that seeding proceeds perpendicular to the wind direction. Subsequently, we would like to call attention to some basic features of importance. Experience says that it takes about 1/2 hour to develop precipitation in a Stratus deck and it takes also about 1/2 hour for the seeding effect to spread to a total width of 3 miles (5 km) or 1 1/2 miles to either side (2 1/2 km), if seeding is done with Dry Ice in the "curtain mode" from the cloud tops. The seeding pattern shall then be such that it combines to one large modified area about at a distance of 1/2 hour wind translation. It is assumed that the seeding pattern is flown as a race track or a flat pattern eight, fixed to the earth surface and such that the distance between the two flight legs does not exceed 3 miles or 5 km. Figure 13 shows three patterns for a windspeed (or drift velocity of the cloud deck) of 10, 20, and 30 m/sec and a flight velocity of 4 km/minute; the flight pattern itself it a racetrack pattern 10 km long and 2.5 wide. The figure shows that the pattern will no longer close in 30 minutes on one end even before the wind velocity reaches 20 m/sec. The flat pattern "8" however, if the turns are made against the wind is good to almost 30 m/sec. (Figure 14). Depending on the purpose of the seeding project there exists a great variety of seeding patterns which are designed to make optimum use of the source of water in the cloud layer. Some may be flown in a Lagrangian mode, upwind or downwind, for some two or more aircraft are needed. Of course, it needs to be said, that also here wind shear needs to be considered. Use of the proper pattern will enable the experimenter to manipulate the areal development of the precipitating snow clouds. We observed during a seeding experiment in November 1971 that a seeding pattern as in Figure 15 for a wind speed of 20 m/sec caused the cloud deck to become arranged in parallel lines of increased dynamic development. The convective development with a strong undersun in the foreground is seen on 15. There can be no doubt that we are only in the beginning of understanding the areal and downwind development of seeded areas under conditions of a convective cloud deck.

7. Results of snow enhancement projects

The reliable measurement of snowfall is one of the most difficult measurements in meteorology; this should always be kept in mind. Table 2 points to some results after seeding of convective Statocumulus layers, from which artificial snowshowers precipitated (Weickmann [24]). One such shower, that of November 25, 1968, is shown in Figure 16. The time between seeding end and precipitation onset was determined a few times to be between 26 and 36 minutes from clouds which were about 1500 m thick. Leskov [25] reports precipitation increases after aerial seeding for a period of 2 to 3 hours downwind with an intensity varying between 0.30 and 0.40 mm/hr. He remarks that increases between 50% and 200% occur, but it was particularly interesting that he emphasizes (Leskov [26]) "...frontal clouds cannot be considered reservoirs of possible additional moisture; they are really generators of natural precipitation." He cannot find redistribution of the available precipitable water, i.e., a decrease downwind, but he remarks that the network was too small, since it did not permit study of the development of precipitation to at least 5 hours after seeding. He is somewhat at variance with Litvinov and Ruzheinikovz [27] who state that "directly beyond the zone of increased amount of precipitation a zone of decreased amount of precipitation occurs so that the overall effect of the increase due to modification is equal to zero." It is interesting to note that in the USA reports to the contrary gain momentum, namely that further increases of precipitation occur at distances between 100 and 200 miles (Grant [19], Elliott [18]). A definition of clouds for systematic modification in the Volga Basin is given by Kondratova [15]. This author finds essentially three groups: Group A . These are clouds 400 to 500 m thickm water content 0.16 to 0.20 g/m^3. Group B. Clouds with a thickness of 500 to 600 m, but the thickness can vary between 300 and 1000 m depending on location. Liquid water content nearly as in Group A. Group C. This cloud group is most efficient in the production of artificial precipitation, yet their thickness is similar as in Group B. A general assessment of the seeding potential of winter time clouds from so-called "dry fronts" is given by B.N. Leskov, et al. [14]. These authors estimate that the precipitation of the cold period could be increased by not more than 3 to 5%.

References

[1] Gunn, K.L.S., 1967: The number flux of snow crystals at the ground. Ross Gunn Memorial Volume, Monthly Weather Rev. 95, 921-924.

Bergeron, T., 1950: Uber den Mechanismus der augiebigen Niederschlage, Berichte, Deutsch, Wetterd., US-Zone (Bad Kissengen) Vol. 12, pp. 225-232.

[3] Weickmann, H.K., 1973: The Modification of Great Lakes Winter Storms. NOAA Tech. Rep. ERL 265-APCL 26, Dept. Commerce, Boulder, CO., 103 pp.

[4] Jiusto, J. and H. Weickmann, 1973: Types of Snowfall to be publ. in forthcoming issue of Bull. Amer. Met. Soc.

[5] Chappell, C., 1971: Modification of cold orographic clouds. Dept. Atm. Sc., C.S.U., Paper No. 173, Ft. Collins, CO., 196 pp.

[6] Hall, F., 1957: III. The Weather Bureau ACN Project. Cloud and Weather Modification. Meteorology Monographs 2, 11, A.M.S., Boston, Mass., 24-26.

[7] Lavoie, R.L., 1972: A mesoscale numerical model of Lake-effect storms. J.A.S., 29, 1025-1040.

[8] Magono, C., 1971: On the localization phenomena of snowfall. J. Met. Soc. of Japan. Vol. 49, Dec. 1971, 824-835.

[9] Bugaev, V. A., 1973: Dynamic climatology in the light of satellite information. Bull. Amer. Met. Soc. 54, 394-418.

[10] McVehil, G. E., C. W. C. Rogers and W. J. Eadie, 1968: The structure and dynamics of lake-effect snowstorms. Tech. Report CAL No. VC-2559-P-1, Cornell Aeronautical Lab., Buffalo, N.Y., 14221, 49 pp.

[11] Jiusto, J. E., and E. W. Holroyd III, 1973: Great Lakes snowstorms, Pt. I, Cloud physics aspects, Grant No. E22-49-70(G), ESSA-APCL, Atmospheric Sciences Res. Center, State Univ. of New York, Albany, N.Y.

[12] Lavoie, R. L., 1968: A numerical model of the atmosphere on the mesoscale with applications to lake-effect storms. PhD thesis, The Pennsylvania State University, University Park, Pa., 102 pp.

[13] Whiteman, C. D., 1973: Some climatological characteristics of seedable upslope cloud systems in the high plains. NOAA Tech. Rept. ERL 268-APCL 27, 43 pp.

[14] Leskov, B. N., L. N. Mogila and S. P. Polovina, 1971: Possible amount of artificial precipitation from cloud layers of "dry" fronts. Trudy, UKR. NIGMI, Issue 99, pp. 52-57.

[15] Kondratova, A. V., 1968: Evaluation of the water content of supercooled stratiform clouds which do not yield precipitation. Leningrad Institut Eksperimental noi meteorologii, Trudy, No. 3: 44-54.

[16] Grunow, J., 1960: Snowcrystal analysis as a method of indirect aerology. AGU Geophys. Monogr. No. 5, Physics of Precipitation. 130-141 (Waverly Press, Inc., Baltimore, Md.).

[17] Weickmann, H., 1957: The snow crystal as aerological sonde. Artificial Stimulation of Rain, Amer. Meteorol. Soc., Woods Hole, Mass., 315-326 (Pergamon Press, New York, N.Y.).

[18] Elliott, R. D., and K. J. Brown, 1971: The Santa Barbara II Project - downwind effects. International Conference on Wea. Mod., Proceedings, September 6-11, 1971, Canberra, Australia, 179-184.

[19] Grant, O. G., Ch. F. Chappell and P. W. Mielke, Jr., 1971: The Climax Experiment for seeding cold orographic clouds. International Conf. on Wea. Mod., Proceedings, Canberra, Australia, 6-11 Sept. 1971, 78-84.

[20] Leskov, B. N., 1969: Isolation of zones of increased precipitation during frontal cloud modification. Trudy Ukr. NIGMI, Issue 86, 23-32.

[21] Leskov, B. N., 1970: Method and preliminary results from experiments on precipitation redistribution. Trudy Ukr. NIGMI, Issue 89- 65-75.

[22] Braham, R., 1966: Project Whitetop - A convective cloud randomized seeding project.
Part I - Design of the Experiment
Part II - Summary of Operations
The University of Chicago, Chicago, Ill., 155 pp.

[23] Weickmann, H., 1957: Current understanding of the physical processes associated with cloud nucleation. Beiträge, Phys. der Atmosphäre 30, 97-118.

[24] Weickmann, H. K., 1972: Man-made weather patterns in the Great Lakes Basin. Weatherwise, Vol. 25, No. 6, December 1972, 260-268.

[25] Leskov, B. N., 1971: Change of intensity of artificial precipitation with time during frontal cloud modification. Trudy Ukr. NIGMI, Issue 99, pp. 41-52.

[26] Leskov, B. N., 1971: Preliminary results of comparison of amount of artificial precipitation and the water reserves of seeded frontal clouds. Trudy Ukr. NIGMI Issue 106, pp. 37-41.

[27] Litvinov, I. V., and Ju. V. Ruzheinikova, 1968: Frequency of clouds in the Podmoskov'ye area suitable for artificial modification. Leningrad Institut Experimental'noi Meteorologii, Trudy, No. 3, 35-43.

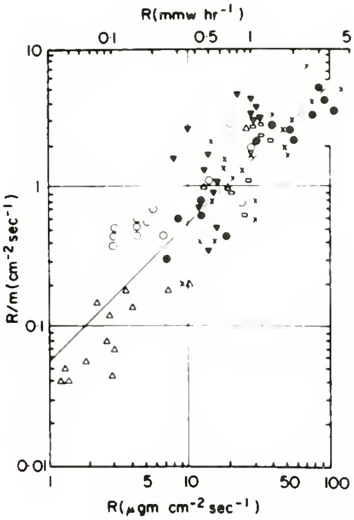

Figure 1 Snow Crystal flux R/m ($m^{-2}sec^{-1}$) versus rate of precipitation R(mmw hr^{-1}) according to Gunn [1].

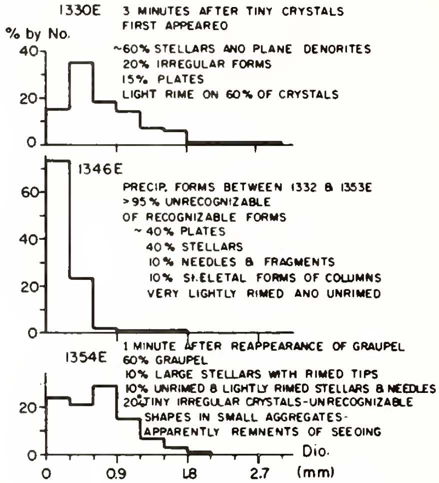

Figure 2 Size distributions of snow crystals collected at S. Dayton on 21 Nov. 1969.

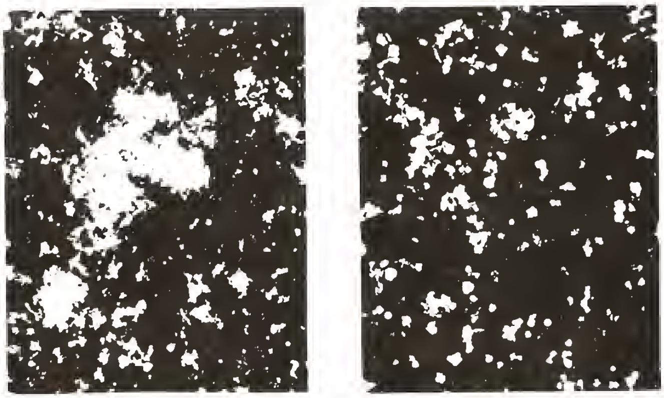

1346E SAMPLE OBTAINED FROM SEEDED REGION

1354E SAMPLE OBTAINED FROM TRAILING EDGE OF SEEDED SHOWER

Figure 3 Photographic pictures of snow crystals collected at S. Dayton on 21 Nov. 1969.

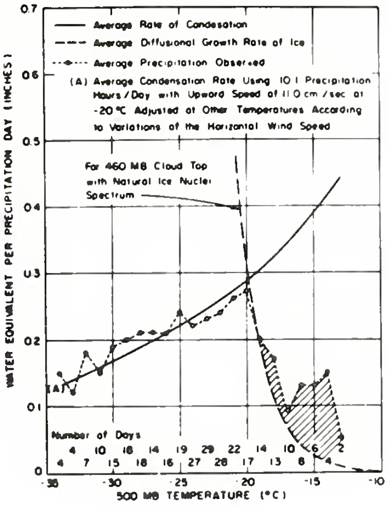

Figure 4 Distribution of non-seeded precipitation at High Altitude Observatory as a function of 500 mb temperature compared to a theoretical distribution computed using the mean diffusional model. Precipitation data are from Climax 1 sample (251) and values are a running mean over a two-degree temperature interval.

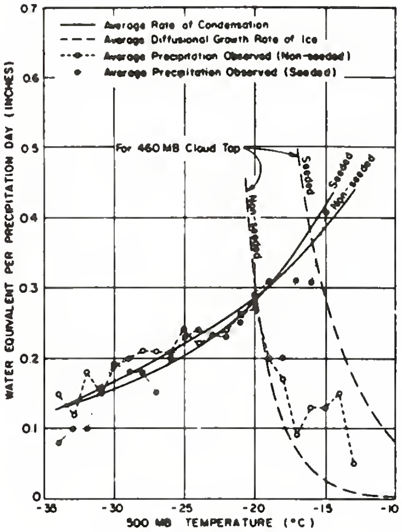

Figure 5 Distributions of seeded and non-seeded precipitation at High Altitude Observatory as a function of 500 mb temperature compared to a theoretical distribution computed using the mean diffusional model. Precipitation data are from Climax 1 sample (251) and values are a running mean over a two-degree temperature interval.

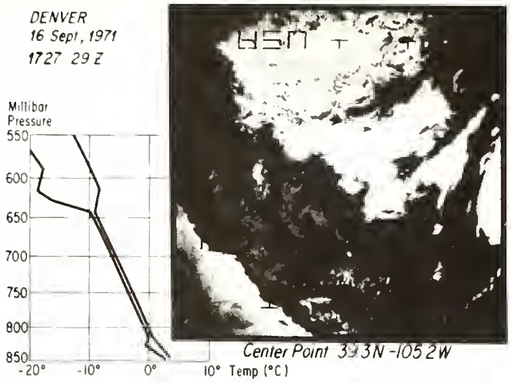

Figure 6 Satellite picture of western USA with large upslope cloud system flowing from east to west against Rocky Mountains. (Note: location of counter crossmark is approximately the location of Denver.) Left side of picture shows Denver Radiosonde and the atmospheric profile of the cloud layer.

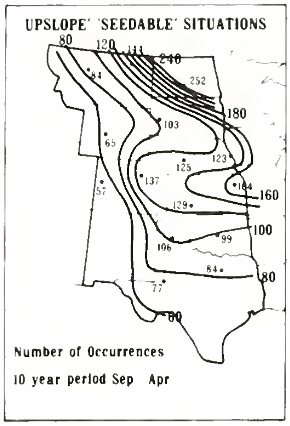

Figure 7 Number of upslope seedable situations in 10 years during winter over the US High Plains area.

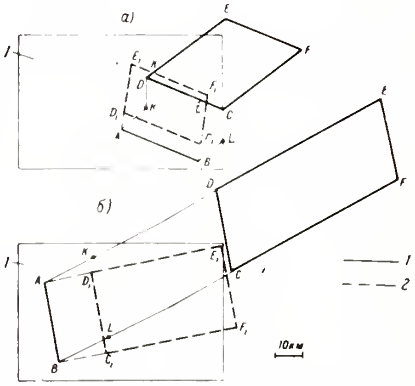

Comparison of results of isolated zones of increased precipitation using the Leskov (1) and Leonov (2) methods. (Leakov 1969)

Figure 8a Definition of target area according to Leonov and Leskov.

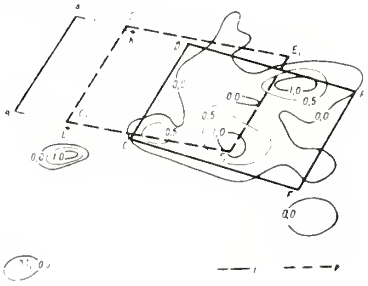

Actual zone of increased precipitation in comparison with the Leskov (1) and Leonov (2) method of determination. (Leskov 1969)

Figure 8b Target area as defined by Leskov and isohyets of precipitation in target area.

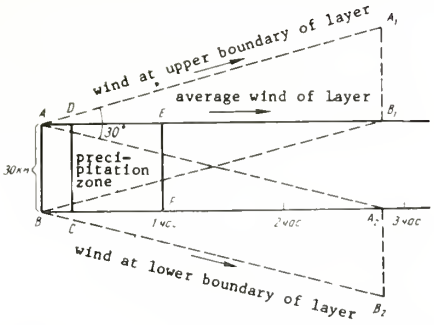

Definition of modification zone due to shift of wind direction in the layer to be seeded (Leskov 1970).

Figure 8c Additional sophistication of target area definition according to Leskov.

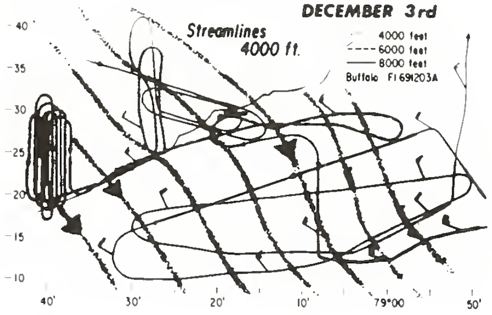

Figure 8d Flight path during seeding and analysis phase on 3 December 1969. Picture illustrates low level wind field as streamlines.

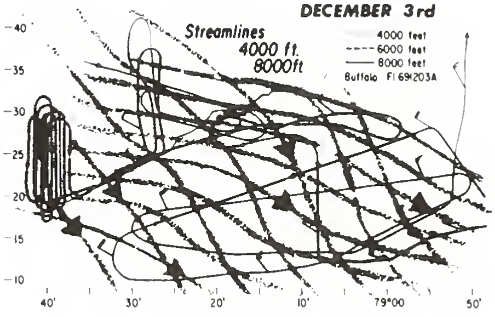

Figure 8e Same as Figure 8d but high level streamlines have been added.

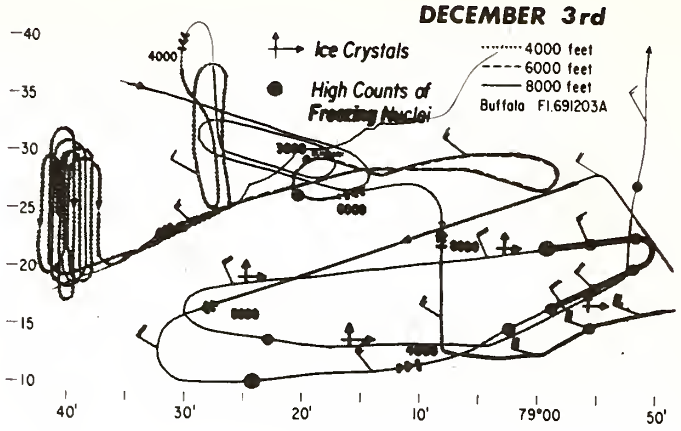

Figure 8f Shaded area defines target area affected by the seeding, freezing nuclei observations along analysis flight path, diamond dust was observed along flight path.

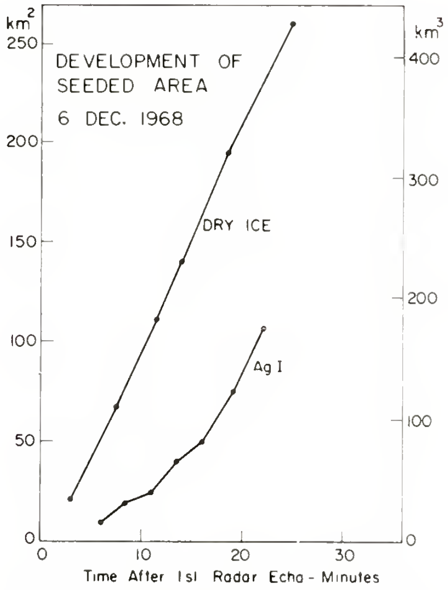

Areal spreading of AgI and dry ice seeding.

Figure 9 Development of seeded areas after seeding with Dry Ice and AgI on 6 Dec. 1968.

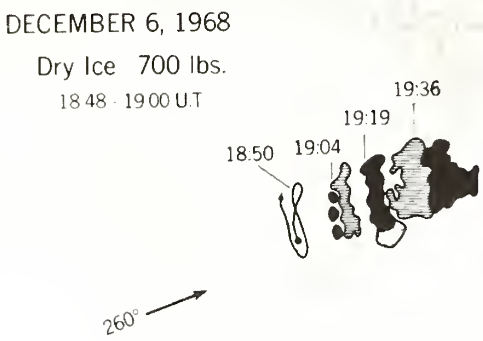

Figure 10a

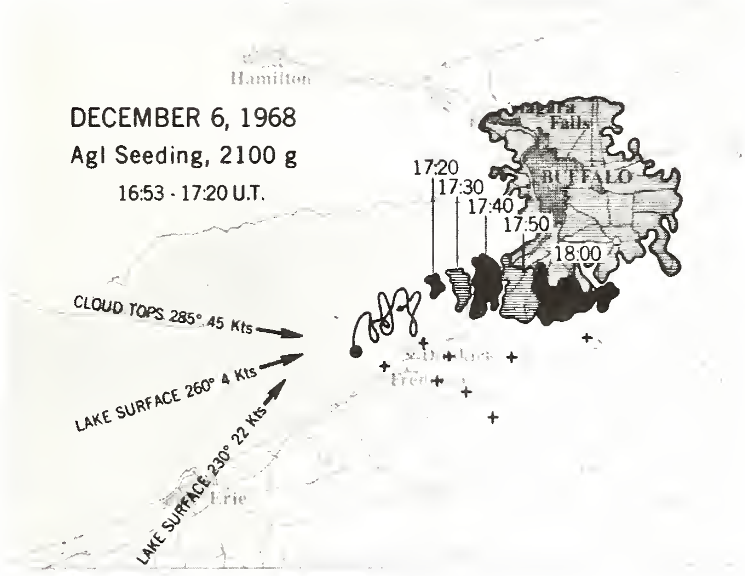

Figure 10b

Figures 10 a, b Seeding effects in cloud layer on 6 Dec. 1968.

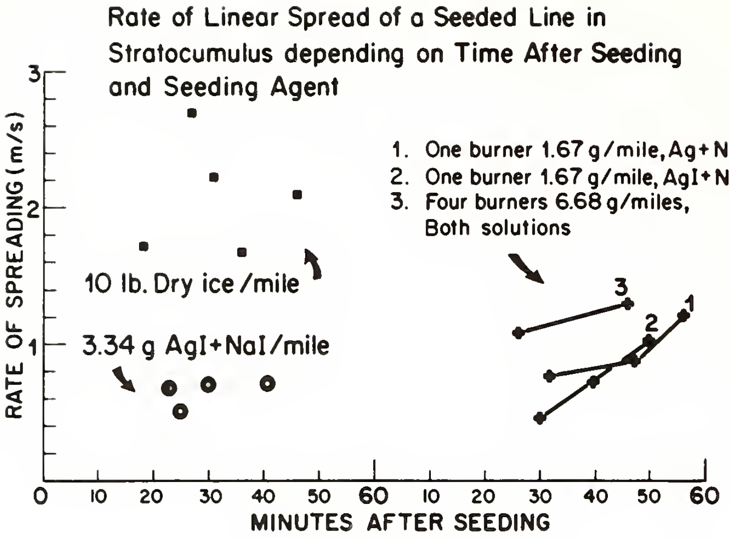

Figure 11 Rate of linear spreading of seeded line in Stratocumulus depending on time after seeding and seeding agent. Data from 21 February 1971, cloud base 1500m at -6°C, cloud tops 2100m at -7.5°C. Data for right side of Figure from 24 Feb. 1971, cloud base 1500m at -8.5°C, tops 2100m at -10.8°C.

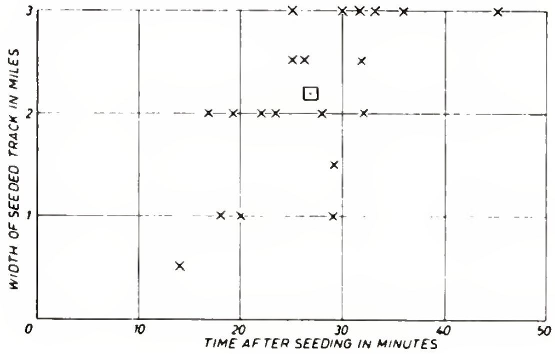

Figure 12 Lateral spread of a seeded line.

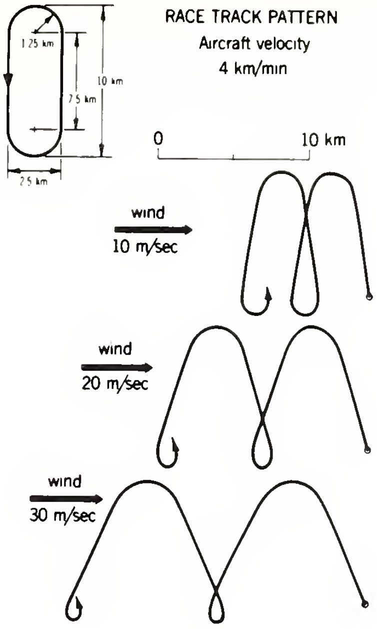

Figure 13 Development of race track seeding track in Stratocumulus layer for various wind speeds.

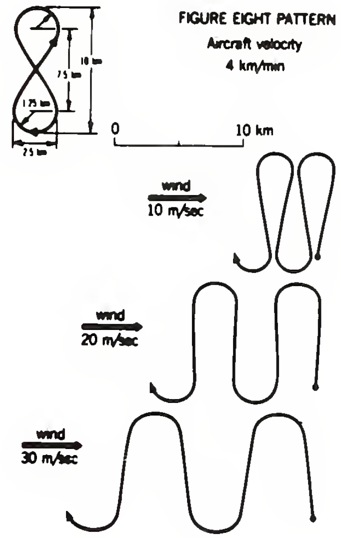

Figure 14 Development of figure eight seeding track in Stratocumulus layer for various wind speeds.

Figure 15 Intensive development of seeded area in a convective Stratocumulus deck, apparently caused through combination of two race track seeding lines as in Figure 13.

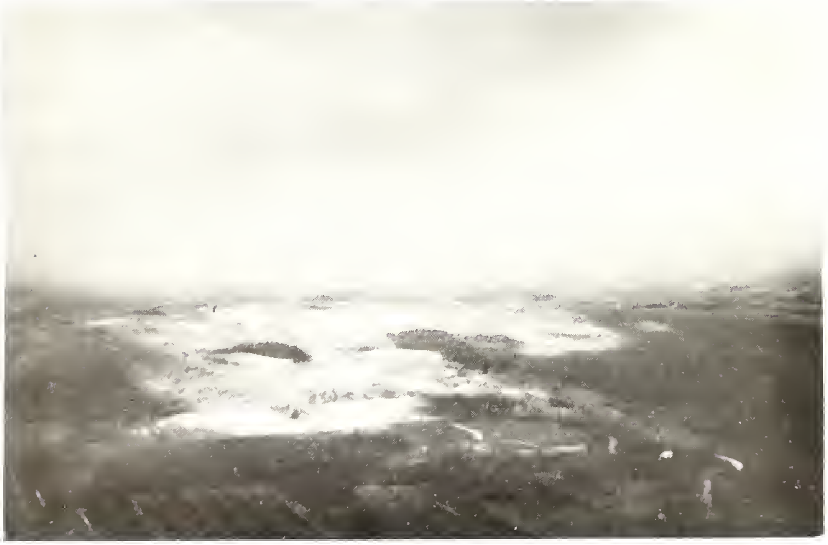

Figure 16 Artificial snow shower on 25 Nov. 1968 over south shore of Lake Erie, NY. Note sunshine behind shower as sign of effective snow-out.

Reprinted with permission of Beitrage zur
Physik der atmosphare, Vol. 46. Band, 1973.

Atmospheric Aerosols: Residence Times, Retainment Factor and Climatic Effects

H. K. Weickmann and R. F. Pueschel

1. Introduction

At present there is much concern about man's impact on his environment. Realizing that in historic times the climate has changed on many time scales without any contribution from anthropogenic sources, a fair evaluation of man's impact on the earth's climate is a near impossible task. However, numerous instances, mostly unnoticed, of local inadvertent weather modification occur due to anthropogenic sources. We frequently had the opportunity to observe such effects in connection with our research in the Great Lakes Basin. Smoke stacks from metal foundries are prolific sources of freezing and condensation nuclei. Freezing nuclei concentrations up to 2×10^3 per liter against a background of $5\ l^{-1}$ and strong glaciation in supercooled Stratus have been measured downwind from industrial plumes. During proper cloud conditions, snow showers developed downwind of cities and industrial centers.

In the following, we will try to evaluate the present situation concerning world-wide pollution from such sources. Without any intention to neglect the significance of gaseous pollutants, the emphasis in the following discussion is placed on aerosols. Atmospheric particles potentially affect climate and weather, respectively, through their influence on the earth's radiation budget and their active participation in cloud formation and modification as condensation and freezing nuclei.

2. Atmospheric Aerosol Budget

Let us first assess the relative significance of worldwide natural and artificial aerosol production. ROBINSON and ROBBINS (1971) in a recent survey estimate that the annual production from natural sources amounts to 2312×10^6 tons, or 88.5 % of the total, while the concentration from man-made sources amounts to 296×10^6 tons, or 11.5 % of the total. For the natural sources we would like to point out that the oceanic production roughly equals land production, whereby soil dust constitutes quite a large portion. It is important to realize that the artificial production is limited to the world's industrial centers. Considering that these are located mainly in the Eastern USA, Europe, Japan and part of Australia, we find that the 296×10^6 tons of man made aerosols are produced every year on only about 2.5 % of the surface of the globe. The natural production over this same area amounts to 58×10^6 tons or only about 20 % of the artificial production. If we consider that the energy demand has increased with time drastically in the past (COOK, 1971) with no limit in sight, then there can be little doubt that inadvertent weather modification on a scale large enough to affect man's well being might soon become a reality.

There is evidence of a deteriorated environmental quality in direct proportion to the density of anthropogenic pollution sources: The American traveler in Europe is struck by the permanently poor visibility in almost all European countries which seldom is better than 10 km. On the other hand, during non-consecutive climatic conditions it is possible to see the island of Hawaii when leaving Honolulu by plane, corresponding to a visibility of well over 300 km (the theoretical visibility limit based on molecular Rayleigh scattering is 350 km). On a more quantitative basis, conductivity measurements showed a steady increase in aerosol concentrations near the surface during the last 60 years over the North Atlantic Ocean, but not over the South Pacific Ocean (COBB and WELLS, 1970). Above the boundary layer, for instance on the Mauna Loa Observatory (MLO), Hawaii, above the tradewind inversion, careful measurements of atmospheric electrical parameters such as conductivity, potential gradient and ion density during 1960 and 1968 yielded no change whatsoever (Table 1), indicating that the steady increase of the atmospheric CO_2 content due to the hydrocarbon combustion (also measured on MLO) is not matched by a corresponding increase of the aerosol content (COBB, 1973). Also, solar radiation measurements on Mauna Loa do not reveal any effect of man's activity on atmospheric turbidity (ELLIS and PUESCHEL, 1971) other than natural-volcanic dust-turbidity in the stratosphere. (ELLIS and PUESCHEL, 1971; DYER and HICKS, 1968; VIEBROCK and FLOWERS, 1968).

- Table 1 Atmospheric Electric Parameters on Mauna Loa Observatory Measured in 1960 and 1968
- Tabelle 1 Luftelektrische Parameter am Observatorium Mauna Loa, gemessen 1960 und 1968

Parameter	1960	1968
Potential Gradient	120 Vm^{-1}	130 Vm^{-1}
Total Conductivity	$7.2 \times 10^{-14}\ \Omega^{-1}\ m^{-1}$	$7.2 \times 10^{-14}\ \Omega^{-1}\ m^{-1}$
Small Ion Density	960 cm^{-3}	960 cm^{-3}

A literature survey readily shows that the available data on atmospheric particulate materials do not provide sufficient information for a comprehensive analysis of atmospheric aerosols in the global, or sometimes even in the regional environment. However, realizing the potential effects of certain classes of particles on weather and climate, we attempt in the following to parameterize atmospheric aerosol systems.

We define an atmospheric retainment factor R for aerosols as being the ratio between the aerosol concentration that is retained by the atmosphere and the annually produced aerosol mass. It appears practical to apply this quantity to three atmospheric layers: the lower boundary layer which reaches from the surface to the top of the Ekman layer (about 1200 m) over the continent, or the top of the trade inversion (about 2000 m) over the oceans, the troposphere between the top of the boundary layer and the tropopause, and the stratosphere. Generally, the residence time for particles in these layers amounts to days for the boundary layer, weeks to months for the troposphere and months to years for the stratosphere. ROBINSON and ROBBINS (1971) present global particulate emission calculations based on data for industrial operations and fuel combustions combined with proper emission factors for typical aerosol systems. Whereas it is possible to estimate quite reliably the emissions of particulate materials from industrial operations, combustion sources and natural processes, a proper evaluation of existing atmospheric concentrations of specific aerosols is hampered by the lack of proper analytical techniques. Based on existing data, however, we calculated retainment factors for various aerosol masses and constituents. The results for background locations are summarized in Table 2. Urban data have not been considered because of their strong dependence on meteorological variables resulting in a large variability.

The source data are the global sum of natural and man-made emissions except for lead which is strictly man-made. No distinction between these two sources has been made because of the general impossibility to distinguish the origin of atmospheric constituents with presently existing analytic techniques. The published concentration values measured in remote areas ($\mu g/m^3$) were converted to metric tons by multiplying with the volume of air in the boundary layers over oceans and continents, respectively, and within the total troposphere and stratosphere. Hence, the retainment factors R are conservative estimates for the northern hemisphere in which most of the artificial aerosol production centers are located.

3. Discussion

Average retainment factors for continental, marine and tropospheric conditions derived from Table 2 (excluding the anomalous values for pesticides) are 1.75×10^{-3}, 1.61×10^{-3} and 0.95×10^{-3}. This close agreement between the boundary layer retainment factor and the tropospheric value for most aerosol systems permits the important conclusion that it is the residence time typical of boundary layer condition which determines the retainment factor. This conclusion is valid for particles which originate at the surface. A volcanic aerosol which is emitted into the stratosphere directly is retained in agreement with stratospheric residence times.

■ Table 2 Annual Production rate $\dot{M}$, Atmospheric Concentrations M and Atmospheric Retainment Factor R for Various Aerosol Systems

■ Tabelle 2 Jahresproduktion $\dot{M}$, Konzentration M und Retainment Faktor R für verschiedene Aerosole

Aerosol Type	Prod. Rate (a) $\dot{M}$ (10^6 tons/yr)	Boundary Layer				Troposphere		Stratosphere	
		Continental		Marine					
		M ($\mu g/m^3$)	R	M ($\mu g/m^3$)	R	M ($\mu g/m^3$)	R	M (10^6 tons)	R
Total	2 608	23 (b)	1.3×10^{-3}	10 (c)	2.8×10^{-3}	1.7 (c)	3.3×10^{-4}		
	227	1.1 (b)	7.4×10^{-4}	2.0 (c)	6.0×10^{-3}	0.5 (c)	1.7×10^{-3}		
		3.0 (e)	2.0×10^{-3}						
Sea Salt	1 000			4.6 (c)	3.3×10^{-3}				
Soil Dust	200	10 (k) (b)	7.5×10^{-3}	2.5 (k)	2×10^{-3}				
Pb	0.23	2×10^{-2} (g)		8×10^{-4} (d)	2.1×10^{-5}	7×10^{-4} (d)	3×10^{-4}		
		2.2×10^{-2} (o)	1.3×10^{-4}	1×10^{-3} (*l*)	3.1×10^{-5}	2×10^{-4} (m)	8.9×10^{-5}		
		2×10^{-2} (p)		1.7×10^{-3} (n)	5.3×10^{-5}	5×10^{-4} (m)	2.2×10^{-4}		
Zn	0.28			1.1×10^{-2} (d)	2.7×10^{-4}	2.8×10^{-3} (d)	1×10^{-3}		
Volcanic	4							4 (i)	1.0
$SO_4^=$	350	4.0 (b)	1.7×10^{-3}			0.1 (j)	3×10^{-3}		
		1.0 (e)	4.3×10^{-4}						
NO_3^-	460	0.7 (b)	2.3×10^{-4}	0.15 (f)	2.4×10^{-5}				
Pesticide	8×10^{-3} (n)	10^{-2} (h)	2×10^{-1}	10^{-6} (h)	10^{-4}				

(a) ROBINSON, E., and R. C. ROBBINS (1971): SRI Project SCC-8507 Final Report.
(b) U.S. Public Health Service (1968): Publ. No. APTD-68-9, 1968.
(c) PUESCHEL, R. F., B. A. BODHAINE and B. G. MENDONCA, J. Appl. Met., March 1973.
(d) SIMPSON, H. J. (1972): J.G.R. **77**, 5266.
(e) GEORGII, H. W. (1970): J.G.R. **75**, 2365.
(f) LODGE, J. P., A. J. MacDONALD and E. VIHMAN (1960): Tellus **12**, 184.
(g) LUDWIG, J. H., G. B. MORGAN and T. B. McMULLEN (1970): EOS **51**, 468–475.
(h) JEGUI, Z. (1969): An. N. Y. Acad. Sci., **160**(1), 143–54.
(i) MITCHELL, J. M. Jr. (1970): In "Global Effects of Environmental Pollution", S. F. Singer, Ed., Reidel, Oodrecht, Holland.
(j) JUNGE, C. E. (1963): Air Chemistry and Radioactivity, Academic Press, N. Y.
(k) PROSPERO, J. M. (1968): Bull. Am. Met. Soc., **49**(6), 645–52.
(l) CHOW, T. J., J. L. EARL and C. F. BENNETT (1969): *Env. Sci. Tech.* **3**, 737.
(m) EGOROV, V. V., T. N. ZHIGALOVSKAYA, S. G. MALAKHOV (1970): J.G.R. **75**, 3650.
(n) JERNIGAN, E. L., B. J. RAY, R. A. DUCE (1971): Atm. Env., **5**, 881.
(o) McMULLEN, T. B., R. B. FAORO, G. B. MORGAN (1970): JAPCA **20**, 369.
(p) CHOW, T. J., J. L. EARL, C. B. SNYDER (1972): Science **178**, 401–402.

Of the aerosol subsystems considered in Table 2, it appears that the lead aerosol has the shortest tropospheric residence times. This agrees with the observation of large variations of lead concentrations with distance from urban areas (ATKINS, 1969), indicating the dominant role played by vehicles as the source of lead aerosols. The decrease with distance from the source is enhanced by dilution and mixing with cleaner air as urban air masses move across rural areas and by scavenging processes that are continually removing lead aerosol particles from the air mass. The possibility exists that our observations of high concentrations of ice crystals downwind of cities is caused by ice nuclei formation from lead in automobile exhaust (SCHAEFER, 1966, MORGAN and ALLEE, 1968).

On the opposite end of the activity spectrum are stable (mostly organic) aerosol particles. It is known that these substances are not only hydrophobic themselves but in interaction with condensation nuclei impair their activity. The residence times of these organic aerosols are consequently the longest, and comparable to that of soil dust whose particle size is in a category where scavenging is at a minimum.

This difference in residence times of different aerosol subsystems points towards distinctive effects which each might have on weather and climate. Whereas active condensation and freezing nuclei, such as the lead halides, will affect the local weather, long term effects on the climate are predominately influenced by aerosol residence times. Differences in retainment factors will lead to an accumulation of one subsystem relative to another. It is conceivable that on a secular scale the long-lived organic aerosol is more important than is the generally short-lived inorganic aerosol, particularly so since an effect on climate will be determined by its absorptivity spectrum of solar and terrestrial radiation. It has been suggested that an increase of particulate loading would lead to cooling or warming of the earth's surface, depending on the amount of radiation absorbed in relation to that scattered by the aerosol system (CHARLSON and PILAT, 1969; MITCHELL, 1971).

BARRETT (1971) has presented a rigorous numerical model which predicts the depletion of solar and sky irradiance due to aerosols but neglects absorption and longwave effects. For low particulate loads (less than 1000 g/ha), percent depletion is a linear function of aerosol mass and may be represented by $D = 0.013\ M$ (at latitude 20 N) where D = percent depletion and M = global aerosol load in g/ha. Barrett's model can be applied to estimate the particulate load of the stratosphere from existing solar radiation data. The Mt. AGUNG (1963) eruption caused an observed 2 % depletion of solar radiation at Mauna Loa, Hawaii (ELLIS and PUESCHEL, 1971) and in Arizona (HEIDEL, 1972). According to Barrett's model this corresponds to an addition into the stratosphere of about 150 gm/ha, or a total of about 8×10^6 tons. MITCHELL (1970) estimates independently that the eruption ejected approximately 15×10^6 tons, assuming that one percent of order-of-magnitude estimates of dust ejections computed by LAMB (1970) reached the stratosphere. The agreement is excellent in view of the approximations involved.

On a global long-term basis, the earth's surface must achieve radiative equilibrium with the received energy from the sun. Neglecting absorption effects, the global annual mean temperature will descrease with increase in particulate loading. The magnitude of this effect has been calculated by BARRETT (1971). The temperature changes resulting from the aerosol systems considered in this paper are shown in Table 3. Column 2 contains the atmospheric aerosol concentrations in tons, which is the product of annual production rate and retainment factor. Column 3 contains the atmospheric concentrations in grams per hectare, and Column 4 gives the expected temperature changes according to Barrett's model. The total accumulative value for the tropospheric aerosol amounts to − 1.3 °C.

Considering that man is responsible for about 10 % of the global aerosol load, his influence on the climate amounts at most to about 0.13 centigrade temperature changes. Relatively high are the temperature effects of sea salt and soil dust which are both portions of the natural background aerosols. However, these two atmospheric constituents prevail over the oceans and the continent, respectively. If their effects are weighed accordingly in global climate evaluations, their cumulative temperature effect amounts to only − 0.4 °C rather than − 0.7 °C which would be expected were they distributed evenly over the globe.

(This and uncertainties in the background aerosol concentration measurements are the reasons why the cumulative effects of the tropospheric aerosol subsystems in Table 3 do not add up exactly to the total trophospheric aerosol effect.)

■ Table 3 Atmospheric Concentrations and Corresponding Sea-level Temperature Changes Below that for a Clean Atmosphere According to Barrett (1971)

■ Tabelle 3 Konzentrationen und entsprechendes Absinken der Temperatur in Seehöhe unter die für eine reine Atmosphäre geltenden Werte (Nach Barrett (1971))

Aerosol Type	$T = \dot{M} \times R$	C	ΔT
	(10^6 tons)	(g/ha)	°C
	Tropospheric		
Total	7.3	145	-1.3
Volatile	1.4	25	-0.2
Pb	2.77×10^{-4}		negl.
Zn	1.78×10^{-3}		negl.
$SO_4^=$	0.6×10^{-1}	10	-0.08
NO_3^-	6×10^{-2}		negl.
Pesticide	1.5×10^{-3}		negl.
Sea Salt	3.3	65	-0.5
Soil Dust	1.5	30	-0.2
	Stratospheric		
Volcanic	4.0	80	-0.6

It can be seen that volcanic aerosols, although comprising only 0.015 percent of the total aerosol production, exhibit the strongest influence on global temperatures due to extended stratospheric residence times and a relatively small stratospheric air mass. Surprisingly high is the effect of photochemically produced volatile substances which amount to about 10 percent of the total aerosol production.

Clearly, these examples point towards the necessity of paying greater attention to the possible increase of certain aerosol types with more pronounced effects. The outlook for a global increase of the atmospheric aerosol burden can be derived from data on present energy consumption (COOK, 1971). The incremental increase in power requirements during 1969 was more than 10 %. If we assume a levelling off at 10 % per year and assume further that the present power consumption is compatible with the present aerosol production, then simple arithmetic would indicate that in about 23 years the aerosol production reaches the amount of the natural production and the atmospheric aerosol content may then have doubled. While this need not be alarming, it may nevertheless signal the beginning of global inadvertent weather modification. Since we are only just now beginning to combat air pollution, we are convinced that the problem can be solved within 23 years.

While the problem of planetary cooling through man's activities appears remote, immediate attention must be given to surveys and monitoring of potentially active aerosols, such as freezing and cloud condensation nuclei. It is apparent that urban activity does increase the concentration of the efficient atmospheric nuclei. The effects of manmade freezing nuclei upon supercooled clouds in the vicinity of industrial centers has been mentioned above.

References

P. R. ATKINS, Lead in a Suburban Environment, J. Air Poll. Contr. Assoc., **19,** 591, 1969.

E. W. BARRETT, Depletion of Short-Wave Irradiance at the Ground by Particles Suspended in the Atmosphere, Solar Energy **13**, 323–337, 1971.

R. J. CHARLSON and M. J. PILAT, Climate: The Influence of Aerosols, J. Appl. Meteor., **8,** 1001–1002, 1969.

W. E. COBB, Oceanic Aerosol Levels Deduced from Measurements of the Electrical Conductivity of the Atmosphere, J. Atm. Sci. 30, 100–105, 1973.

W. COBB and H. J. WELLS, The Electrical Conductivity of Oceanic Air and its Application to Global Atmospheric Pollution, J. Atm. Sci., **27,** 814–819, 1970.

E. COOK, The Flow of Energy in an Industrial Society, Scient. American **225,** 135–144, 1971.

A. J. DYER and B. B. HICKS, Global Spread of Volcanic Dust from the Bali Eruption of 1963, Quart. J. Roy. Met. Soc., **94,** 545, 1968.

H. T. ELLIS and R. F. PUESCHEL, Solar Radiation: Absence of Air Pollution Trends at Mauna Loa, Science **172,** 845–846, 1971.

K. HEIDEL, Turbidity Trends at Tucson, Arizona, Science **177,** 882–883, 1972.

H. H. LAMB, Volcanic Dust in the Atmosphere, Phil. Trans. Roy. Soc. London, 266A, 425, 1970.

J. M. MITCHELL, Jr., in: Global Effects of Environmental Pollution, S. F. Singer, Ed., Reidel Publ. Co., Oodrecht, Holland, 1970.

J. M. MITCHELL, Jr., The Effect of Atmospheric Aerosols on Climate with Special Reference to Temperature near the Earth's Surface, J. Appl. Meteor. **10,** 703, 1971.

G. M. MORGAN, Jr. and P. A. ALLEE, The Production of Potential Ice Nuclei by Gasoline Egines, J. Appl. Metor. **7,** 241–246, 1968.

E. ROBINSON and R. C. ROBBINS, Emissions, Concentrations and Fate of Particulate Atmospheric Pollutants, SRI Project SCC-8507, Final Report 1971.

V. J. SCHAEFER, Ice Nuclei from Automobile Exhaust and Iodine Vapor, Science **154,** 1555, 1966.

J. H. VIEBROCK and E. C. FLOWERS, Comments on the Recent Decrease in Solar Radiation at the South Pole, Tellus **20,** 400–411, 1968.

Reprinted from NOAA Technical Report ERL 281-APCL 29,
27 pages, October 1973.

COMPUTER SIMULATION OF MULTI-AIRCRAFT FLIGHTS: AN AID TO MISSION PLANNING

Stephen D. Whitaker

To aid advanced planning in multi-aircraft research flights, a computer program was developed in APCL to simulate a multi-aircraft flight. With this program a scaled, graphic display of each aircraft's position can be obtained at any desired time into the mission. During the development of the program we emphasized flexibility so that flight parameters can be readily changed and the simulated flight re-run for comparison. The program, also, incorporates certain computational aids to provide for aircraft rendezvous and takeoff timing. This report contains a description of the program elements and their operation.

Reprinted from NOAA Technical Report ERL 268-APCL 27,
43 pages, March 1973.

SOME CLIMATOLOGICAL CHARACTERISTICS OF SEEDABLE UPSLOPE CLOUD SYSTEMS IN THE HIGH PLAINS

C. D. Whiteman

A model of seeding opportunity recognition is developed for shallow wintertime cloud systems in the High Plains of the United States. The model uses rawinsonde network data for the High Plains to determine climatological characteristics of "seedable" upslope cloud systems. Included are annual, monthly, and diurnal frequencies of occurrence of seedable cloud systems as well as characteristics of the cloud systems themselves. Such characteristics include cloud thicknesses, heights of cloud tops and bases, lapse rates, cloud top temperatures, upslope wind components, and the relative frequencies of precipitating and nonprecipitating cloud systems.

Reprinted from NOAA Technical Report ERL 287-APCL 31,
43 pages, March 1973.

VARIABILITY OF HIGH PLAINS PRECIPITATION

C. D. Whiteman

Precipitation statistics are presented for the High Plains area of the United States. These include measures of the variability of annual, monthly, cold season, and crop-growing season precipitation. Maps show the spatial distribution of coefficients of variation. The natural variability of High Plains precipitation is compared with that of other parts of the country having similar annual amounts of precipitation.

1. INTRODUCTION

The High Plains area is the western, higher elevation portion of the Great Plains of the United States. It extends eastward from the foothills of the Rocky Mountains for approximately 800 km. The elevation varies between 3000 and 150 m above mean sea level (MSL).

The High Plains states, as delineated in figure 1, cover 2,890,000 sq km and contain 23,019,000 people, of which 28 percent live in rural areas. Because agriculture is a substanital part of the economy, the region is dependent on the climate, especially the annual precipitation.

The climate of the High Plains varies from semi-arid over the Western Plains in the "rain shadow" of the Rocky Mountains to sub-humid grassland climate farther east. The precipitation regime is characterized by relatively small mean annual precipitation with large year-to-year variability. Need for additional precipitation exists through most of the area but the degree varies with location and time of year.

A major national precipitation enhancement experiment may soon begin at a site in the High Plains. Many factors must be considered in selecting a site for the proposed program. A precipitation climatology is one that should have an important bearing on the final selection of the site, as well as aid in the design of the statistical and physical experiments.

The ultimate verification of the success of a seeding experiment is determined by a statistical analysis of the amount of precipitation that reaches the ground. To find statistically significant increases or decreases in precipitation at the ground, precipitation during the seeding experiment must be shown to differ significantly from that in an adjacent unseeded area, or, from precipitation expected on the basis of historical records. Alternatively, the seeded days in the target area must be shown to differ from the unseeded days in the same target. Several factors are important in choosing the location of a seeding experiment. The need for additional precipitation may be a strong factor for locating an experiment in a dry area. Experimental concerns, especially the ease of verifying the seeding effect, may be a strong factor for locating the experiment in a different area that has more favorable natural precipitation characteristics. In general, the most favorable area for statistically verifying the effects of seeding are those having low variabilities in the distribution of natural precipitation in space and time.

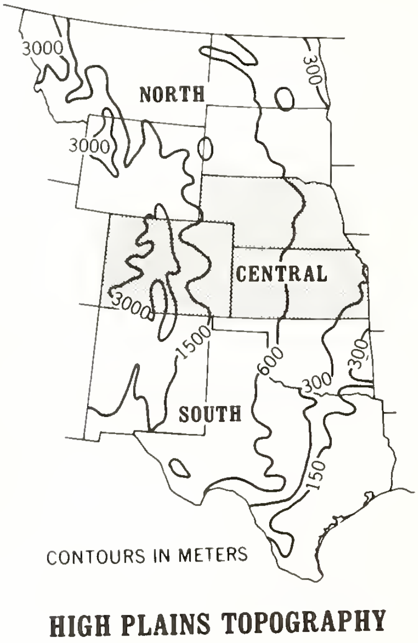

Figure 1. High plains topography and regions.

This paper presents statistics that define the spatial and temporal distributions of High Plains precipitation. This information should be useful in the location and design of future precipitation modification experiments in the High Plains.

☆ U. S. GOVERNMENT PRINTING OFFICE 1975 - 677-240/1254 Reg. 8

PENN STATE UNIVERSITY LIBRARIES
A000072832851